# Water resistance properties of water-based biopolymer films

Alison Louise Tasker

Submitted in accordance with the requirements for the degree of

Doctor of Philosophy

The University of Leeds

School of Food Science and Nutrition

August 2013

The candidate confirms that the work submitted is her own, except where work which has formed part of jointly-authored publications has been included. The contribution of the candidate and the other authors to this work has been explicitly indicated below. The candidate confirms that appropriate credit has been given within the thesis where reference has been made to the work of others.

The article **Kinetics of Food Biopolymer Film Dehydration: Experimental Studies and Mathematical Modelling** by Rammile Ettelaie, Alison Tasker, Jianshe Chen, and Stefan Alevisopoulos, doi 10.1021/ie3033075, is based on work found in Chapters 2 and 3 of this thesis.

This copy has been supplied on the understanding that it is copyright material and that no quotation from the thesis may be published without proper acknowledgement.

The right of Alison Louise Tasker to be identified as Author of this work has been asserted by her in accordance with the Copyright, Designs and Patents Act 1988.

© 2013 The University of Leeds and Alison Louise Tasker

## Acknowledgements

First and foremost I would like to thank my supervisors Dr Jianshe Chen and Dr Rammile Ettelaie, without the guidance and support of both of whom I would not have been able to complete this Ph.D. Also many thanks are given to my industrial supervisor Dr Stefan Alevisopoulos, and others at Henkel GMBH, Dusseldorf, for partially funding this work, and for helpful meetings, guiding me to keep my work industrially relevant. I must also express my gratitude to the EPSRC for funding this work, without which I would not have had the opportunity to undertake this project.

I cannot forget all the helpful conversations and encouragement from the staff in the School of Food Science and Nutrition, and particularly the help from Mr Ian Hardy, Dr Mel Holmes and Professor Malcolm Povey on the numerous times the equipment broke! Thank you to the colloids group for allowing me to present my work and for providing constructive feedback for me to improve my work. Particular thanks must go to Dr Nicholas Watson for all his initial guidance on using ultrasound, without which I would have been a fish out of water!

Finally, I would like to thank my parents for supporting me both financially through my entire education and by always encouraging me to achieve my goals and aspirations. The support of my friends and family has been second to none and a special thanks must go to my partner Chris for putting up with the tears, tantrums and stress of the last few months, and just

believing in me! I never thought this day would come and I would never have got here without all of you, so I am grateful to each and every one of you.

## Abstract

This thesis addresses both the theory and simulation of diffusion of moisture in water-based biopolymer films, whose preliminary use is as adhesives on glass bottles in the labelling industry. The first part explores the kinetics of dehydration of thin films of these biopolymer materials. The second part of the thesis deals with moisture intake into both dried thin films and into the wet biopolymer gel network.

Mathematical simulations based on Fick's laws of diffusion have been developed as a tool to understand the underpinning mechanisms of diffusion and of evaporation to discover which, if either plays a more dominant role in controlling the dehydration process. By inputting a series of different initial and final moisture contents, a full spectra of scenarios has been examined to aid understanding of the dehydration process. Numerical calculations where diffusion is the controlling mechanism as well as simulations where evaporation controls the process have been considered and discussed. Models in which a combination of both diffusion and evaporation are equally important are also studied. Fixed and moving boundary conditions are applied to the models and compared with dehydration results obtained experimentally. A simple method has been developed to assess the rehydration process of a dried biopolymer film and similar simulations have also been constructed to describe the rehydration of a water droplet into the thin, dried films.

A novel method to investigate the migration of water into casein biopolymer gels using acoustic techniques has been developed and validated. The

preliminary results are promising, highlighting the potential capability of the method. As the composition of a material changes, the speed of a wave of sound being passed through the material changes, so by monitoring this change as a function of time, concentration profiles of the biopolymer material can be constructed. Simulated concentration profiles were successfully produced based on Fick's second law of diffusion, to obtain a diffusion coefficient dependent on both time and position.. By fitting these curves to the experimental data, diffusion coefficients are obtained with values of the same order of magnitude as those calculated from the experiments on a dehydrating thin film of the same composition.

# Table of Contents

**Acknowledgements** ..... **iii**
**Abstract** ..... **v**
**Table of Contents** ..... **vii**
**List of Figures** ..... **xi**
**List of Tables** ..... **xvii**
**Chapter 1. Introduction** ..... **1**
1.1 The importance of diffusion ..... 1
1.1.1 The diffusion equations ..... 2
1.2 Objectives ..... 4
1.3 Biopolymers ..... 5
1.3.1 Casein ..... 6
1.3.1.1 Casein extraction ..... 7
1.3.2 Starch ..... 9
1.4 The diffusion coefficient and types of diffusion ..... 11
1.5 Measuring diffusion ..... 17
1.5.1 Food applications ..... 18
1.5.2 Building applications ..... 21
1.5.3 Polymer applications ..... 28
1.6 Microscopy techniques ..... 32
1.6.1 SEM, scanning electron microscopy ..... 33
1.6.1.1 Preparation of samples ..... 36
1.6.2 CLSM, confocal laser scanning microscopy ..... 36
1.7 Outline of this work ..... 38
**Chapter 2 Modelling and simulating the dehydration of thin biopolymer films** ..... **40**
2.1 Introduction ..... 40
2.1.1 What is mathematical modelling? ..... 40
2.1.2 Models available in the literature ..... 42
2.2 Theoretical considerations for modelling a drying film ..... 45
2.2.1 Diffusion in a drying film ..... 45
2.2.2 Evaporation from the surface of a drying film ..... 48
2.3. Simulations to model drying in thin films ..... 62

2.3.1 The standard curve – drying with constant D and no shrinkage ..... 63
2.3.2 Incorporating shrinkage into models ..... 64
2.3.3 Moisture dependent diffusion ..... 66
2.3.4 Drying Limited by Evaporation. ..... 70
2.3.5 Modelling dehydration that is controlled by both diffusion and evaporation ..... 73
2.4 Conclusions ..... 74
**Chapter 3 Dehydration of thin biopolymer films ..... 77**
3.1 Introduction ..... 77
3.1.1 Mechanisms of dehydration ..... 77
3.1.2 Structural changes during dehydration ..... 78
3.1.3 Methods used to investigate drying in the literature ..... 79
3.1.4 Modelling the dehydration process ..... 80
3.2 Materials and methods ..... 83
3.2.1 Materials ..... 83
3.2.2 Dehydration of thin biopolymer films ..... 83
3.2.3 Monitoring shrinkage of biopolymer films ..... 84
3.3 Results and discussion ..... 85
3.3.1 Film shrinkage during biopolymer dehydration ..... 85
3.3.2 Dehydration of thin biopolymer films ..... 88
3.4 Dehydration of adhesive films ..... 102
3.5. Conclusions ..... 106
3.6. Future work ..... 108
**Chapter 4 Using Acoustics to Monitor Water Diffusion into Biopolymer Systems ..... 110**
4.1 Introduction ..... 110
4.1.1 What is Ultrasound? ..... 111
4.1.2 Why is Ultrasound an important technique? ..... 112
4.1.3 Applications of Ultrasonic measurements ..... 114
4.2 Using acoustic techniques to develop a novel method for monitoring diffusion in biopolymer systems ..... 116
4.3. Materials and Methods ..... 117
4.3.1 Materials ..... 117
4.3.2 Measuring the speed of sound in pure water and biopolymer system and different temperatures and concentrations ..... 117

4.3.3 Measuring the speed of sound in biopolymer systems as water diffuses into it ..... 118
4.4 Results and Discussion ..... 120
4.4.1 Measuring the speed of sound in pure water and biopolymer system and different temperatures and concentrations ..... 120
4.4.2 Measuring the speed of sound as pure water diffuses into a biopolymer system using the Acoustiscan method .. 123
4.4.2.2 Using Sound velocity as a function of concentration to create a concentration profile as water diffuses into sodium caseinate solution ..... 126
4.4.3 Modelling concentration profiles ..... 128
4.5. Conclusions ..... 135
4.6. Further work ..... 135
**Chapter 5 Rehydration of thin biopolymer films ..... 137**
5.1 Introduction ..... 137
5.1.1 Why is the rehydration behaviour of thin films important? ..... 137
5.1.2 Properties affected by the intake of moisture ..... 138
5.1.3 Methods used to measure moisture intake ..... 139
5.2 Materials and methods ..... 140
5.2.1 Materials ..... 140
5.2.2 Monitoring rehydration of water into biopolymer films ..... 140
5.3 Results and discussion ..... 142
5.3.1 Kinetics of rehydration of thin biopolymer films ..... 143
5.3.2 Microstructural analysis of biopolymer systems ..... 154
5.3.3 Modelling rehydration ..... 160
5.4 Conclusions ..... 174
5.5 Further Work ..... 176
**Chapter 6 Conclusions ..... 177**
6.1 Key findings ..... 178
6.1.1 Dehydration of thin biopolymer films ..... 178
6.1.2 Modelling dehydration of thin biopolymer films ..... 180
6.1.3 Novel acoustic monitoring of water transport into biopolymer solutions ..... 181
6.1.4 Rehydration of thin biopolymer films ..... 181
6.2 Further research ..... 182
6.3 Limitations of this work ..... 185

6.4 Concluding statement..... 185
**References..... 187**
**List of Abbreviations..... 195**
**Appendix 1..... 197**

# List of Figures

**Figure 1.1 - Computational prediction of the structure of casein – from (United States Department of Agriculture, Agricultural Research Service. Dairy and Functional Foods: Molecules. 2010) ..... 7**

**Figure 1.2 - Orientation of glucose monomers in amylose, with 1,4-glycosidic bonds. ..... 9**

**Figure 1.3 - Orientation of glucose monomers in amylose, with 1,4- and 1,6-glycosidic bonds. ..... 10**

**Figure 1.4 - Schematic diagram of the apparatus used for measuring moisture diffusivity of green mango (from Seth & Sarkar, 2004) ..... 19**

**Figure 1.5 - Graphs of *W*, weight loss* vs. time at 50 °C and 70°C respectively under controlled air flow and humidity conditions. • = experimental data, - = exponential regime, ... = first linear regime, and --- = second linear regime. (from Seth & Sarkar, 2004). ..... 20**

**Figure 1.6 - Graph showing *W** vs. Fourier number ($D_\infty t/L^2$) with model predictions. • = experimental data, - = exponential regime, ... = first linear regime, and --- = second linear regime. (from Seth & Sarkar, 2004) ..... 21**

**Figure 1.7 - Schematic diagram of sorption apparatus (from Drchalova & Cerny, 2003). ..... 23**

**Figure 1.8 - Comparison of moisture diffusivity functions using various methods (from Drchalova & Cerny, 2003). ..... 24**

**Figure 1.9 - Diagram to show experimental apparatus setup (from Nizovtsev *et al,* 2008). ..... 27**

**Figure 1.10 - Graphs showing curve fits of experimental moisture uptake for 1 mm thick samples conditioned at 50 C, immersed in water (a) absorption and (b) desorption (from Mubashar *et al,* 2009a). ..... 31**

**Figure 1.11 - Schematic diagram of an SEM ..... 35**

**Figure 1.12 - Schematic diagram of a CLSM ..... 37**

**Figure 2.1 - The "standard" curve calculated from Fick's law with constant diffusion coefficient and constant film thickness. ..... 64**

**Figure 2.2 - Numerically calculated drying curves for constant diffusion and film shrinkage for different final moisture contents.–= standard curve, – = $V_f$ 0.48, – = $V_f$ 0.4, – = $V_f$ 0.3, – = $V_f$ 0.2, – = $V_f$ 0.1, – = $V_f$ 0.02. In all cases *K* is infinite and $V_{in}$ = 0.5. ..... 65**

**Figure 2.3 - Numerically calculated drying curves for constant diffusion and film shrinkage for different initial moisture contents. – = standard curve, – = $V_{in}$ 0.2, – = $V_{in}$0.4, – = $V_{in}$ 0.6, – = $V_f$ 0.8. In all cases *K* is infinite and $V_f$ = 0.02..... 66**

**Figure 2.4 - Numerically calculated drying curves for variable diffusion and film shrinkage for different final moisture contents. – = standard curve (with constant diffusion and film thickness), – = $V_f$ 0.48, – = $V_f$ 0.4, – = $V_f$ 0.3, – = $V_f$ 0.2, – = $V_f$ 0.1, – = $V_f$ 0.02. In all cases *K* is infinite and $V_{in}$ = 0.5. ..... 67**

**Figure 2.5 - Numerically calculated drying curves for variable diffusion and film shrinkage for different initial moisture contents. – = standard curve, – = $V_{in}$ 0.2, – = $V_{in}$0.4, – = $V_{in}$ 0.6, – = $V_f$ 0.8. In all cases *K* is infinite and $V_f$ = 0.02..... 68**

**Figure 2.6 - Comparison between drying curves for different initial moisture contents obtained for constant and variable diffusion coefficients, when *K* is infinite and $V_f$ = 0.02. – = constant *D*, – = variable *D*. ..... 69**

**Figure 2.7 - Mathematical model prediction for evaporation limited dehydration with constant film thickness..... 70**

**Figure 2.8 - Evaporation limited drying curves with film shrinkage and different final moisture contents. --- = evaporation curve with fixed volume, – = $V_f$ 0.1, – = $V_f$ 0.05, – = $V_f$ 0.02, – = $V_f$ 0.01,– = $V_f$ 0.005. In all cases $V_{in}$ = 0.5. ..... 71**

**Figure 2.9 - Evaporation limited drying curves obtained, with film shrinkage and different initial moisture contents. --- = evaporation curve with fixed volume, – = $V_{in}$ 0.8, – = $V_{in}$ 0.6, – = $V_{in}$ 0.5, – = $V_{in}$ 0.4, – = $V_{in}$ 0.2. In all cases $V_f$ = 0.02. ..... 73**

**Figure 2.10 - Graphs showing the effect of increasing importance of evaporation in the diffusion limiting simulations. . – = K∞, – = *K*= 0.1, – = *K* = 0.01, – = *K*= 0.001, – = *K*= 0.0001. In all cases *D* = 5.48x10$^{-10}$ m$^2$s$^{-1}$, $V_{in}$ = 0.5 and $V_f$ = 0.02. ..... 74**

**Figure 3.1 - apparatus setup for monitoring film shrinkage. ..... 85**

**Figure 3.2 - Changing film thickness of 18wt% sodium caseinate solution at different temperatures ♦=30°C, ■=40°C, ▲=50°C at 25 ± 5% RH plotted against time. ..... 86**

**Figure 3.3 - Changing film thickness of 7wt% starch solution at different relative humidities ♦=20 °C, ■=30 °C , ▲= 40 °C at 25 ±5% RH, plotted against time. ..... 87**

**Figure 3.4 – Plots of $\Gamma = (L(t)\phi(t)-L(\infty)\phi^{eq})/(L(0)\phi(0)-L(\infty)\phi^{eq})$ against time for three systems at RH 30% a) 18 wt% sodium caseinate solution, b) 7 wt% starch solution, and c) 9 wt% sodium caseinate:4.5 wt% starch mixture solution at different temperatures ♦=30°C, ■=40°C, ▲=50°C at 30% RH. ..... 89**

**Figure 3.5 - Plots of $\Gamma$ against time for three systems at 30 °C a) 18 wt% sodium caseinate system, b) 7 wt% starch system, and c) 9 wt% sodium caseinate:4.5 wt% starch mixture system at different relative humidities ♦=20% RH, ■=30% RH, ▲=40% RH at 30°C. ..... 91**

**Figure 3.6 - Drying rate vs. time graphs at 30% RH for a) 18 wt% sodium caseinate solution, b) 7 wt% starch solution, and c) 9 wt% sodium caseinate:4.5 wt% starch mixture solution at different temperatures ♦=30°C, ■=40°C, ▲=50°C ..... 93**

**Figure 3.7 - Drying rate vs. time graphs at 30 °C for a) 18 wt% sodium caseinate solution, b) 7 wt% starch solution, and c) 9 wt% sodium caseinate:4.5 wt% starch mixture solution at different relative humidity values ♦=30% RH, ■=40% RH, ▲=50% RH ..... 93**

**Figure 3.8 – Numerically calculated drying curves, showing $\Gamma = (L(t) - L(\infty)) / (L(0) - L(\infty))$ plotted against scaled time ($\pi^2 Dt/(4L(0)^2)$), for diffusion limited dehydration. The graphs are for a) a system with constant *D* and *L* (red), b) constant *D* and film shrinkage (blue), c) with a moisture dependent water diffusion coefficient and shrinkage (green). The inset shows the magnified graphs for the initial stages of drying. ..... 95**

**Figure 3.9 – Experimental data of Figure 3.4 and Figure 3.5, scaled on a single master curve. The solid line shows the best fit to the results using a numerically calculated diffusion dominated dehydration curve, which includes film shrinkage and a constant moisture diffusion coefficient. ..... 97**

**Figure 3.10 - Comparison of the theoretically predicted drying curves for evaporation controlled dehydration with the experimental data. The black line is for a model that includes the film shrinkage, while the blue line represents the results for a model without shrinkage. ..... 100**

**Figure 3.11 - Change in volume for different weights of sodium caseinate in the solution, used to calculate density, where the volume increase is plotted against the amount of casein added. ..... 101**

**Figure 3.12 – The experimental data, all scaled onto to a single curve, compared with numerical predictions from a model combining evaporation with fast but finite diffusion, as well as film shrinkage. ..... 102**

**Figure 3.13 - Adhesive samples dried with labels attached at 25 °C fitted to model for the case where diffusion is the limiting factor with shrinkage. ♦= saced01b, ■= saced02b, ▲= saced06b, ∗= syntacol300. ..... 104**

**Figure 3.14 - Adhesive samples dried with labels attached at 25 °C fitted to model for the case where evaporation is the limiting factor with shrinkage. ♦= saced01b, ■= saced02b, ▲= saced06b, ∗= syntacol300. ..... 105**

**Figure 3.15 - Adhesive samples dried with labels attached at 25° C fitted to model for the case where evaporation is the dominating process with fast but finite diffusion and with shrinkage. ♦= saced01b, ■= saced02b, ▲= saced06b, ∗= syntacol300..... 106**

**Figure 4.1 - Schematic representation of a longitudinal wave. ..... 112**

**Figure 4.2 - Acoustiscan experimental setup. ..... 116**

**Figure 4.3 - Speed of sound as a function of temperature for 18wt% sodium caseinate solution and pure water..... 121**

**Figure 4.4 – Speed of sound as a function of concentration for sodium caseinate solutions upto 18wt% at different temperatures. ..... 122**

**Figure 4.5 - Waterfall plot showing the change in speed of sound through the casein-water cell as a function of both height and time at 25 °C..... 124**

**Figure 4.6 - Speed of sound as a function of cell height at different time intervals for 18wt% caseinate solution at 25 °C. ..... 125**

**Figure 4.7 - Speed of sound as a function of caseinate concentration ..... 126**

**Figure 4.8 - Concentration profiles at t= 3h, 13h, 23h and 48h for 18wt% caseinate solution..... 127**

**Figure 4.9 - Fitting mathematical model of concentration profile to the experimental data at t= 3h..... 130**

**Figure 4.10 - Fitting mathematical model of concentration profile to the experimental data at t= 8h. ..... 131**

**Figure 4.11 - Fitting mathematical model of concentration profile to the experimental data at t= 13h. ..... 132**

**Figure 4.12 - Fitting mathematical model of concentration profile to the experimental data at t= 18h. ..... 132**

**Figure 4.13 - Fitting mathematical model of concentration profile to the experimental data at t= 48h. ..... 133**

**Figure 4.14 - Fitting mathematical model of concentration profile to the experimental data at t= 56h. ..... 134**

**Figure 5.1 - Schematic of a droplet on a substrate showing radius, *R*, contact radius, *a*, and height of droplet, *h*, used in calculating volume of a partial sphere. ..... 141**

**Figure 5.2 - Droplet volume normalised by contact area with respect to time for sodium caseinate 18 wt% films at constant relative humidity, 25%. ■= 15 °C, ▲ = 25 °C, and ♦ = 35 °C. ..... 144**

**Figure 5.3 - Rate of change of droplet volume normalised by contact area with respect to time for sodium caseinate 18 wt% films at constant relative humidity, 25%. ■= 15 °C, ▲ = 25 °C, and ♦ = 35 °C. ..... 145**

**Figure 5.4 - Normalised droplet volume as a function of contact area with respect to time for sodium caseinate 18 wt% films at constant relative humidity, 25% ± 5% and 30 °C, dehydrated at ■ = 30 °C, and ♦ = 20 °C. ..... 146**

**Figure 5.5 - Normalised droplet volume as a function of contact area with respect to time for sodium caseinate 18 wt% films at constant relative humidity, 25% ± 5%, and 30 °C.▲ = 0.1 wt% cross-linker, ■ = 0.2 wt% cross-linker, and ♦ = no cross-linker. ..... 148**

**Figure 5.6 - Normalised droplet volume as a function of contact area with respect to time for 7 wt% starch films at constant relative humidity, 25% ± 5%. ■= 15 °C, ▲= 25 °C, and ♦ = 35 °C. ..... 149**

**Figure 5.7 - The t0.5 as a function of rehydration temperatures for films made from 7 wt% starch..... 151**

**Figure 5.8 - Normalised droplet volume as a function of contact area with respect to time at 30 °C and constant relative humidity, 25% ± 5%. ♦ = 7 wt% starch with 1 wt% caseinate, ∗ = 7 wt% starch with 2 wt% caseinate,▲ = 7 wt% starch with 3.5 wt% caseinate, ■ = 7 wt% starch with 7 wt% caseinate, and × = 7 wt% starch with 14 wt% caseinate. ..... 152**

**Figure 5.9 - The $t_{0.5}$ measured at 30 °C and a constant relative humidity, 25% ± 5%, for rehydration of films of different composition. ..... 153**

**Figure 5.10 - A SEM image of a starch film dried at 25 °C and 30% relative humidity. ..... 155**

**Figure 5.11 - SEM image of caseinate film dried at 25 C and 30% relative humidity. ..... 156**

**Figure 5.12 - A CLSM image a of casein film dried at 25 °C and 30% relative humidity. ..... 157**

**Figure 5.13 - A CLSM image of a starch film dried at 25 °C and 30% relative humidity. ..... 158**

**Figure 5.14 - CLSM images of the surface of dried films with a) 1% casein and 7% starch, b) 3.5% casein and 7% starch, c) 7% casein and 7% starch, and d) 14% casein and 7% starch. The scale bar represents 300 μm length. ..... 160**

**Figure 5.15 - Finding the volume of a partial sphere in terms of *R* and *a*..... 161**

**Figure 5.16 - Droplet with a curvature of *R* and is in contact with the surface by a circular region of radius, *a*..... 163**

**Figure 5.17 - Schematic of a "pinned" droplet drying..... 164**

**Figure 5.18 - Illustration a circular patch on top of a substrate, modelled using COM-SOL..... 164**

**Figure 5.19 - Using *R* and *a* values from droplets placed on a metal substrate to calculate the evaporation constant. ■= 15 °C, ▲=25 °C, and ♦ =35 °C..... 169**

**Figure 5.20 - Evaporation constants plotted against temperature for a droplet evaporating from an impermeable substrate..... 170**

**Figure 5.21 - Using R and a values from droplets placed on casein films to calculate the evaporation constant. ■= 15 °C, ▲=25 °C, and ♦ =35 °C..... 171**

**Figure 5.22 - Using R and a values from droplets placed on a metal substrate to calculate the evaporation constant. ■= 7 wt% starch with 3.5 wt% casein and ♦ = 7 wt% starch with 7 wt% casein..... 172**

# List of Tables

**Table 1.1 - Comparison of constituents of acid casein and sodium caseinate (adapted from (Sutermeister, 1939). ..... 8**

**Table 1.2 - Amylose:amylopectin content in some common starches. ..... 10**

**Table 1.3 - Typical moisture diffusivities of food materials at 30°C (adapted from Saravacos and Maroulis, 2001). ..... 12**

**Table 1.4 - Coefficients of Dual Fickian model determined by curve fitting to absorption data (from Mubashar *et al,* 2009a)..... 29**

**Table 1.5 - Coefficients of Fickian model determined by curve fitting to desorption data (from Mubashar *et al,* 2009a)..... 29**

**Table 4.1- Ultrasound categories - taken from Practical Sonochemistry (Mason T. J. 2002). ..... 112**

# Chapter 1. Introduction

## 1.1 The importance of diffusion

Diffusion is a fundamental process that occurs in almost every application in everyday life, as well as many important chemical applications. Whilst the basic concept underlying the phenomenon is simple, diffusion is a very difficult phenomenon to measure accurately. Diffusion is defined as the spontaneous movement of a component from a region of high chemical potential in a system, to one which is a lower chemical potential. It is caused by random molecular motion along a concentration gradient and is driven by the need to reach the lowest free energy state (i.e. equilibrium state) (Cussler, 1997).

Diffusion occurs in gases, liquids, and solids and is the subject of many areas of research studies because of its importance in providing a better understanding of how mass transfer in complex systems occurs. Study of diffusion is a multi-disciplinary endeavour, as it takes place in a huge variety of situations, from biological transport processes in the body, to a pollutant spreading through a river, to moisture loss from a drying object. A particularly prominent research area recently concerns ordered porous solids, such as those used as catalysts, storage or separation (Krishna, 2009, Bouchard et al., 2013). Materials investigated include carbon nanotubes, which are important for storing gases such as hydrogen for future use as a fuel source (Alonso et al., 2012, Wang and Ronnebro, 2005), molecular sieves, used for separating small molecules from large ones (Al-

Asheh et al., 2004), particularly in the petrochemical industry, and zeolites, used as catalysts in petrochemical processing (Chen et al., 2012).

While all these examples are different in nature, the underlying process is essentially the same, and in the majority of cases can be described by Fick's laws of diffusion or its extensions.

### 1.1.1 The diffusion equations

The modern view of diffusion was developed by Thomas Graham, and later Adolf Fick (Cussler, 1997). Graham, (1805-1869) was the pioneer of diffusion, focussing his research on diffusion of gases in a diffusion tube. Hydrogen gas was placed in a tube sealed at one end with a plug, and at the other with a water reservoir. He observed that hydrogen diffused out of the tube and air diffused in, but the rates of diffusion were different, resulting in a change in the water level. From this work he postulated that the rate of effusion of a gas is inversely proportional to the square root of its molecular weight (Graham, 1833). This discovery resulted in Graham's law:

$$\frac{R_1}{R_2} = \sqrt{\frac{M_2}{M_1}}, \qquad \textbf{1.1}$$

where, $R_1$ and $R_2$ are the rates of effusion of gas 1 and gas 2 respectively, and $M_1$ and $M_2$ are the molar mass of the respective gas. Later in his career Graham also conducted a significant amount of work on diffusion in liquids, where he discovered that diffusion rates in liquids are several orders of magnitude slower than those for gases.

Another major advance in diffusion came later, in the findings of Adolf Fick. Fick was a mathematician who spent the majority of his research career

focussing on physiology as opposed to diffusion. It was he who first described diffusion using the same mathematical basis as Fourier's law of heat transfer (Fick, 1995). His work led to the two laws of diffusion commonly used today.

Fick's First Law relates the diffusive flux to the concentration gradient. It implies that a steep change in concentration will result in faster diffusion. In a uniaxial dimension:

$$\boldsymbol{J = -D\frac{\partial C}{\partial x}}, \qquad \textbf{1.2}$$

where $J$ is the diffusive flux (mol.m$^{-2}$.s$^{-1}$), $C$ is the concentration (mol.m$^{-3}$), $D$ is the diffusion coefficient (m$^{2}$.s$^{-1}$), and $x$ is the distance (m) along the system in which the diffusion is taking place.

Fick's Second Law, also known as the diffusion equation, relates the rate of change of concentration at a certain point to the spatial variation of the concentration at the point i.e. the rate of change of concentration is proportional to the variation of the concentration flux with respect to distance. If the concentration gradient changes greatly from point to point, then the concentration changes rapidly with time. The diffusion equation is:

$$\boldsymbol{\frac{\partial C}{\partial t} = \frac{\partial}{\partial x}\left(D\frac{\partial C}{\partial x}\right)}, \qquad \textbf{1.3}$$

where $t$ = time (s). Fick's second law is a consequence of Fick's first law combined with the concentration of mass.

## 1.2 Objectives

In this work the diffusion of moisture into and out of water-based biopolymer films is investigated. Biopolymer films have great importance in the food industry, drug industry, adhesives industry, paints industry and for many more coatings applications. It is therefore important to understand the drying and rehydration of these films, particularly in relation to how they act as a barrier towards water in their dry state.

The problem that formed the basis of this project, while it can be applied to all of the applications mentioned above, stemmed from issues faced by the adhesive labelling industry, specifically concerning the labelling of beer and wine bottles.

The issues can be split into two parts. The first part relates to the beer bottling process. In Europe, beer is typically bottled at low temperatures, between 4°C and 10°C, prior to the label being applied. Due to the cold surface of the bottle, water vapour from the surrounding air condenses on the bottle. This leads to the wet adhesive being washed away when the label is applied, before it has had time to set and adhere to the bottle, resulting in the label becoming distorted, creased, or falling off completely.

The second part of the problem involves the dried adhesive long after the labelled bottle has left the shelves. In restaurants and bars, when wine is served the bottle is often placed in a wine cooler of ice water. The water from the cooling bucket penetrates the adhesive over time, resulting in a change in the properties of the adhesive, which becomes more fluid like as opposed to its solid, dry form, and thus less sticky. This leads to a failure in

the adhesion properties of the adhesive, causing the label to no longer stick to the bottle.

To address the first problem, the diffusion of water from drying water-based biopolymer thin films of different compositions, similar to those used in industry, are examined over a range of conditions, and mathematical simulations based on Fick's laws of diffusion are conducted and fitted to the experimental data. Besides needing to know how the film dries, because of the condensation present on the bottle when labelling occurs, it is also important to understand how water ingresses into the wet biopolymer. A novel technique is presented and validated using ultrasound to monitor the influx of water into a water-based casein biopolymer. A numerical solution using Fick's second law of diffusion is implemented and fitted to the experimental data in order to extract a diffusion coefficient to describe the water influx.

With regard to the second problem, another novel method has been designed. A camera is used to monitor the disappearance of a water droplet placed on the surface of dried biopolymer films of different composition under different temperature conditions. Once again a numerical solution expressing the changing droplet volume in terms of evaporation and diffusion flux has been derived and used to map the droplet size as a function of time.

## 1.3 Biopolymers

Most of the water-based adhesives used until recently in industry contained casein or starch as the biopolymer element. However, nowadays a move

away from casein to synthetic polymers has been made as casein is an animal based product. This was not the case at the start of this project, so casein is still investigated.

### 1.3.1 Casein

Casein is a phosphoprotein found in milk and cheese, accounting for upto 80% of the total protein in these foods. It exists in four forms, αs1-, αs2-, β-, and κ-casein, which have different amounts of calcium bound to them, except κ-casein, which has no calcium associated with it. Casein exists almost completely as dispersed structures called micelles (Fiat and Jolles, 1989). It is the κ-casein which is responsible for the colloidal stability of these micelles. A casein micelle is accepted to be colloidal aggregates of casein macromolecules surrounded by κ-casein (Lucey, 2002). Casein has relatively little tertiary structure, as it has no disulphide bridges. It also contains mainly inert proline amino acids, which tend to disrupt the secondary structure. The macromolecular structure of casein has been the subject of much debate over the years (Horne, 2002, Qi et al., 2001, Swaisgood, 1982), however, Figure 1.1 displays a commonly accepted depiction of a casein submicelle. The blue-grey part is κ- casein, the white part $\alpha_{s1}$-casein, the red part represents β-casein, and the pink parts are a mixture of $\alpha_{s1}$-casein and β-casein.

Swaisgood (Swaisgood, 1982) was one of the pioneers of the school of thought that caseins were neither globular nor random coil proteins and that they potentially composed of distinct functional domains. The next major advance came from Holt and Sawyer (1993) who suggested the structure was more fluid and dynamic, and that casein does not form a rigid structure

until aggregates begin to form. The most recent view of the structure of casein believes it to be a stable, open structure of rigid rods joined by flexible elements (Qi et al., 2001).

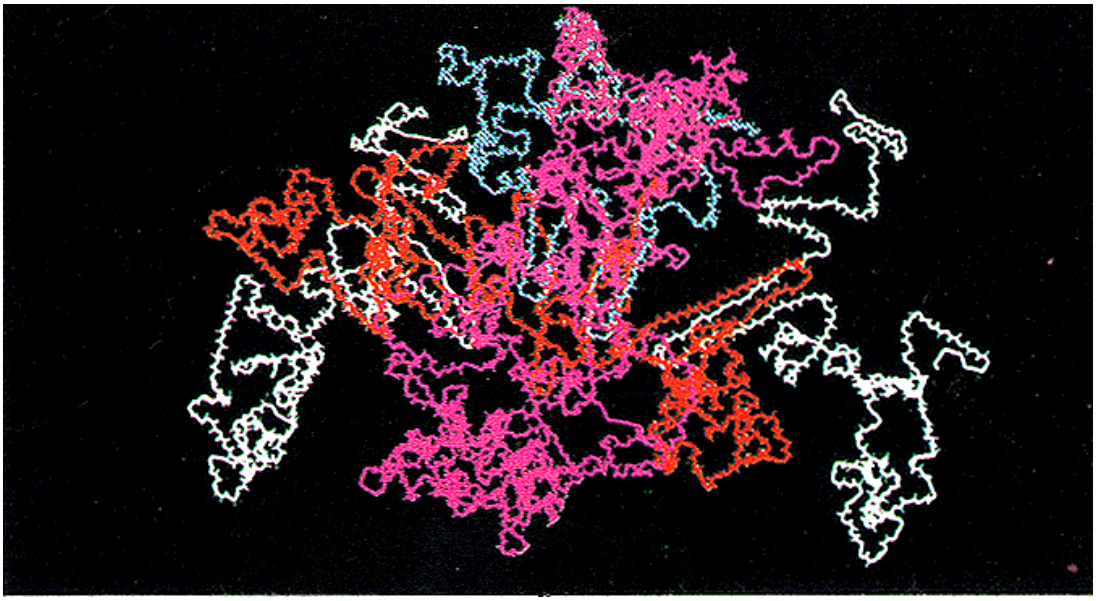

**Figure 1.1 - Computational prediction of the structure of casein – from (United States Department of Agriculture, Agricultural Research Service. Dairy and Functional Foods: Molecules. 2010)**

### 1.3.1.1 Casein extraction

Casein is precipitated at pH 4.6, the isoelectric point, where all the charges in the molecule balance. Whole milk is separated by centrifugation to give skimmed milk, and this is the raw material used to make casein products.

Acid casein is the product used to prepare the adhesives discussed in the objectives, but sodium caseinate is the starting material used to prepare the caseinate model systems in this work as it is water soluble without modifying the external conditions.

Acid casein is prepared by acidification of the skimmed milk by adding HCl or $H_2SO_4$, lowering the pH from 6.6 to around 4.6 and forming an insoluble, acidic precipitate. When the casein has been precipitated, the mixture is 'cooked', causing the particles to shrink, expelling whey, and clump together to form curds. This is separated from the whey by washing several times, then the water is removed by centrifugation. The remaining curd is dried with hot air, before being cooled and conditioned to ensure an even moisture distribution between large and small particles, milled, sifted and then blended to ensure uniformity.

Sodium hydroxide 2.5 M, 2 %w/w, is mixed with a slurry of casein curd or powder in water to give sodium caseinate.

Table 1.1 shows the comparisons between sodium caseinate and acid casein;

**Table 1.1 - Comparison of constituents of acid casein and sodium caseinate (adapted from (Sutermeister, 1939).**

| | Moisture % | Protein % | Lactose % | Fat % | Na % | Ca % | pH | Solubility in $H_20$ % |
|---|---|---|---|---|---|---|---|---|
| Na-caseinate | 3.8 | 91.4 | 0.1 | 1.1 | 1.3 | 0.1 | 6.5-6.9 | 100 |
| Acid casein | 11.4 | 85.4 | 0.1 | 1.3 | <0.1 | 0.1 | 4.6-5.4 | 0 |

As casein is formed of many polymer chains, it is possible to strengthen the structure using a cross-linker. A cross-linker is a compound which causes

the polymer chains in a material to bind together, either covalently or ionically, in order to strengthen and provide rigidity to the structure.

Cross-linkers can be chemical compounds such as the one used in this work, aluminium sulphate, or physical cross-linkers which use heat, pH or other changes in conditions to induce cross-linking (Ghosh et al., 2009).

### 1.3.2 Starch

Starch is a polysaccharide found in maize, tapioca, potato, wheat and rice. It consists of glucose monomers joined together to form a polymer by either 1,4-glycosidic bonds or 1,6-glycosidic bonds. It consists of two types of molecules, which depend on the type of glycosidic bond formed. Typically, starch contains approximately 20-25% amylose, and 75-80% amylopectin, depending on the plant source. Amylose is the straight chained starch molecule where the glucose monomers are joined in the 1,4- confirmation. Amylopectin however forms a branched structure, as the glucose molecules are joined together in the 1,6- formation.

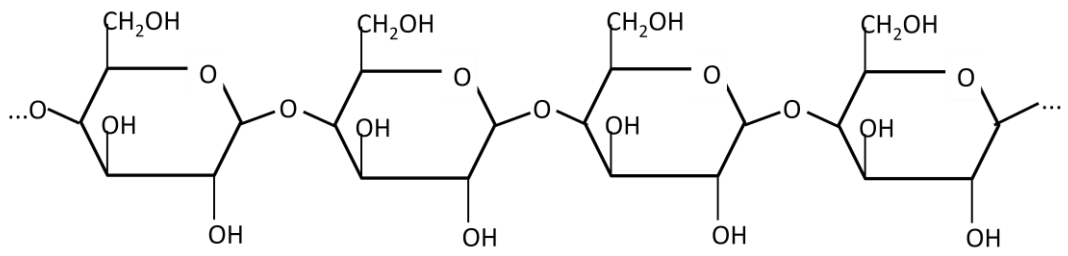


**Figure 1.2 - Orientation of glucose monomers in amylose, with 1,4-glycosidic bonds.**

Figure 1.2 and Figure 1.3 depict the straight-chain and branched structures of amylose and amylopectin respectively. Depending on the source of starch, there will be different relative amounts of amylose and amylopectin.

Table 1.2 shows some typical values.

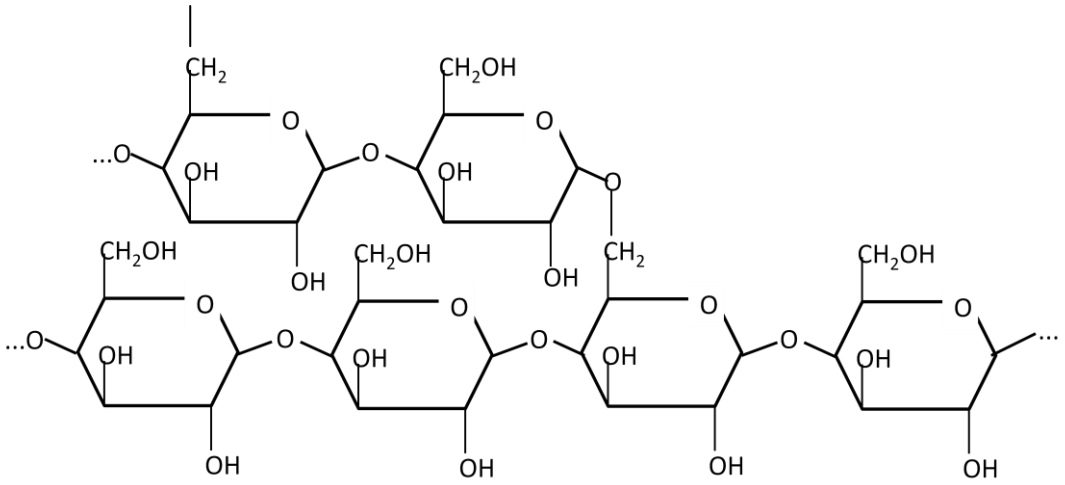


**Figure 1.3 - Orientation of glucose monomers in amylose, with 1,4- and 1,6-glycosidic bonds.**

**Table 1.2 - Amylose:amylopectin content in some common starches.**

| Starch source | Amylose content/% | Amylopectin content/% |
|---|---|---|
| Potato | 20 | 80 |
| Corn | 25 | 75 |
| Rice | 2 | 98 |
| Tapioca | 15-18 | 72-75 |
| Waxy Maize | 0 | 100 |
| Wheat | 25 | 75 |

When starch is cooked, gelatinisation occurs, where the less branched amylose molecules leach out of the granules, forming a network which traps water and by forming physical cross-links causes an increase in viscosity, and a loss of the original semi-crystalline structure. As the cooking continues, a thick paste forms, but as the paste cools, retrogradation occurs the crystalline structure partially recovers, and some of the trapped water is able to escape. Some starches are called "waxy". Waxy starches are modified starches which contain 100% amylopectin. This means that when they are cooked, they form a much more stable paste, and retrogradation does not occur. The branched structure of amylopectin makes it harder for it to form ordered crystalline structures.

In this work a diphosphorylated waxy maize starch and sodium caseinate are used, and in some cases mixes of the two are considered in an attempt to optimise performance by taking the strengths of each of the biopolymers and combining them.

## 1.4 The diffusion coefficient and types of diffusion

The diffusion coefficient *D*, usually defined as the effective moisture diffusivity, is an overall transport property which incorporates a number of transport mechanisms, including diffusion, molecular effusion, capillary diffusion, and Knudsen diffusion. Table 1.3 shows a list of typical *D* values for some common food materials adapted from (Saravacos and Maroulis, 2001).

**Table 1.3 - Typical moisture diffusivities of food materials at 30°C (adapted from Saravacos and Maroulis, 2001).**

| Food Material | Moisture (kg/kg dm) | Diffusivity ($x10^{-10}$ $m^2/s$) |
|---|---|---|
| Corn kernel | 0.20 | 0.40 |
| Rice | 0.20 | 0.40 |
| Dough | 0.40 | 5.00 |
| Cookie | 0.15 | 0.50 |
| Pasta | 0.15 | 0.30 |
| Potato | 0.30 | 5.00 |
| Peas | 0.10 | 3.00 |
| Carrot | 0.30 | 2.00 |
| Apple | 0.50 | 2.00 |
| Raisins | 0.40 | 1.50 |
| Pork Sausage | 0.20 | 0.50 |
| Cod | 0.50 | 2.00 |

*D* can be calculated using experimental techniques in combination with mathematical modelling. Determination of mass diffusivity in solid and semi-solid materials is crucial for the control and quantitative analysis of several mass transfer operations, including drying and adsorption. (Saravacos and Maroulis, 2001).

In a polymer system, the diffusion of small molecules such as solvents, salts and sugars is important to many physical and chemical processes. One

indication of the transport mechanism of water in such systems is the sorption kinetics test. Gravimetric sorption data, usually of a thin film of polymer, are compared to the generalised sorption equation (Peppas and Brannonpeppas, 1994).

$$\frac{M}{M_e} = kt^n, \qquad \textbf{1.4}$$

where $M$ and $M_e$ are the moisture contents after sorption time $t$ and at equilibrium, $k$ is a constant, and $n$ is the diffusion index. The diffusion index shows the type of diffusion in the system (Saravacos and Maroulis, 2001). When:

| | |
|---|---|
| n = 0.5 | Fickian diffusion occurs |
| 0.5 < n < 1 | Non-Fickian/ Knudsen diffusion occurs |
| n = 1 | Type II diffusion occurs |

Fickian diffusion occurs when the mean free path of the diffusant is much smaller than the pore size and most collisions are between molecules as opposed to with the walls. It is applicable to Brownian motion, where each movement is independent of the previous one. Non-Fickian, or Knudsen diffusion is the term used to describe the type of diffusion that occurs when the above conditions are not met, and type II diffusion occurs when a non-solvent molecule diffuses with a steep concentration profile at a constant rate leading to an increase in weight proportional to time (Peterlin, 1977).

If diffusion is Fickian, sorption data at a constant temperature can be used to determine $D$, as the drying constant $h$ is related to the moisture diffusivity $D$ and sample thickness $L$:

$$h = 4\left(\frac{D}{\pi L^2}\right)^{0.5}, \qquad \textbf{1.5}$$

The effective moisture diffusivity *D* depends strongly on the structure of the polymer itself. Values of *D* in the order of $10^{-14}$ are expected for glassy state materials, whilst in the rubbery state *D* increases to the order of around $10^{-11}$ (Saravacos and Maroulis, 2001). Sorption data can also be obtained using inverse phase gas chromatography.

The transport of water in solids is assumed to be controlled by molecular diffusion, so for analysis and calculation, Fick's diffusion equation is applied. There are several important methods of measurement and estimation of the effective moisture diffusivity, and these include sorption kinetics, discussed above, permeability and drying kinetics, each of which is applicable in a certain circumstance, for example sorption kinetics is applicable to moisture adsorption in systems, while drying kinetics is applied to drying applications.

Drying was the first method used to determine the effective moisture diffusivity in solid systems (Sherwood, 1931). It is a complicated process of both heat and mass transfer (Zogzas and Maroulis, 1996), and it is influenced by both the external conditions and the internal structure of the material. The transport of water is fundamentally important to the drying of solids, and is the main rate-determining mechanism in drying operations. There are three stages to the drying process; first, water is removed by a hydrodynamic gradient and capillary forces, secondly by vapour diffusion, and finally by desorption (Saravacos and Maroulis, 2001). These stages are usually split into the constant rate and the falling rate periods (Zogzas and Maroulis, 1996, Perry and Green, 1997). During the constant rate period, free water exists at the surface and the rate is controlled by external conditions including temperature, humidity, and air velocity. A moisture

gradient begins to build up inside the material, determining the start of the falling rate period (Seth and Sarkar, 2004). During the falling rate period moisture diffuses from the interior to the exterior of the material, along the moisture gradient. During this period the main resistance to mass transfer is movement within the bulk (Saravacos and Maroulis, 2001). To calculate the moisture diffusivity *D* in the falling rate period, the diffusion equation is applied to a suitable shaped sample, either slab, cylinder, or sphere. For a thin film polymeric sample, it would be most appropriate to use the equation for a slab (Crank, 1975):

$$\boldsymbol{Y = \frac{X - X_e}{X_0 - X_e} = \frac{8}{\pi^2} \sum_{n=1}^{\infty} \frac{1}{(2n+1)^2} e^{\left(-\frac{(2n+1)^2 \pi^2 Dt}{L^2}\right)},} \qquad \textbf{1.6}$$

where *X* is the mean moisture after time *t*, $X_0$ is the initial moisture content, $X_e$ is the moisture content at equilibrium, and *L* is the sample thickness. *Y* is often used to represent the moisture ratio. However this equation assumes constant diffusivity throughout the drying process, whereas in reality the moisture diffusivity changes significantly with moisture content (Nizovtsev et al., 2008, Pel et al., 1996, Saravacos and Maroulis, 2001, Wang and Fang, 1988). Also, the equation assumes a constant film thickness, whereas in many cases the film shrinks as the drying progress progresses.

The equation for a sample with spherical geometry (Crank, 1975) is:

$$\boldsymbol{Y = \frac{X - X_e}{X_0 - X_e} = \frac{6}{\pi^2} \sum_{n=1}^{\infty} \frac{1}{n^2} e^{\left(\frac{-n^2 Dt}{r^2}\right)},} \qquad \textbf{1.7}$$

where *r* is the radius of the sphere.

The equation used when the geometry is cylindrical (Crank, 1975) is:

$$\boldsymbol{Y = \frac{X - X_e}{X_0 - X_e} = \frac{4}{r_a{}^2} \sum_{n=1}^{\infty} \frac{1}{\beta_n{}^2} e^{\left(\beta_n{}^2 Dt\right)},} \qquad \textbf{1.8}$$

where $r_a$ is the radius of the cylinder and $\beta_n$ is the root of the Bessel function of first kind and zero order. Bessel functions are the standard solutions, y(x), of Bessel's differential equation:

$$\boldsymbol{x^2 \frac{d^2 y}{dx^2} + x \frac{dy}{dx} + (x^2 - \propto^2) y = 0,} \qquad \textbf{1.9}$$

The ingress of water into a polymer matrix can result in mechanical stresses in the polymer system. The importance of this phenomenon can be estimated using a dimensionless number known as the Deborah number, *De*, which expresses the relative importance of relaxation in a polymer system to diffusion. It is an index of the fluid or solid behaviour of a material. When water enters a polymer system mechanical stresses occur, which can result in major changes to the polymer structure such as chain rearrangements and characteristic swelling and relaxation phenomena. These phenomena can significantly affect the transport mechanisms and properties of water in the system. The Deborah number relates diffusion properties to the viscosity properties of a material. It can be calculated from the following equation:

$$\boldsymbol{De = \frac{D\varphi}{L^2},} \qquad \textbf{1.10}$$

where $\varphi$ is the relaxation time and $L^2/D$ is the diffusion time, where $L$ is the sample thickness. When

$De >> 1$, slow relaxation

$De << 1$, very fast relaxation

*De = 1*, diffusion is controlled by molecular relaxation.

Small Deborah numbers are characteristic of liquid-like behaviour, whereas large Deborah numbers characterise a more solid-like behaviour.

## 1.5 Measuring diffusion

Measuring diffusion of water both into and out of materials is important across a wide range of disciplines. Some of these include, food (Mayachiew et al., 2010), pharmaceuticals (Marucci et al., 2011), dental composites (Rahim et al., 2012b) , paints (Zhang and Niu, 2003), adhesives (Roy et al., 2006), building materials (Drchalova and Cerny, 2003) and many physiological processes (Datta and Rakesh, 2009). In food systems for example, it is important to understand the mechanisms behind the ingress of small molecules such as oxygen and water in order to provide a barrier to protect the food product and prevent premature decay to improve shelf life and reduce waste. It is also advantageous to be able to control the rate of dehydration of foods in order to optimise processing and again to improve shelf life.

The simplest method used to determine moisture diffusivity uses the gravimetric approach, recording change in mass vs. drying/sorption time (Drchalova and Cerny, 2003, Li and Kobayashi, 2005, Seth and Sarkar, 2004, Wang and Fang, 1988, Zogzas and Maroulis, 1996). Other methods include the use of microscopically powerful techniques using magnetic resonance, infrared, UV or gamma rays to investigate the moisture gradient build-up, and then moisture diffusivity. These technologically advanced techniques have seen an increase in popularity over the last few years,

particularly for investigations on building materials. The desire for deeper knowledge of moisture diffusivity does not however limit itself to the building materials research. It also has applications in the food industry in particular, and polymer research.

### 1.5.1 Food applications

One of the main areas interested in determining the moisture diffusivity of products is the food industry. There are many reasons for investigating the moisture diffusivity including improvement of shelf-life of products, storage, physico-chemical stabilisation and product stability (Babalis and Belessiotis, 2004, Baez-Gonzalez et al., 2004, Ruiz-Cabrera et al., 2005, Seth and Sarkar, 2004). The most popular method used for investigating moisture diffusivity in foods uses drying data. This is a straightforward procedure to carry out experimentally, where the sample is dried under controlled temperature and relative humidity, under controlled air flow conditions. The sample is weighed over set time intervals, either by removing the sample from the apparatus for a short period of time, or by using electronic sensors built in to the apparatus to record the weight without having to change the surroundings. The complication in the method arises from the interpretation of the data as will be discussed later.

Seth and Sarkar (2004) used a simple, gravimetric method to measure the effective moisture diffusivity of green mango. They used an experimental set up where the sample was suspended horizontally from a balance, in a vertical glass column, which had heated air forced through it (Figure 1.4).

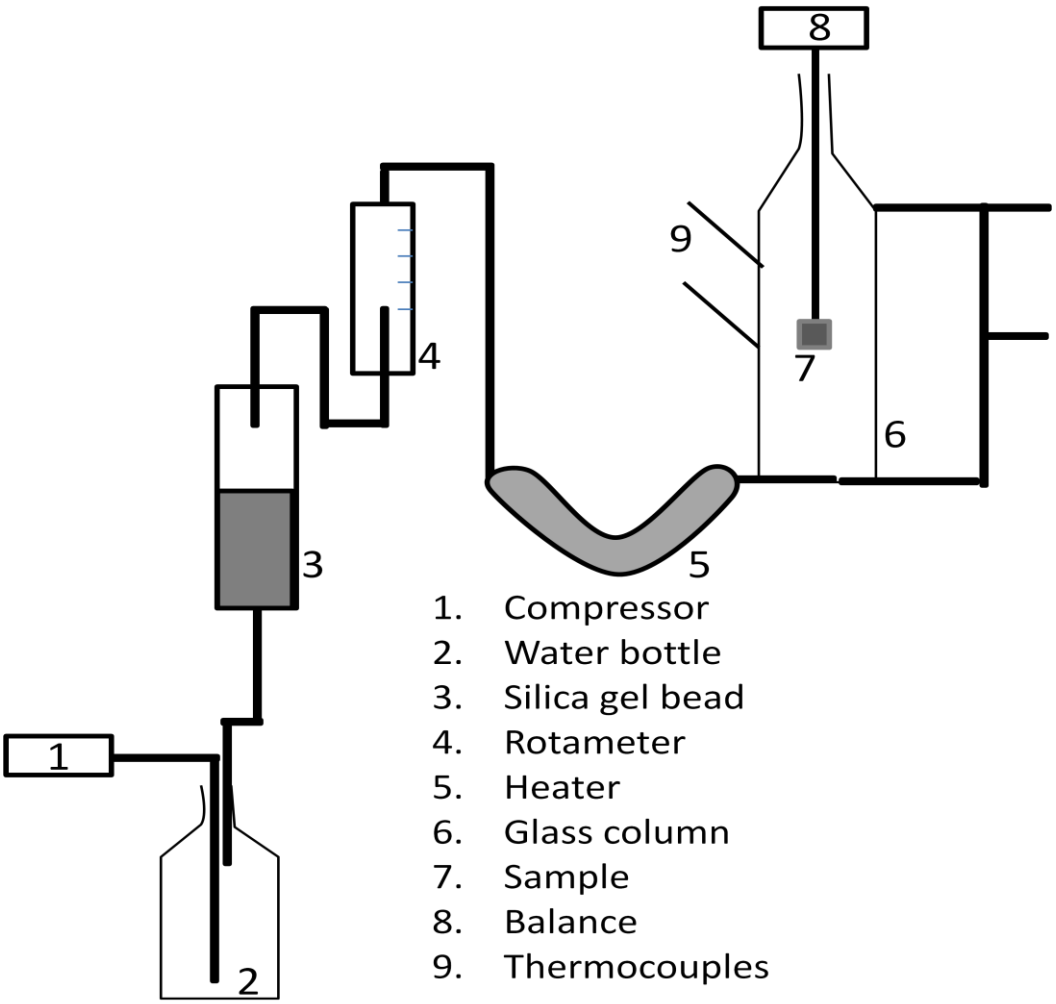


**Figure 1.4 - Schematic diagram of the apparatus used for measuring moisture diffusivity of green mango (from Seth & Sarkar, 2004)**

They monitored the inlet and outlet temperature, as well as the sample temperature continuously throughout the experiment. The sample was weighed *in situ* every 5 minutes up to 20 minutes, then every 10 minutes after that. Weight loss was plotted against time to give a drying curve with two distinct regimes corresponding to alternative types of moisture removal for example free and bound moisture. Results were plotted as $W^*$, the weight ratio against time Figure 1.5.

The mathematical model used to analyse the results was based on Fick's law of diffusivity for a cylindrical sample based on variable diffusivity, as they

found that many of the experimental results did not fit with the constant diffusivity equation. Log of *W**, from the diffusivity equation was plotted against time to give the moisture diffusivity from the gradient.

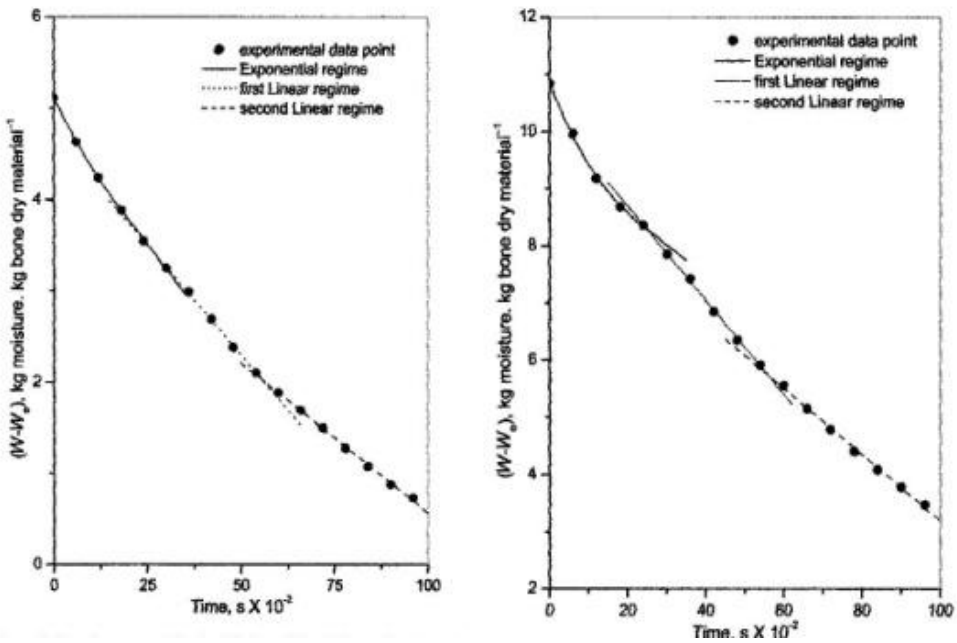


**Figure 1.5 - Graphs of *W*, weight loss* vs. time at 50 °C and 70°C respectively under controlled air flow and humidity conditions. • = experimental data, - = exponential regime, ... = first linear regime, and --- = second linear regime. (from Seth & Sarkar, 2004).**

However they found the straight line to deviate towards the end, thus moisture diffusivity was only calculated for values of *W** less than 0.6. To model the data three curves were generated with different diffusion conditions using different boundary conditions based on Fourier number ($D_{\infty}t/L^2$), which incorporates shrinkage into the model. They concluded that Fick's law of constant diffusivity cannot accurately predict the drying kinetics observed experimentally, with an error of ± 27%, and the most accurate prediction, with an error of ± 7%, used Fick's law with variable diffusivity, with the diffusion coefficient varying exponentially, followed by two linear lines (Figure 1.6).

The method described here has the advantage of being a simple procedure which is easy to carry out, although the determination of moisture diffusivity is only accurate for certain values of *W**. Another disadvantage is that the mathematical modelling is quite complicated, with three different curves having to be fitted to the different regions of the plot, but still it does not yield very satisfactory results. Large deviations between predictions of mathematical models and actual results are evident in many such experiments.

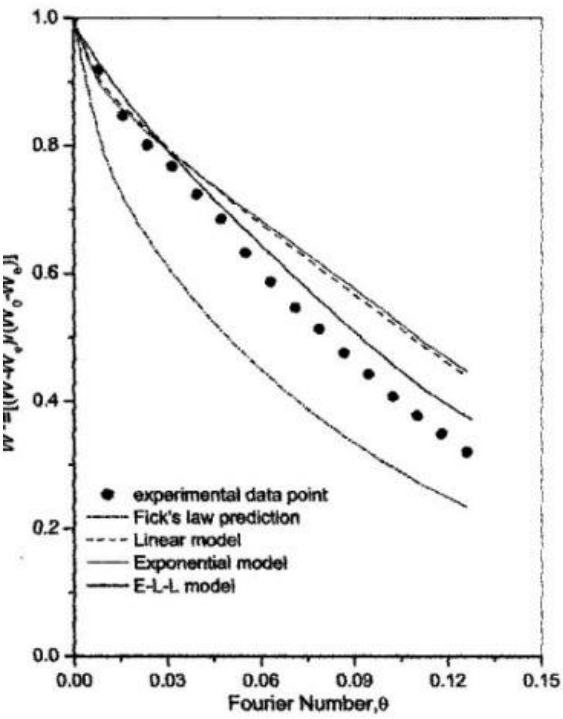


**Figure 1.6 - Graph showing *W** vs. Fourier number ($D_\infty t/L^2$) with model predictions. • = experimental data, - = exponential regime, ... = first linear regime, and --- = second linear regime. (from Seth & Sarkar, 2004)**

### 1.5.2 Building applications

Much research has been conducted on porous building materials to investigate the moisture diffusivity, particularly using sorption data

(Drchalova and Cerny, 2003, Nizovtsev et al., 2008, Pel et al., 1996, Wang and Fang, 1988). It is highly important for engineers to know how different materials will react to water uptake during industrial processes and also over long periods of time, to assess their durability and suitability to be used in the building industry.

Drchalova and Cerny (2003) used a gravimetric method to determine moisture diffusivity, however the data they used was from sorption kinetics. Their aim was to determine the effective moisture diffusivity with regard to moisture content throughout a building material sample. They did so by placing the sample on a viscous sponge, and allowing it to suck the moisture from the free water surface (Figure 1.7).

The sample was water and vapour-proofed on all edges except the one in contact with the sponge, and the one in contact with the air to prevent any undesired water transport. The sample was removed from the sponge in order to record the change in mass every 10s. A curve of mass vs. $t^{1/2}$ was plotted and several points were chosen to determine mass diffusivity, $k$, using a mathematical equation derived from partial moisture densities:

$$\boldsymbol{m_m(\tau) - S(\rho_1 + \rho_2)\frac{d}{2} + \frac{2dS}{\pi^2}(\rho_1 - \rho_2)\sum_{n=1}^{\infty}\frac{1}{n^2}.[1 - \cos(n\pi)].exp - \left[\frac{kn^2\pi^2\tau}{d^2}\right] = 0}\ , \qquad \textbf{1.11}$$

where $\rho_1$ and $\rho_2$ are the maximum and initial partial moisture densities respectively, $d$ is the thickness of the sample in the direction of water flux, $\tau$ is the time interval, and $S$ is the surface area.

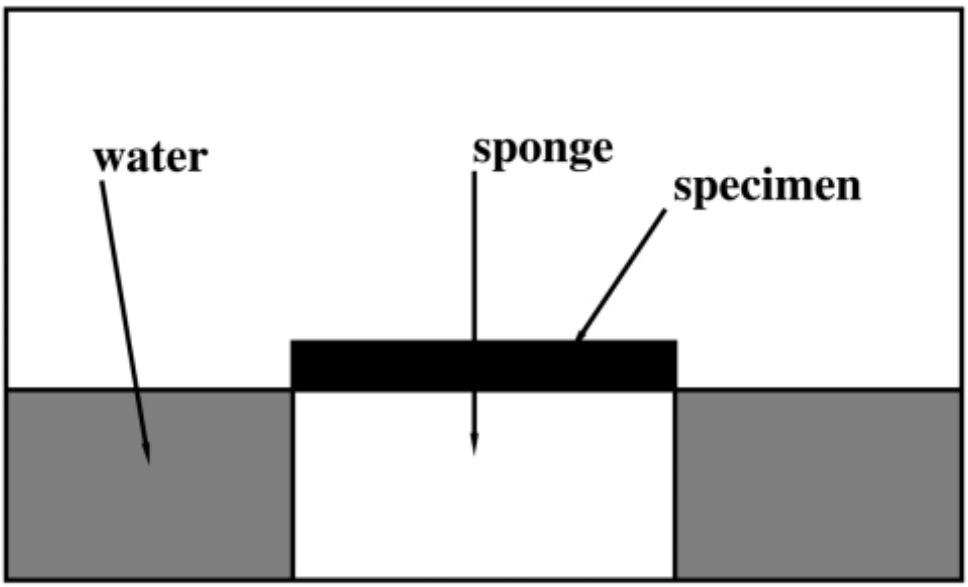


**Figure 1.7 - Schematic diagram of sorption apparatus (from Drchalova & Cerny, 2003).**

The average moisture diffusivity calculated from the chosen points was assigned to the average moisture content, calculated using a simple equation, $\rho_{mc} = \frac{m_{m(\tau)}}{2Sd} + \frac{\rho_1+\rho_2}{2}$, where $\rho_{m(\tau)}$ is the partial moisture density at time, $\tau$. The experiment was repeated using samples with different initial moisture contents. The resulting graph allowed the authors to tell if the sample was anisotropic or not. The results were compared to those obtained from the classic Matano method but they were not in good agreement for the majority of moisture contents (Figure 1.8). The Matano method is based on a graphical integration of Fick's second law. They concluded that their method was only accurate at high moisture contents, around 60-80%.

Due to the poor agreement of results with a classic method, this method will not be used to calculate the moisture diffusivity of the thin polymer films used in this work. However it could be useful in determining the structural properties of the film.

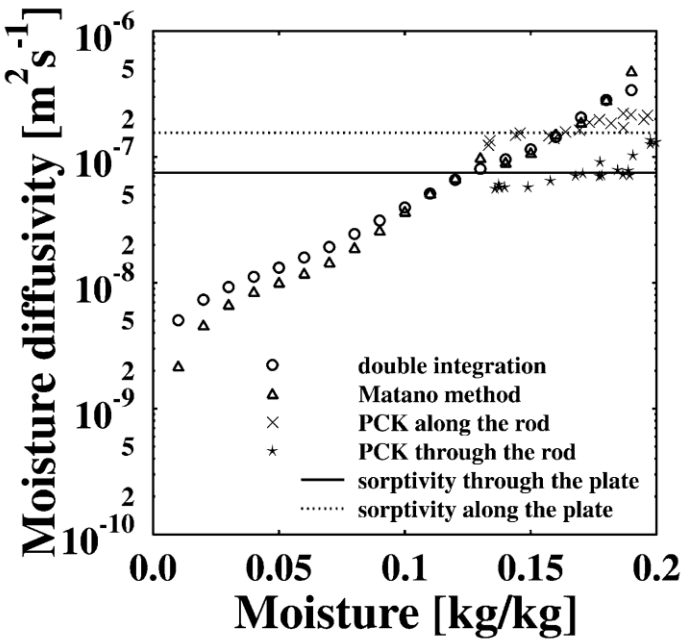


**Figure 1.8 - Comparison of moisture diffusivity functions using various methods (from Drchalova & Cerny, 2003).**

In recent years there has been an increase in the use of more microscopically powerful techniques such as nuclear magnetic resonance (NMR) methods, and gamma ray methods. Drying methods which use drying curves to determine diffusion coefficients have to be based on the assumption that *D* is related to the moisture content, however by measuring the moisture concentration profile, the diffusion coefficient can be calculated directly. Moisture concentration profiles were measured as opposed to drying curves, allowing the moisture diffusivity to be determined directly.

Pel, Brocken and Kapinga (1996) used NMR to determine moisture concentration profiles in porous samples. NMR methods can be made sensitive to only hydrogen, and therefore water. Also, free and bound water can be distinguished from each other. If a known magnetic field is applied, the resonance condition is dependent on the spatial position of the nuclei spatially, so the moisture distribution can be measured without having to

move the sample. The small, cylindrical sample was placed in a Teflon holder with an open top. The air flow was kept constant at 20°C and 45% relative humidity. A coil was placed around the sample to create and received the radio frequency fields required for the experiment. To measure an entire moisture profile over the 25 mm length of sample, with a 1% inaccuracy, took around 40 min. Each measurement was time stamped, and the moisture concentration profile was obtained by “interpolating subsequent experimental profiles with time using least squares fit with cubic spline”, a typical statistical function. Three different materials were tested, each for a period of 40 h or more. To calculate the moisture diffusivity, Fick’s law of diffusion was applied, and integrated with respect to the length, *x*. They found, from plotting the moisture diffusivity against moisture content, that three regimes could be distinguished. At high moisture concentrations, where the moisture transport was dominated by liquid transport, the profiles were nearly horizontal, corresponding to a high moisture diffusivity. As the moisture content decreased, moisture diffusivity decreased, as the large pores were drained and so no longer contributed to liquid transport. Below the critical moisture content, water no longer formed a continuous phase and therefore has to be transported by vapour, controlled by vapour pressures, and for very low moisture contents the moisture diffusivity began to increase again. The minimum moisture diffusivity is therefore representative of the change from liquid to vapour transport. Computer simulations were carried out to check the accuracy of the moisture diffusivity calculations and to identify the significance of the errors due to noise, resolution and grid scanning. They found that the moisture diffusivity was reproduced accurately over the range of the moisture profile, with the only deviation being the

minimum moisture diffusivity, which was overestimated slightly. They concluded that NMR is both an accurate and reliable method for determining the moisture concentration profiles in porous media, allowing moisture diffusivity to be determined directly, with only experimental noise and inhomogeneity of the material being sources of error.

Due to the accuracy of the moisture diffusivity determination, the method utilising NMR could be useful in this work, however it is a particularly time consuming and expensive procedure, and the specialist equipment required is not easily available. All the samples used by Pel *et al*, (1996) were porous, so it is unclear whether the method would be suitable for the polymeric samples being investigated here.

Nizovtsev *et al.* (2008) conducted an experimental gamma ray study of moisture transfer processes in porous materials. Gamma radiation is a type of electromagnetic radiation which has a high frequency, of above $10^{19}$ Hz. Gamma rays have very high energies of around 100 KeV, and a very small wavelength, around $10^{-12}$ m. The method used was contactless and could be used to determine the thermophysical properties of the sample material. The procedure involves raying a sample with a narrow beam of gamma rays. The gamma rays in a wet sample will be attenuated by the skeleton of the material and then by the moisture contained in its pores, so to accurately predict the gamma ray intensity of a moist material, the intensity transmitted for the dry material needs to be known. The gamma ray method allows moisture concentrations to be measured with high precision over a range of moisture contents. The sample was placed in a container with separate sealed upper and lower chambers, with a reservoir of sorbent in the upper chamber and water in the lower one. Gamma quanta were fired at a certain

position at the sample and transmitted radiation was measured using a scintillation counter. The sample was moved in relation to the gamma beam in order to measure the transmitted rays at different cross sections (Figure 1.9). Relative humidity and temperature were constant and monitored throughout the experiment.

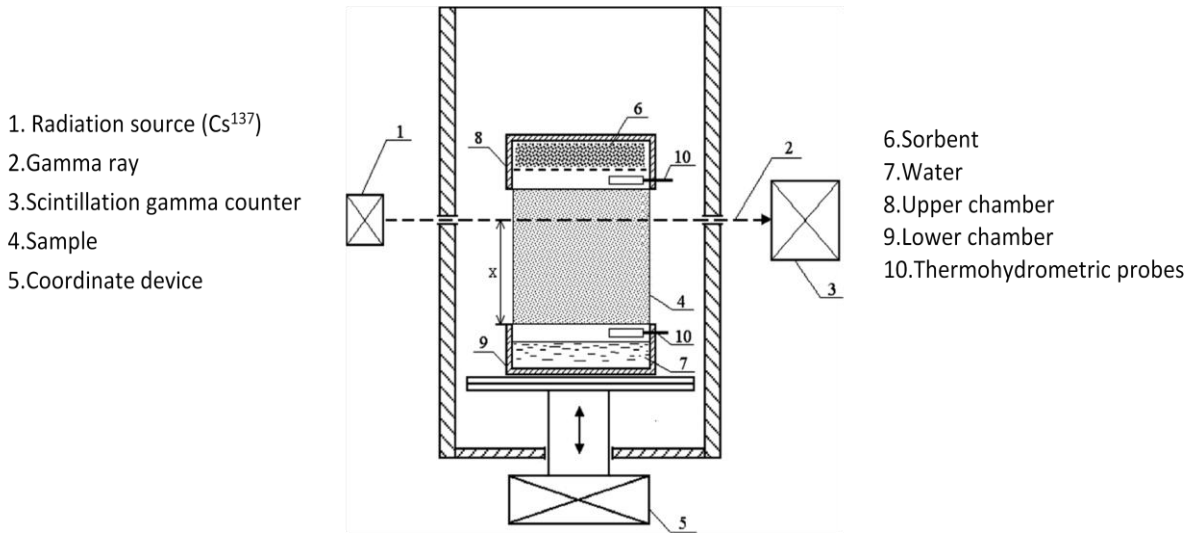


**Figure 1.9 - Diagram to show experimental apparatus setup (from Nizovtsev *et al,* 2008).**

From the gamma ray attenuation factor, moisture content was determined for a given cross section, and repeated measurements at different cross sections allowed moisture profiles to be constructed as a function of time. The moisture diffusivity could be determined from the moisture profiles using the Matano technique based on a solution of the time dependent diffusion equation. Initial and boundary conditions need to be considered in order to determine the moisture diffusivity, and automodel variables also need to be used to construct the moisture profiles. The moisture diffusion coefficient was determined using the equation:

$$\boldsymbol{D_w(W) = -\frac{1}{2}\frac{1}{\frac{\partial W}{\partial S}}\int_{W_0}^{W} S\partial W,} \qquad \textbf{1.12}$$

where $W$ is the moisture content of the material, and $S = \frac{x}{t^{0.5}}$, a variable in the model dependent on time and the spatial coordinates. They found that the calculations used were adequate and could therefore be used to process analytical data. They concluded that moisture diffusivity increased with increasing moisture content when moisture content was both high, and very low, however between 5 and 30% moisture content, only a small increase in moisture diffusivity was observed.

Although this method has many advantages; it is highly accurate and sensitive, it is a non destructive technique, and requires only a short measurement time, it has two major disadvantages with regard to my current project. Firstly, the initial moisture distribution is required to be uniform throughout the sample, and secondly the sample needs to be large, in the region of 500 $cm^3$, neither of which are fulfilled by the thin polymeric films which require testing.

### 1.5.3 Polymer applications

Polymer and adhesive technology is another area which has a great deal of interest in moisture diffusivity (Day et al., 1992, Mubashar et al., 2009a, 2009b, Reid and Buck, 1987). As water diffuses in and out of polymer systems, their structure can change significantly and with it the properties of the system such as strength, viscosity and shear strain. These changes can lead to failure of the system, particularly in adhesives where an increase in water uptake can result in a weaker, less viscous polymer solution, which will no longer adhere to the substrate. Methods used to investigate polymer systems are dominated, once again by the gravimetric method.

Mubashar *et al.* (2009a) used a gravimetric method to investigate the cyclic moisture uptake in an epoxy adhesive. They characterised the diffusion behaviour of such adhesives over three absorption - desorption cycles in which the desorption cycles were carried out in an oven at 50 °C, a temperature well below the glass transition temperature of the adhesive.

**Table 1.4 - Coefficients of Dual Fickian model determined by curve fitting to absorption data (from Mubashar *et al,* 2009a).**

| Cycle | $D_{1\infty}$ mm$^2$/h | $D_{2\infty}$ mm$^2$/h | $M_{1\infty}$ wt% | $M_{2\infty}$ wt% |
|---|---|---|---|---|
| 1 | 0.014 | 4.47x10$^{-4}$ | 1.78 | 1.92 |
| 2 | 0.024 | 6.46x10$^{-4}$ | 2.32 | 1.68 |
| 3 | 0.025 | 9.55x10$^{-4}$ | 2.23 | 1.97 |

**Table 1.5 - Coefficients of Fickian model determined by curve fitting to desorption data (from Mubashar *et al,* 2009a).**

| Cycle | $D$ mm$^2$/h | $M_\infty$ wt% |
|---|---|---|
| 1 | 0.017 | 3.7 |
| 2 | 0.025 | 4.0 |
| 3 | 0.035 | 4.2 |

An electric balance was used to weigh the samples at chosen time intervals throughout the procedure. They found that the overall diffusion coefficient was not constant and changed with increasing concentration (Table 1.4 and Table 1.5). In the dual Fickian process, two different Fickian processes are considered to occur simultaneously, helpful when representing anomalous behaviour when modelling although it does not explain this anomalous

behaviour, and thus two *D* and two *M* values are obtained as seen in Table 1.4. Also the diffusion coefficient and saturated mass uptake both increased with the number of absorption - desorption cycles. The desorption diffusion coefficient increased during the first and second cycles but not the third (Figure 1.10).

They concluded that absorption of moisture in the adhesive is non Fickian and the rate of absorption is dependent on the moisture history of the adhesive. Also, desorption is a Fickian process but the rate of desorption increases with moisture cycling. In addition, as the diffusion rates for absorption and desorption are different, and they have different dependency on the moisture history, they deduced that for an accurate prediction a model which includes moisture history must be used.

This method is useful in that it relates directly to polymeric adhesives and can be replicated for the relevant starch and casein models to be used in this work, however it provides no information on how accurately the diffusion coefficient can be determined, only that it changes throughout the process, therefore this method may be better suited to examining the physical properties of the polymer systems rather than to determine the moisture diffusivity.

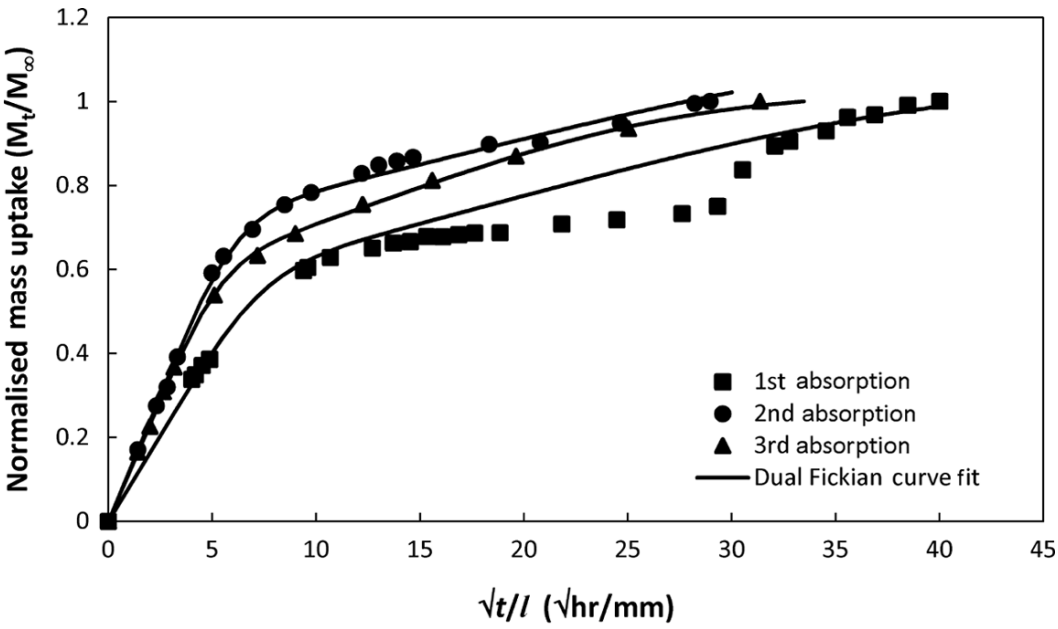


(a)

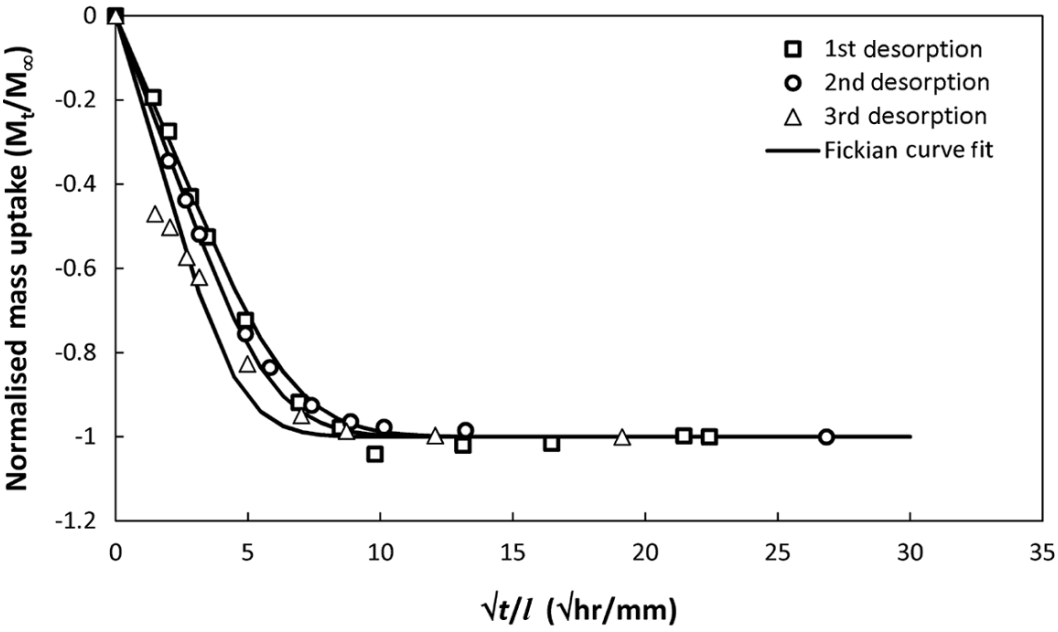


(b)

**Figure 1.10 - Graphs showing curve fits of experimental moisture uptake for 1 mm thick samples conditioned at 50 C, immersed in water (a) absorption and (b) desorption (from Mubashar *et al,* 2009a).**

The final technique to be discussed for determining moisture diffusivity uses dielectric measurements. Day, Shepard and Craven (1992) used micro-dielectric sensors to monitor moisture diffusion in polymer systems. They coated several micro-dielectric sensors with a thin film of polymer and cured

them for various times at either 177 °C or 220 °C. Once the polymer had dried onto the sensors, they were placed in a moist environment and the dielectric response was monitored as a function of time. Once the sensors detected no change in readings, they were placed in a dessicator and the dielectric response was monitored during the drying process until no further change occurred. They found that the procedure did not work for 100% relative humidity, or total immersion in water, however it was accurate up to 85-90% relative humidity. They found that thin films exposed to moisture could be modelled for one-dimensional diffusion across the film thickness using Fick's diffusion equation. Their diffusion coefficients were in good agreement with literature values, and the Fickian model which was used to model changes in permittivity gave a good correlation between data and theoretical values. They also found that the curing time had no effect on the diffusion coefficient and that the moisture uptake increased with cross-link density of the polymer.

The method above has two major advantages over other methods. When used with thin films, both the diffusion coefficient and the degree of moisture uptake can be determined very quickly. However the major disadvantage in this case is the cost required to carry out the experiment.

## 1.6 Microscopy techniques

An important property of the materials used in this work relating to their diffusion behaviour is the microstructure. This means an investigation of the biopolymer surface both before and after it has dried on a micro scale. The microstructure of a material has a strong influence on the physical properties of a material, for example, strength, temperature behaviour, and resistance

to wear. It is therefore important to understand the microstructure this controls the application of a material.

Some irregularities in the surface will be at a level not visible to the naked eye, thus optical microscopy alone is not an appropriate tool under these circumstances, due to its limited magnification capabilities. SEM, scanning electron microscopy is commonly employed to investigate surface structure at a high magnification up to 200000x. An alternative method which has some advantages over SEM is CLSM, confocal laser scanning microscopy. CLSM allows imaging throughout the entire structure rather than just the surface, and because it does not require a vacuum, wet samples can be examined as well as completely dry ones. Both techniques have been used in this work, and their principles are discussed below.

### 1.6.1 SEM, scanning electron microscopy

As its name suggests, the SEM uses electrons which are focussed onto the surface of a sample and are reflected into a detector, allowing a high resolution image of the surface to be generated. Figure 1.11 shows a schematic of a typical SEM.

The electron gun is situated at the top of the SEM and it is here that the beam of electrons is produced. A filament generates the electrons and it is housed in the Wehnelt cylinder, which has a small hole in the bottom for the electrons to exit through. Most electron guns use a heated tungsten wire as the filament, although more expensive guns use tungsten or lanthanum hexaboride crystals which can be heated, or a large electrical potential can be applied to pull the electrons out. The more voltage that is put through a filament, the more electrons are emitted, until a saturation point is reached

where no extra electrons are emitted when the current is increased. It is important to know when this point occurs to prolong the lifespan of the filament and prevent it from burning out.

Below the electron gun is an anode which attracts the electrons away from the filament, followed by a series of electromagnetic lenses and apertures which are used to reduce the size of the electron beam and focus the electrons onto the sample. The current that flows through the electromagnetic lens produces a magnetic field perpendicular to the current, into the hole through the centre of the lens. This magnetic field shapes the negatively charged electrons into a spiral which travels through the hole. The focal length can be adjusted by varying the current through this magnetic lens.

There are two sets of lenses in the SEM, the condenser lens and the objective lens. The condenser lens converges the electron beam to a spot which then flares into a cone before being converged a second time by the objective lens. The height at which the condenser lens converges the beam influences the spot size – the closer it is to the lens, the smaller the spot. The main role of the objective lens is to focus the electron beam onto the sample.

The SEM is operated under high vacuum. A high vacuum leads to minimal scattering of the electron beam. This is important to ensure a high resolution and to optimise collection of secondary electrons.

Secondary electrons usually form the image of the surface when SEM is used. These are low energy electrons (~50 eV) formed by inelastic scattering when an incident electron excites an electron in the sample, which

escapes from the surface of the sample if it has gained sufficient energy. These electrons are detected by the secondary electron detector which has a positively charged grill attached to it, to attract the electrons. Secondary electrons are used to examine the surface topography and give better resolution than back-scattered electrons and x-rays (Egerton, 2005).

Back-scattered electrons have higher energies than secondary electrons and are incident electrons which undergo elastic collisions in the sample with the atoms' nuclei before being ejected back out of the sample. Back-scattered electrons produce a contrast image and are useful when investigating chemical composition.

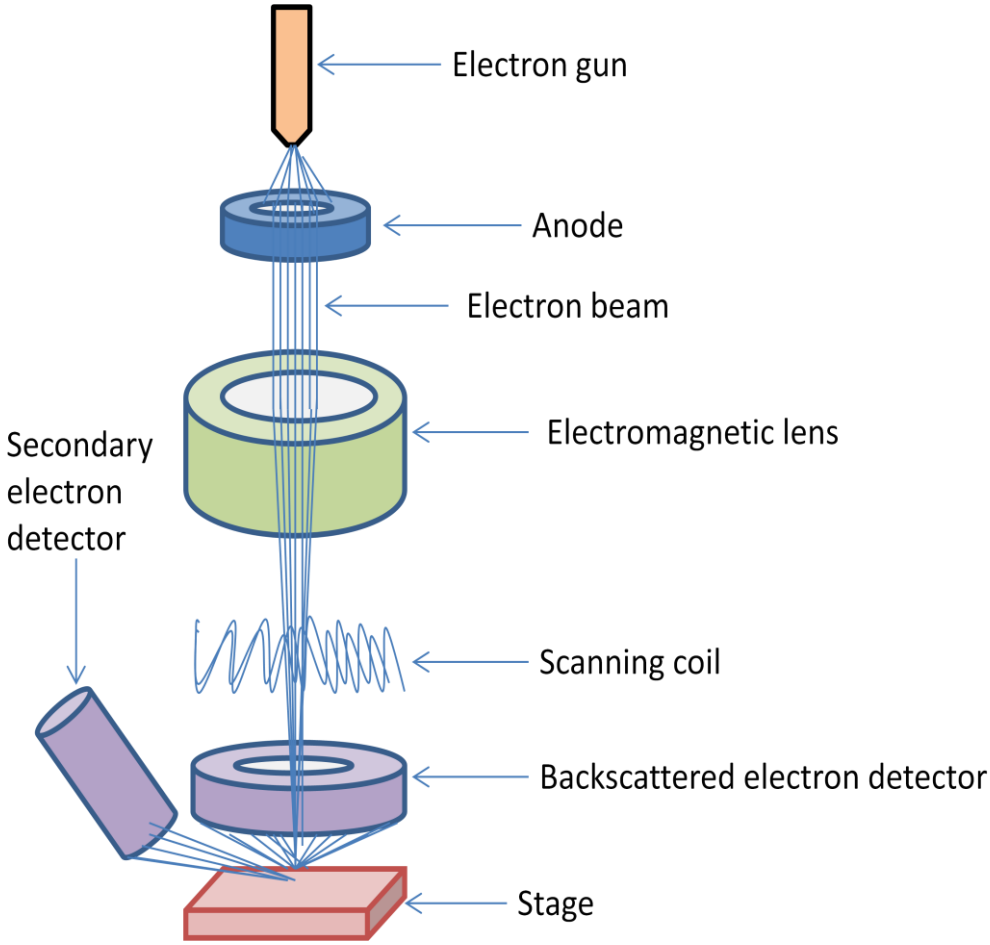


**Figure 1.11 - Schematic diagram of an SEM**

#### 1.6.1.1 Preparation of samples

To prepare biopolymer films for the SEM, a sample of the degassed film is mounted onto a short stub using carbon tape, secured with carbon paste. Once the paste is dried, the samples are coated with conductive gold particles in a sputter chamber. The stubs are placed inside the chamber and the pressure is reduced to 0.05 torr. Once this pressure is reached, the chamber is purged with argon gas atoms, which bombard the gold target, causing gold atoms to be released. These atoms coat the sample over 4 min to give a coating of a few nm. The gold coating allows the sample to be viewed under the SEM without it charging. Without this coating, electrons accelerated at the samples would not conduct away from the site of absorption leading to a buildup of charge in one spot. This causes an electrostatic field which deflects secondary electrons causing contrasts inconsistent with the actual sample.

### 1.6.2 CLSM, confocal laser scanning microscopy

Confocal laser scanning microscopy offers some advantages over the more traditional electron microscopes in that it can be used to scan through the sample easily and it rejects out of focus light which can often result in a low contrast, poor image. Charging is also not an issue with confocal so there is no need to coat samples with an electron conductive material prior to observation. Another advantage, more specific to this work is the ability to be able to view both wet and dry samples under the microscope, a limitation of SEM.

Figure 1.12 shows a schematic of a typical CLSM. A laser beam is directed towards a pair of mirrors, which scan the light in two directions x and y, by a

dichroic mirror, that is a mirror which reflects specific colours determined by the wavelengths set by the user. The light is directed to the microscope objective and onto a fluorescent sample. The fluoresced light then passes back through the objective and is descanned by the two mirrors, before passing through the dichroic mirror through a pinhole in the conjugate focal plane of the sample, emerging to be measured by a detector. The presence of the pinhole allows all out of focus light to be rejected, resulting in a high contrast image which is reconstructed in 2D on a computer (Prasad et al., 2007).

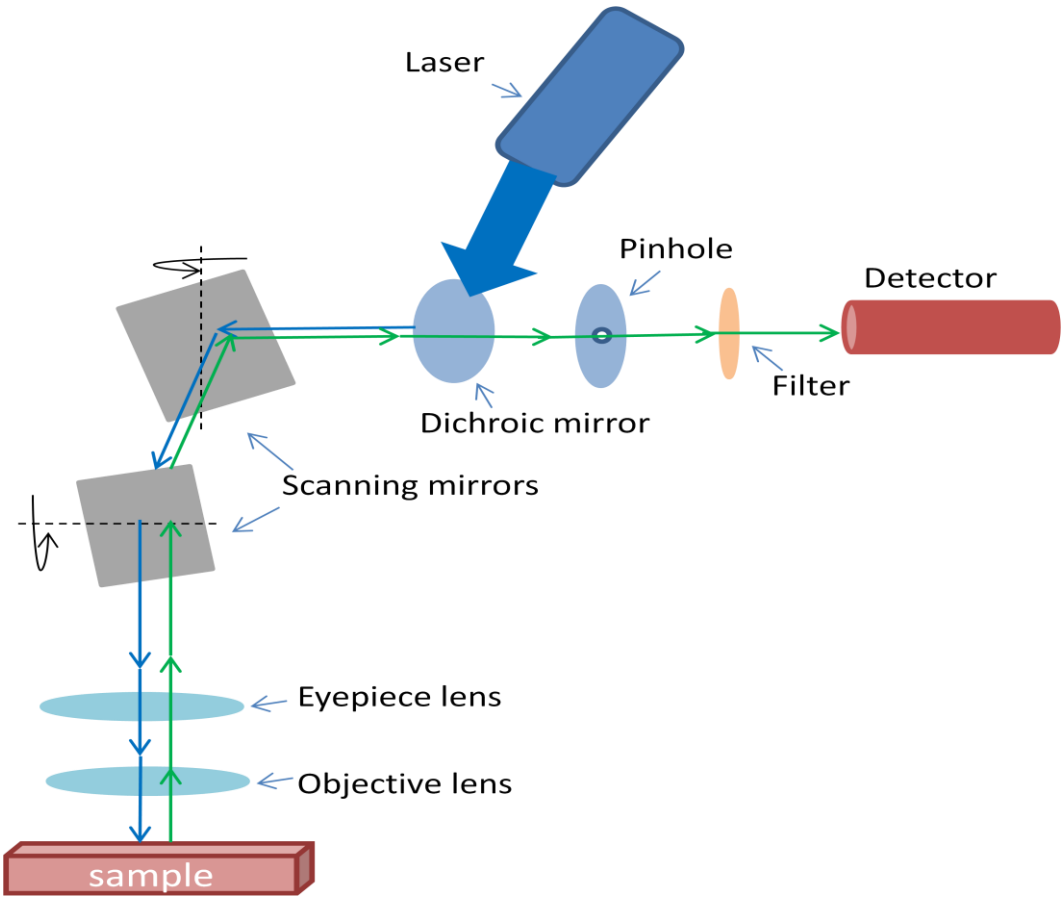


**Figure 1.12 - Schematic diagram of a CLSM**

It is very easy to prepare a sample for confocal observation. A fluorescent dye with specific binding properties to the component in question is added to

the solution of the material during its production stage. Care must be taken however to ensure the fluorscence is not lost, as it is light sensitive, so once dyed, the sample should be stored in dark conditions if immediate analysis is not possible. In the case of the samples used in this project, rhodamine B has been used to stain the protein within the samples.

## 1.7 Outline of this work

In this thesis the diffusion of moisture both into and out of thin biopolymer films of different composition is investigated under different external conditions, including temperature and relative humidity. In Chapter 2 several theoretical models based on Fick's second law of diffusion combined with evaporation equations are derived and implemented for a series of initial and final moisture conditions. They are also used to demonstrate the effects of film shrinkage on the rate of moisture loss and the importance of including this property in the simulations.

Chapter 3 presents the experimental results for a series of dehydration experiments carried out in a purpose built chamber with temperature and air humidity control. The numerical calculations presented in Chapter 2 are fitted to the experimental data for the cases where

1) diffusion is the limiting factor with infinitely fast evaporation,

2) evaporation is the limiting factor with infinitely fast diffusion,

3) film shrinkage and fixed volume films, examined for both 1) and 2),

and finally

3) evaporation dominated dehydration, with fast, but finite diffusion is studied.

From the fittings of these models, diffusion coefficients and evaporation constants can be obtained for the different systems and conditions.

In Chapter 4 a novel method for measuring water diffusion into biopolymer films using acoustic data is presented. The method uses ultrasound waves to scan a rectangular cell containing the biopolymer gel with a reservoir of water on top. The change in speed of sound with height of the cell, and time, can be correlated with data on the sound velocity for different concentrations of the biopolymer, so that concentration profiles can be constructed. Fick's laws can again be used to generate model concentration profiles, which are fitted to the experimental data to obtain the diffusion coefficient. The method has been validated using sodium caseinate solution at 25 °C, and future work includes expanding the method to observe temperature and composition effects on diffusion.

Finally in Chapter 5, water ingress into dried, thin biopolymer films is examined. Again, a novel approach is presented, where a droplet of water is depositied onto the biopolymer film, and its disappearance monitored as a function of time using a videocamera. Images are analysed to assess droplet height and contact with the film, and used to plot droplet volume as a function of contact area with time. Experimental evidence shows that after an initial period of adjustment of a few seconds, for some film compositions the droplet remains at a fixed contact area throughout drying. Numerical solutions are therefore derived for droplet evaporation and diffusion for such a "pinned" droplet. Models are fitted to experimental data with a view to obtaining evaporation constants and diffusion coefficients. The effect of microstructure on the rehydration properties of the films is also discussed in this chapter.

# Chapter 2 Modelling and simulating the dehydration of thin biopolymer films

## 2.1 Introduction

### 2.1.1 What is mathematical modelling?

By definition, mathematical modelling is “the process of constructing mathematical objects whose behaviour or properties correspond in some way to a real world system” (Maki, 2006). Mathematical models attempt to represent reality using mathematical symbols, relations and concepts. They are an important tool to improve understanding of a process, by discovering important factors and how they relate to each other; and to predict or simulate what may happen in the future where it is impractical or impossible to experiment directly with the real system, for example weather predictions (Banasiak, 2013).

By constructing a mathematical model, real objects or processes are represented by mathematical ones (Maki, 2006). The first part normally involves simplifying the real situation, neglecting some factors completely whilst simplifying others in an attempt to discover the most important factors behind the process.

Modelling may also allow some sort of control or intervention to take place in a process. It is a particularly useful tool, as devising an accurate model is a cost effective alternative to directly experimenting (Basmadjian, 2003)

It is important to realise that when modelling a real system there will be no perfect model (Maki, 2006), as it is necessary to place more importance on one of accuracy, cost or flexibility, at the expense of the others.

It is useful to think of modelling as a process which evolves as follows. The problem to be modelled arises in the real world, and the study of this real world system is the first step in the modelling process. This could involve quantitative measurements of the system, or knowledge of how it works. The next step in the process is to simplify the problem. This is achieved by identifying the basic concepts, and eliminating any unnecessary information. In order to do this, one needs to consider what aspects of the system are to be investigated and predicted, and how accurate does the prediction need to be. This step, consisting of simplifying, idealising and approximating, formulates the model. It is particularly important to conduct proper background research of the literature as it may be that good models exist for parts of the system, that can be put together to represent the whole system, or that there is a good model for a different process which could be modified to apply to the process in question. The review of the literature will be discussed in the next section of this chapter.

Once the model has been created, the next step is to apply mathematical theories and techniques to the model in order to find new information about the system of interest and develop conclusions and predictions. These findings can then be used to test the model against the real world system to determine how effective the model is.

In this work, the process of interest is the mass transfer of moisture in biopolymer thin films. The ultimate aim of this work is to establish a mathematical model which adequately describes the dehydration behaviour of thin biopolymer films.

When considering a drying biopolymer film it is important to first consider the theory behind the process in order to be able to construct a mathematical model which can be applied to predict the behaviour of such a system. A lot of work in the literature is based on designing mathematical models to predict diffusion (Brennan et al., 2009, da Silva et al., 2009, Evingur and Pekcan, 2011b, Henshaw et al., 2006, Mubashar et al., 2009a, Nahimana et al., 2011, Oner et al., 2011), however the majority of these are simple models, based on Fick's laws of diffusion.

### 2.1.2 Models available in the literature

From a thorough examination of the literature it is clear that mass transfer models are based on Fick's laws of diffusion. In many cases when thin films are dried, the controlling factor is diffusion of the moisture within the film (Ruiz-Lopez et al., 2012, Zogzas and Maroulis, 1996). The rate of evaporation when moisture reaches the surface is assumed rapid enough to be almost instantaneous and therefore does not influence the drying rate of the film. This is reflected in the simplest mathematical models by taking the moisture content at the surface of the film as always being at equilibrium with the moisture in the air above. Furthermore, such models are mostly based on Fick's second law of diffusion with either a constant diffusion coefficient (Czaputa et al., 2011, Day et al., 1992, Nizovtsev et al., 2008, Ramirez et al., 2011), or in some cases a variable diffusion coefficient that changes with moisture content (Seth and Sarkar, 2004). Ruiz-Lopez *et al* (2012). developed and validated an analytical model, based on Fick's second law of diffusion. This was used to evaluate mass transfer properties and describe drying kinetics in shrinkable food products. They used a simple, gravimetric method to obtain experimental data to compare to the

numerical scheme. The models can be used to accurately describe food drying with the assumption that the food temperature remains constant throughout the drying process. The mathematical model used by Seth and Sarkar (2004) to simulate the effective moisture diffusivity of green mango was based on Fick's law of diffusivity for a cylindrical sample with variable diffusivity, as they found that many of the experimental results did not fit with the constant diffusivity equation. They concluded that Fick's law of constant diffusivity cannot accurately predict the drying kinetics observed experimentally, with an error of ± 27%, and developed their own model. To model the data three curves were generated with different diffusion conditions using different boundary conditions based on Fourier number ($D_{\infty}t/L^2$), which incorporates shrinkage into the model. The most accurate prediction, with an error of ± 7%, used Fick's law with a variable diffusion coefficient which varied exponentially, followed by two linear lines (see Figure 1.6).

More sophisticated models attempt to take shrinkage of the drying material into account, by using moving boundary conditions (Nahimana et al., 2011, Thuwapanichayanan et al., 2011). Ramirez et al (2011) modelled the drying of apples using two models based on Fick's laws. Both of these models assumed one dimensional drying in the axial direction, with negligible moisture loss from the sides and bottom of the apple slices. The first model assumed negligible shrinkage with constant diffusivity, and the second model assumed a variable diffusion coefficient, which took into account the physical properties of the film. This model was found to give a good fit to the experimental data, although some deviation was observed. Czaputa et al (2011) investigated the drying of polymer coatings, with cylindrical or

spherical geometry. Film shrinkage was taken into account by using non-dimensional coordinates on a fixed domain. They found that at very small values of initial film thickness, geometry hardly influenced the drying process. For cases with no substrate, the diffusion equation was solved on time dependent domains, and when a substrate was present, diffusion was solved numerically using the Crank-Nicolson scheme. Results were validated against analytical solutions for drying filaments and droplets with a vanishing substrate radius.

In most cases these simple mathematical models have been found to give a reasonable fit to experimental data, and in the literature many use these as a satisfactory approximation (Cerny et al., 1996, Saravacos and Maroulis, 2001). However, as this work demonstrates, a more complex model may be required to give a more reliable representation of the drying process (Zogzas and Maroulis, 1996).

In this chapter, the drying process for a thin biopolymer film will be discussed from a theoretical point of view, beginning with the simplest case, where diffusion is the limiting factor for a fixed boundary situation. Following on from this, the cases where shrinkage of the film occurs, ie a moving boundary, will be considered for both a constant diffusion coefficient and a diffusion coefficient which varies as a function of moisture content. In this section it is demonstrated how the initial and final moisture volume fractions affect the drying curve and how they deviate from the simple standard curve, where the diffusion coefficient and thickness of sample remain constant throughout the drying process.

In some cases, diffusion is not the dominating factor limiting the drying rate, it is in fact evaporation. Again, the simple case, with fixed boundaries will be discussed, followed by the case with a moving boundary.

It is important to realise that while one of these processes may dominate the drying process, the other cannot be completely disregarded, therefore to conclude, the effect of the evaporation constant used in the diffusion limited simulations will be discussed.

## 2.2 Theoretical considerations for modelling a drying film

### 2.2.1 Diffusion in a drying film

In this section, the drying process for a film is considered, as applied to biopolymer solutions, from a theoretical point of view. Within the body of the film, the process of moisture transfer involves diffusion of water. On the upper surface of the film, i.e. the surface exposed to the surrounding air, the loss of water is due to evaporation. It is assumed that there is no loss of moisture through the substrate underneath the film and moisture loss through the side surfaces is also negligible. First, some of the issues and complications that can arise in association with each of these two processes will be highlighted, before mathematical analysis of the drying model is presented. As mentioned previously, in the simplest case, one can assume that the volume of the film remains constant throughout the drying process. This occurs when the solid fraction in the polymer film has formed a porous layer through which water can migrate to the surface. The yield stress of the porous structure formed in such a case must be sufficient to withstand any capillary stresses induced during the loss of moisture. Under such

circumstances the diffusion of the solid fraction is much smaller than that of the moisture thus it can be ignored. Since the loss of water from any region in the film is not accompanied by a change in the volume of that region, the partial molar volume of the water phase, on scales larger than the size of pores, can be taken as being effectively zero. When either the internal diffusion or the surface evaporation is the dominant rate limiting process, simple models of drying result. Analytical solutions for both of these models have been obtained and extensively discussed in the literature (Zogzas and Maroulis, 1996, Saravacos and Maroulis, 2001). Due to their inherent simplicity, and the presence of closed form analytical solutions for each model, these have widely been used in the fitting of the data from many drying experiments under a variety of circumstances (Saravacos and Maroulis, 2001). In fact, their popularity has been such that they have been considered even in situations where various assumptions inherent in the models, such as the requirement for a constant volume of the sample, have not been strictly valid. In such cases often an empirical effective diffusion coefficient, that is somewhat different to the real diffusion coefficient of water in the film, is often used in order to partially compensate for the shrinkage and other complications not present in the simple model (da Silva et al., 2009).

Where the changes in the volume of the film during drying are large, for example if there are no stress-supporting structures formed by the solid fraction, the approaches discussed above can no longer be used. One immediate problem is that of specifying a reference frame against which the diffusion fluxes are measured. As was originally pointed out by Hartley and Crank (1949) there are many frames of reference that can be considered.

For example the diffusion fluxes may be specified relative to the substrate side of the sample or to the film-air interface side. For a shrinking film these two frames result in different measured fluxes. Other possibilities have been considered involving mean mass, mean molar or mean volume reference frames (Hartley and Crank, 1949, Cussler, 1997). As long as partial molar volumes of the components in the film are not composition dependent, then diffusion coefficients measured in one reference frame can easily be related to those obtained in another frame (Brady, 1975). Unless stated otherwise, in what follows we shall assume that the diffusion process and all the related diffusion coefficients are specified in the so called laboratory frame of reference, relative to the substrate.

There are two main factors that can contribute to changes in the volume of the sample. Firstly, the more obvious one associated with the loss of the moisture. However, provided the partial molar volumes of the components in the polymer solution are constant, independent of the composition of the solution, the problem simplifies greatly. Here the reduction in the volume remains strictly proportional to the amount of water that is lost at any stage throughout the drying process. This makes it simpler to determine the location of the moving air-film interface. This information is required for an analytical or numerical solution to the drying problem. The second factor influencing changes in the volume of the film arises from the variation of the partial molar volumes of the two components with the mix ratio. This frequently occurs in problems involving inter-diffusion of two metals or metal oxides to form alloys (Greskovi and Stubican, 1970). Variations arising as a result of changes in the partial molar volumes add a substantial degree of complication to the analysis of the diffusion process. Mathematical models of

diffusion have been extended to account for these more complex cases in relation to metal couples (van Loo, 1990). Of course in such problems, unlike drying, the total mass of the system remains a conserved quantity. This makes the use of constant mass reference frame a more appropriate choice (Cussler, 1997). In the drying problem, this type of variation in the volume makes it that much more difficult to determine the location of the moving upper boundary. However, since this information is crucial in obtaining a solution to the equations describing the drying process, the use of the constant mass reference frame is not as useful. A reference frame with respect to the substrate is preferable in this case. Fortunately in many practical situations involving the drying of food related biopolymer films, including the systems studied here, the partial molar volumes remain reasonably constant over a wide range of mixture ratios. Since a theoretical analysis of changes arising from the variation of partial molar volumes has not been fully considered in the context of the drying of the biopolymer films, it is useful to first provide such a general treatment. The more familiar and widely studied cases, involving constant partial molar volumes, emerge then as special limits of this more general model. Before this analysis is presented, the evaporation of water from the upper surface of the film will be examined.

### 2.2.2 Evaporation from the surface of a drying film

The conditions prevalent at the air–film interface determine the rate at which water evaporates from the film. These conditions include the nature of the solid phase, air temperature and flow above the film and the amount of moisture in the film just beneath the interface. For any given set of conditions there will be an equilibrium value of water content (molar

concentration), $c_w^{eq}$, in the film that will be in equilibrium with the moisture in the air above. The $c_w^{eq}$ values relating to the systems and conditions used in the experimental investigation into drying films can be seen in Appendix 1. Over a long period of time the water concentration in the film will approach $c_w^{eq}$ everywhere in the dried film. In general the rate of water loss per unit surface area of the film will be a function of ($c_w(L,t) - c_w^{eq}$), where $c_w(L,t)$ is the concentration of water on the surface at time $t$ and $L$ is the thickness of the film. The function can be expanded in powers of ($c_w(\mathrm{L},t) - c_w^{eq}$ ) and providing the difference between $c(L)$ and $c_w^{eq}$ is small, only the linear term needs to be retained.

$$f(c_w(L,t) - c_w^{eq}) \approx -K(c_w(L,t) - c_w^{eq}) \qquad \textbf{2.1}$$

The approximation remains a rather good one, even for relatively large values of ($c_w(\mathrm{L},t) - c_w^{eq}$ ). The value of $K$ captures all the temperature dependence and other factors related to the evaporation of the water from the film on the surface, but otherwise is a constant for a given set of conditions. It is known as the drying constant (Zogzas and Maroulis, 1996).

If the diffusion of moisture is a relatively fast process in the film, then the only important factor limiting drying is evaporation. This occurs for sufficiently small $K$, large water diffusion coefficient, $D$, and in thin films where $D/(KL) >> 1$. Under such circumstances the water concentration gradients across the film thickness are small. Thus the concentration of water can be taken as being uniform throughout the film $c_w(\mathrm{z},t) = c_w(L,t) = c_w(t)$, where $z$ is the distance into the film as measured from the substrate. For cases with no shrinkage this leads to a very simple model that can readily be solved to give an exponential decrease in the concentration of

water with time, (Strumillo et al., 1986) $c_w(t) = c_w^{eq} + (c_w(0) - c_w^{eq})\exp(-Kt)$ . Therefore, when considering the more interesting case where the thickness of the film decreases during the drying process, the basic equation to solve now becomes

$$\frac{d\left(c_w(t)L(t)\right)}{dt} = L(t)\frac{dc_w(t)}{dt} + c_w(t)\frac{dL(t)}{dt} = -K\left(c_w(t) - c_w^{eq}\right) \qquad \textbf{2.2}$$

The rate of shrinkage of the film, $dL/dt$, can be related to the rate of water loss from the film through the partial molar volume of the water, $V_w$, at any given time

$$\frac{dL(t)}{dt} = -V_w(\alpha)K\left(c_w(t) - c_w^{eq}\right) \qquad \textbf{2.3}$$

The possible dependence of $V_w$ on the molar fraction of water in the mixture, $\alpha = c_w(t) / (c_w(t) + c_s(t))$, is indicated by writing this as $V_w(\alpha)$. As the molar concentrations of water and the solid phases, $c_w(t)$ and $c_s(t)$, change with time, so will the value of $\alpha$ and therefore $V_w(\alpha)$. The total amount of solid phase in the film obviously will not alter. Therefore we also have

$$c_s(0)L(0) = c_s(t)L(t) \qquad \textbf{2.4}$$

There is one further important relation that relates the values of $c_w(t)$ and $c_s(t)$ to each other, namely

$$c_s(t)V_s(\alpha) + c_w(t)V_w(\alpha) = 1 \qquad \textbf{2.5}$$

Provided the variation of $V_w$ and $V_s$ with the water mole fraction $\alpha = c_w(t) / (c_w(t) + c_s(t)$ is known, then in principle for any given value of $c_w$ the above

equation can be solved to yield the corresponding value of $c_s$. In practice however, the equation is non-linear, and requires a numerical solution or an approximate expression. Assuming that, for a particular system such an exact or approximate expression has been obtained, where $c_s = g(c_w)$, then, using equations 2.3 and 2.4 to substitute for d$L$/d$t$ and $L$ in equation 2.2, we arrive at

$$\frac{c_s(0)L(0)}{g(c_w)}\frac{dc_w}{dt}+\left(1-c_wV_w\left(\frac{c_w}{c_w+g(c_w)}\right)\right)K\left(c_w-c_w^{eq}\right)=0 \qquad \textbf{2.6}$$

Whether an analytical solution to the above differential equation can be obtained or not depends on the actual form of the functions $g(c_w)$ and $V_w(\alpha)$. Such a solution can be found for the early stages of the drying process, by linearising the functions around the initial value of $c_w$. Another special but important case, involves systems for which $V_w$ and $V_s$ are constant. As mentioned before, many biopolymer solutions behave in this way, at least down to the very last stages of drying. For these systems it is easier to work with the volume fraction of water $\phi = c_wV_w$. The volume fraction of the solid phase is then $1-\phi = c_sV_s$. With partial molar volumes independent of the composition, function $g(c_w) = (1-c_wV_w) / V_s = (1-\phi) / V_s$. Multiplying both sides of equation 2.6 by $V_w$ we find

$$\frac{d\phi}{dt}=\frac{-K}{(1-\phi(0))L(0)}(1-\phi)^2\left(\phi-\phi^{eq}\right) \qquad \textbf{2.7}$$

where $\phi(0)$ is the initial volume fraction of the water in the film and $\phi^{eq}$ is the equilibrium value. The above differential equation can be solved to give an

explicit relation between time $t$ and volume fraction of water $\phi$ in the system as follows**:**

$$\frac{1}{(1-\phi)} - \frac{1}{(1-\phi(0))} + \frac{1}{(1-\phi^{eq})}\ln\left[\frac{(1-\phi(0))(\phi-\phi^{eq})}{(1-\phi)(\phi(0)-\phi^{eq})}\right] = \frac{-K(1-\phi^{eq})}{L(0)(1-\phi(0))}t \qquad \textbf{2.8}$$

The results predicted by equation 2.8 is substantially different to that of the simple model not accounting for the film shrinkage, when $\phi^{eq}$ and $\phi(0)$ are not so small. However, for small values of these quantities i.e. $\phi^{eq} << 1$ and $\phi(0) << 1$, the equation predicts the same exponential behaviour

$(\phi - \phi^{eq}) / \phi(0) - \phi^{eq}) = exp(-Kt/L(0)$ as the one obtained by the simple model. This is because at small values of $\phi^{eq}$ and $\phi(0)$, the term $c_w(dL/dt)$ becomes much smaller that $L(dc_w/dt)$ in equation 2.2, and hence the shrinkage of the film can be safely neglected. In the next chapter, results obtained from equation 2.8 will be compared with the experimental data involving drying of casein and starch based biopolymer films.

### 2.2.3 General Model for the Drying Film.

In this section the drying process will be discussed in which diffusion, evaporation and shrinkage of the film are all significant and none may be ignored. The diffusion process has to satisfy a number of basic relations, the most obvious of which is the continuity equation for both the solid and the water phase within the film:

$$\frac{\partial c_i}{\partial t} = -\frac{\partial j_i}{\partial z} \qquad \textbf{2.9}$$

In equation 2.9 $j_i$ is the molar flux of component *i*, where suffix *i*=*w* or *i*=*s,* refers to the water or the polymer phases, respectively. Provided that the local equilibrium is also maintained at each point in the film, the concentrations of the two phases are also related to each other throughout the system. Once the composition ratio, $\alpha$, is known at a point, then so are the values of $c_w$ and $c_s$ through equations

$$c_s(z,t)V_s(1-\alpha)+c_w(z,t)V_w(\alpha)=1 \qquad \textbf{2.10}$$

which is equation 2.5 now applied locally to each point *z*, and

$$(1-\alpha)c_w(z,t)-\alpha c_w(z,t)=0 \qquad \textbf{2.11}$$

Thus, it suffices to only focus on the diffusion of one component (e.g. water), since diffusion of the other component (solid phase) will simply follow suit. The relationship between $c_w$ and $c_s$ is a simple linear one for the cases where partial molar volumes are constant. This leads to the well-known situation for which the diffusion coefficient of both components are identical, often referred to as the inter-diffusion coefficient (Brady, 1975, Cussler, 1997). To relate the diffusion of the two components in these more general cases, both sides of equation 2.10 are differentiated with respect to *z*. We have

$$V_w\frac{\partial c_w}{\partial z}+V_s\frac{\partial c_s}{\partial z}=0 \qquad \textbf{2.12}$$

The above equation is obvious when $V_w$ and $V_s$ are composition independent, but it also holds more generally. This can be seen from the fact that

$$c_w \frac{\partial V_w}{\partial z} + c_w \frac{\partial V_w}{\partial z} = (c_w + c_s)\left(\alpha \frac{dV_w}{d\alpha} + (1-\alpha)\frac{dV_s}{d\alpha}\right)\frac{\partial \alpha}{\partial z} = 0 \qquad \textbf{2.13}$$

That the term in the bracket in the above equation is zero follows from the generalised form of Denham-Gibbs equation, valid for all partial molar quantities (Atkins and De Paula, 2006). It can easily be derived by considering changes in the volume of a uniform mixture of $n_w$ moles of water and $n_s$ moles of polymer solid phase and the fact that the volume, $V$, is a function of state. In other words $\partial^2 V/(\partial n_w \partial n_s) = (\partial V_s/\partial n_w) = (\partial V_w/\partial n_s)$.

A very similar argument can be applied to the derivative of equation 2.10 with respect to time to obtain

$$V_w \frac{\partial c_w}{\partial t} + V_s \frac{\partial c_s}{\partial t} = 0, \qquad \textbf{2.14}$$

which in combination with the continuity equations, equation 2.9, may also be written as

$$V_w \frac{\partial j_w}{\partial z} + V_s \frac{\partial j_s}{\partial z} = 0, \qquad \textbf{2.15}$$

Equations 2.9 to 2.15 apply quite generally to any two phase system, so long as the local equilibrium is maintained at each point throughout the system. They are valid irrespective of the laws that govern the dependence of the diffusion fluxes on concentrations. However, at this stage a choice has to be made with regards to the relations governing the dependence of diffusion fluxes on gradients of thermodynamic quantities. Several such laws have been suggested over a number of years of which Fick's first law, Maxwell-Stefan's law or Onsager's flux law are amongst the best known and most widely used (Cussler, 1997). In this work it is assumed that the flux relation

for the water phase, though not necessary the solid phase, can be described by Fick's law

$$j_w = -D_w(\alpha)\frac{\partial c_w}{\partial z}. \qquad \textbf{2.16}$$

The symbol $D_w(\alpha)$ in the above equation denotes the compositional dependent diffusion coefficient of water, as measured in the chosen laboratory reference frame. It must be stressed that this is a phenomenological relation, the validity of which would have to be verified experimentally for the particular system of interest. It should be noted that there are many situations, and particularly with regards to diffusion of water in glassy polymer films, where Fick's law is not always obeyed (Durning and Tabor, 1986, Karger, 2005, Pogany, 1976). In other situations an equation similar to equation 2.16 can be developed only by redefining the length scale in a position dependent manner, and by expressing the concentrations in units consistent with this variable (Hartley and Crank, 1949, Frisch and Stern, 1983). Substituting equation 2.16 into equation 2.9 for the water phase, leads to the familiar Fick's second law

$$\frac{\partial c_w}{\partial t} = \frac{\partial}{\partial z}\left( D_w(\alpha)\frac{\partial c_w}{\partial z} \right). \qquad \textbf{2.17}$$

As the concentration of moisture evolves with time across the film thickness, the concentration of the solid phase, $c_s$, has to follow suit in a manner dictated by equations 2.10 and 2.14. Since the aim is to eliminate all references to $c_s$ in the equations governing the drying process, the temporal variation of $\alpha$ at each point will be considered, instead of $c_s$. This is also useful as, more often than not, the experimental data for partial molar

volumes are given as functions of the mole fraction of the constituent components. To obtain the required equation, we express $c_w$ in terms of $\alpha$ using equations 2.10 and 2.11; $c_w = \alpha / [(1-\alpha)V_s + \alpha V_w]$. Differentiating both sides of this equation with respect to time and rearranging we obtain

$$\frac{\partial \alpha}{\partial t} = \left[\frac{((1-\alpha)V_s + \alpha V_w)^2}{V_s}\right]\frac{\partial c_w}{\partial t} = \left[\frac{((1-\alpha)V_s + \alpha V_w)^2}{V_s}\right]\left[\frac{\partial}{\partial z}\left(D(\alpha)\frac{\partial c_w}{\partial z}\right)\right] \qquad \textbf{2.18}$$

Equation 2.18 is particularly convenient for use in finite difference or other similar numerical schemes (da Silva et al., 2009, Tabor et al., 2012b), since ($\partial c_w/\partial t$) is determined at each time step using equation 2.17. By updating the value of $\alpha$ throughout the system the values of $V_w$ and $V_s$ can be refreshed at each point too.

Equations 2.17 and 2.18 have to be solved by imposing the appropriate boundary conditions to the film. At the bottom surface, in contact with the substrate, these are $j_w(0,t) = j_s(0,t) = 0$, leading to

$$\frac{\partial c_w}{\partial t} = \frac{\partial c_s}{\partial t} = 0. \qquad \textbf{2.18}$$

At the upper surface, where the evaporation of water takes place, we have

$$c_w \frac{dL}{dt} - j_w = -K(c_w(L,t) - c_w^{eq}) \qquad \textbf{2.19a}$$

for the water phase. The corresponding equation for the solid phase reads as follows:

$$c_s \frac{dL}{dt} - j_s = 0 \qquad \textbf{2.20b}$$

The rate of change of the film thickness is denoted by *dL*/*dt*. These conditions follow directly from equation 2.1 for the evaporation and the continuity equations for each phase at the air–film interface.

Multiplying equation 2.20a by $V_w$ and equation 2.20b by $V_s$ and adding the two together we have the rate of shrinkage of the film given by

$$\frac{dL}{dt} = V_w j_w + V_s j_s - V_w K(c_w(L,t) - c_w^{eq}) \,. \qquad \textbf{2.20}$$

The flux ($V_w\, j_w$ + $V_s\, j_s$ ) in equation 2.21 above, when not equal to zero, indicates the presence of the so called Darken velocity (Crank, 1975, Darken, 1948) and the related Kirkendall effect (Paul et al., 2004, Smigelskas and Kirkendall, 1947) rather well known in the field of metallurgy. This effect manifests itself as a movement of marker non-diffusing entities relative to the substrate. From a theoretical view, the effect has been analysed in great detail in many different studies and has been the subject of several excellent reviews in the literature (Frisch and Stern, 1983, Danielewski and Wierzba, 2009). It suffices here to mention that for a system where the local equilibrium conditions are achieved quickly, and thus equation 2.10 prevails throughout the film, it can only occur if the partial molar volumes change with the mixture ratio. Conversely, the presence of the effect in a two component system where partial molar volumes are constant indicates that the two constituent components are not in local equilibrium with each other, at least in some regions in the system.

The reference to the solid phase can once again be removed from the above equation by expressing $j_s$ in terms of $j_w$. To do so we integrate eq 2.15 from 0 to a given height z into the film to obtain

$$j_s(z,t) = -\int_0^z \frac{V_w}{V_s}\frac{\partial j_w}{\partial z'}dz' = -\frac{V_w}{V_s}j_w + \int_0^z j_w \frac{\partial(V_w/V_s)}{\partial\alpha}\frac{\partial\alpha}{\partial z'}dz' \,. \qquad \textbf{2.21}$$

With equation 2.22 substituted in 2.21, we finally obtain the required equation describing the shrinkage of the film purely in terms of the concentration and diffusion fluxes for the water phase:

$$\frac{dL}{dt} = V_s\int_0^z j_w(z',t))\frac{\partial(V_w/V_s)}{\partial\alpha}\frac{\partial\alpha}{\partial z'}dz' \; - V_w K(c_w(L,t) - c_w^{eq}) \,. \qquad \textbf{2.22}$$

Equations 2.16 to 2.18, together with the boundary conditions 2.19 and 2.20 and equation 2.23 for the rate of shrinkage of the biopolymer film completely describe the diffusion–evaporation process. Furthermore, they do so in a way that is fully consistent with the presence of local equilibrium, as imposed by equation 2.10 at each point. Using these equations, a numerical scheme can now be easily implemented to simulate the drying process. In such a scheme, it would be even more convenient if the integral term in the above equation could be reduced to a form which only involves local quantities at the air–film interface. Such an expression for the integral has not been obtained. The presence of this integral term in equation 2.23 reflects the fact that the shrinkage of the film depends on the changes in the mix ratio and thus those in the values of the partial molar volumes, occurring not only on the surface but throughout the whole of the film, all the way down to the substrate. Of course, when the partial molar volumes are constants, then no such considerations will arise and this non-local term should disappear. This is clearly the case in equation 2.23. We shall discuss the special case involving constant partial molar volumes next and show how the equations derived above take on their more familiar forms in such a circumstance.

### 2.2.4 Systems Involving Constant Partial Molar Volumes.

When the partial molar volumes of the constituent components are not dependent on the composition ratio, the equations describing the drying process simplify significantly. In many biopolymers solutions this condition is satisfied quite well over a large range of composition mix ratios. It is only at the very last stages of the drying, where major changes in the structure of the film may occur, that the assumption begins to be violated. As in the analysis of the case involving the drying process limited by evaporation, once again it is easier to work with the volume fraction of water, $\phi = V_w c_w$. Thus, multiplying both sides of equation 2.17 by $V_w$ the moisture diffusion equation becomes

$$\frac{\partial \phi}{\partial t} = \frac{\partial}{\partial z}\left( D_w(\phi) \frac{\partial \phi}{\partial z} \right). \qquad \textbf{2.23}$$

The variation of the compositional dependent diffusion coefficient is assumed to be provided in terms of $\phi$ rather than $\alpha$. It is also immediately apparent that the diffusion equation for the evolution of the volume fraction of the solid phase $(1-\phi)$ is identical to equation 2.24, implying the expected result, $D_w(\phi) = D_s(\phi)$. So long as the diffusion coefficients are given as a function of $\phi$, equation 2.18 is redundant and need not be considered further. The fact that the partial molar volumes are constant implies that the volume is now a conserved quantity in the problem. That is, the volume of the remaining film and that of the evaporated water together always equal the initial volume of the film. This requires

$$\frac{dL}{dt} = -K(\phi - \phi^{eq}) \,. \qquad \textbf{2.24}$$

The above equation also results directly from equation 2.23 when $V_w$ and $V_s$ are constant, whereupon the integral term in the equation vanishes. Finally, the boundary condition 2.19 at the substrate side remains the same, while eq 2.20a at the air–film interface, $z = L$, can now be written as

$$D(\phi)\frac{\partial \phi}{\partial z} = -K(1-\phi)(\phi - \phi^{eq}) \,. \qquad \textbf{2.25}$$

The presence of a moving boundary condition in the problem is not desirable. It can be difficult to implement in a simple finite difference type numerical scheme and may require redefinition of the grid as the film shrinks relative to the grid size. This can be a source of numerical errors in the solution. One possible way to avoid such a problem would be to use a set of coordinate systems, $y$, where the length scale is continuously redefined by the thickness of the film at time $t$:

$$y = \frac{z}{L(t)} \,. \qquad \textbf{2.26}$$

In the new coordinate systems the air–water interface is always at $y = 1$. $\theta$ is also defined as

$$\theta = L(t)\phi \qquad \textbf{2.27}$$

such that

$$\int_0^{L(t)} \phi \, dz = \int_0^1 \theta \, dy \qquad \textbf{2.28}$$

In terms of the new length scale, the diffusion coefficient becomes $D^* = D_w/(L(t))^2$, while the diffusion equation, equation 2.24, now turns into a diffusion-convection equation:

$$\frac{\partial\theta}{\partial t} = \frac{\partial}{\partial y}\left(D^* \frac{\partial\theta}{\partial y} + \frac{y}{L}\frac{dL}{dt}\theta\right). \qquad \textbf{2.29}$$

Numerically it is much more convenient to implement a solution to equation 2.30, which now has to be solved with a fixed boundary condition

$$D^* \frac{\partial\theta}{\partial y} = -K\left(1-\frac{\theta}{L}\right)\left(\frac{\theta}{L}-\phi^{eq}\right) \qquad \textbf{2.30}$$

at $y$ = 1, rather than the moving boundary condition for equation 2.24. We have implemented a simple finite difference scheme to solve equation 2.30 in conjunction with equation 2.25. The solutions thus obtained will once again be compared to our experimental results once they are discussed in the next chapter.

To express the diffusion equation, equation 2.24, in terms of a new set of variables $y$ and $\theta$, as defined by equations 2.27 and 2.28 constitutes a continuous redefinition of the length scale, such that the unit of length is always the thickness of the film, $L(t)$, at any given time $t$.

We note that $L$ is a function of $t$ only. Therefore the right hand side of equation 2. 24 can simply be written as

$$\frac{\partial}{\partial z}\left(D_w(\phi)\frac{\partial\phi}{\partial z}\right) = \frac{1}{L}\frac{\partial}{\partial y}\left(D^* \frac{\partial\theta}{\partial y}\right), \qquad \textbf{2.31}$$

with $D^* = D_w/L^2$. As for the left hand side of equation 2.24, we have

$$\left(\frac{\partial \phi}{\partial t}\right)_z = \left(\frac{\partial \phi}{\partial t}\right)_y + \left(\frac{\partial \phi}{\partial y}\right)_t \left(\frac{\partial y}{\partial t}\right)_z = \left(\frac{\partial \phi}{\partial t}\right)_y - \frac{y}{L}\left(\frac{dL}{dt}\right)\left(\frac{\partial \phi}{\partial y}\right)_t, \quad \textbf{2.32}$$

where the subscript following each bracket indicates the quantity that is being kept fixed for that differential. Furthermore,

$$\left(\frac{\partial \phi}{\partial t}\right)_y = \frac{1}{L}\left(\frac{\partial \theta}{\partial t}\right)_y - \frac{\theta}{L^2}\left(\frac{dL}{dt}\right). \quad \textbf{2.33}$$

Thus upon substituting equation 2.34 into equation 2.33 and equating the result with equation 2.32, we arrive at

$$\frac{1}{L}\left(\frac{\partial \theta}{\partial t}\right)_y - \frac{\theta}{L^2}\left(\frac{dL}{dt}\right) - \frac{y}{L^2}\left(\frac{dL}{dt}\right)\left(\frac{\partial \theta}{\partial y}\right)_t = \frac{1}{L}\frac{\partial}{\partial y}\left(D^* \frac{\partial \theta}{\partial y}\right). \quad \textbf{2.34}$$

Multiplying both sides of the above equation by *L,* and following a slight rearrangement, the required diffusion-convection equation, equation 2.30 is obtained. Although equation 2.30 is seemingly more complicated than the original diffusion equation, it is actually easier to implement numerically since now the condition imposed at the moving boundary $z=L(t)$ becomes one at a fixed point $y=1$. This alleviates the need for re-meshing or redefining the grid size, as the film shrinks to a small fraction of its original size during the calculations. The presence of a convective term in equation 2.30 arise from the fact that a point at a fixed height *z* from the substrate, now moves with a velocity $-(y/L)(dL/dt)$ in the newly defined *y* coordinate system.

## 2.3. Simulations to model drying in thin films

### 2.3.1 The standard curve – drying with constant D and no shrinkage

Here, the simplest case, where diffusion is constant throughout the drying process, and the film has fixed boundaries, i.e. no film shrinkage occurs, as discussed in the previous section, is considered. All simulations in this section have an initial volume fraction of 0.5 for consistency, unless stated otherwise. Figure 2.1 shows the curve generated for these conditions. As the boundaries are fixed, and the diffusion coefficient is constant throughout, the initial and final moisture conditions have no effect on the curve. In other words, whatever conditions are inputted into the program, this same normalised curve is generated. It is therefore termed the standard curve, and this has been used as an appropriate tool for modelling experimental data (Huang and Haghighat, 2002). However, as seen in the literature, this curve does not always predict the drying behaviour particularly well, and it is often necessary to consider the physical properties of the system, such as the film thickness as a function of time. By normalising $t$ by $D/L^2$, and $L$ by $L(0)$ it is possible to scale simulations for any given diffusion coefficient and any film thickness onto the same curve. This is reflected in the x-axes of the following figures of diffusion-limited simulations.

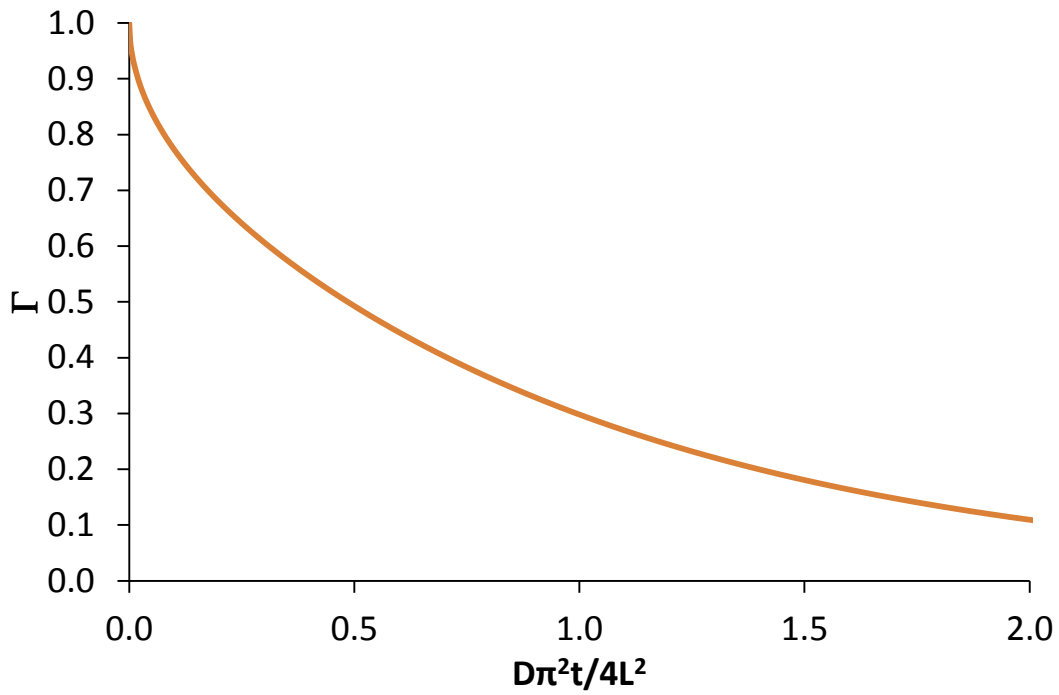


**Figure 2.1 - The "standard" curve calculated from Fick's law with constant diffusion coefficient and constant film thickness.**

### 2.3.2 Incorporating shrinkage into models

Moving boundary conditions are much more appropriate to use in the simulation when considering biopolymer film dehydration, as it is unlikely that stress supporting structures are formed as moisture is lost, at least for a large portion of the drying process. Experimental data presented in the following chapter supports the claim that the film thickness reduces during the drying process. By incorporating this physical change into the simulation, one can see that the curves produced deviate away from the standard curve, and the influence of the initial and final moisture conditions become apparent. Figure 2.2 shows several simulations, all with an initial moisture volume fraction of 0.5, but with varying final volume fractions, between 0.48 and 0.02.

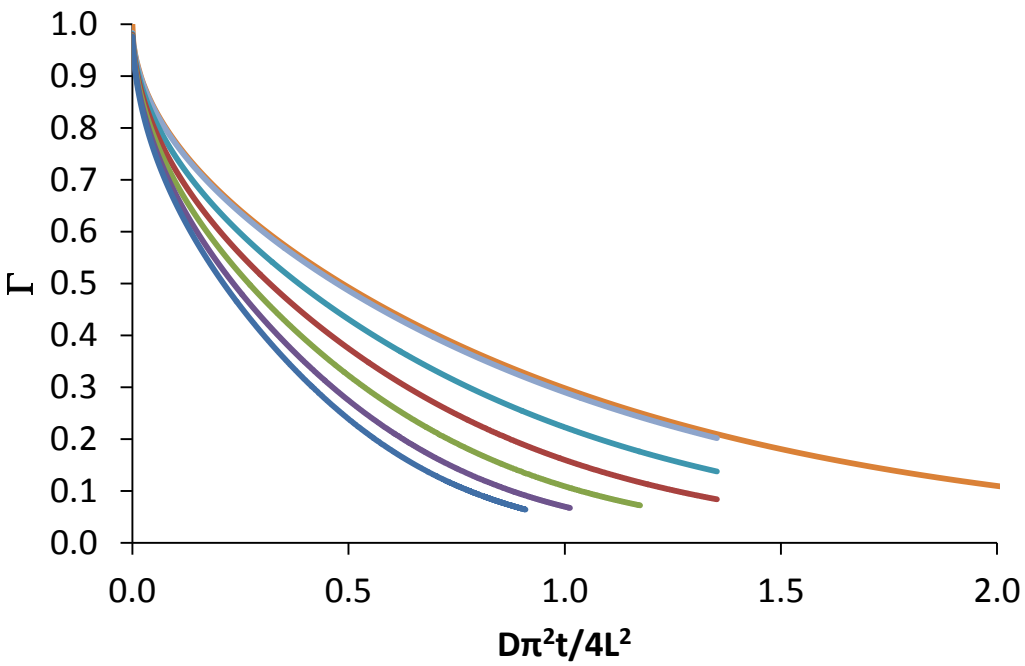


**Figure 2.2 - Numerically calculated drying curves for constant diffusion and film shrinkage for different final moisture contents. — = standard curve, — = $V_f$ 0.48, — = $V_f$ 0.4, — = $V_f$ 0.3, — = $V_f$ 0.2, — = $V_f$ 0.1, — = $V_f$ 0.02. In all cases *K* is infinite and $V_{in}$ = 0.5.**

It is clear that the more moisture that is lost results in a larger deviation from the original standard curve, thus highlighting the importance of including film shrinkage in the simulation.

Figure 2.3 demonstrates the effect of changing the initial moisture conditions. Each curve has the same final moisture content of 0.02. As the initial moisture content within the film is increased the curve becomes steeper suggesting an increased drying rate. This is likely to occur in a real life system as with a higher initial moisture content there will be a larger moisture concentration gradient driving the diffusion process.

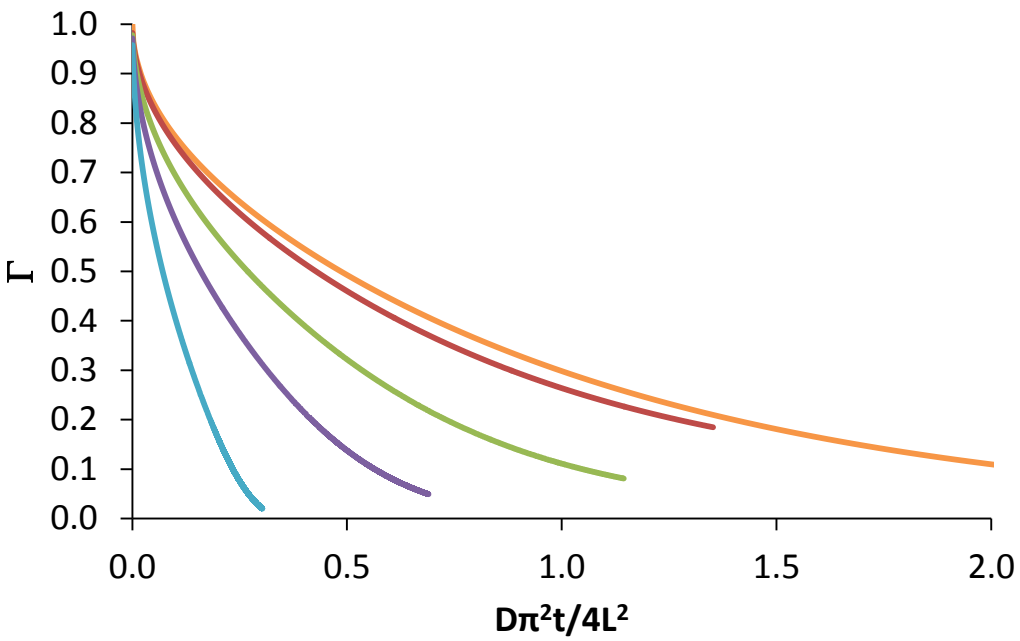


**Figure 2.3 - Numerically calculated drying curves for constant diffusion and film shrinkage for different initial moisture contents. — = standard curve, — = $V_{in}$ 0.2, — = $V_{in}$0.4, — = $V_{in}$ 0.6, — = $V_{in}$ 0.8. In all cases *K* is infinite and $V_f$ = 0.02.**

As in Figure 2.2, this figure demonstrates the importance of using the correct parameters when modelling the real life system, as great deviation is also seen when different initial moisture contents are used. This further supports the importance of incorporating film shrinkage into the model, and the unsuitability of the standard curve as an acceptable fit to all real life drying slabs.

### 2.3.3 Moisture dependent diffusion

From the literature it is clear that in many cases of dehydration the diffusion coefficient is moisture dependent. That is, as more moisture is lost, diffusion becomes slower. This could be due to several factors for example, a change in the properties of the material leading to plasticisation as the moisture is lost, or a surface skin, where the surface dries more than the bulk, trapping

water inside the material, and making diffusion more difficult, both of which result in a reduced diffusion rate.

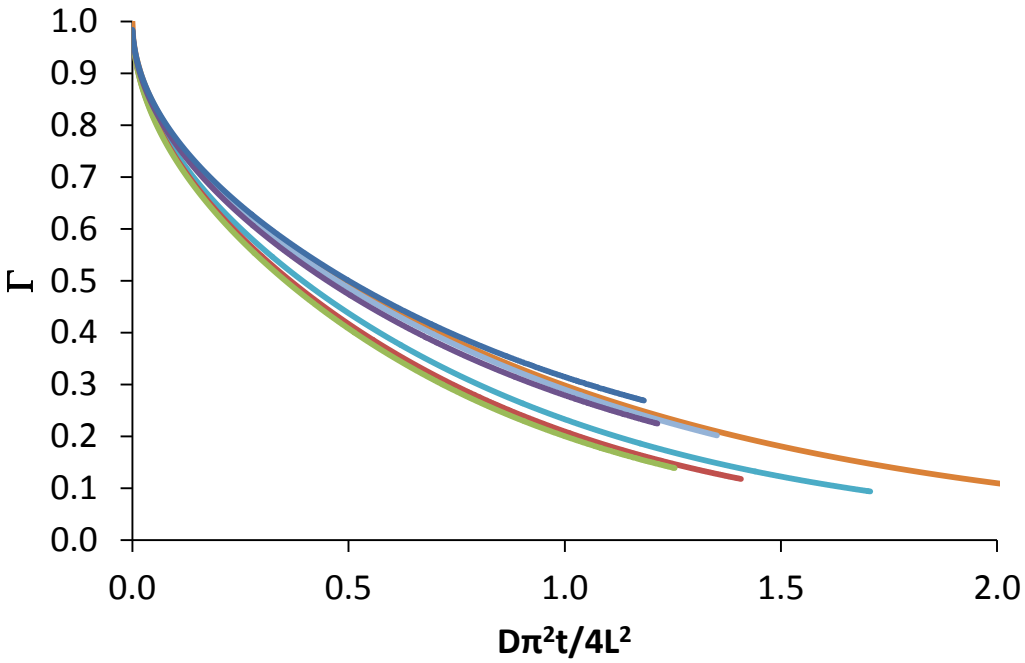


**Figure 2.4 - Numerically calculated drying curves for variable diffusion and film shrinkage for different final moisture contents. — = standard curve (with constant diffusion and film thickness), — = $V_f$ 0.48, — = $V_f$ 0.4, — = $V_f$ 0.3, — = $V_f$ 0.2, — = $V_f$ 0.1, — = $V_f$ 0.02. In all cases *K* is infinite and $V_{in}$ = 0.5.**

Figure 2.4 shows what happens when diffusion is variable throughout the dehydration process. In this simulation, the diffusion coefficient has been varied so that it corresponds to previous simulations, for the constant *D* case, at the point where 50% of the moisture loss has occurred. Again, the initial and final moisture contents lead to deviation from the standard curve, although it appears that the effect of film shrinkage and variable diffusion cancel each other out somewhat, when initial conditions remain constant, as even at low final moisture content, the curves lie much closer to the standard than for the cases with constant diffusion and shrinkage. One thing that is

particularly interesting is that the curves that most closely match the standard curve, besides the case where there is hardly any moisture lost (0.48), are those with the lowest final moisture contents of 0.1 and 0.02. From the simulations shown here, it is clear why, in some cases, the standard curve is sufficiently accurate to model dehydration, even though this may not be expected.

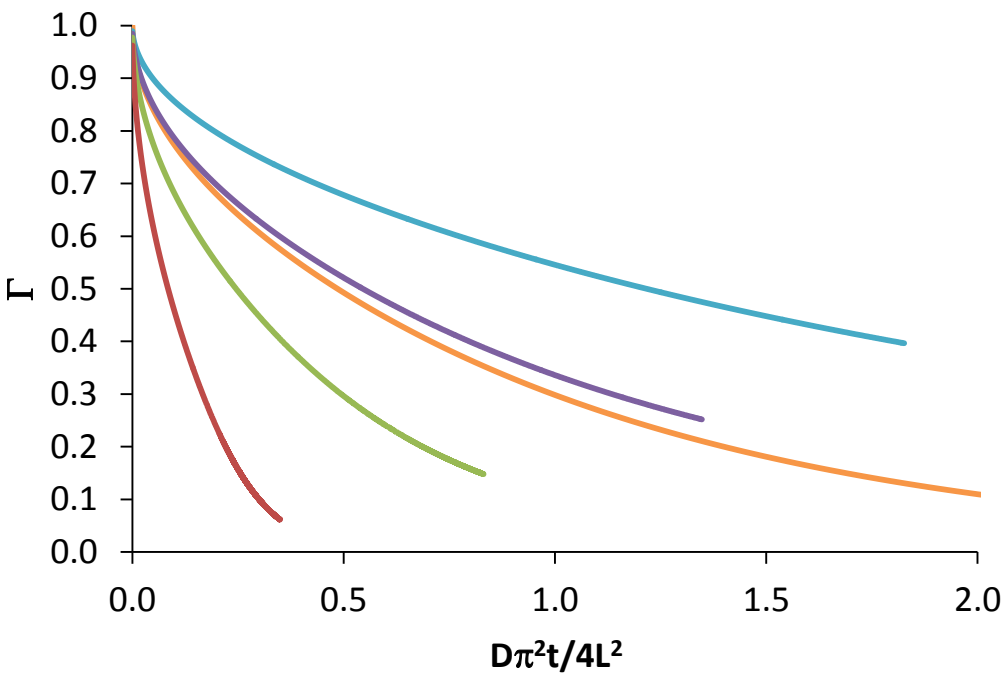


**Figure 2.5 - Numerically calculated drying curves for variable diffusion and film shrinkage for different initial moisture contents. — = standard curve, — = $V_{in}$ 0.2, — = $V_{in}$0.4, — = $V_{in}$ 0.6, — = $V_f$ 0.8. In all cases *K* is infinite and $V_f$ = 0.02.**

Figure 2.5 compares the simulation results for variable diffusion with different initial moisture contents. Again, as with constant diffusion, as the initial moisture content is increased the curve becomes steeper. Interestingly, the curve which deviates least from the standard curve has an

initial moisture content of 0.4, whereas when diffusion was constant the curve with the smallest deviation had an initial moisture content of 0.2. It is clear that there are several situations which can be modelled to an acceptable degree by the standard curve.

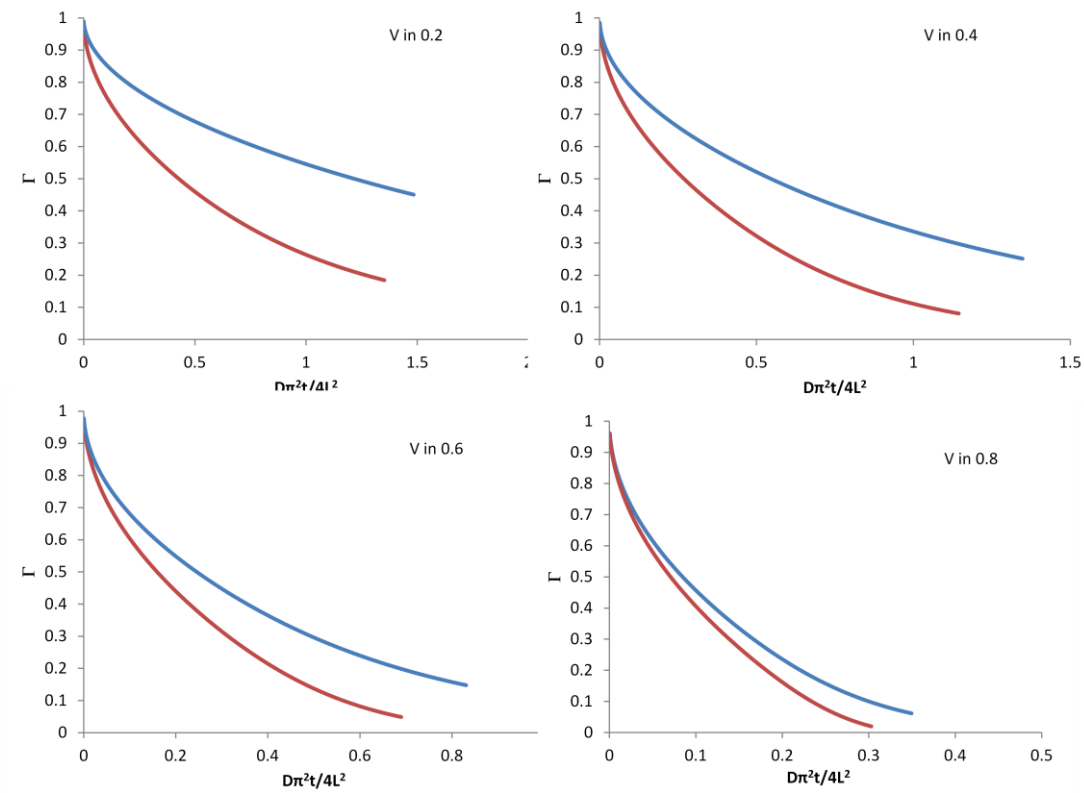


**Figure 2.6 - Comparison between drying curves for different initial moisture contents obtained for constant and variable diffusion coefficients, when *K* is infinite and $V_f$ = 0.02. — = constant *D*, — = variable *D*.**

In Figure 2.6 a comparison is made between the simulated drying curves for each initial moisture content with either constant or variable diffusion in order to highlight the deviation from the curves for a constant diffusion coefficient, when diffusion is varied with moisture content. It is interesting to see that as the initial moisture content increases, the deviation between constant and variable diffusion becomes less pronounced.

### 2.3.4 Drying Limited by Evaporation.

As discussed in the theoretical considerations section, when evaporation is taken to be the limiting factor in the dehydration of biopolymer films, and diffusion is infinitely fast so as not to have any effect on the drying, a simple curve is produced, if the assumption is made that there is no film shrinkage. This curve can be seen in Figure 2.7, and shows an exponential decrease in concentration with respect to time $c_w(t) = c_w^{eq} + (c_w(0) - c_w^{eq})\exp(-Kt)$. The axis Kt/L0 is used as equation 2.8 is implemented to obtain the plot.

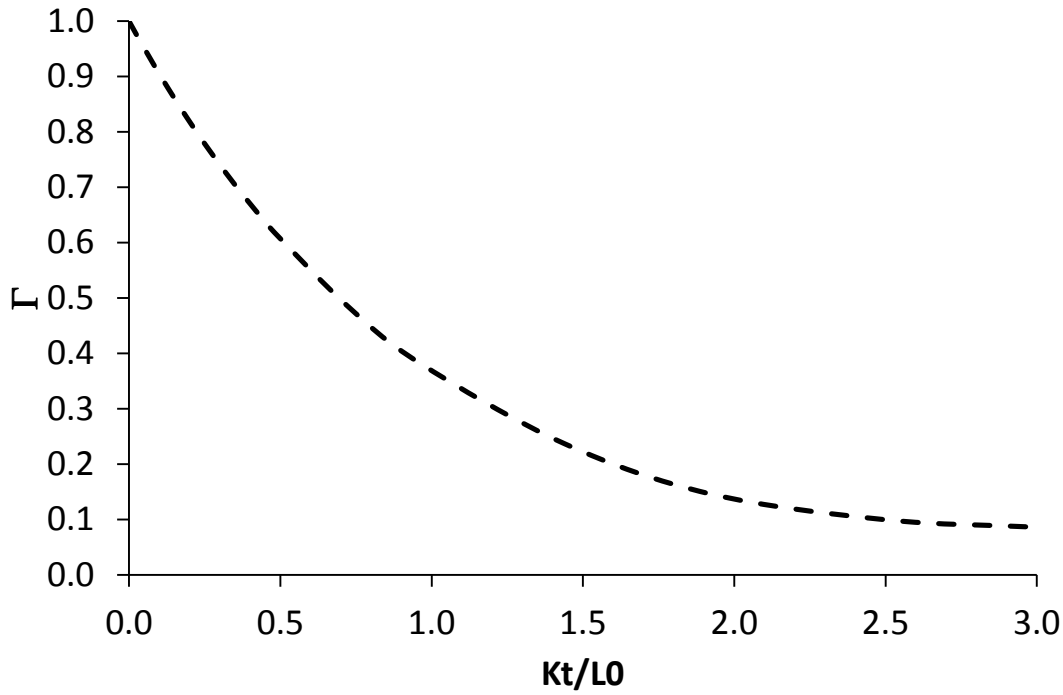


**Figure 2.7 - Mathematical model prediction for evaporation limited dehydration with constant film thickness.**

Of course, as seen with the diffusion limited simulations, when film shrinkage is taken into account we see a rather different picture, and once again the initial and final moisture contents have a distinct effect on the final shape of the curve. In Figure 2.8 the effect of the final moisture content is demonstrated. Once again, by changing the final moisture content, the

overall path of the curve is altered, however the shape of the curve remains the same for all final moisture contents. As the final moisture content becomes smaller, the gradient of curve becomes steeper. As the final moisture content becomes less than 0.01, there is only a slight effect on the curve generated. This is most likely because by the time the moisture content has reached 0.01 there is very little moisture remaining so only slight deviations will be seen towards the very end of the curve.

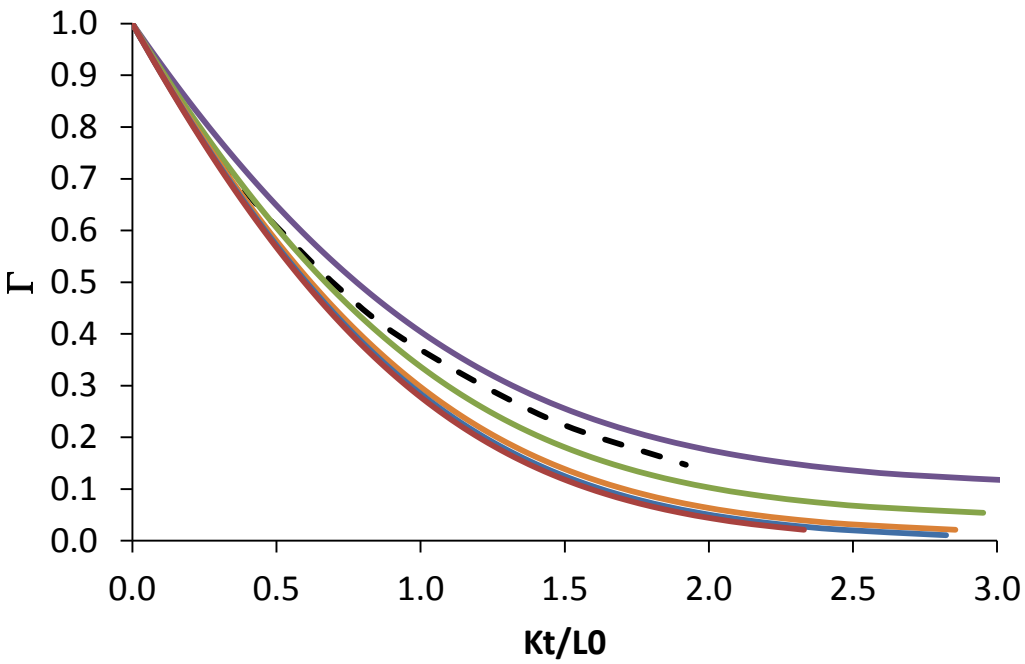


**Figure 2.8 - Evaporation limited drying curves with film shrinkage and different final moisture contents. --- = evaporation curve with fixed volume, — = $V_f$ 0.1, — = $V_f$ 0.05, — = $V_f$ 0.02, — = $V_f$ 0.01,— = $V_f$ 0.005. In all cases $V_{in}$ = 0.5.**

It is clear that all the curves generated for $\Gamma$ show a much more linear decrease with time than those generated in the diffusion limited simulations, showing that the two mechanisms affect the dehydration in very different ways. With changes in the film thickness included in the analysis, the dehydration curve is described by eq 8. This equation does not admit a

simple scaling relation between $\Gamma$ and scaled time $t/\tau$. However, if a system where $\phi^{eq} << \phi(0)$, is considered, then $\phi(t)L(t) >> \phi^{eq} L(\infty)$ for a considerable portion of the dehydration process. We can write $(1-\phi^{eq}) \approx 1$, $L(\infty) \approx (1-\phi(0)L(0)$ and $\Gamma \approx \phi(t)L(t)/(\phi(0)L(0))$. With these approximations, equation 2. 8, expressed in terms of $\Gamma$ now reads

$$\left(1-\phi(0)\right)\ln(\Gamma)+\phi(0)(1-\Gamma)=-\frac{Kt}{L(0)} \qquad \textbf{2.35}$$

For the initial stages of dehydration, where we have $(1-\Gamma) << 1$, the above equation gives an identical result to the exponential curve, i.e. $\Gamma \approx 1-\left(Kt/L(0)\right)$. At longer times, the shape of the curve is dependent on the initial moisture content.

Figure 2.9 shows the curves generated when different initial moisture concentrations are used. Again this figure demonstrates the importance of inputting the correct initial moisture content as it has a significant effect on the shape of the resulting curves. It is apparent that as the initial moisture content is increased the resulting curve becomes more linear. This is important because if the value input for the initial moisture concentration did not match the actual moisture content of the system being modelled, the results would not be expected to fit the experimental data. Interestingly, for the case where the initial moisture content is 0.2, very little deviation is seen from the exponential curve. This is likely to be due to the large amount of solid present in the film at the start of drying, which may permit only a relatively small change in film thickness. As the initial moisture content is increased, the curve becomes steeper and deviates further, and sooner, from the exponential curve as seen in Figure 2.9.

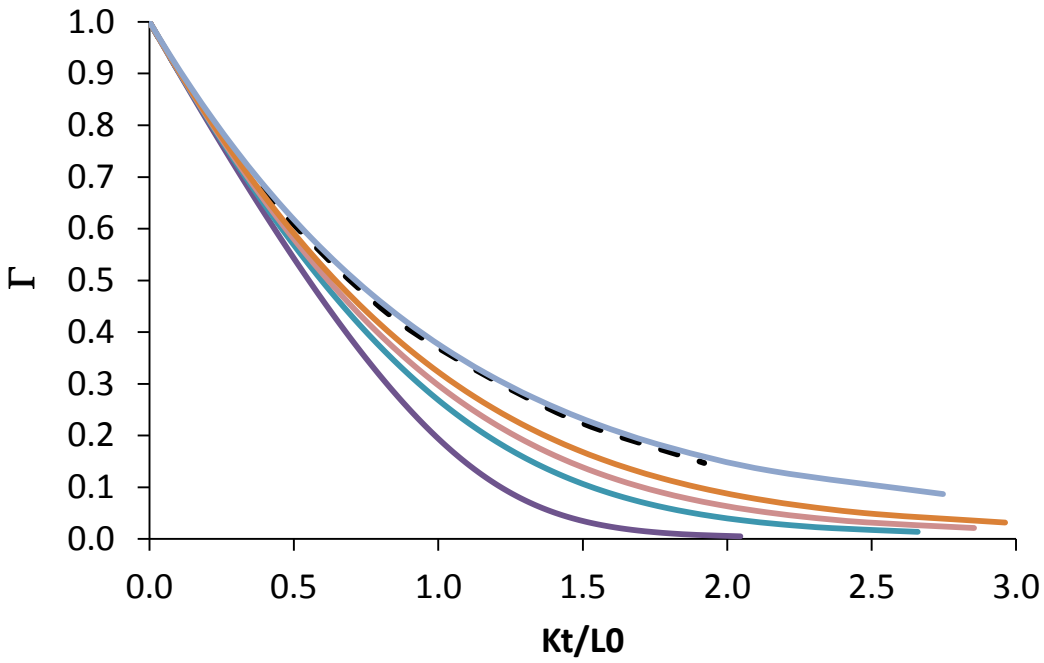


**Figure 2.9 - Evaporation limited drying curves obtained, with film shrinkage and different initial moisture contents. --- = evaporation curve with fixed volume, — = $V_{in}$ 0.8, — = $V_{in}$ 0.6, — = $V_{in}$ 0.5, — = $V_{in}$ 0.4, — = $V_{in}$ 0.2. In all cases $V_f$ = 0.02.**

### 2.3.5 Modelling dehydration that is controlled by both diffusion and evaporation

In a real life system it is unlikely that dehydration would be controlled by just one of these two mechanisms. In this section, simulations which take both the effect of internal diffusion and the effect of surface evaporation into account are considered. The simulations used to construct the diffusion limited models have also been used to construct the models shown here, however the evaporation term used has been modified by several orders to emphasise its importance. In Figure 2.10 the curves have initial and final moisture contents of 0.5 and 0.02 respectively, and the value of D used is

that of previous simulations 5.48 x$10^{-10}$ $m^2s^{-1}$. The evaporation constant is varied from being infinite, where evaporation is fast enough to be assumed instantaneous, to a value four orders of magnitude less, resulting in a much slower and limiting evaporation. It is obvious that as evaporation becomes the more dominant limiting factor the resulting curve becomes more linear, and completely different from the curve generated for the case where diffusion in the only limiting factor.

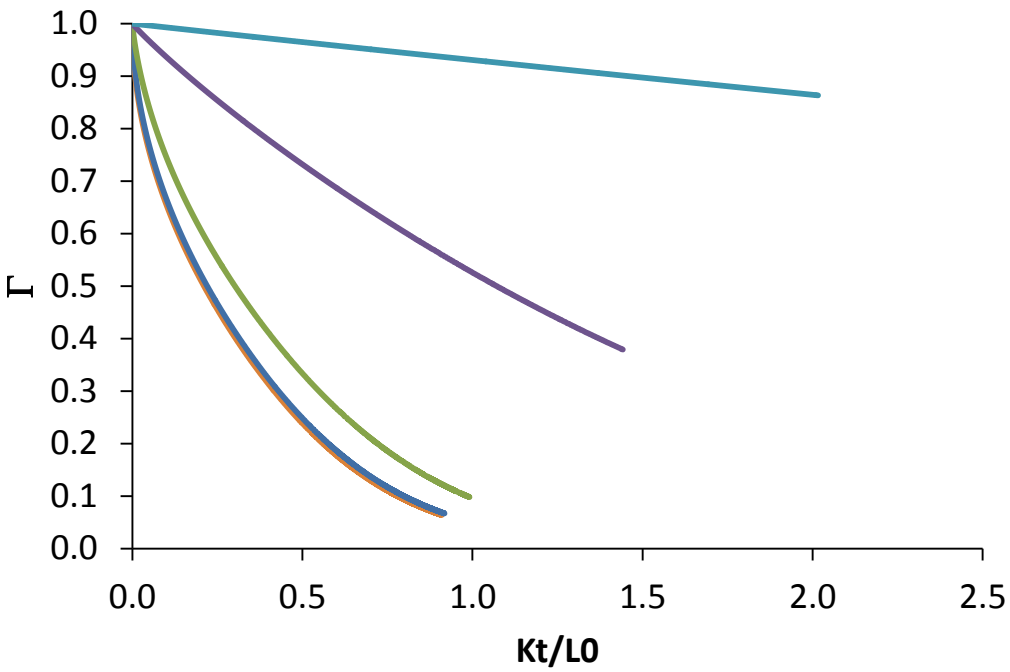


**Figure 2.10 - Graphs showing the effect of increasing importance of evaporation in the diffusion limiting simulations. . — = K∞, — = *K*= 0.1, — = *K* = 0.01, — = *K*= 0.001, — = *K*= 0.0001. In all cases *D* = 5.48x$10^{-10}$ $m^2s^{-1}$, $V_{in}$ = 0.5 and $V_f$ = 0.02.**

## 2.4 Conclusions

In this chapter the dehydration of thin biopolymer films has been explored from a theoretical point of view. Models were created to numerically calculate dehydration under different initial and final moisture conditions, initially based on Fick's laws to investigate diffusion, followed by a numerical

solution for evaporation limited dehydration. It was found that when a diffusion coefficient that varied with moisture content was used, for any final moisture concentration, there was much less deviation from the standard curve than when the diffusion coefficient was constant. This suggests that by having a variable diffusion coefficient, the effect of film shrinkage is partially compensated for, thus it becomes apparent why, in some cases, the standard curve is sufficient to describe the drying behaviour of some materials. Unlike most previous calculations, this scheme allows for the changes in film thickness occurring as a result of the variation of local partial molar volumes with evolving composition, as the drying progresses. This is in addition to the more usual shrinkage due to the loss of moisture. Under most circumstances the partial molar volume of water in mixed systems of water and biopolymer can be considered as almost constant. However, the main motivation for considering such a generalised situation was to derive a set of equations applicable to the drying, even when the structure of the solid phase changes appreciably during the dehydration process. A particular example is when the solid phase in an initially fluid biopolymer solution begins to develop a stress supporting porous structure. In such a system the loss of water will no longer lead to the shrinkage of the film. This can be modelled by taking the effective partial molar volume as a composition dependent variable which approaches zero once a solid structure with a sufficient yield stress is formed. This model could be used in future to investigate dehydration in thin films where such changes in the structure of the biopolymer solutions are prevalent. The effect of including film shrinkage in the diffusion and indeed evaporation equation causes significant deviation from the standard curves produced for diffusion limited, or evaporation

limited cases, where film thickness remains constant throughout the dehydration process. Incorporating film shrinkage into the models, the importance of the initial and final moisture contents of the film in question has been highlighted. Finally combining both diffusion and evaporation into the simulation, the shape of the curve becomes more linear, demonstrating that the diffusion coefficient and evaporation rate are both potentially important factors in the dehydration of thin biopolymer films.

# Chapter 3 Dehydration of thin biopolymer films

## 3.1 Introduction

Thin biopolymer films have many important applications in industry, particularly as adhesives (Price et al., 1997), paints (Henshaw et al., 2006), in the food industry as edible coatings (Janjarasskul and Krochta, 2010), and the pharmaceutical industry as drug delivery systems (Janjarasskul and Krochta, 2010, Guo et al., 2011). The requirements and criteria are often very different for different dehydration applications. It is therefore important to understand the mechanisms involved in the drying process of these biopolymer films. For instance, if a film dries too rapidly, defects such as cracks and large voids can occur which weaken the films and reduce their performance. On the other hand, if a film dries too slowly, dripping may occur, an undesirable effect in the case of coating and labelling applications.

### 3.1.1 Mechanisms of dehydration

Temperature, relative humidity and air flow velocity are all important external parameters when controlling drying rate. However, the diffusion of moisture within the internal film structure is also a major factor when considering how the film dries. In some cases drying can be split into an initial constant rate period where free moisture from the surface is removed, followed by two falling rate periods whereby diffusion in the bulk is the main transfer mechanism. However, this only applies to systems which start with a layer of saturated moisture on their surface and the initial moisture loss can be compensated fully by the fast moisture diffusion.

Water can be present in different molecular environments depending on its interactions with the surrounding molecules. Initially, most of the water molecules in a polymer network are in free water status ($a_w$ = 1) like those in bulk phase water, surrounded by other water molecules, and so can diffuse through the system without significant restriction. An exception to this, however, is if the material has small pores throughout the bulk, in which case capillary pressures may limit this diffusion. This so-called free water is lost during the constant rate and the first falling rate period.

Once all the free water has evaporated, the rate of dehydration slows and the second falling rate period becomes apparent. Loosely bound water requires extra energy for breaking up hydrogen bonding. Practically, it is very difficult to differentiate the different mechanisms involved in moisture diffusion. Therefore, an effective, moisture dependent diffusion coefficient is used in the analysis of rate of dehydration. This allows all the different mechanisms discussed in Chapter 1 to be taken into account in one single diffusion coefficient. In most dehydration applications bound water remains untouched in the dried film. Often, and in particular in foods, an initial constant rate period is not observed (Saravacos and Maroulis, 2001).

### 3.1.2 Structural changes during dehydration

During dehydration, changes in the structure of the polymer film may occur. The most common structural change encountered is film shrinkage, which is directly related to moisture loss due to drying (Ramirez et al., 2011). As the film dries and moisture is lost, a pressure imbalance between the inside and outside of the film develops. This pressure imbalance results in the build up of mechanical stress within the film, which leads to possible shrinkage,

collapse or cracking of the film in order to release the stress. The increase of stress and its subsequent decrease due to structural relaxation within a drying film has been experimentally measured by Chen *et al* (2009). The dynamics of stress evolution within the film depends significantly on the internal structure of the film.

Film cracking is most prevalent in the drying of colloidal particulate dispersions, or solutions of film forming polymers below their glass transition temperature, where the structural relaxation times are long (Dragnevski et al., 2010, Georgiadis et al., 2011). A porous structure allows moisture to migrate to the surface through channels without film shrinkage or loss of volume occurring during the drying process. Various models of transport, dealing in particular with the presence of porous structures in foods and similarly related biological systems, have been reviewed by Datta (Datta, 2007a, 2007b, Datta and Rakesh, 2009).

### 3.1.3 Methods used to investigate drying in the literature

There are many different methods reported in the literature to monitor and investigate aspects of drying. These range from advanced analytical techniques to simple gravimetric methods.

NMR diffusion measurements have been used to investigate microstructural changes during drying (Griffith et al., 2009). This is a non-invasive technique which provided an insight into the behaviour of individual droplets within detergents. Schmidt-Hansberg *et al* (2009) used reflectometry to monitor the drying kinetics of polymer films. A laser beam was shone on the sample and the reflected beam was detected using a silicon photodiode, throughout the drying process, in order to collect data on the film thickness which was used

to create moisture loss vs time curves. The intensity of fluorescence given off by polymers as they dry has also been monitored (Evingur and Pekcan, 2011a, Tari et al., 2011) where, as more water is released from a polymer, an increase in intensity of the pyranine- based fluorescence is seen. Results obtained using this method are supported by gravimetric and volumetric data, and type II diffusion models, where Fick's laws cannot describe the entire process, fit the data well.

The simplest method for monitoring drying kinetics is the gravimetric method. This is a macroscopic method that is the most prevalent of the techniques that are reported in the literature (Ramirez et al., 2011, Day et al., 1992, Seth and Sarkar, 2004, Thuwapanichayanan et al., 2011). It is easily applicable to all shapes and sizes for a wide range of materials. It is a straightforward procedure where the sample is dried under a controlled temperature and relative humidity, and the sample is weighed over set time intervals. The method is popular because the weight change with time is easy to measure, and if carried out *in situ*, does not cause any disturbance to the sample's drying environment which could potentially lead to inaccuracies in the drying data. The method has also been used in the study of rehydration and ingress of water into polymer coatings, although this is a somewhat different problem to that of dehydration considered in this chapter (Krzak et al., 2012) and will be considered further in Chapter 5.

### 3.1.4 Modelling the dehydration process

Assumptions made in mathematical models to simulate such drying processes as those discussed above must reflect these diverse behaviours

in order to provide an accurate and reliable representation of the drying process. A further explanation of this can be found in Chapter 2.

During the drying of the biopolymer films, initially, as moisture is lost from within the film, the film shrinks due to the lack of a stress supporting structure. There comes a point however, at which although moisture continues to be lost there is no further shrinkage and the solid fraction forms a porous structure with a yield stress that can support the stresses developed in the film. No further volume changes occur at this point. In order to be able to model the entire dehydration process, encompassing both these different behaviours, it is important to consider the general case where the effective molar volumes, if not the true values, of both the solid and the water phases alter during the process. This was discussed in greater detail in Chapter 2.

In most cases when thin films are dried, the controlling factor is diffusion of the moisture within the film (Ruiz-Lopez et al., 2012, Zogzas and Maroulis, 1996). The rate of evaporation when moisture reaches the surface is assumed rapid enough to be almost instantaneous and therefore it does not constitute the controlling factor of the drying of the film. This is reflected in the simplest mathematical models by taking the moisture content at the surface of the film as always being at equilibrium with the moisture in the air above. Furthermore, such models are mostly based on Fick’s second law of diffusion with either a constant diffusion coefficient (Ramirez et al., 2011, Day et al., 1992, Seth and Sarkar, 2004, Czaputa et al., 2011, Nizovtsev et al., 2008), or in some cases a variable diffusion coefficient that changes with moisture ratio. More sophisticated models attempt to take shrinkage of the drying material into account, by using moving boundary conditions

(Thuwapanichayanan et al., 2011, Nahimana et al., 2011). In most cases these simple mathematical models have been found to give a reasonable fit to experimental data, and in the literature many use these as a satisfactory approximation. However, as our work demonstrates a more complex model may be required to give a more reliable representation of the drying process (Zogzas and Maroulis, 1996).

In this chapter, mass transfer during dehydration of several thin biopolymer films under controlled temperature and relative humidity is examined. Experimental results are compared with several mathematical models based on Fick's second law of diffusion and incorporating the following different scenarios:

i) the dehydration involves both constant and variable diffusion coefficients, as well as film shrinkage, with the evaporation rate being high and therefore not the limiting factor in the drying process;

ii) the diffusion is instantaneous and the evaporation rate is the controlling factor; and

iii) both diffusion and evaporation have a role in controlling the drying rate.

These models have already been discussed in detail in Chapter 2. The ultimate aim of this work is to establish a mathematical model which adequately describes the dehydration behaviour of thin biopolymer films as found in the present work.

## 3.2 Materials and methods

### 3.2.1 Materials

The biopolymers investigated in the dehydration experiments were 18 wt% sodium caseinate (purchased from Acros organics, Belgium) solution, 7 wt% purity starch (provided by Henkel, Germany) solution, and a mixture containing 9 wt% sodium caseinate and 4.5 wt% starch. The samples were prepared by dissolving the powder in distilled water at 90 °C under magnetic stirring for 1.5 h. Sodium azide (0.02 wt%) was added as a preservative, and 10 drops of defoamer (Agitan 299, Munzing corporation) were added to avoid the formation of bubbles. All samples were stored at operating temperature and used within three days of preparation.

### 3.2.2 Dehydration of thin biopolymer films

The dehydration experiments were carried out in a purpose built, wood framed Perspex chamber, with dimensions of 710 mm × 445 mm × 705 mm (length × width × height), designed and made in house. The chamber has an accurate temperature control that allows the chamber to be set at any temperature between room temperature and 50 °C, with an accuracy control of ±0.5°C. The relative humidity was controlled reliably by continuous supply of dry air and wet air, bubbled through pure water, into the chamber at a combined rate of 10L/min. The dry air was obtained by passing controlled air through a drying column (Beko drypoint, UK). The ratio of wet to dry air can be controlled to achieve the desired relative humidity within the chamber. The chamber also has a fan to create a gentle air flow so that air homogeneity can be maintained throughout the entire system. The relative humidity conditions investigated include 20%, 30%, 40% and 50%,

measured by hygrometer, with the temperatures set to 30 °C, 40 °C and 50 °C. The chamber houses a beam coating system which consists of a moveable platform with a stainless steel beam (80 mm x 12.6 mm x 0.4 mm) attached. On the left hand side wall of the chamber is a coating gate of 0.4 mm. A small volume of thermally equilibrated sample was first deposited on the beam. The beam is then pulled through the coating gate at a constant speed using a stepper motor to ensure an even coating of film, with a thickness of 0.4 mm and width of 10.6 mm, across the full length of the beam. This setup and procedure has also been applied, and illustrated in a previous study where the stress measurements within drying films were reported (Chen et al., 2009). The coated beam is then placed on a balance inside the chamber and the weight loss is monitored *in situ* at set time intervals, of 2 minutes for the first hour then every 30 minutes for 4 hours.

### 3.2.3 Monitoring shrinkage of biopolymer films

To measure film shrinkage of the biopolymer films as they dried, the apparatus shown in Figure 3.1 was used, consisting of a Perspex chamber with temperature control provided by a Peltier fan system (Stable Micro Systems, UK). The shrinkage was investigated at the temperatures indicated in 3.2.2, used for the drying experiments. Relative humidity was monitored, and found not to vary dramatically between experiments, at 25 ± 5%. First, a stainless steel metal beam, as used in 3.2.2 was coated with biopolymer solution at the desired temperature using the coating gate also described in 3.2.2. The coated beam was transferred to the chamber and positioned on a stage in front of a CCD video camera (Optivision, UK) with microscope attachment. There was a time lapse of under two minutes in transferring the beam from one device to the other and positioning correctly for focussed

images to be obtained. The drying film was captured at a frame-rate of 0.25 fps (frames per second) over the entire drying period, and the resulting video was converted to individual jpeg images for analysis. The total height of the film was measured using ImageTool 2.0 freeware.

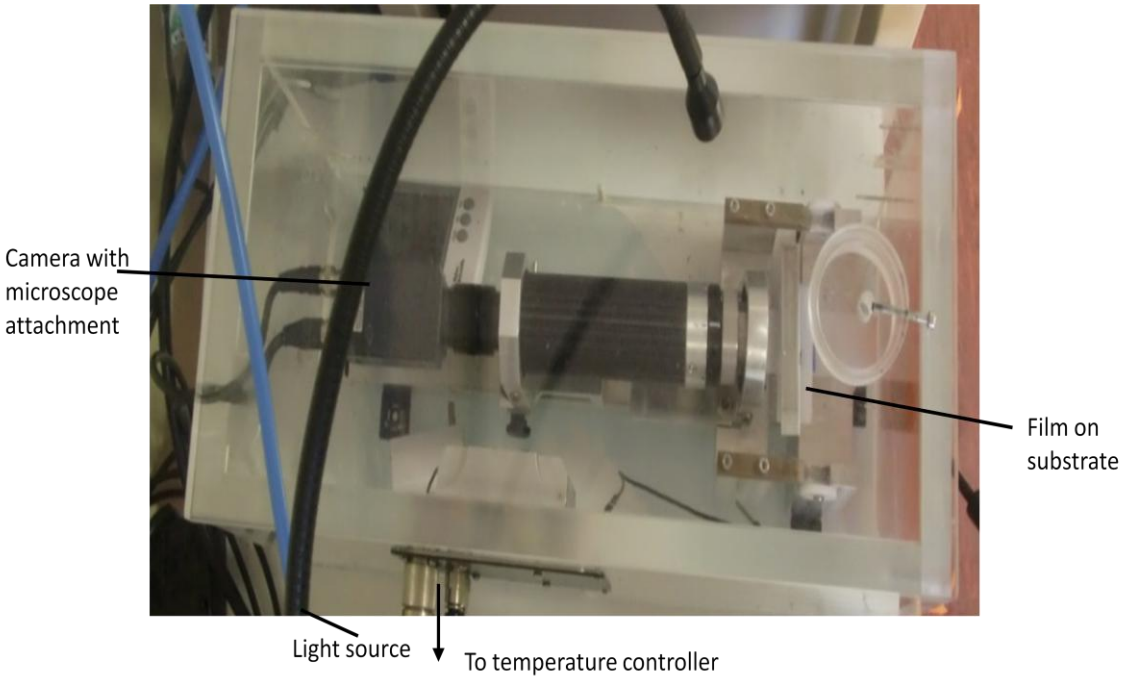


**Figure 3.1 - apparatus setup for monitoring film shrinkage.**

## 3.3 Results and discussion

### 3.3.1 Film shrinkage during biopolymer dehydration

In this section, the results of the film shrinkage investigation will be discussed. Film shrinkage is an important phenomenon to consider because, as demonstrated by the results presented in Chapter 2 regarding the modelling of diffusion and indeed evaporation limited dehydration, the drying curves will be considerably different when shrinkage occurs as opposed to the volume remaining fixed. The main objective here is to establish whether the films are shrinking or not as they dry. Figure 3.2 and Figure 3.3 show the

film shrinkage as a function of time at different temperatures for 18 wt% sodium caseinate and 7 wt% starch solutions.

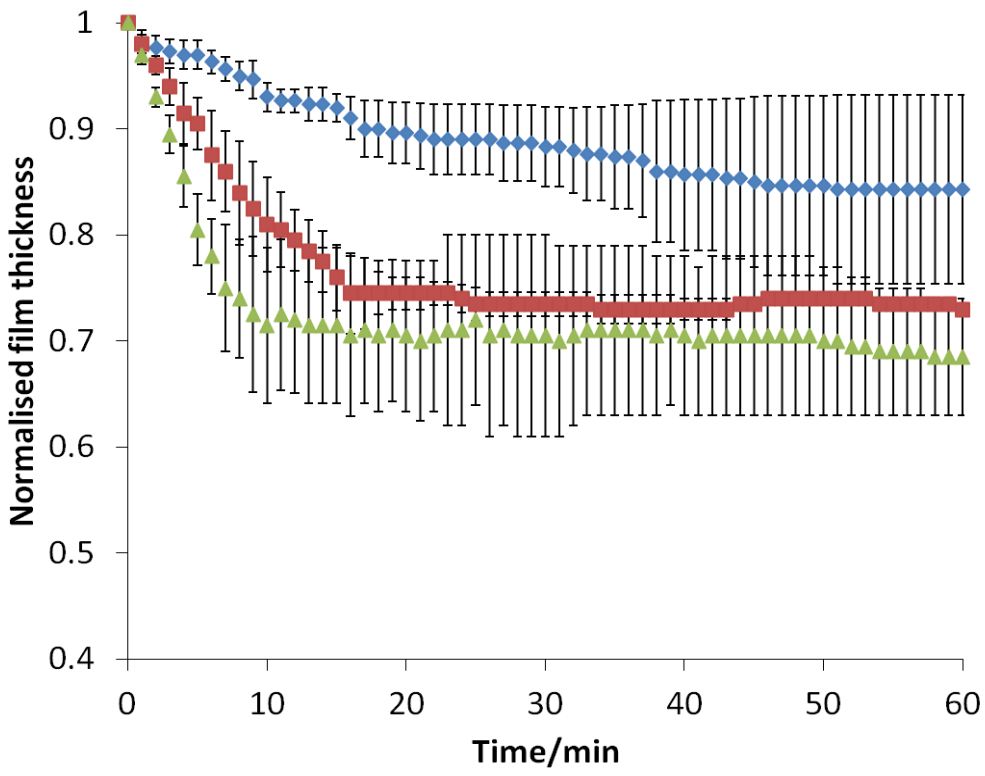


**Figure 3.2 - Changing film thickness of 18wt% sodium caseinate solution at different temperatures ♦=30°C, ■=40°C, ▲=50°C at 25 ± 5% RH plotted against time.**

These data clearly show that in both systems significant film shrinkage is occurring during the drying process. In both cases the film shrinks during the initial period of drying, with the caseinate film reaching a reasonably smooth plateau after only approximately 15 minutes. When comparing these results to those shown in Figure 3.4 in the following section, it is obvious that moisture loss continues long after the film has reached a constant volume. This suggests that after this point the film structure is strong enough to support further stresses caused by further moisture loss. It is likely that a porous structure may have formed to allow the continued moisture loss that

is seen later in this chapter. A similar trend can be seen for starch at 30 °C and 40 °C. At 20 °C however, after 60 minutes the film still appears to be losing volume. Temperature appears to have more effect on the starch system than the caseinate system with respect to the rate of film shrinkage, an interesting result when compared with figure 3.4, where temperature affects the moisture loss of caseinate more than starch.

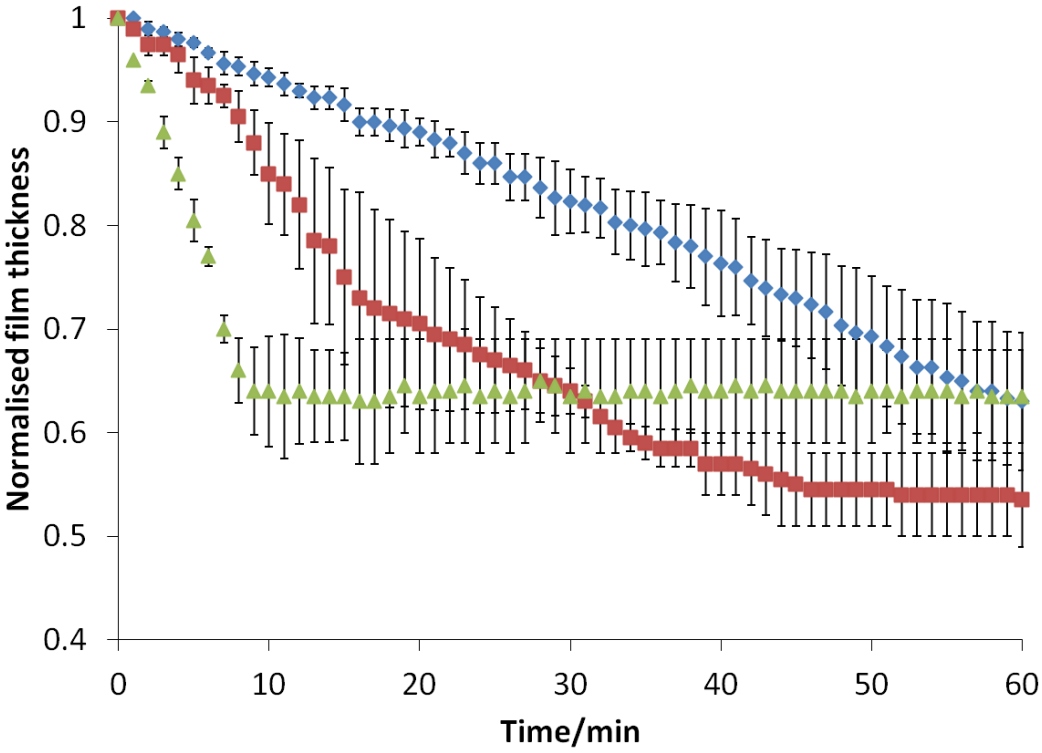


**Figure 3.3 - Changing film thickness of 7wt% starch solution at different relative humidities ♦=20 °C, ■=30 °C , ▲= 40 °C at 25 ±5% RH, plotted against time.**

The receding boundary at the film air interface will continually increase the moisture gradient formed inside the film as compared to if the boundary was in a fixed position. This means that the driving force behind the diffusion of moisture to the surface is higher, resulting in faster moisture loss. This was clearly demonstrated in Chapter 2 Figure 2.2 where the effects of including

film shrinkage into the drying simulations are compared to cases not involving shrinkage.

The data is quite noisy, with large error bars seen in Figure 3.2. This error is likely a systematic one, due to the lack of ability to control relative humidity. This means that experiments conducted at different times of day may have had different external conditions, leading to a higher relative humidity than for other samples of the same composition. Although the reproducibility of the data is not excellent due to this, and the other experimental limitations of having to move the coated substrate from one piece of apparatus to the other, and the time lost in focussing the camera, it is sufficient to confirm that the films are in fact shrinking as they dry, supporting the necessity of inclusion of a moving boundary if the numerical calculations are to be fitted to the experimental drying curves.

### 3.3.2 Dehydration of thin biopolymer films

#### 3.3.2.1 The kinetics of dehydration of biopolymer films

The three biopolymer systems used were chosen for their highly contrasting structures and properties. Casein and starch are both commonly used in industry in the formulation of edible films, though the films they form have vast differences. Casein forms a strong homogeneous protein network whereas starch, being a polysaccharide, has a more granular, brittle film structure prone to cracks and faults.

A mixed system of casein and starch was also investigated to see if the addition of casein could help the film formation in polysaccharide based systems. Starch is considerably cheaper than casein and so replacing even a small proportion of casein with starch would significantly reduction in the

commercial costs of the product. The concentrations used were chosen so as to give similar viscosity and flow behaviour for all solutions.

Figure 3.4a-c show how the drying behaviour of sodium caseinate, starch, and sodium caseinate-starch mixed films respectively, changes under different temperature conditions, under a constant relative humidity of 30%.

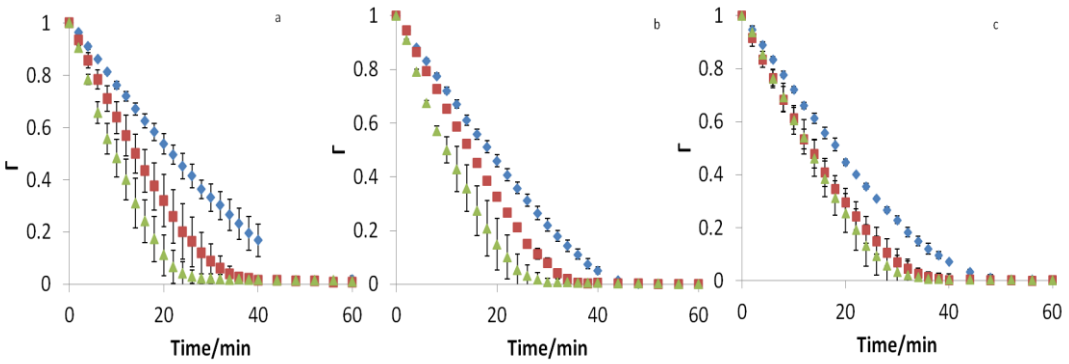


**Figure 3.4 – Plots of $\Gamma = (L(t)\phi(t)-L(\infty)\phi^{eq})/(L(0)\phi(0)-L(\infty)\phi^{eq})$ against time for three systems at RH 30% a) 18 wt% sodium caseinate solution, b) 7 wt% starch solution, and c) 9 wt% sodium caseinate:4.5 wt% starch mixture solution at different temperatures ♦=30°C, ■=40°C, ▲=50°C at 30% RH.**

The moisture ratio, $\Gamma$, defined as $(L(t)\phi(t) - L(\infty)\phi^{eq})/(L(0)\phi(0) - L(\infty)\phi^{eq})$, was plotted against time. The quantities $\phi_t$, $\phi^{eq}$, and $\phi_0$ are the moisture content at time *t*, the final equilibrium moisture content, and the initial moisture content respectively, calculated from the film mass, with *L(t),(0) and* (∞) being the film thickness at time t, initially and at t∞ respectively. In all cases, one can see that as temperature increases, the rate of drying also increases, as indicated by the more rapidly falling curves. This is because of two factors. At higher temperatures, the water molecules within the film have more kinetic energy (Atkins and De Paula, 2006), and thus can diffuse more

quickly to the surface, where moisture loss occurs, resulting in a faster rates of drying than that at lower temperatures. Secondly, an increase in temperature will also result in faster evaporation from the surface of the film. However, the effect of increasing the temperature is noticeably greater for the sodium caseinate system as compared to the starch and mixed systems. In particular, it should be noted that a temperature increase from 40 °C to 50 °C in the mixed system only results in a very small increase in drying rate, a behaviour that differs from both sodium caseinate and starch based systems. This suggests that the two components may have some sort of synergic interactions leading to networks that have a larger water holding capability.

As expected, relative humidity also plays a role in the drying behaviour, as seen in Figure 3.5a-c. As relative humidity of the surrounding air increases, the rate of moisture loss decreases. An increase in relative humidity means that the surrounding air is more saturated and so the moisture gradient between the surface of the film and its surroundings is smaller, thus limiting the rate of moisture loss. However, below 30%, the relative humidity has little effect on the drying of starch films, with the moisture ratio vs time curves at 20% and 30% relative humidity being almost identical to each other. At 40% relative humidity however, a slightly slower decline in moisture ratio is observed. This result suggests that for starch films, the external relative humidity of the surrounding air plays a lesser role than the temperature in the drying process. Conversely, changing the relative humidity conditions has more of an impact on the drying curves for the mixed system as compared to temperature.

It is constructive to examine the data in graphs of Figure 3.4 and Figure 3.5 to see if a constant rate period and two distinct falling rate periods, often reported in the literature on drying of foods, can be identified here. This has been done in the graphs of Figure 3.6 and Figure 3.7. Figure 3.6a-c display the time variation of the drying rate for the three systems, at three different temperatures.

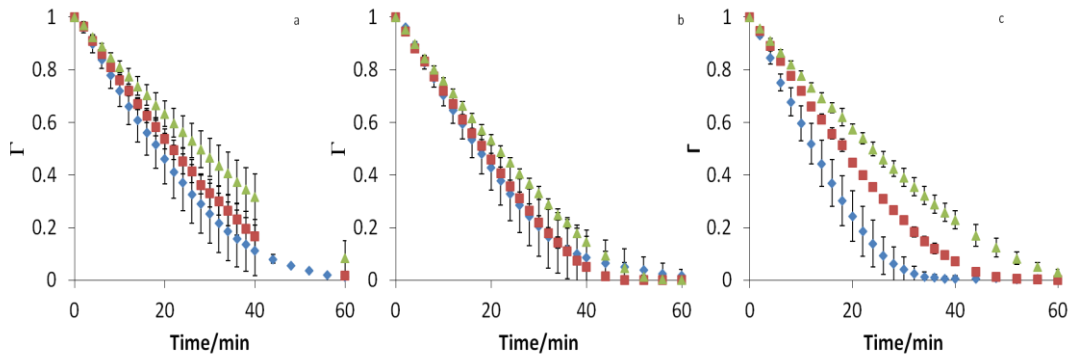


**Figure 3.5 - Plots of *Γ* against time for three systems at 30 °C a) 18 wt% sodium caseinate system, b) 7 wt% starch system, and c) 9 wt% sodium caseinate:4.5 wt% starch mixture system at different relative humidities ♦=20% RH, ■=30% RH, ▲=40% RH at 30°C.**

The drying rate is calculated as $(W_n - W_{n+1})/W_\infty(t_{n+1} - t_n)$, where $W_n$ is the weight of the film at the $n^{th}$ reading. i.e. the difference between two consecutive weight measurements, divided by the final weight recorded at equilibrium, and the time interval between the two. The equilibrium film weights can be found in Appendix 1 for the different compositions and conditions. Data of this type, involving finite differences, are normally quite noisy and the results are no exception in this respect, therefore the data presented in Figure 3.6 and Figure 3.7 use a 3 point average in order to make the results easier to interpret. The graphs in Figure 3.7a-c show the same data but now obtained at different values of air humidity. No clear

constant rate period is evident in any of the cases presented here. In general for all graphs shown in Figures 3.6 and 3.7, the drying rate is fastest at the start of drying, dropping rapidly to a lower value later on as the process progresses further. This phenomenon was observed for all three systems and may suggest that the surface of the films are drying quicker than the bulk, thus resulting in the decrease in drying rate observed in Figure 3.6 and Figure 3.7. Also it is evident that in some cases there appears to be no obvious transition between the two expected distinct falling rate periods. These different drying regimes are assumed to be associated with different mechanisms of movement of moisture to the surrounding air (Datta, 2007b). In the constant drying period there is sufficient free water on the surface. The rate of drying is fixed in accord with equation 2.1, with the surface moisture concentration remaining constant, the same as that for free water. Typically, during the falling rate period moisture is migrating through the bulk of the film to the surface, and the drying rate is decreasing with time. In the first falling rate this is in the form of liquid water. The second falling rate would occur when the surface is almost completely dry and dehydration involves removal of the partially bound water molecules and transport of this water within the interior pores to the surface. However our systems do not exhibit any clear trends towards this behaviour. Therefore, if diffusion is the controlling factor in the dehydration process, it seems more appropriate to interpret the drying rate curves in terms of a changing diffusion coefficient, $D$, for water molecules, varying smoothly with the amount of moisture present at any point in the film. In fact, it turns out that evaporation is the main factor in control of the drying, not diffusion, as will be shown shortly.

The continuously falling nature of the drying rate becomes even more pronounced as temperature decreases (Figure 3.6) and relative humidity increases (Figure 3.7). Again, as highlighted in Figure 3.5b, the effect of relative humidity on the starch system is minimal.

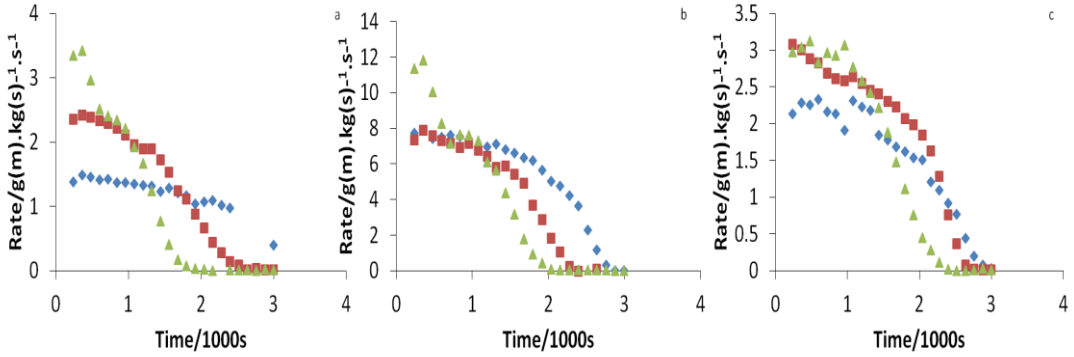


**Figure 3.6 - Drying rate vs. time graphs at 30% RH for a) 18 wt% sodium caseinate solution, b) 7 wt% starch solution, and c) 9 wt% sodium caseinate:4.5 wt% starch mixture solution at different temperatures ♦=30°C, ■=40°C, ▲=50°C**

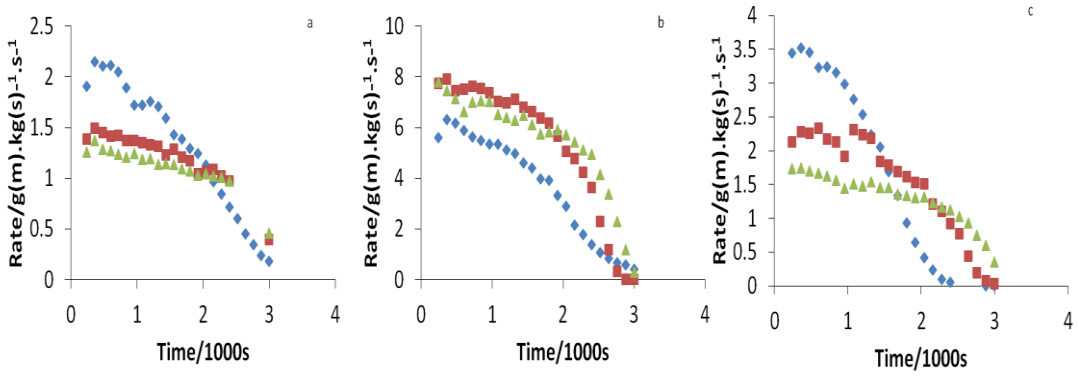


**Figure 3.7 - Drying rate vs. time graphs at 30 °C for a) 18 wt% sodium caseinate solution, b) 7 wt% starch solution, and c) 9 wt% sodium caseinate:4.5 wt% starch mixture solution at different relative humidity values ♦=30% RH, ■=40% RH, ▲=50% RH**

### 3.3.2.2 Comparison of theoretical and experimental data of biopolymer film dehydration

Mathematical models were constructed as described in Chapter 2. Figure 3.8 shows three different curves simulating the dehydration process based

on Fick's second law of diffusion, as described by equation 2.17. In all these cases, it is assumed that the diffusion process is the limiting factor in determining the drying rate, with evaporation being rapid enough to maintain the surface moisture at equilibrium with the air above. The systems chosen are

a) one with a constant diffusion coefficient and constant volume,

b) with a constant diffusion coefficient, but involving film shrinkage as described in section 2.3.2, and

c) a system with both a variable moisture dependent diffusion coefficient and film shrinkage.

The diffusion coefficient for the two constant $D$ cases was chosen to be $8.5\times10^{-11}$ $m^2.s^{-1}$, typical of that in solid food systems (Saravacos and Maroulis, 2001), such as vegetables. For the system with moisture dependent diffusion, we used the model proposed by Maroulis et al (Maroulis et al., 2001), which itself is based on the analysis of a large number of reported experimental data in the literature. $D = (1.72\times10^{-10}\phi)+(1.75\times10^{-11}(1-\phi))$ $m^2s^{-1}$ was chosen, with the value of the diffusion coefficient half way through the drying process being the same as that for the two constant $D$ systems. In all three systems the initial moisture volume fraction was $\phi(0) = 0.875$, while the final equilibrium value $\phi^{eq} = 0.02$. The initial thickness of the film was $4\times10^{-4}$m. The data are presented as the reduced moisture ratio $\Gamma=\phi(t)L(t)-\phi^{eq}L(\infty))/(\phi(0)L(0)-\phi^{eq}L(\infty)) = (L(t)-L(\infty))/(L(0)-L(\infty))$, plotted against the reduced time $t/\tau$, where the time scale $\tau = 4L(0)^2/(\pi^2 D)$. Plotted in this way, the results for all systems with constant volumes and a constant diffusion coefficient lie on a single master curve

(Crank, 1975), irrespective of the values of $L(0)$, $D$, $\phi(0)$ and $\phi^{eq}$. For systems where there is a variation in diffusion coefficient or film shrinkage, the initial values of $D$ and $L$ were used to calculate $\tau$. Of course, in these latter cases the same universal scaling is not to be expected.

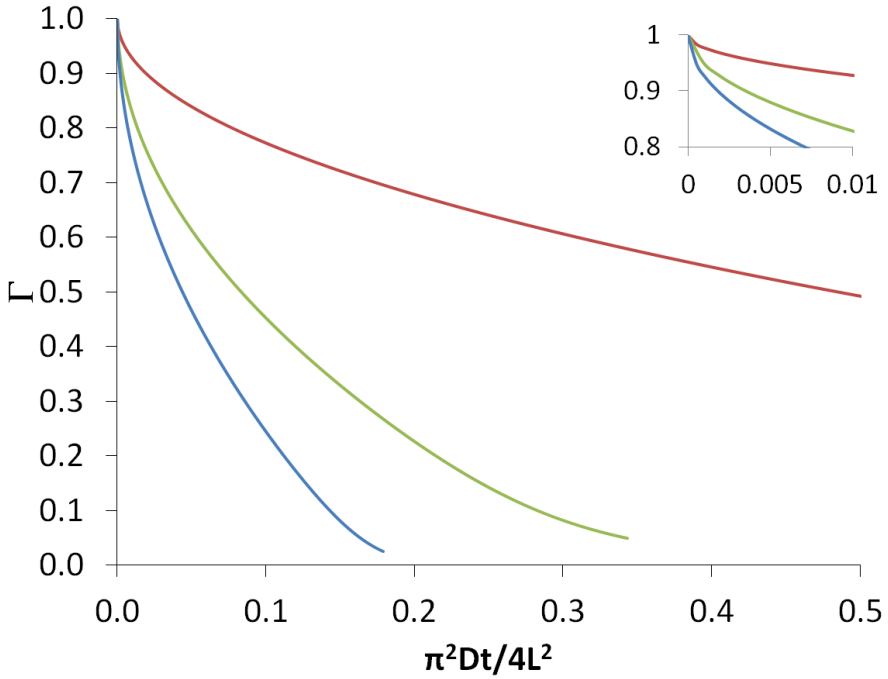


**Figure 3.8 – Numerically calculated drying curves, showing $\Gamma = (L(t) - L(\infty)) / (L(0) - L(\infty))$ plotted against scaled time ($\pi^2 Dt/(4L(0)^2)$), for diffusion limited dehydration. The graphs are for a) a system with constant $D$ and $L$ (red), b) constant $D$ and film shrinkage (blue), c) with a moisture dependent water diffusion coefficient and shrinkage (green). The inset shows the magnified graphs for the initial stages of drying.**

While all three curves in Figure 3.8 follow similar trends, it is noticeable from the inset in the figure that the graphs deviate from each other very early on. In particular, the drying curve for the system with a constant $D$ but film shrinkage (blue) falls much more rapidly than the one that doesn't involve a change in the film thickness (red). This also means that the assumption regarding the diffusion being the limiting factor at the start of the film drying,

might not apply throughout the whole process. As the film shrinks, the diffusion path becomes shorter and therefore diffusion is faster and so is no longer the dominant resistance to loss of moisture. However, the effect can to some extent be compensated by the decrease in the water diffusion coefficient, as the moisture content of the film decreases. This is demonstrated by the green line of Figure 3.8, showing a faster drying than the one with a constant *D* and *L*, but slower than the system with constant *D* but variable *L*. It could well be then that in some practical cases, the effects of a reduction in *D* and a decrease in the film thickness largely cancel each other out. This allows the familiar analytical equation (Crank, 1975) for the standard case to be fitted to the dehydration of such materials.

In Figure 3.9 an attempt has been made to scale all of the experimental drying data, obtained for different systems at various temperatures and humidity conditions, on to a single master curve. This was achieved by plotting moisture ratio $\Gamma$ against the scaled time $t/\tau$ for each system, where $\tau$ is an adjustable parameter chosen for each set of data to provide the best possible scaling. These values are available in Appendix 1. The data for different sets of systems, presented in Figure 3.4 and Figure 3.5, all show a remarkably good level of scaling when plotted in this way. The only possible small discrepancy between the results arises towards the very last stages of the drying process, where very contrasting behaviour for starch and casein based films would be expected. The good scaling of the data suggests that the drying process is either predominantly controlled by evaporation, where the time scale $\tau = L/K$, or alternatively largely dominated by moisture diffusion, with $\tau = 4L^2 / (\pi^2 D)$. If both factors were equally significant in the drying of these films, such scaling as that seen in Figure 3.9 would not be

possible. One of the two processes is too fast relative to the other and therefore at best, can only cause a small perturbation to the results otherwise obtained by its omission.

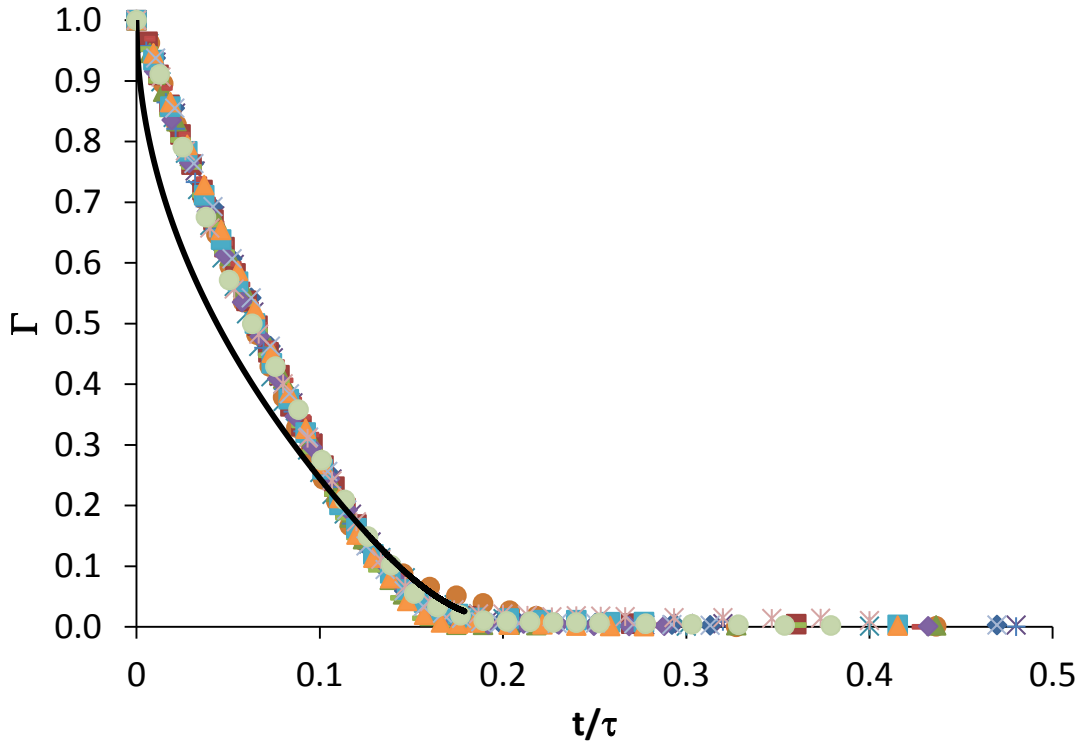


**Figure 3.9 – Experimental data of Figure 3.4 and Figure 3.5, scaled on a single master curve. The solid line shows the best fit to the results using a numerically calculated diffusion dominated dehydration curve, which includes film shrinkage and a constant moisture diffusion coefficient.**

The time dependence of scaled experimental results indicates that moisture diffusion is unlikely to be the controlling factor. Attempts have been made to fit the scaled data in Figure 3.9 using numerically generated drying curves, obtained for systems where the evaporation is rapid and diffusion the controlling mechanism. Irrespective of whether the film shrinkage was taken into account or not, and the use of constant or moisture dependent diffusion coefficients, none of the results provide a good fit to the experimental data. The black line in Figure 3.9 shows one of these attempts, calculated for a

system with constant *D* but decreasing thickness. By applying statistical analysis to the data in the form of an f-test and a t-test with critical p values of 0.05 in each test, values of 0.000537 and 0.0438 respectively were obtained, showing that the experimental data and simulated curve are statistically significantly different. The essential point is that for all of the diffusion limited drying curves the initial moisture loss follows a relation of the form (1-$\Gamma$)~$\sqrt{t}$ . In contrast, the experimental results are better described by (1-$\Gamma$)~ *t*. The poor fit to the experimental data, even in the best case, confirms that diffusion is not the limiting factor in the dehydration of these polymer films. This is likely due to a combination of the very thin film and relatively mild drying conditions, which allow diffusion to occur fairly easily.

Following the above findings, the evaporation controlled case was considered. The simple exponential curve, obtained when the film shrinkage is neglected, results in a better fit to the experimental data at short times; $\Gamma = \exp(-Kt/L) \approx 1-(Kt/L)$. However, as clearly seen in Figure 3.10 (blue line), the predictions grossly overestimate the remaining moisture content at longer times. With changes in the film thickness included in the analysis, the dehydration curve is described by equation 2.8. This equation does not admit a simple scaling relation between $\Gamma$ and scaled time $t/\tau$. However, if a system is considered where $\phi^{eq} << \phi(0)$, as is the case here, then $\phi(t)L(t) >> \phi^{eq} L(\infty)$ for a significant portion of the dehydration process. We can write $(1-\phi^{eq}) \approx 1$, $L(\infty) \approx (1-\phi(0))L(0)$ and $\Gamma \approx \phi(t)L(t)/(\phi(0)L(0))$. With these approximations, equation (2.3-8), expressed in terms of $\Gamma$ now reads

$$(1-\phi(0))\ln(\Gamma) + \phi(0)(1-\Gamma) = -\frac{Kt}{L(0)} \qquad \textbf{3.1}$$

For the initial stages of dehydration, where we have (1-$\Gamma$) << 1, the above equation gives an identical result to the exponential curve, i.e. $\Gamma \approx 1-\left(Kt/L(0)\right)$. At longer times, the shape of the curve is dependent on the initial moisture content. However, it turns out that all the systems studied here have a very similar initial moisture volume fraction. The caseinate based systems have a solid weight fraction of 18%. To convert this to a volume fraction value the density of the caseinate in the solution is required. This was obtained by measuring the volume of a series of solutions, prepared with the same amount of water but different masses of added sodium caseinate. The results of this can be seen in Figure 3.11. The gradient of the linear data gives the inverse density. The density of sodium caseinate was therefore found to be 1.53 $gcm^{-3}$, in good agreement with reported values in the literature for relatively short protein chains (Fischer et al., 2004). Using this value, the initial water volume fraction was estimated to be 0.875 for our caseinate solutions. A similar procedure for starch based systems gave the starch density as 1.35 $gcm^{-3}$ and the initial water volume fraction as 0.9 for our solutions.

We have calculated $\phi(t)$,$L(t)$ = (1-$\phi(0)$)$L(0)$/(1-$\phi(t)$) and hence $\Gamma$ = (L(t)-L(∞))/(L(0)-L(∞)) using equation 2.8 with an initial water volume fraction $\phi(0)$ = 0.875 and a small final moisture volume fraction of 0.02. It is worth stressing that once the initial volume fraction of water is specified, the shape of the dehydration curve, $\Gamma$ vs. $t/\tau$, is entirely determined. There are no adjustable free parameters. The black line in Figure 3.10 displays the theoretically determined dehydration results, with $\tau$= $L(0)/K$. The model gives a curve that fits the experimental data very well, as indicated by the f-test

and t-test with critical p values of 0.05 in each test, values of 0.184 and 0.181 respectively were obtained, showing that the experimental data and simulated curve are statistically significantly different. indicating the important roles of evaporation and film shrinkage on one hand, and the relative insignificance of diffusion on the other. Nevertheless, even further modest improvement in describing the experimental data is possible if the diffusion process is not entirely neglected.

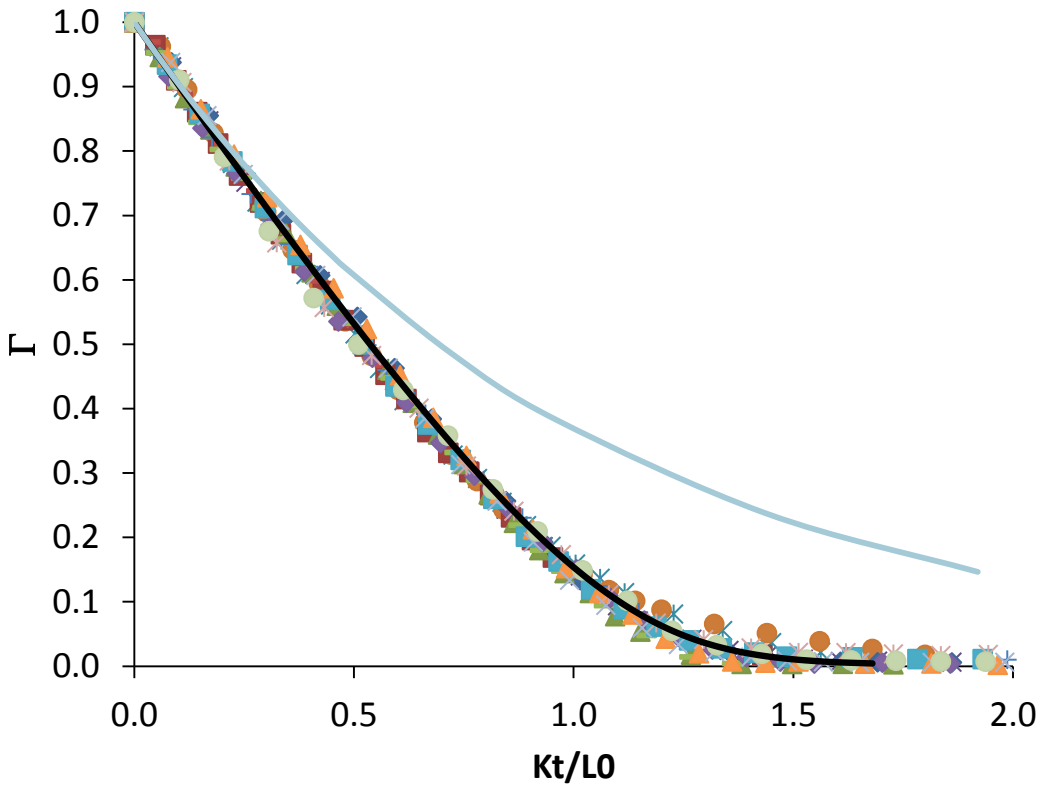


**Figure 3.10 - Comparison of the theoretically predicted drying curves for evaporation controlled dehydration with the experimental data. The black line is for a model that includes the film shrinkage, while the blue line represents the results for a model without shrinkage.**

In Figure 3.12, the result of the numerical calculations, based on equations 2.30 and 2.31, together with the experimental scaled master curve are

shown. The diffusion coefficient was chosen to be large but finite. The best fit was obtained when $D/(KL(0)) \approx 55$. The excellent correspondence between the experimental and theoretical results is evident and supported statistically by an f-test and a t-test with critical p values of 0.05 in each test, values of 0.097 and 0.407 respectively were obtained, showing that the experimental data and simulated curve are statistically similar. Analysing the data using our model then, we find the evaporation constant $K$ to lie between $1.2\times10^{-7}$ $ms^{-1}$, for casein at lower temperatures and large air humidity, to $3.6\times10^{-7}$ $ms^{-1}$ at higher temperatures, 40 °C, and low air humidity. With a film thickness of 0.4 mm, used for all the experiments, the best estimate for $D$ is $5\times10^{-9}$ $m^2s^{-1}$ for the diffusion of water in our biopolymer based films.

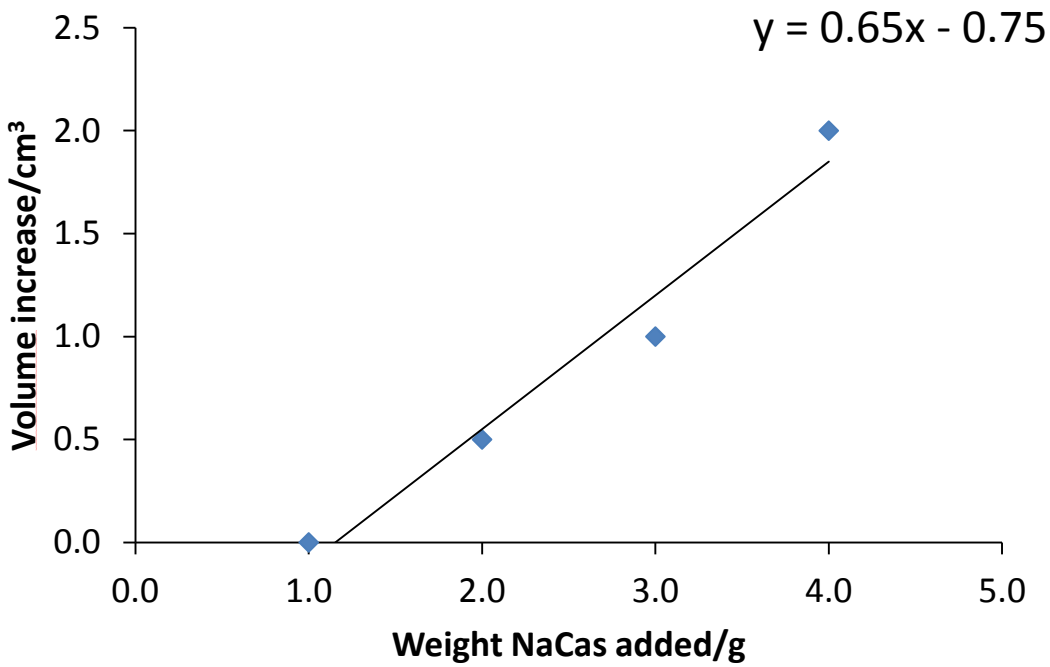


**Figure 3.11 - Change in volume for different weights of sodium caseinate in the solution, used to calculate density, where the volume increase is plotted against the amount of casein added.**

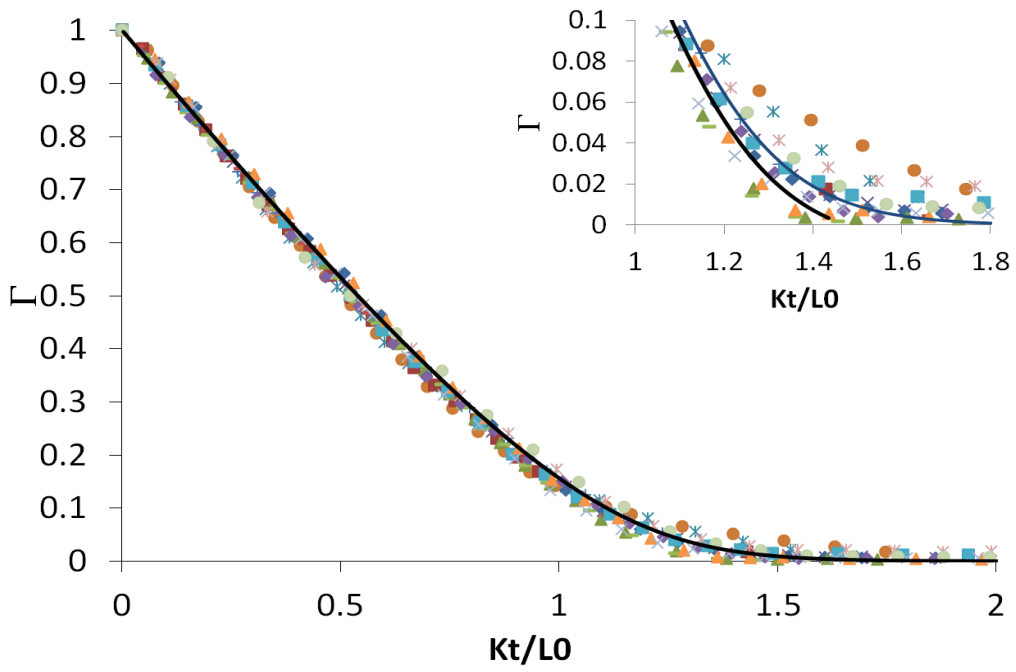


**Figure 3.12 – The experimental data, all scaled onto to a single curve, compared with numerical predictions from a model combining evaporation with fast but finite diffusion, as well as film shrinkage.**

## 3.4 Dehydration of adhesive films

Drying data of several variations of starch and casein based adhesives used in industry was provided by Henkel GmbH. They collected gravimetric data for several adhesive samples which were used to attach a paper label to a glass bottle and dried in a controlled environment. The samples were different compositions of the Saced water-based adhesive and Syntacol 300 water-based adhesive. The Saced adhesives have casein as the major component and Syntacol is starch based. The starch used in this formulation is Purity SCS A, the same di-phosphorylated starch used in the model starch system investigated throughout this work. These data were normalised and the moisture ratio was plotted against time as for the model systems described in section 3.3.2.1. Again the time was scaled by the adjustable parameter $\tau$, chosen for each set of data to provide the best possible

scaling. The adhesive samples investigated had a moisture content of approximately 55% and a density of 1.12g.cm$^{-1}$. From this information the volume fraction of moisture was calculated to be 0.62, and so this was the value used in the numerical simulations. The final moisture content was set as 0.02, as this gave the best fit when used for the model systems. Figure 3.13 shows the good scaling of three different adhesive samples, again suggesting that one of either evaporation or diffusion will dominate the drying process over the other. The model where diffusion is constant with infinite evaporation and film shrinkage is fitted to the adhesive data in this case. It is clear that as with the model systems in 3.2.2 the experimental drying curves are much more linear than the simulated curve, with a $(1-\Gamma) \sim t$ relationship. Initially, the predicted dehydration is faster than the experimental results, although towards the end of the drying process the numerical calculation results appears to fit the data better.

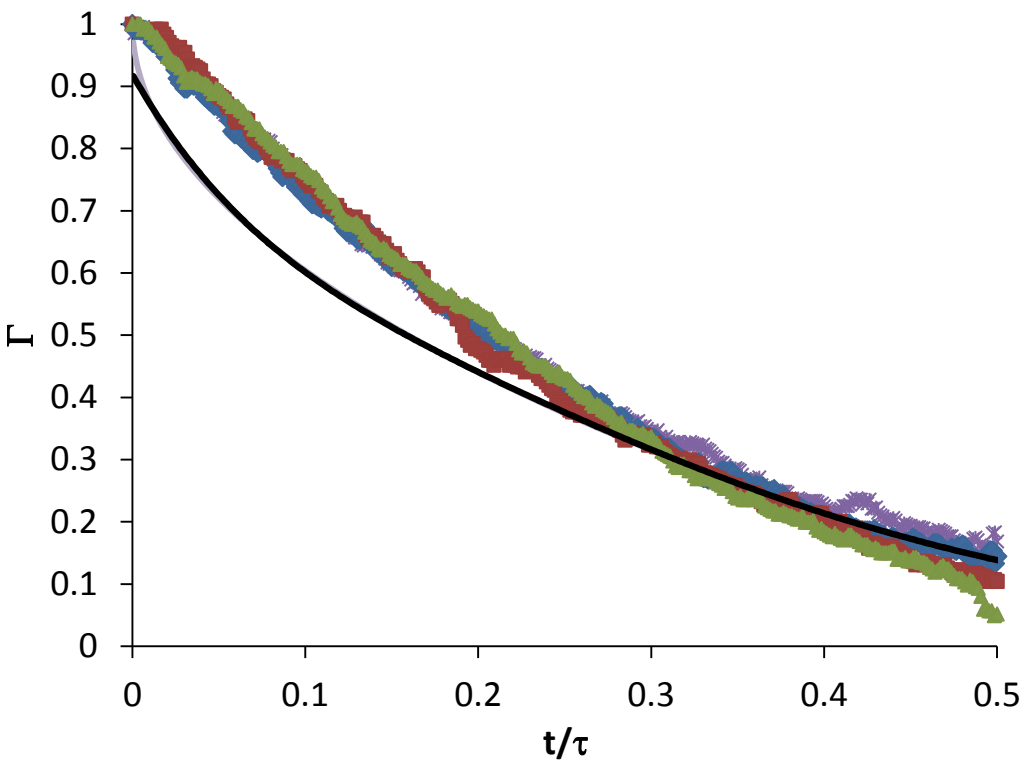


**Figure 3.13 - Adhesive samples dried with labels attached at 25 °C fitted to model for the case where diffusion is the limiting factor with shrinkage. ◆= saced01b, ■= saced02b, ▲= saced06b, *= syntacol300.**

In Figure 3.14 the experimental data is compared with the numerical model for the case where evaporation is the dominate limiting factor and diffusion is infinitely fast. As before the film shrinkage is included. Here, once again, a much better fit is seen with the initial stages of the data, although slight deviation is apparent in the latter parts of the dehydration process. The dotted line indicates the numerical calculation for the case where shrinkage does not occur.

The pattern of the normalised data of the adhesive samples is supported by that seen previously for the model starch and caseinate films, so the next logical step is to fit the simulation for the case where evaporation is the

dominant mechanism of dehydration, with a fast but still finite diffusion. The results for this exercise are shown in Figure 3.15.

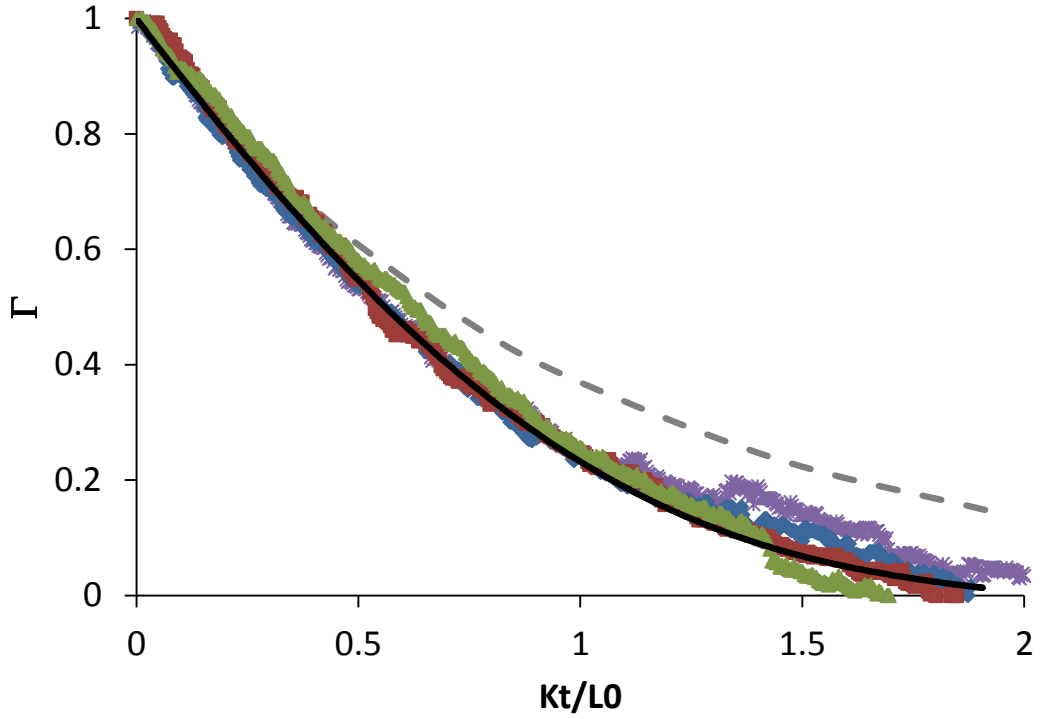


**Figure 3.14 - Adhesive samples dried with labels attached at 25 °C fitted to model for the case where evaporation is the limiting factor with shrinkage. ◆= saced01b, ■= saced02b, ▲= saced06b, *= syntacol300.**

As with the model systems investigated earlier in the chapter, this model provides an excellent fit to the experimental data for both starch and casein adhesive films. This is a somewhat surprising result when applied to the actual adhesive systems, considering that the adhesive in this case is sandwiched between a glass bottle and paper label, thus the moisture also has to pass through a paper label before it can evaporate, however as the film applied to the label is so thin, evaporation is still the rate limiting factor, as diffusion is so fast through the very thin film.

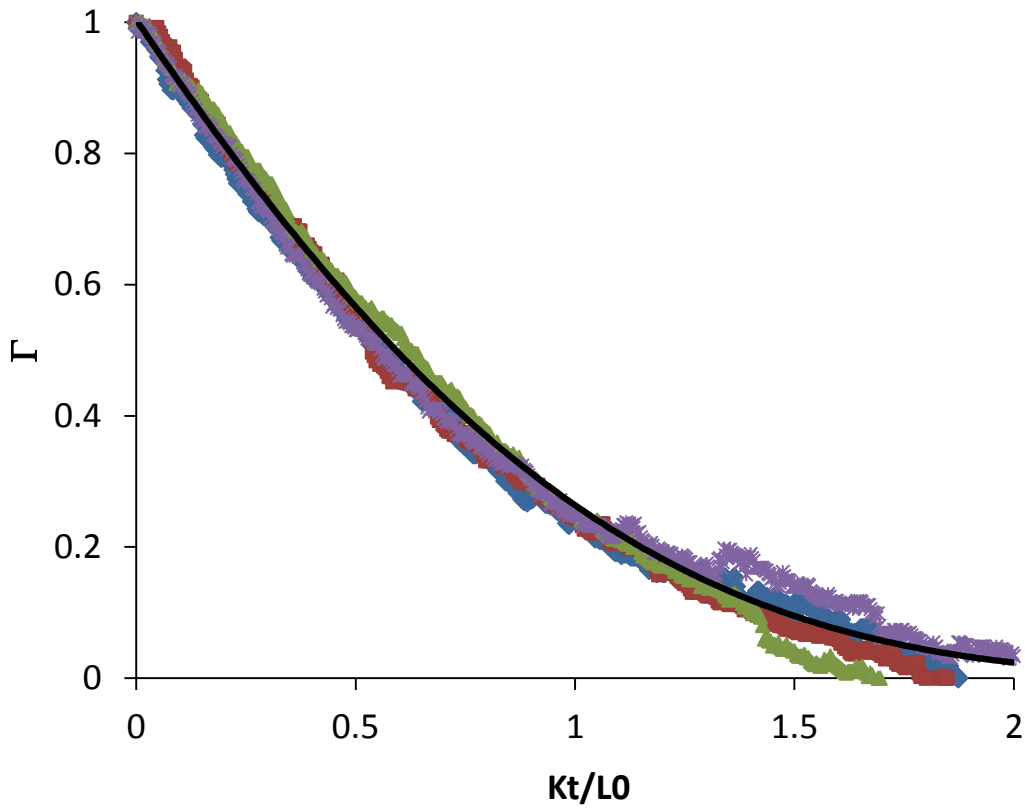


**Figure 3.15 - Adhesive samples dried with labels attached at 25° C fitted to model for the case where evaporation is the dominating process with fast but finite diffusion and with shrinkage. ◆= saced01b, ■= saced02b, ▲= saced06b, *= syntacol300.**

Assuming a film thickness of 0.4 mm, as used in the model experiments, the evaporation constant lies between $2.6\times10^{-7}$ $ms^{-1}$ and $3.7\times10^{-7}$ $ms^{-1}$, and the diffusion coefficient between $4.35\times10^{-9}$ $m^2s^{-1}$ and $5.95\times10^{-9}$ $m^2s^{-1}$, values which are in good agreement with the model starch and casein systems used in the rest of this work

## 3.5. Conclusions

In this chapter the dehydration in thin biopolymer films consisting of solutions of casein and starch, as well as those comprising of a mixture of the two, have been compared. The two biopolymers chosen typify the two wide

classes of macromolecules encountered in food systems, namely protein and polysaccharides. Dehydration curves as expressed by the moisture ratio plotted against time, studied under a range of air humidity and temperature conditions, have been found to all superimpose onto a single master curve, by a simple scaling of time for each system. It has been shown that moisture diffusion dominated drying, whether involving a constant or a variable water diffusion coefficient, with or without film shrinkage, cannot accurately describe experimental dehydration curves obtained in this work. The analytical expression for the moisture content in a film as a function of time, derived in chapter 2, for a drying process in which the evaporation dominates and in which the film thickness decreases with the loss of moisture, provides an accurate description of the experimentally obtained master curve. This highlights the crucial importance of accounting for the film shrinkage in theoretical calculations describing the dehydration process of such biopolymer films. The good correspondence between the experimental and the theoretical results also indicates the much more dominant role played by surface evaporation as compared to bulk diffusion. This is to some extent expected for thin films.

Situations where both evaporation and diffusion may be equally important have also been considered, using a generalised scheme derived in Chapter 2 for numerically solving such cases.

Application of the above model to the simpler case with constant partial molar volumes, under the condition where evaporation was the main limiting mechanism for the loss of water was studied. In these models the diffusion coefficient, $D$, was large but still finite, resulting in a slight perturbation to our analytical expression obtained by assuming $D$ to be infinite. It was found that

in this case, the theoretical predictions of the model were in excellent agreement with the experimental data for the dehydration of our biopolymer films.

Finally, the above models were applied to drying data of adhesive samples used in industry. The results indicate that the model systems sufficiently describe the drying behaviour of such adhesive thin films, as the theoretical predictions were once again in excellent agreement with the experimental data provided for the dehydration of several starch and casein based adhesive samples.

## 3.6. Future work

Further work to continue the investigation of dehydration in biopolymer films can be split into two main areas. The first of which would be more applicable to industry. Throughout the course of this project, casein based adhesives have started to be phased out of use and replaced with synthetic alternatives. These synthetic adhesives are based on an acrylic polymer mixed with starch. Therefore a sensible and useful route would be to repeat the dehydration experiments for a model acrylic system to see if the synthetic polymer film can be modelled successfully to give the same mechanism of dehydration, i.e. with evaporation as the dominant process and diffusion fast but not infinite. More importantly, the scaled curve obtained from the model systems can be examined to see if it can also incorporate the scaled data of such synthetic polymers.

Secondly, it would be interesting to repeat the experiments with films of different thicknesses. Due to apparatus limitations, this could not be done

using the current setup for large film thicknesses, but an experimental setup could be designed to cope with thicknesses upto 1-2 cm. By increasing the film thickness the importance of the role of diffusion in the drying process should become more prominent, and eventually diffusion will become the controlling mechanism. Similarly, the drying experiments should be repeated under more severe drying conditions where the evaporation from the surface of the film is very fast. This would be a useful investigation to demonstrate how the mechanism of dehydration for any type of polymer film can be controlled by controlling the film thickness.

# Chapter 4 Using Acoustics to Monitor Water Diffusion into Biopolymer Systems

## 4.1 Introduction

The diffusion of water into biopolymer coatings is becoming a more and more important problem (Karbowlak et al., 2008, Tabor et al., 2012a). Water diffusion has a significant effect on the properties of polymers which can affect their performance in many different applications, for example in edible food coatings there are many reasons for investigating the moisture diffusivity including improvement of shelf-life of products, storage, physico-chemical stabilisation and product stability (Camirand et al., 1992, Gennadios, 2002, Janjarasskul and Krochta, 2010, Karbowlak et al., 2008). Other areas where this is of interest are in dental composites (Rahim et al., 2012a, Sideridou and Karabela, 2011) and adhesives (Day et al., 1992, Henshaw et al., 2006, Mubashar et al., 2009a). A common problem in the adhesives industry is that as water diffuses into and out of polymer systems, their structure can change significantly and with it the properties of the system such as strength, viscosity and shear strain. These changes can lead to failure of the system, particularly in adhesives where an increase in water uptake can result in a weaker, less viscous polymer, which will no longer adhere to the substrate. By altering the properties of the biopolymer it may be possible to slow down the water diffusion into the system, so it is therefore important to understand how the diffusion process occurs in these biopolymers.

The most common approach to investigate this uses gravimetric data from either drying experiments (Babalis and Belessiotis, 2004, Czaputa et al., 2011, Ramirez et al., 2011), or sorption data (Anderberg and Wadso, 2008, Baez-Gonzalez et al., 2004, Drchalova and Cerny, 1998), however in this work we present a novel technique which uses ultrasound waves to scan the system and monitor diffusion over time (Povey, 1997). Considerable advances have been made in ultrasonic velocity measurement in the last few decades as it has many advantages over other characterisation methods in that it is fast, non-destructive, accurate and relatively low cost, and it can be used to characterise everything from particle dispersions, emulsions and solutions to soft solids, in particular opaque materials can be analysed (Povey, 1997). A major advantage of this method compared to other available methods is that localised concentrations can be determined at a particular *x*, height, value.

### 4.1.1 What is Ultrasound?

Sound is transmitted through a system as vibrations at a molecular level, with molecules colliding with each other to form a longitudinal wave (Mason T. J., 2002). A series of vertical lines with different separation between them – areas with small separation are known as compressions and areas with larger separation are rarefactions, are typically how a sound wave is represented schematically, as seen in Figure 4.1.

The hearing threshold for humans is around 18 KHz for adults although younger persons have a threshold of 20 KHz. Anything above 20 KHz is classed as ultrasound (Mason T. J., 2002). Ultrasound can be divided into three categories as seen in Table 4.1.

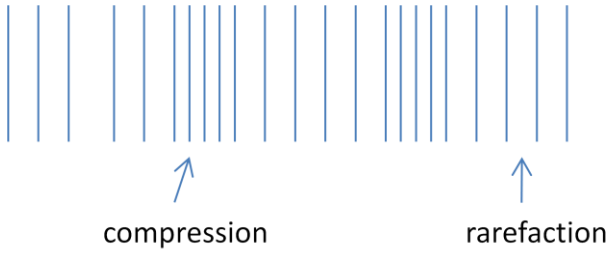


**Figure 4.1 - Schematic representation of a longitudinal wave.**

**Table 4.1- Ultrasound categories - taken from Practical Sonochemistry (Mason T. J. 2002).**

| | |
|---|---|
| 20 KHz -100 KHz | Power Ultrasound used for industrial processing and sonochemistry |
| 100 KHz – 2MHz | Extended sonochemistry range |
| 5MHz - 10MHz | Low power high frequency ultrasound used for diagnostics |

The study and application of sound waves above the human hearing threshold is called ultrasonics (Blitz J., 1963). The theory of sound is based in classical physics, with Newton's second law, force is equal to mass multiplied by acceleration, being of particular importance. Wood (1941) offered experimental support to the theory developed by Raleigh (1877), leading to the theoretical basis used today (Wood, 1941). Changes in the sound velocity and attenuation can be used to monitor the progress of a reaction, or for quality control purposes where composition is examined.

### 4.1.2 Why is Ultrasound an important technique?

Wood (1941) stated that the physical properties of a medium which influence the speed of sound as it passes through it are the elasticity and density, or

the mass and stiffness of a particle. As a wave passes through, the density and volume of the system fluctuate around their normal values. The properties of the medium in addition to the applied forces control the magnitude of these fluctuations. The ratio of the change in volume to the original volume is known as dilatation, and the ratio of the change in density to the original density is known as condensation (Wood, 1941). The compressibility of a medium is a property that can be measured, and is the inverse of the bulk modulus of elasticity. This allows the speed of sound to be calculated from equation 4.1, first observed by Wood, then developed by Urick who generalised it to solid particle suspensions (Urick, 1947). The key assumption for the Urick equation was that the mixture behaves as an ideal liquid, with extremely small particle sizes, so scattering effects can be assumed negligible. The equation is known as the Urick equation (Povey, 1997)

$$v = \frac{1}{\sqrt{\kappa\rho}} \qquad \textbf{4.1}$$

Where, $v$ is the sound velocity, $k$ is the compressibility and $\rho$ is the density.

In many cases for emulsions and suspensions, the Urick equation does not describe the sound velocity adequately (Dickinson et al., 1997). Scattering effects cause significant deviation from the Urick equation in concentrated emulsions. Previous work in the literature found that the simple application of the Urick equation was unsuitable to calculate the volume fraction in solutions of sodium caseinate above 6 wt% reliably (Pinfield et al., 1995). To account for this they modified the equation to account for scattering.

The renormalisation method (Pinfield et al., 1995) allows concentration profiles to be calculated from sound velocity measurements. It requires only the continuous phase velocity and initial volume fraction and assumes that the dispersed phase volume is conserved throughout the experiment. The particle size distribution must also remain constant.

### 4.1.3 Applications of Ultrasonic measurements

The applications of the ultrasound can be split into two categories, both of which use sound velocity and frequency. One of these uses the process of cavitation, forming and destroying low pressure bubbles, and the other uses measurement of sound velocity and attenuation.

Cavitation is a widely used ultrasonic process and the mechanism behind many applications of ultrasound. By altering the ultrasonic frequency and acoustic amplitude, the size of bubbles formed can be controlled in sonochemical reactions. By controlling bubble radius, the impact of their collapse can be controlled. Violently collapsing bubbles can lead to localised high temperatures and pressures leading to chemical effects on a system. If these bubbles collapse close to an interface, mechanical effects can also be induced (Merouani et al., 2013, Tsochatzidis et al., 2001). Another common use of ultrasound in this context is for decontamination purposes. Chlorinated phenols are a common constituent of preservatives, dyes and lubricants. These chemicals are highly toxic to the environment and detrimental to human health, and they are also particularly resistant to chemical destruction. Zhao (2013) applied sonication to produce Pd/Fe nanoparticles which could be used to de-chlorinate the dangerous phenolic compounds. Emulsification is another process which commonly employs

ultrasonic techniques in order to generate highly stable emulsions in the sub-micron range with relatively little surfactant required (Povey, 1997, Chemat et al., 2011, Kaltsa et al., 2013).

The other way in which ultrasound can be a useful tool, and perhaps of greater relevance to this work, involves time of flight, i.e. sound velocity, and amplitude measurements. Measurements of this kind are non-destructive and have many potential applications. By monitoring time of flight measurements, and changes in amplitude throughout a particular system, a time-frequency analysis can be conducted allowing location and severity of damage to be deduced, for example on a metal part of a landing gear. Changes in time of flight would indicate damage positions, and a larger change would point to more severe damage (Thursby et al., 2006).

Emulsion instability has also been investigated using these types of measurement. Work by Povey *et al* measured the time of flight across the height of a glass cell containing an emulsion as a function of time. As the emulsion creamed and flocculated, changes in the time of flight were observed. The results were used to create volume fraction profiles which clearly showed the inhomogeneous nature of the emulsion over time (Dickinson et al., 1997, Pinfield et al., 1996, Povey, 1997). It is the method used here that provides the basis to investigate the diffusion of water into a biopolymer system in this work. Essentially, this process is like a reversal of a separating emulsion, and so the same principles should be applicable to the system in question, i.e. as water diffuses into the biopolymer, the time of flight should change.

## 4.2 Using acoustic techniques to develop a novel method for monitoring diffusion in biopolymer systems

In this work we investigate the diffusion of water into a casein biopolymer solution using the Acoustiscan, an ultrasonic velocity scanning device developed at the University of Leeds (Povey, 1998). The Acoustiscan scans a rectangular glass cell containing the sample, between 10 mm and 250 mm and plots acoustic parameters, such as speed of sound and attenuation, as a function of height. The transducers are moved by a stepper motor system. The process can be repeated numerous times in order to build up a spatial and temporal picture of what is happening to the sample over time. The acoustic signal is very sensitive to small changes in the sample thus the device is able to accurately detect any small volumes of water diffusing into the sample. This method assumes the effect of gravity on diffusion to be negligible. Figure 4.2 shows a schematic of a cell within the Acoustiscan.

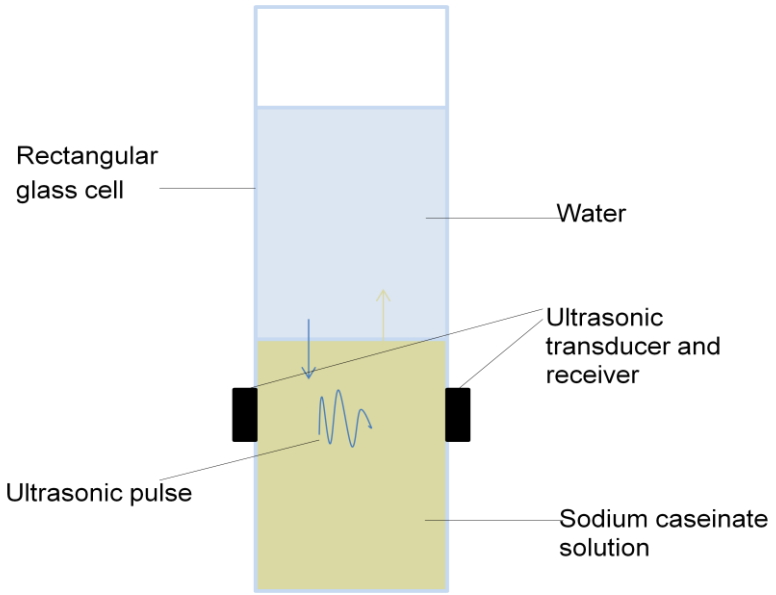


**Figure 4.2 - Schematic diagram of Acoustiscan cell.**

## 4.3. Materials and Methods

### 4.3.1 Materials

The biopolymer system used to validate this novel technique for monitoring the diffusion of water into a biopolymer system was 18 wt% sodium caseinate. Sodium caseinate was obtained from Sigma Aldrich, and used as received. The solution was prepared as described previously in Chapter 3, Materials and Methods.

### 4.3.2 Measuring the speed of sound in pure water and biopolymer system and different temperatures and concentrations

To measure the speed of sound through a sample of known concentration with varying temperature, the Resoscan is used. The Resoscan is a fully automated instrument which can determine the velocity and attenuation of acoustic waves in liquid samples as a function of temperature or time. Samples are placed in small cells of 0.17 mm housed in a Peltier block, allowing control of temperature accurate to ± 0.001 °C. Speed of sound measurements can be measured with high accuracy and reproducibility across the range of temperatures 5 °C – 85 °C. The technique is non destructive and the liquid being tested does not need to be transparent or optically active. The Resoscan works by converting an electronic signal into an ultrasonic wave using a piezoelectric transducer. The ultrasonic wave propagates through the sample and is converted back into an electronic signal by a second piezoelectric transducer. Resoscan software records the speed of sound and attenuation data in a spreadsheet.

The effect on speed of sound is investigated in the temperature range 5 °C - 40 °C for a range of concentrations of each of the samples from the Acoustiscan experiments described previously. Eight concentrations are measured for the sodium caseinate based samples between 18 wt% and 2 wt%; four concentrations for the starch system, between 7 wt% and 1 wt%; and five concentrations for the mixed sodium caseinate and starch system from 9:4.5 wt% to 1:0.5 wt%. The speed of sound through pure water is also measured at each temperature.

From the data collected, standard curves can be produced for each system, of speed of sound as a function of concentration at a specific temperature. This is then used to construct a concentration profile from the speed of sound measurements obtained from the Acoustiscan experiments.

### 4.3.3 Measuring the speed of sound in biopolymer systems as water diffuses into it

To measure the change in concentration of a system as water diffuses in, the Acoustiscan, a device built and developed at the University of Leeds, was used. The Acoustiscan scans a rectangular glass cell containing the sample, between 10 mm and 250 mm and plots acoustic parameters, such as speed of sound and attenuation, as a function of height. The process can be repeated numerous times in order to build up a picture of what is happening to the sample over time. The acoustic signal is very sensitive to small changes in the sample thus the device is able to detect small volumes of water diffusing into the sample.

The Acoustiscan is housed in a refrigeration unit for temperature control, and has a six cell sample changer incorporated into the design in order to allow

for multiple samples being scanned simultaneously. The available temperature range is between 5 °C and 40 °C. A pair of probes scan the sample cell using a pitch- catch arrangement, where a pulse of sound is transmitted from the transducer probe, through the sample, and is detected by the receiver probe positioned at the opposite side of the sample cell. The process is repeated for the desired height of the cell, at pre-determined step intervals.

For this experimental procedure, the cell is filled to a height of 100 mm with the desired polymer solution, sodium caseinate, starch or acrylic based polymers. Milli-Q water is then added carefully on top using a pipette to prevent surface disruption, to a height of 200 mm. The cell is placed into the carousel along with two repeat cells and the cell details are programmed into the software. The software allows complete automation of the scanning, and is set to scan a total height of 100 mm, with large steps, between scans, of 5 mm between the heights of 10 mm to 35 mm and 65 mm to 100 mm. Between 35 mm and 65 mm the step size is 1.0 mm, as this area, around the water – biopolymer interface, is the area where most change in sound speed is anticipated. Each cell is scanned in turn, with each scan taking approximately half an hour to complete. The scans for each cell are programmed to run every hour for 56 hours.

The acoustic data collected by the Acoustiscan can be correlated with the data collected from the Resoscan, reported in section 4.3.2, to produce a concentration profile across the height of the sample with time.

## 4.4 Results and Discussion

### 4.4.1 Measuring the speed of sound in pure water and biopolymer system and different temperatures and concentrations

In order to be able to interpret the results obtained from the Acoustiscan, it is necessary to first collect speed of sound data for the biopolymer system at different concentrations. As water diffuses into the biopolymer, the system becomes less concentrated and thus the speed of sound will change accordingly.

#### 4.4.1.1 Speed of sound vs Temperature

It is well known that as temperature increases by 1 °C, the speed of sound in pure water increases by 3 $m.s^{-1}$ (Del Grosso and Mader, 1972, Marczak, 1997, Povey, 1997). The effect of temperature on the speed of sound is shown by equation 4.2.

$$c_p - c_v = -T\left(\frac{dP}{dV}\right)_T \left(\frac{dV}{dT}\right)_P^2 \qquad \textbf{4.2}$$

$C_p$, $c_v$ are the specific heat capacities at constant pressure and volume respectively.

This is quite a significant change and demonstrates the importance of maintaining a constant temperature throughout the diffusion experiment, as results will fluctuate dramatically if the desired temperature is allowed to deviate. In Figure 4.3, the Resoscan data for speed of sound in pure water is displayed. This confirms that there is a linear relationship between the speed of sound and temperature. In the literature, the speed of sound through pure water at 25 °C is 1497.98 $ms^{-1}$ (Marczak, 1997). The experimental data

obtained here agrees with the literature, with a speed of sound through pure water at 25 °C of 1497.3 m.s$^{-1}$.To generate the data, the temperature was reduced stepwise from 40 °C to 15 °C, and then ramped back up to 40 °C, in order to account for any effects on the material that a change in temperature may induce. This is not so important for pure water as for the biopolymer system, as permanent structural changes may occur which lead to the speed of sound being altered, giving a different set of results.

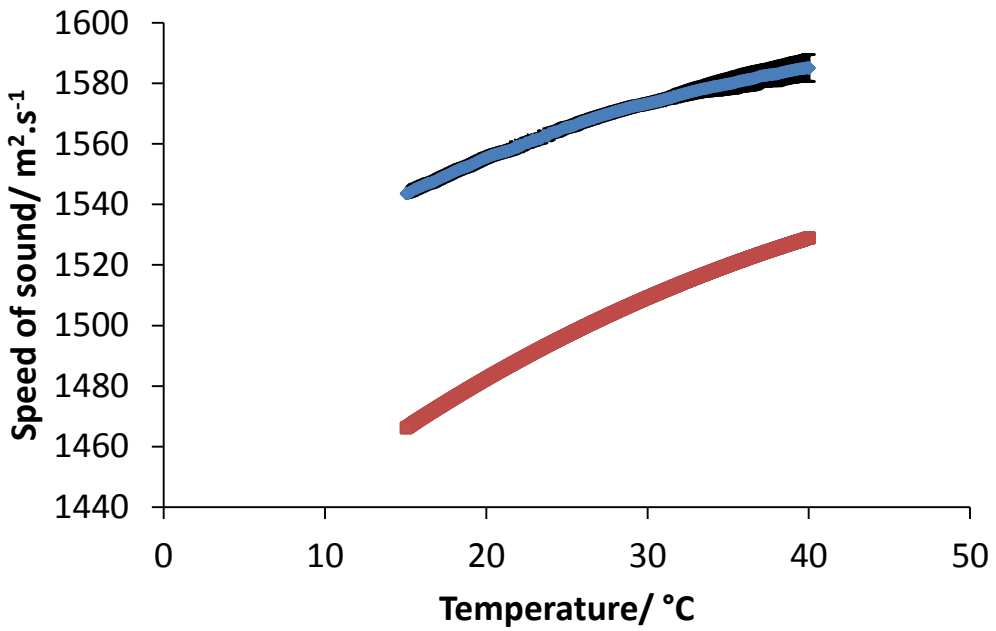


**Figure 4.3 - Speed of sound as a function of temperature for 18wt% sodium caseinate solution (♦) and pure water (■).**

Figure 4.3 also shows the results obtained for the speed of sound in an 18 wt% caseinate solution throughout the same temperature range. Again, we see a linear relationship between the speed of sound and temperature. The results for increasing temperature are identical to those where the temperature was decreased, except at the highest temperatures, showing that temperature has no significant irreversible effect on the structure of the biopolymer matrix, particularly in the temperature range 15 – 30 °C.

From the results shown in Figure 4.3, the large difference in speed of sound in the two media can be seen. For example, at 25 °C the speed of sound in water is 1497.1 m.s$^{-1}$ and in the caseinate solution it is a faster 1566.3 m.s$^{-1}$. Therefore, one would expect that as water diffuses into the caseinate system, the sound velocity will decrease as the caseinate becomes more dilute.

#### 4.4.1.2 Speed of sound vs Concentration

In Figure 4.4, the data collected for speed of sound in different concentrations of sodium caseinate solution is displayed over a temperature range between 7 °C to 40 °C. The concentrations of sodium caseinate used lie between 0% (pure water) up to 18% by weight, the maximum initial concentration to be used in the Acoustiscan.

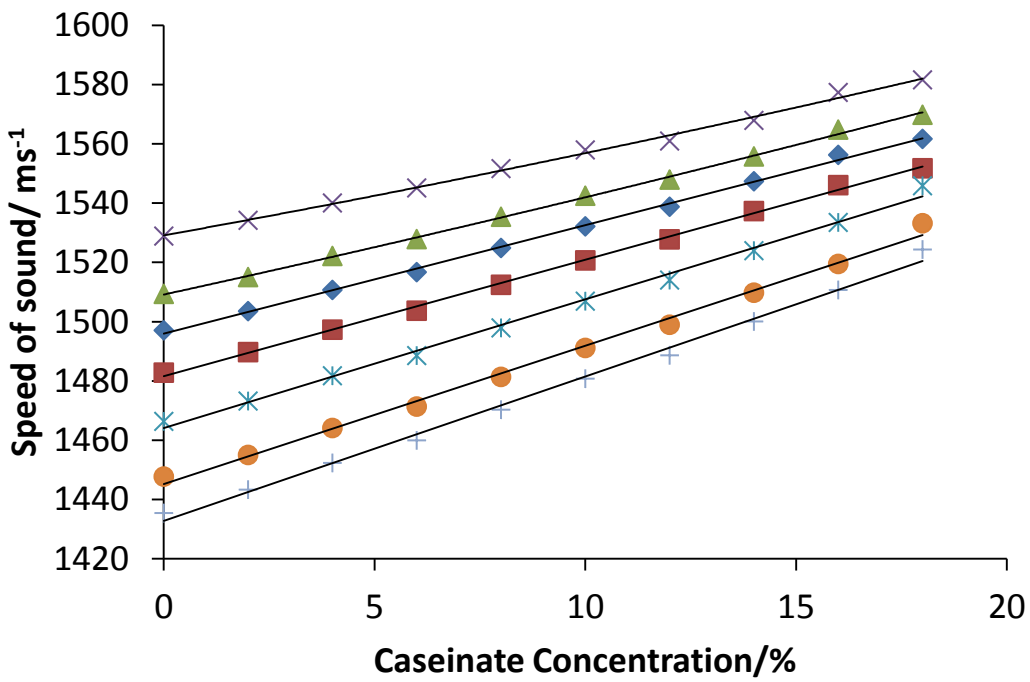


**Figure 4.4 – Speed of sound as a function of concentration for sodium caseinate solutions upto 18wt% at different temperatures + = 7°C, ● = 10°C, * = 15°C, ■ = 20°C, ♦ = 25°C, ▲ =30°C, and x = 40°C.**

At each temperature, a linear relationship is observed. As the caseinate concentration increases, the sound velocity increases. These results support the hypothesis suggested from Figure 4.3 that as water diffuses in to the caseinate system, the speed of sound will be reduced. The linear relationship obtained is a particularly promising result, as it means that a particular speed of sound obtained in the Acoustiscan experiment can be converted to a concentration easily, as the two parameters are proportional.

Also, given that at all temperatures in this range give a linear relationship between concentration and speed of sound, the diffusion of water into the caseinate system can be successfully interpreted using Acoustiscan data at different temperatures.

### 4.4.2 Measuring the speed of sound as pure water diffuses into a biopolymer system using the Acoustiscan method

In this section, the results obtained from the Acoustiscan for 18 wt% sodium caseinate solution are presented. In **4.4.2.1**, the results of speed of sound vs height are discussed, as water diffuses into the biopolymer system, and in **4.4.2.2**, the results generated by the Resoscan are used to convert the speed of sound to concentration in order to generate concentration profiles as a function of height for different time intervals.

#### 4.4.2.1 Speed of sound vs height

In Figure 4.5, sound velocity is plotted in 3D as a function of height and time. The waterfall plot was generated using Matlab. This plot give a good indication of how the speed of sound varies across the system at t=0 right through to t=56h. Initially there is a sharp decrease in the speed of sound at

the boundary position, x=0 mm, where the water meets the biopolymer solution. Gradually this sharp boundary becomes a more gradual transition between the two systems, as water diffuses into the caseinate, and caseinate diffuses into the water. This is a slow process, taking place over many hours, suggesting the rate of diffusion is very slow.

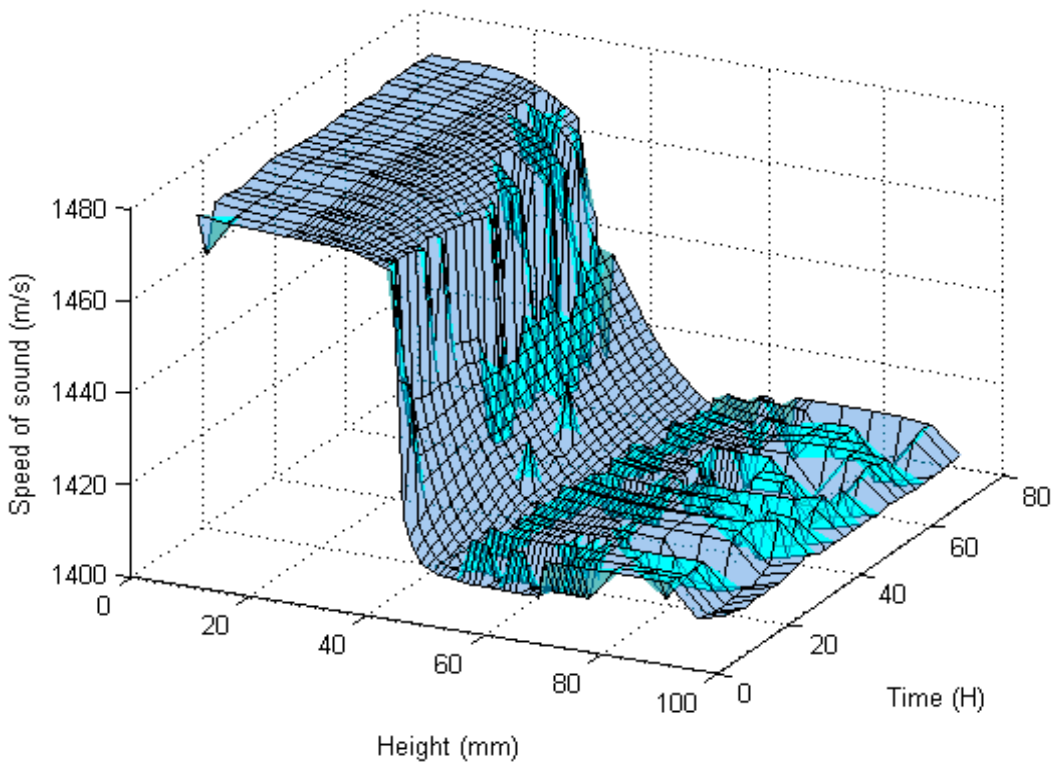


**Figure 4.5 - Waterfall plot showing the change in speed of sound through the casein-water cell as a function of both height and time at 25 °C.**

Figure 4.6 shows the speed of sound as a function of height at four time intervals, t=3h, 8h, 24h and 56h. This figure further supports the slow diffusion process, and demonstrates how the boundary becomes larger with time.

Due to the speed of sound changing as it passes through the glass on either side of the rectangular cell, a correction factor was implemented using the

data generated from the Resoscan, to give the actual speed of sound as it passes through the casein solution and water. As expected, the speed of sound decreases as water diffuses into the caseinate solution. In the water phase at the top of the rectangular cell, deviations in the speed of sound are evident. These are likely due to one of two scenarios, the first being small bubbles of casein being displaced as the water is added and floating to the surface of the water phase. Alternatively, the deviation could be due to small scratches in the glass of the cell wall. The latter is more likely the reason for the small deviation, as it occurs over the full time scale of the experiment and in the same position for each reading. However, due to machine constraints, further work would be required to investigate this further.

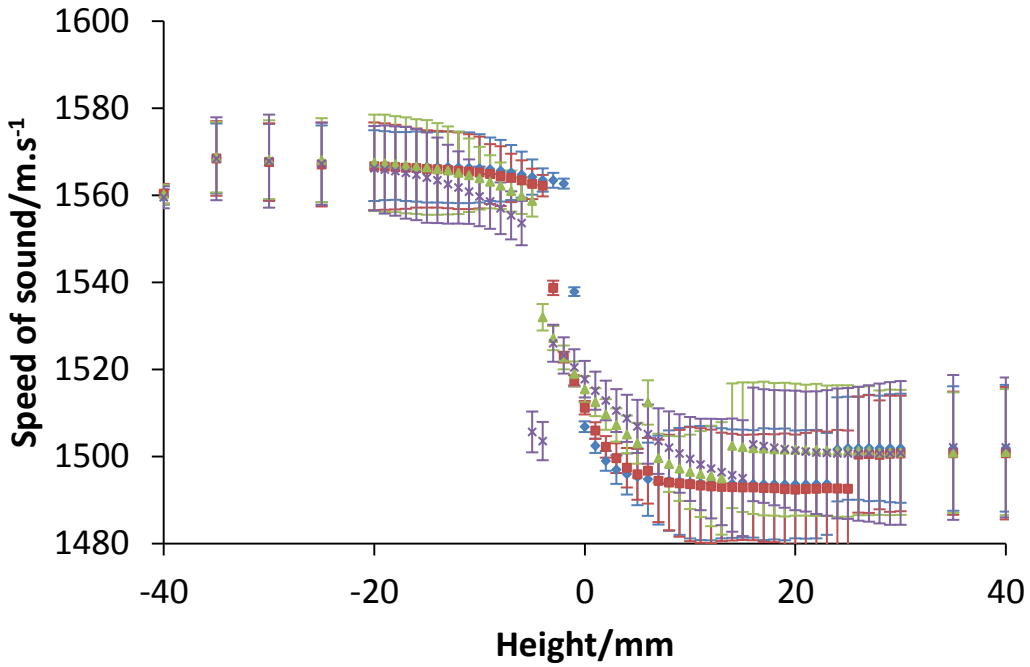


**Figure 4.6 - Speed of sound as a function of cell height at different time intervals for 18wt% caseinate solution at 25 °C. ♦= 3h, ■ = 8h, ▲=28h, and x = 56h.**

#### 4.4.2.2 Using Sound velocity as a function of concentration to create a concentration profile as water diffuses into sodium caseinate solution

In Figure 4.7, the results obtained using the Resoscan for different concentrations of sodium caseinate solution are shown. As described previously, the results give a linear relationship. This means that speed of sound and concentration are proportional, and from the equation displayed in Figure 4.7, the constant relating the two is 0.0027.

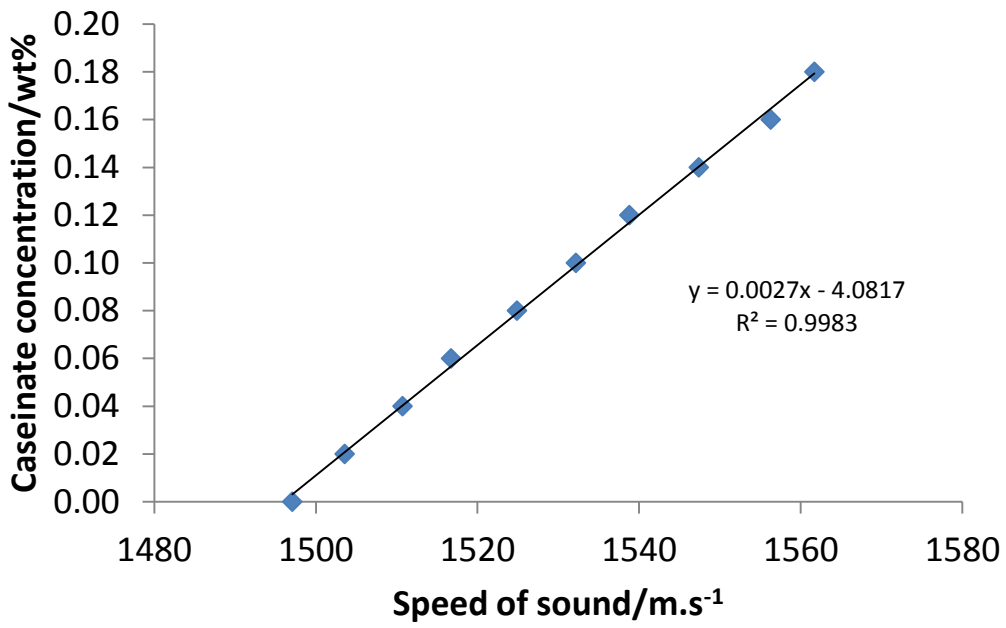


**Figure 4.7 - Speed of sound as a function of caseinate concentration**

Taking Figure 4.7, and applying this constant to the speed of sound data, a concentration profile can be generated. This is shown in Figure 4.8. Figure 4.8 shows the concentration profiles of the entire cell at 3h, 13h, 23h, and 48h. These give a typical shape seen in the literature many times previously for concentration profiles of one substance diffusing into another (Rejl et al.,

2010, York et al., 2011, Povey, 1997). The concentrations have been normalised so pure water is represented as 1, and the caseinate solution is represented as 0. Initially, above the boundary, the water phase is uniformly at 1, and below the boundary the caseinate solution is at 0. The boundary is a sharp interface between the two. As time goes on, diffusion of the two phases occurs, and this is seen as a blurring and spreading of the boundary, as the distinction between the two phases becomes less obvious and more gradual. Figure 4.8, however, demonstrates that the diffusion of the two species is rather slow, with only a noticeable change in shape of the profile after 13h.

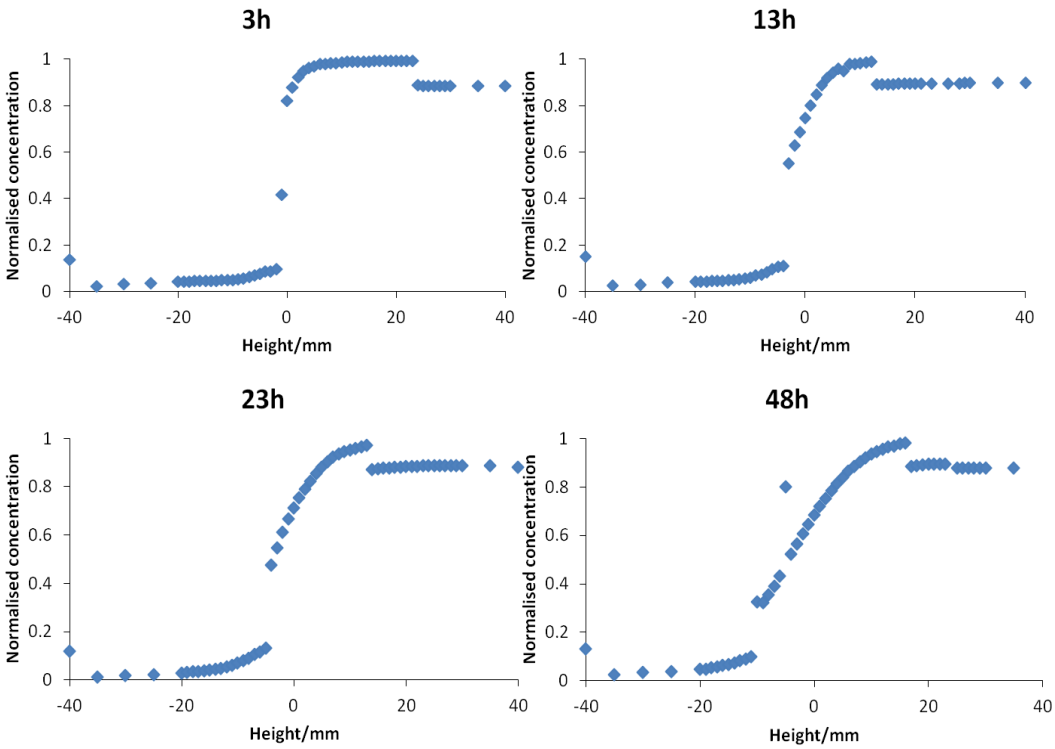


**Figure 4.8 - Concentration profiles at t= 3h, 13h, 23h and 48h for 18wt% caseinate solution.**

### 4.4.3 Modelling concentration profiles

#### 4.4.3.1 Constructing a model to predict the diffusion of water into a biopolymer solution

In order to solve this problem, diffusion through a semi-infinite slab should be considered, as has been the case many times in the literature (Cussler, 1997, Crank, 1975, Treybal, 1980). In this case, the contents of the cell can be thought of as two semi-infinite slabs end to end, meeting at a boundary x=0 (Cussler, 1997).

Starting with Fick's second law of diffusion, relating concentration to both time and position, it is possible to derive an equation which can be used to model such a concentration profile.

$$\frac{dc}{dt} = \frac{d}{dx}\left(D\frac{dc}{dx}\right) \qquad \textbf{4.3}$$

In order to solve this partial differential equation, a new variable must be defined (Cussler, 1997):

$$\zeta = \frac{x}{\sqrt{4Dt}} \qquad \textbf{4.4}$$

From this new variable, the differential equation can be written as:

$$\frac{d^2c}{d\zeta^2} + 2\zeta\frac{dc}{d\zeta} = 0 \qquad \textbf{4.5}$$

The boundary conditions can be defined as:

$$\zeta = 0\,,\, c_{1,x} = c_{1,0}$$

$$\zeta = \infty\,,\; c_{1,x} = c_{1,\infty} \qquad \textbf{4.6}$$

Where $c_{1,x}$ is the concentration at position $x$, $c_{1,0}$ is the concentration at the interface, and $c_{1,\infty}$ is the concentration at infinite distance from the interface.

Applying the boundary conditions shown in equation 4.6, the concentration profile can be defined as (Cussler, 1997):

$$\frac{c_{1,x} - c_{1,0}}{c_{1,\infty} - c_{1,0}} = erf\zeta \qquad \textbf{4.7}$$

This allows a concentration profile to be constructed where the concentration varies with both position and time. The equation can be applied to the caseinate phase and the water phase, and by combining the two, a profile of the entire system can be generated.

#### 4.4.3.2 Applying the model to experimental concentration profiles

By taking the individual concentration profiles for different times, discussed in section 4.4.2.2, it is possible to fit the models to the experimental data. This allows predictions to be made about how other biopolymer systems will behave as water diffuses into them, and it also allows a diffusion coefficient to be calculated. Figures 4.9 to 4.14 show the models fitted to experimental concentration profiles at 3h, 8h, 18h, 48h and 58h. This range was chosen as it gives a good representation across the entire timeframe over which the experiment was conducted.

In the simplest case, diffusion would be constant throughout the experiment, and only the water phase would diffuse into the biopolymer. However, it is unlikely that this is the case here, because the biopolymer phase, 18 wt% caseinate, is largely composed of water to begin with, i.e. the concentration gradient between the two phases is relatively small, and so as more water

diffuses in, the driving force for diffusion will diminish and so the rate of diffusion will become slower.

Figure 4.9 shows the experimental data at 3h with the model described in section 4.4.3.1. To fit the model to the data different diffusion coefficients were applied to equation 4.7 in order to obtain the best possible fit.

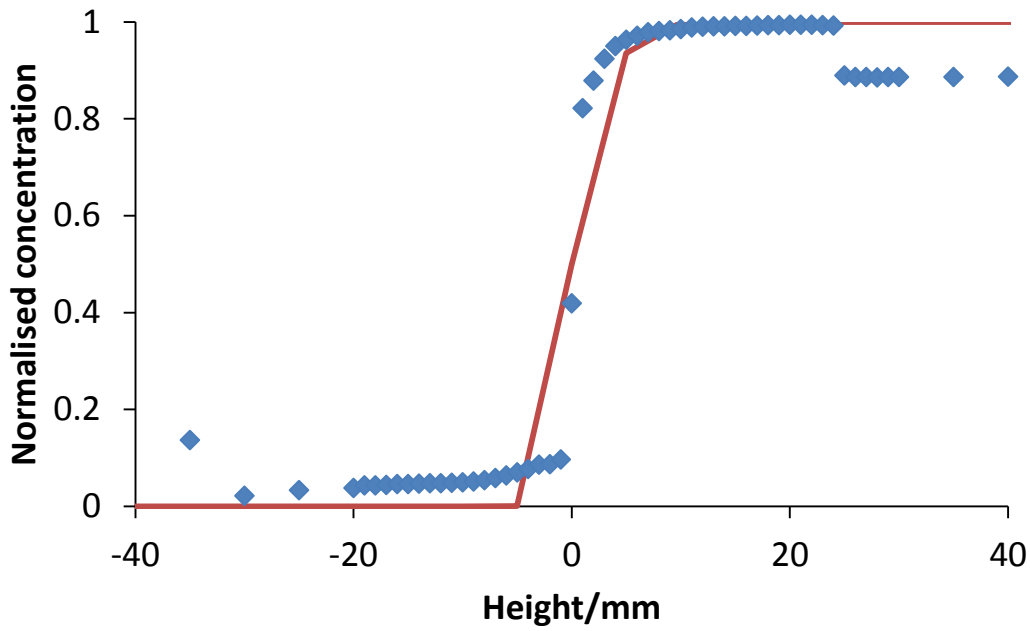


**Figure 4.9 - Fitting mathematical model of concentration profile to the experimental data at t= 3h.**

Applying f and t tests to the data shows the model is statistically similar to the experimental data, with p values of 0.36 and 0.42 respectively. A p value greater than 0.05 is considered to have no significant difference. As both water and caseinate solution are diffusing simultaneously, two diffusion coefficients are applied to the model, $D_1$ for water in the caseinate phase, where x < 0, and $D_2$ for caseinate diffusing into the water phase, where $x$ > 0. In this case $D_1$ is 1.0 x $10^{-10}$ $m^2.s^{-1}$ and $D_2$ is 1.5 x $10^{-9}$ $m^2.s^{-1}$. Interestingly,

$D_2$ is an order of magnitude faster than $D_1$. This could be due to the large viscosity difference between the two phases, 75000-85000 mPas of caseinate as compared to 0.89 mPas of water.

Figure 4.10 shows the model fitted to the experimental data at 8h. Applying f and t tests to the data shows the model is statistically similar to the experimental data, with p values of 0.27 and 0.28 respectively. Here, $D_1$ is $2.5 \times 10^{-10}$ $m^2.s^{-1}$ and $D_2$ is $2.5 \times 10^{-10}$ $m^2.s^{-1}$.

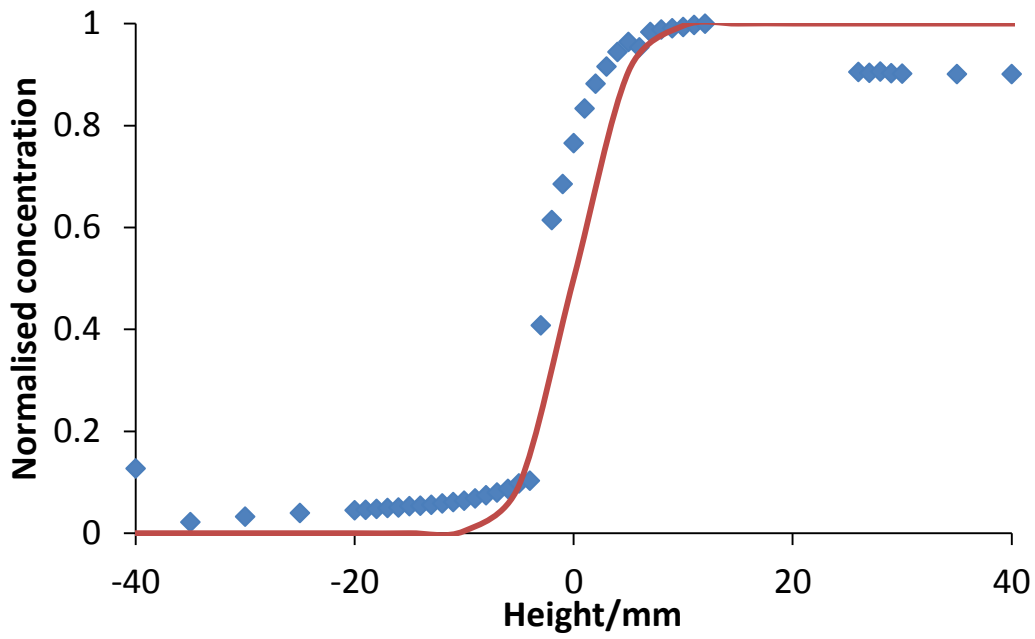


**Figure 4.10 - Fitting mathematical model of concentration profile to the experimental data at t= 8h.**

Clearly the diffusion rate of caseinate into water has slowed down dramatically by 8h, whereas the rate of water diffusion into the caseinate phase has not changed significantly. In Figure 4.11 the model has been fitted with a $D_1$ of $1.8 \times 10^{-10}$ $m^2.s^{-1}$ and a $D_2$ of $1.3 \times 10^{-10}$ $m^2.s^{-1}$ for t=13h. Applying f and t tests to the data shows the model is again statistically similar to the experimental data, with p values of 0.21 and 0.30 respectively.

Caseinate diffusion continues to slow with time, although not by a great amount, and the diffusion of water remains relatively constant.

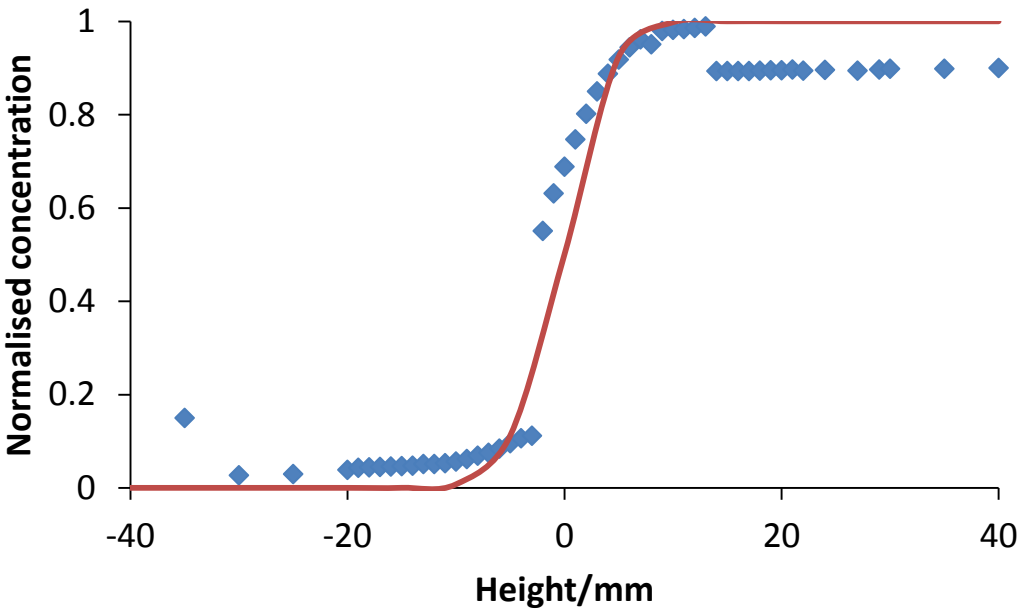


**Figure 4.11 - Fitting mathematical model of concentration profile to the experimental data at t= 13h.**

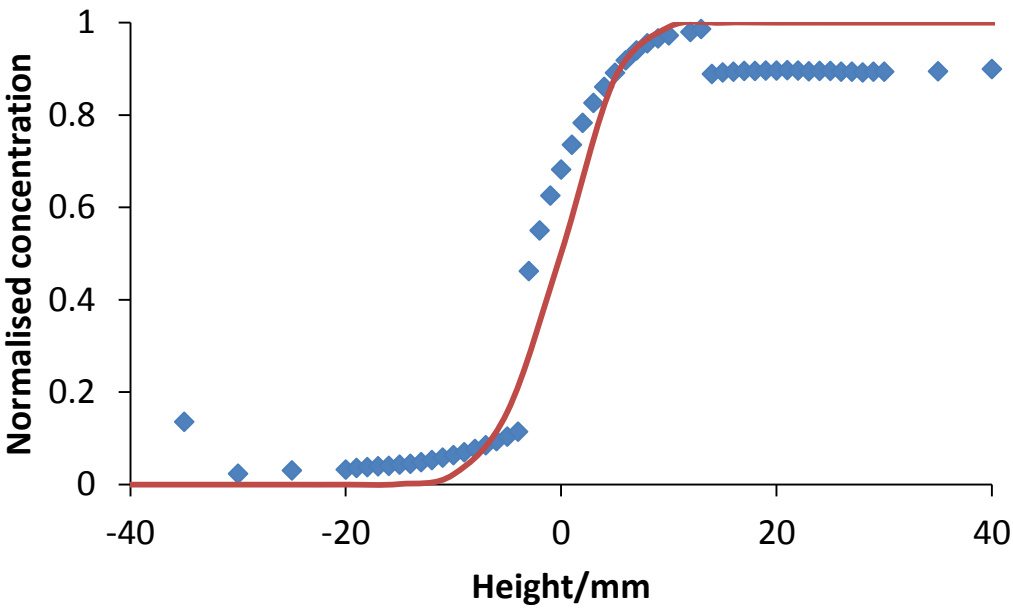


**Figure 4.12 - Fitting mathematical model of concentration profile to the experimental data at t= 18h.**

At 18h, the $D_1$ and $D_2$ values used to fit the model to the data, as shown in Figure 4.12 are 1.9 x $10^{-10}$ $m^2.s^{-1}$ and 1.4 x $10^{-10}$ $m^2.s^{-1}$ respectively. Once again, applying f and t tests to the data shows the model is statistically similar to the experimental data, with p values of 0.18 and 0.36 respectively. These values of diffusion coefficient are relatively constant between 13h and 18h.

At 48 h, in Figure 4.13, the $D_1$ and $D_2$ values used to fit the model to the data are 2.8 x $10^{-10}$ $m^2.s^{-1}$ and 1.4 x $10^{-10}$ $m^2.s^{-1}$ respectively. These values of diffusion coefficient are again relatively constant between 13h and 48h. Applying f and t tests to the data shows the model is statistically similar to the experimental data, with p values of 0.10 and 0.19 respectively.

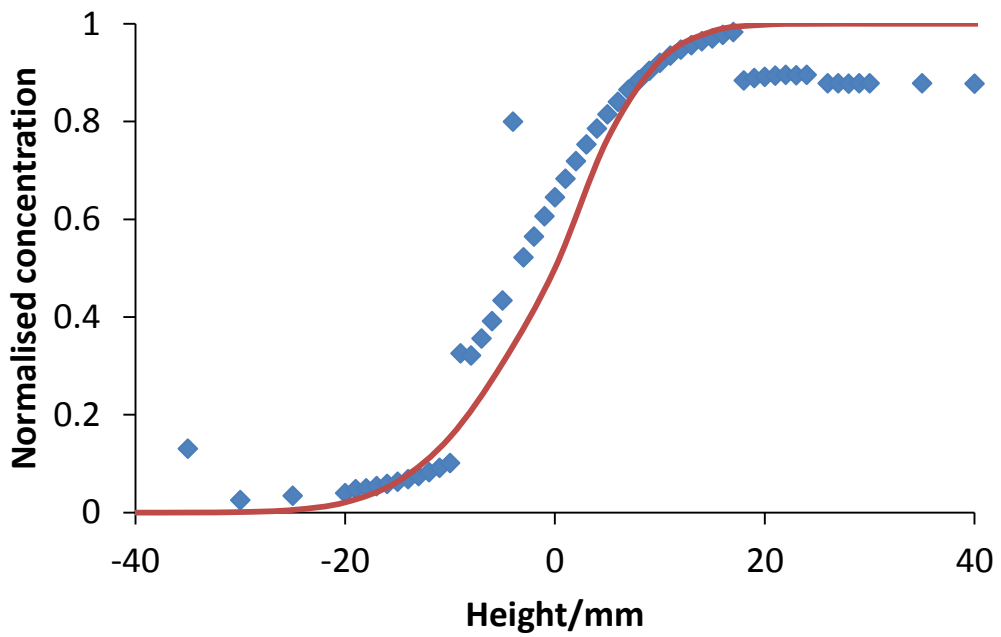


**Figure 4.13 - Fitting mathematical model of concentration profile to the experimental data at t= 48h.**

Finally, in Figure 4.14, at 58h, the model has been fitted to the experimental data with a $D_1$ of 2.2 x $10^{-10}$ $m^2.s^{-1}$ and a $D_2$ of 3.0 x $10^{-10}$ $m^2.s^{-1}$ . Applying f and t tests to the data again shows the model is statistically similar to the experimental data, with p values of 0.22 and 0.17 respectively.

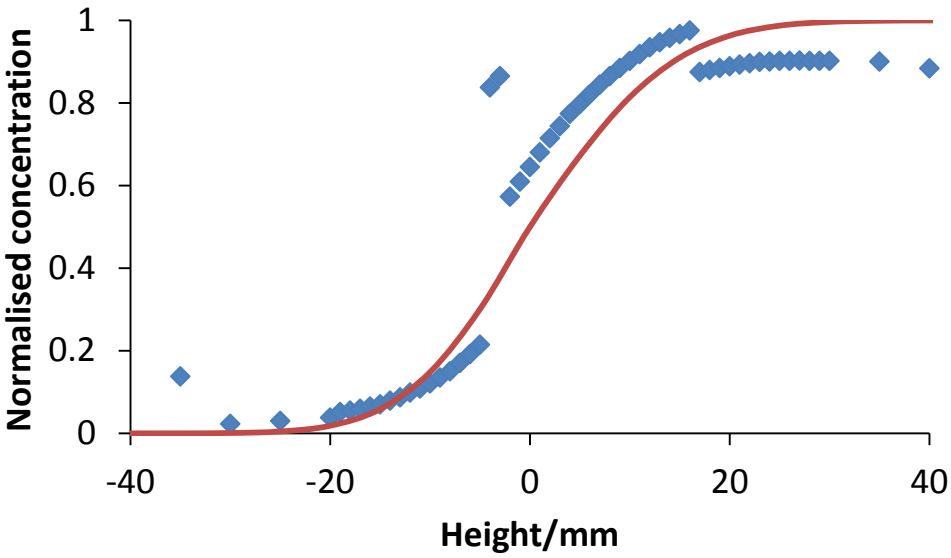


**Figure 4.14 - Fitting mathematical model of concentration profile to the experimental data at t= 56h.**

Overall, from the fitting of data to the mathematical model from 4.4.3.1, the diffusion coefficient of water appears to remain relatively constant throughout the experiment. The diffusion coefficient suggests that the diffusion of water into the biopolymer is very slow, and so it is unlikely the concentration gradient will be reduced enough to limit the intake of more water during the 58h time period, therefore a constant diffusion is an entirely acceptable scenario.

## 4.5. Conclusions

This work has successfully developed a novel method for the investigation of water diffusion into biopolymer solutions using the Acoustiscan device built at University of Leeds. The method has been validated using a sodium caseinate system, tested in replicate to give reproducible results. The procedure has scope to test a variety of different compositions of biopolymer solution over a wide range of temperatures, and therefore is a useful tool in determining the diffusion properties of biopolymer systems. A model based on Fick's second law of diffusion has been successfully fitted to the experimental data at various time intervals. The procedure has confirmed that two way diffusion occurs in the water-biopolymer system and the diffusion coefficients have been found to be in the order of 2.0 $x10^{-10}$ $m^2.s^{-1}$ for water and 1.5 $x10^{-10}$ $m^2.s^{-1}$ for caseinate at t >8h and prior to t=8h an order of magnitude faster at 1.0 $x10^{-9}$ $m^2.s^{-1}$.

## 4.6. Further work

There is a great deal of further work that would be interesting to carry out following the successful validation of this novel method. The effect of temperature on diffusion is easily examined using the Acoustiscan with support from temperature – speed of sound data already collected on the Resoscan for the sodium caseinate system. It would also be interesting and of great merit to this project to develop an understanding of how different composition biopolymer systems behave under the same conditions. The outcomes of these additional experiments will allow better understanding of the effect of temperature on diffusion of water into each sample, and the

effects of adding crosslinkers and mixing systems on the diffusion of water can be examined.

By defining a diffusion coefficient for these different biopolymer systems, for example starch based, and synthetic acrylic based systems, an explanation as to why they behave so differently with respect to the issue of ice water resistance as outlined in chapter 1 could be uncovered. This knowledge could lead to an adhesive being designed which outperforms all currently available water based labelling adhesives.

# Chapter 5 Rehydration of thin biopolymer films

## 5.1 Introduction

In this chapter, dried, thin biopolymer films will be investigated with respect to their behaviour when they are rehydrated. A novel method is developed to monitor ingress of a water droplet into a dried film and analysis of the problem is presented showing how the diffusion coefficient can be inferred in each case. As in chapter 3, the effects of temperature and composition were explored. Confocal microscopy and SEM were used to discover whether the differences in rehydration behaviour could be due to changes in the microstructure of the films.

### 5.1.1 Why is the rehydration behaviour of thin films important?

As mentioned in previous chapters, thin biopolymer films have a wide range of applications, from adhesives and paints to edible food and drug coatings. In the case of coatings suitable for ingestion, it is important to prevent moisture absorption into the films, during storage, for two main reasons. Firstly, microbes thrive in a moist environment, and so if moisture can penetrate the biopolymer coating, potentially dangerous colonies will begin to multiply. This obviously is not desirable because of the possible consequences for causing consumers ill health. Secondly, as moisture penetrates through the biopolymer coatings, the quality, texture and appearance of the food may be altered, resulting in an inedible product (Kamper and Fennema, 1984). Paint coatings are also susceptible to microbial attack, and the penetration of water can reduce the lifespan of the product and cause damage to the substrate below the film (Houghton et al.,

1988). In chapter 1 the problem faced by the adhesive labelling industry was outlined. Preventing water penetration into adhesive films is important to ensure a high performance is maintained (Mubashar et al., 2009b). Again, water absorption can affect the stability and properties of these biopolymer films. It is therefore important to understand the mechanisms behind moisture absorption and how it can be reduced or retarded.

Similar to the dehydration of these films, there are two main mechanisms which can be responsible for moisture intake. The first, and more obvious mechanism is related to Brownian motion and diffusion. This occurs when the moisture intake is driven solely by a concentration gradient existing between the film and the external environment (Kamper and Fennema, 1984, Buonocore et al., 2003). In addition, the water-polymer affinity plays a role in the absorption of water and other small molecules, such as oxygen. In other words, the solubilisation of the polymer film in water will influence its permeability (Buonocore et al., 2005). These two mechanisms work synergistically to control the absorption of water into biopolymer films.

### 5.1.2 Properties affected by the intake of moisture

When water is absorbed by thin biopolymer films many of their physical properties change, resulting in a loss in their mechanical properties (Chick and Ustunol, 1998). As the functional properties of biopolymer films require a dehydrated structure, the influx of moisture can be catastrophic with respect to performance. For example, as moisture penetrates an adhesive film, the biopolymer will gradually become more fluid as the viscosity decreases and so become tacky again. As this occurs the adhesion forces holding the substrates in place become much weaker, potentially resulting in peeling or

complete failure of the adhesive film (Shih and Hamed, 1997). In industry, mechanical properties of such films can be tested by an ice-water resistance test, where an adhesive film is tested by immersing the test subject, two substrates adhered to each other (i.e. glass bottle, and paper label) with the desired adhesive sample into ice-water. Separation of the two substrates is attempted over various time intervals, and the point of failure is noted.

### 5.1.3 Methods used to measure moisture intake

The majority of work in the literature deals with water vapour, as opposed to liquid water investigated in this work. Liquid water rehydration was chosen in this case because of its relevance to the problems faced in the adhesive label industry as described in section 1.2. Sorption data is a common method used to investigate water intake (Dhanpal et al., 2009, Hernandez and Gavara, 1994, Staudt et al., 2013, Metayer et al., 1999). There are several methods to implement this, including using sorption cells where the test material is placed in a special cell with pressure control, and connected to a solvent reservoir (Nizovtsev et al., 2008). The water vapour pressures can then be measured as a function of time. Other work has used a saturated sponge placed on top of the test sample and monitored the water intake gravimetrically (Drchalova and Cerny, 2003).

It is possible for more solid structures such as cement or dental composites to be completely immersed in water over set time intervals, and removed for gravimetric analysis periodically (Costella et al., 2010). Unfortunately, this simple gravimetric method is not appropriate for the thin biopolymer films investigated in this work, as they will quickly dissolve and lose their solid structure. In this chapter an alternative method has been developed to

monitor quantitatively and model a single water droplet being absorbed by a biopolymer film. The method used has been modified from that used to monitor the drying of an ink jet droplet using a camera to film the volume profile of the droplet (Enomae et al., 2012).

## 5.2 Materials and methods

### 5.2.1 Materials

The samples investigated in the rehydration experiments were 18 wt% sodium caseinate (purchased from Acros organics, Belgium) solution, 7 wt% purity starch (provided by Henkel, Germany), and several mixtures of sodium caseinate and starch in the following ratios: 1:7 caseinate:starch, 2:7, 3.5:7, 7:7, and 14:7 wt%. These mixtures were chosen to reflect the full range of caseinate based and starch based mixtures. Preparation of the pure solutions are described in section 3.2.2. The mixed solutions were prepared in the same way, however the two powders were blended thoroughly with mechanical stirring (IKA RW11, UK) at 300 rpm before being added to water.

### 5.2.2 Monitoring rehydration of water into biopolymer films

Dehydrated films were prepared as described in the method of section 3.2.3. The dried film on a stainless steel beam was placed on a platform in a sealed Perspex box with Peltier temperature control (Stable Micro Systems, UK). Relative humidity was monitored and recorded. A 20 μl droplet of Milli-Q water was applied to the film using a microliter syringe. A CCD video camera (Optivision, UK), was set up to record the droplet profile at a frame rate of between 1fps (frames per second) and 0.1fps depending on the

external conditions, monitoring the reduction of volume of the droplet. The video in the form of an .avi file produced was converted into individual Jpeg images which were analysed using Imagetool, an image analysis freeware. The height and contact area of the droplet were measured in pixels. The syringe tip of known diameter was used as a scale to convert the number of pixels to mm.

The following formula for volume of a partial sphere was used to calculate the droplet volume at set time intervals, and this was normalised as a function of the initial volume and plotted against time. A schematic can be seen in Figure 5.1 to illustrate this.

$$\frac{1}{6}\pi h\left(3a^2\right)+h^2 \qquad \textbf{5.1}$$

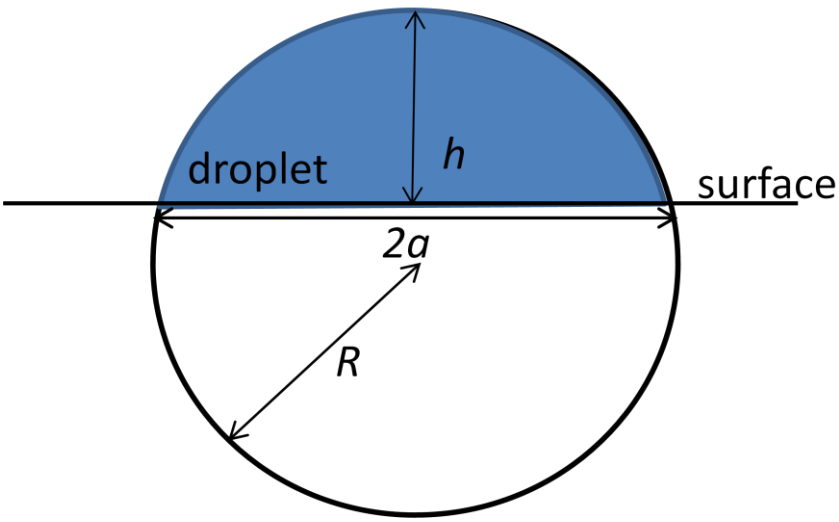


**Figure 5.1 - Schematic of a droplet on a substrate showing radius, *R*, contact radius, *a*, and height of droplet, *h*, used in calculating volume of a partial sphere.**

Taking into account the contact area of the droplet, as demonstrated in equation 5.2, a representation of the ingress of the droplet into the film is

given. Here, the original assumption is that the effect of evaporation is small, and that the main cause of droplet disappearance is due to the flux of moisture into the film. Thus, to account for this effect of evaporation, a droplet of water was deposited onto the metal substrate and monitored as above. The results of change in droplet volume with time were normalised by the surface area of the droplet in contact with the air, *A*, from the formula $A_a=\pi(a^2+h^2)$, and was used as a correction factor when calculating the rate of rehydration of a droplet into each biopolymer film. This analysis gives a rough guide to the flux, as, as demonstrated later in the chapter, evaporation actually plays a large part in the droplet disappearance and so cannot be safely neglected.

$$\frac{\left(\frac{1}{6}\pi h\left(3a^2\right)+h^2\right)}{\pi a^2} \qquad \textbf{5.2}$$

## 5.3 Results and discussion

In this section the different rehydration kinetics of starch and caseinate based films is discussed. Several mixtures of different starch:casein ratios have been chosen to give a full representation of whether the synergistic behaviour between the two biopolymers, seen when the films are dehydrated, Chapter 2, also holds true for water absorption. Images obtained from both SEM and confocal microscopy are presented to provide insight into how the different microstructures and surfaces of the films could affect the moisture rehydration rate. Finally, mathematical models of sorption are applied and fitted to the results to help explain the mechanisms involved in the water absorption.

### 5.3.1 Kinetics of rehydration of thin biopolymer films

In Figure 5.2 the results for the change in droplet size as a function of area, with respect to time are shown for sodium caseinate films dehydrated at 30 °C. In all cases the rehydration was carried out at 15 °C, 25 °C, and 35 °C. Some experiments were conducted below this, at 10 °C, however the rate of evaporation, calculated from the droplet deposited on the clean metal substrate, with no biopolymer film present, was faster than the rehydration at this temperature, so this data did not give a true representation of the rehydration behaviour, and is therefore not included in this work. This is likely due to the variation in relative humidity, i.e. the amount of moisture present in the air compared to how much moisture the air can hold, which is exaggerated as temperature decreases. This is because when air pressure is constant, for the same amount of moisture in the air, relative humidity increases as temperature decreases. The humidity also changes from day to day, which may have affected these results. Whilst temperature control is easily achievable with the apparatus set up used, currently the control of relative humidity is not easy and involves placing saturated salt solutions in the chamber. Whilst this is enough at higher temperatures to keep the humidity within a few percent of the desired 30%, at lower temperatures the relative humidity has to be reduced to 30% before being kept there, which can be quite a challenge. The improving reproducibility and reduction in error can be seen in Figure 5.2.

In each case the trend representing the absorption of the droplet has a slight curvature, suggesting that the rehydration rate is not constant throughout the process. As expected, the rehydration is slowest at 15 °C and fastest at

35°C with good reproducibility, from the three repeats carried out in each case. As the temperature gets lower, the reproducibility drops somewhat due to the longer time periods being dealt with, however it is still within an acceptable range.

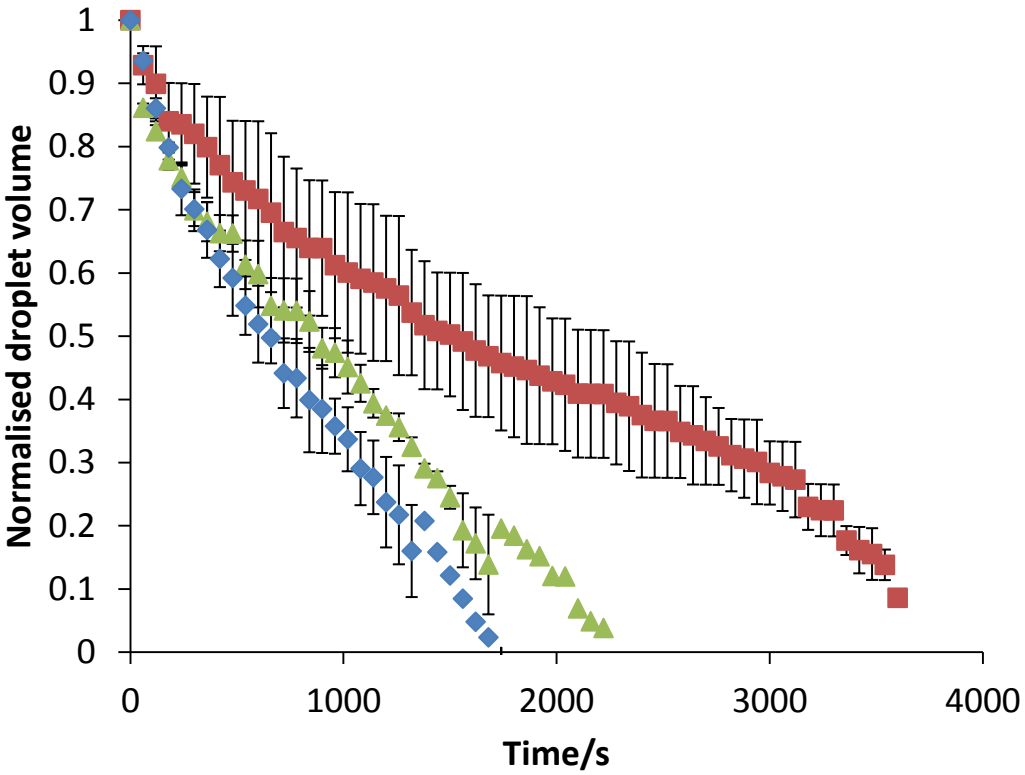


**Figure 5.2 - Droplet volume normalised by contact area with respect to time for sodium caseinate 18 wt% films at constant relative humidity, 25%. ■= 15 °C, ▲ = 25 °C, and ♦ = 35 °C.**

As a comparison between the three temperatures investigated, it is useful to plot the rate of droplet disappearance as a function of time. To give a less noisy curve, a 3-point average has been used to calculate the rate at each time point using the equation $((V_n+V_{n+1}+V_{n+2})/3)/(t_{n+1}-t_n)$, where $V$ is the droplet volume normalised by surface area in contact with the substrate, and $t$ is time at the $n^{th}$ reading. These data are shown in Figure 5.3. As expected,

as temperature is increased, the rate of droplet shrinkage becomes faster. The resulting rate graphs are not linear, suggesting that the diffusive flux does not remain constant throughout the process. Interestingly, the rate drops off rapidly towards the end of the process. This deviation, most noticeable at 15 °C, suggests that evaporation may be more influential in controlling droplet disappearance than first thought. This is considered, and indeed shown, in more depth later in this chapter.

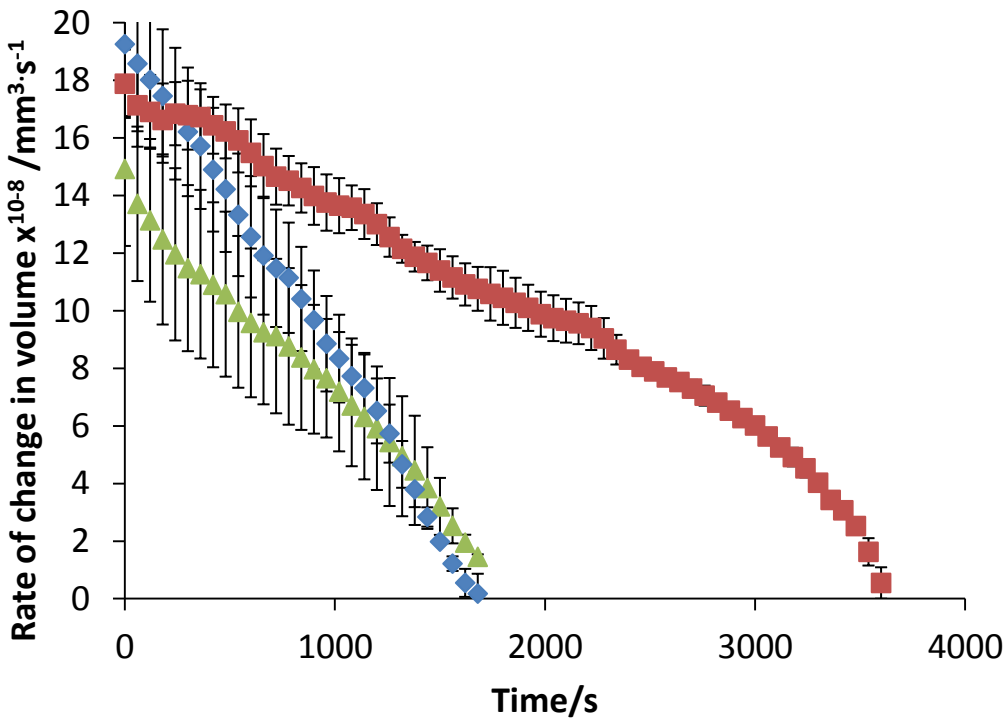


**Figure 5.3 - Rate of change of droplet volume normalised by contact area with respect to time for sodium caseinate 18 wt% films at constant relative humidity, 25%. ■= 15 °C, ▲ = 25 °C, and ♦ = 35 °C.**

It is conceivable that the structures produced as the films dry could differ with an increase in temperature, because, as confirmed in Chapter 3, dehydration is faster at higher temperatures. Thus, if the microstructure of a film which has taken longer to dry, i.e. dried at a lower temperature, is more

open and porous, then subsequent absorption of water will occur at a faster rate. In Figure 5.4 the rehydration of a film produced at 20 °C is compared with a film produced at 30 °C at a rehydration temperature of 25 °C.

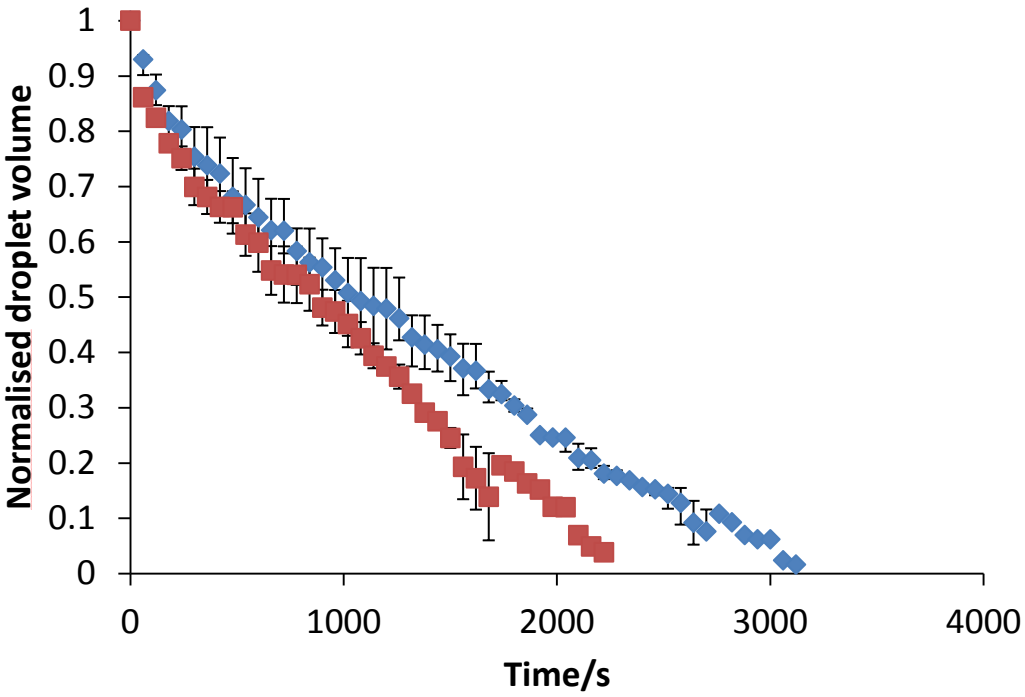


**Figure 5.4 - Normalised droplet volume as a function of contact area with respect to time for sodium caseinate 18 wt% films at constant relative humidity, 25% ± 5% and 30 °C, dehydrated at ■ = 30 °C, and ♦ = 20 °C.**

Figure 5.4 shows that the absorption of water into the film dried at 20 °C is very similar to that of the film dried at 30 °C. The rate of absorption of the water droplet into the two films is almost identical at the beginning of the process, with a slightly greater deviation, with the water droplet volume on the 20 °C film reducing more slowly towards the end of the process. This could be due to slight differences in the humidity of the sealed vessel, as it was not possible to control relative humidity accurately due to the apparatus constraints. An increase in humidity would increase the moisture vapour in

the surrounding air and this could potentially begin to penetrate the film in addition to the droplet, thus decreasing the moisture gradient between the droplet and the film, resulting in a slower absorption. Of course the penetration of water vapour would be a relatively slow process compared to that of liquid water, so the effect would not be all that significant. From the results in Figure 5.4, it is unlikely that an increase in drying temperature of this scale would lead to a different film microstructure, as there is no significant difference in the rehydration between the two films.

It is suggested in the literature that the arrangement of molecules within the polymer affects the rate of rehydration (Evingur and Pekcan, 2011a, Delahaye et al., 1998). Therefore, a cross-linker, aluminium sulphate was added to the caseinate solution to alter its internal structure. By adding a cross-linker, the arrangement of the molecules within the film will become more tightly packed and so it will become more difficult for water to penetrate the polymer as the channels between molecules will be smaller (Saravacos and Maroulis, 2001). Figure 5.5 shows the results for a film produced with 0.1 wt% and 0.2 wt% cross-linker added. The addition of the cross-linker occurs once all the sodium caseinate has been dissolved during the sample preparation. It has been suggested that sodium caseinate forms cross links through the ester phosphate groups (Aoki et al., 1987). These structural changes produce a solution with higher viscosity compared to a non cross-linked caseinate solution, with more tightly packed molecules. This suggests the dried cross-linked films will be more resistant to water penetration.

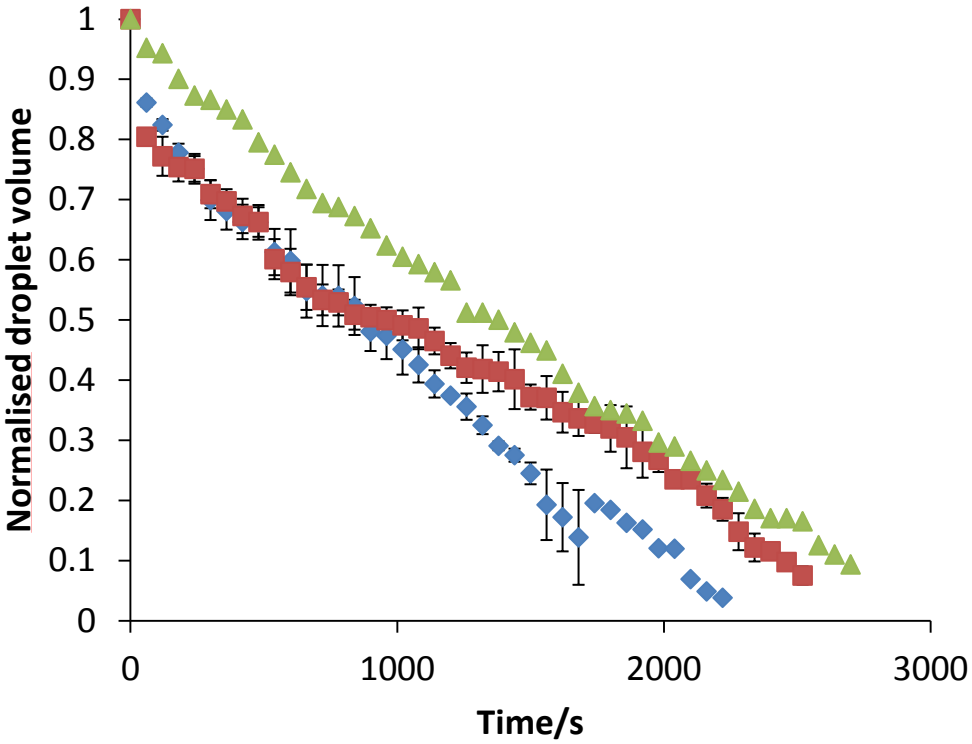


**Figure 5.5 - Normalised droplet volume as a function of contact area with respect to time for sodium caseinate 18 wt% films at constant relative humidity, 25% ± 5%, and 30 °C. ▲ = 0.1 wt% cross-linker, ■ = 0.2 wt% cross-linker, and ♦ = no cross-linker.**

The data in Figure 5.5 does indeed show this trend, however once again there is not really a significant decrease in absorption between the three films. The amount of cross-linker added was chosen as this is a typical amount used in industry in the preparation of water-based biopolymer adhesives. Perhaps an interesting systematic study would be to continue increasing the amount of cross-linker used, but due to time restraints, this must be considered as future work.

The other biopolymer system of interest in this work is 7 wt% starch. As with the caseinate films, these films were all prepared at 30 °C and 30% relative humidity. The pure starch films were rehydrated using the same water

droplet technique at a constant humidity of 25% ±5% across a range of temperatures. The results are shown in Figure 5.6.

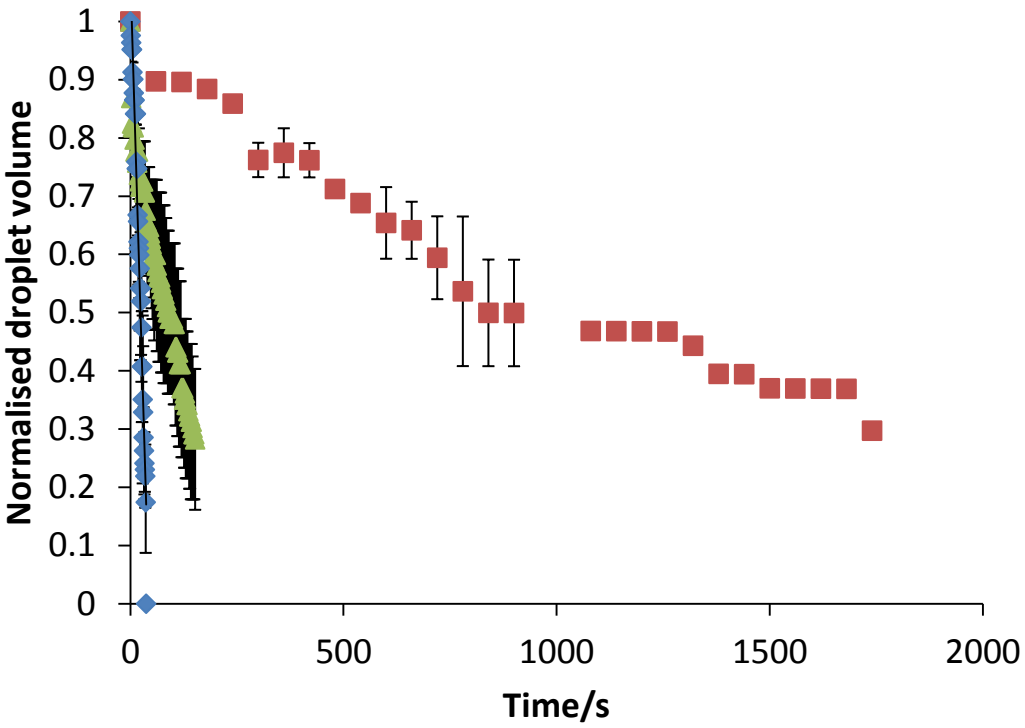


**Figure 5.6 - Normalised droplet volume as a function of contact area with respect to time for 7 wt% starch films at constant relative humidity, 25% ± 5%. ■= 15 °C, ▲= 25 °C, and ♦ = 35 °C.**

Similar to the trend seen for the sodium caseinate films, the water is absorbed faster as temperature is increased, however it is interesting to note that this increase in absorption rate is much more pronounced as compared to the caseinate film. For example the time taken for the droplet to be absorbed at 15 °C is over half an hour whereas at 25 °C it is around 2 minutes and at 35 °C only a matter of seconds. This huge difference in absorption rate could be due to several things. First, as the starch films dry, large stresses build up as the films contract towards the centre. The films cannot withstand this stress and so cracks form to release some of the stress from the system. These cracks occur randomly throughout the film

and some can be on a micro scale so are not visible to the naked eye. If the droplet happened to be deposited in an area with a large frequency of such micro-cracks, it is likely to be absorbed much faster than if there are no cracks, as the crack provide entry routes into the film, and increase the film's surface area in contact with the droplet. The structure of the films will be discussed further in the following section. The reproducibility however is quite good, so it is more likely that the large differences are due to the effect of the surrounding temperature on the films. As the temperature increases, the micro-cracks in the film could expand, providing a larger defect in the surface for the water to penetrate. As the films are so thin, at around 70 µm, it is possible that a crack could run almost the entire thickness of the film, meaning the water droplet could easily run into the film and spread internally. In Figure 5.7 the rate of change in normalised droplet volume is shown as a function of time. There is a sharp increase in the rate between 15 °C and 25 °C, with the rate at 25 °C approximately 100 times faster than at 15 °C. The rate curves at both 25 °C and 35 °C show an initial increase in rate before it begins to decrease with time, then the rate appears to decrease almost linearly with time, suggesting that the diffusive flux is constant for the majority of the process. This could be due to a change in surface area with time counteracting and thus minimising the effect of reducing volume on the rate of droplet absorption.

A key observation was made during the experiment with the starch films that the water droplet spread on the surface of the film initially. This spreading did not occur with the caseinate films, suggesting they are more hydrophobic than the starch films. The higher hydrophilicity of the starch films helps explain why the water penetrates this film composition easily. It is because

of this phenomenon that the contact area of the droplet with the film must be incorporated into the analysis, otherwise the volume presented would not be a true representation of the water absorption.

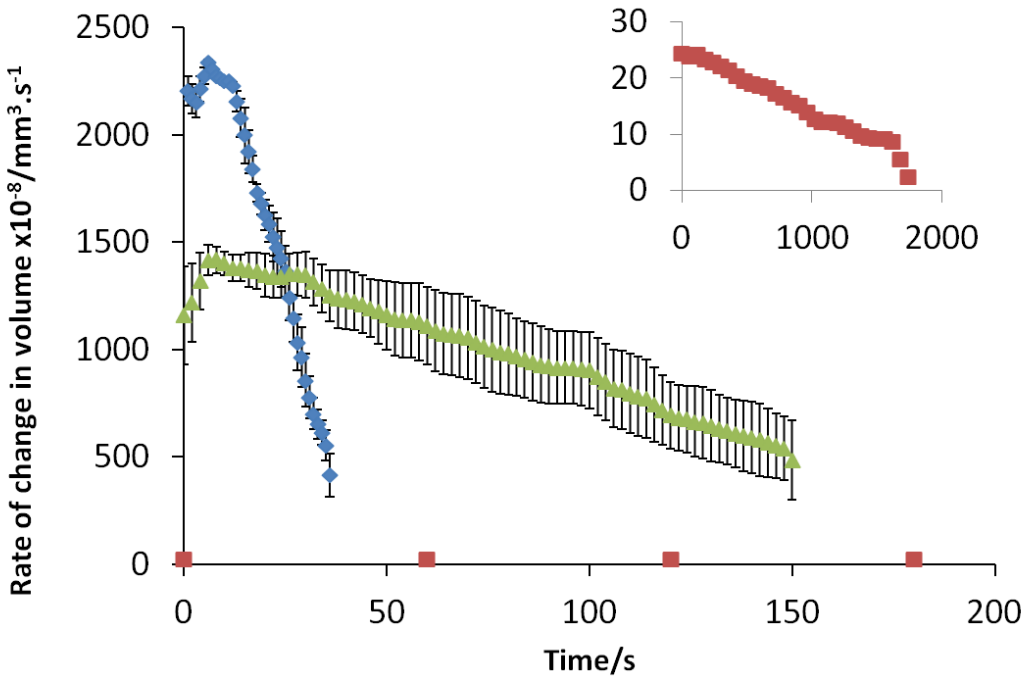


**Figure 5.7 - Rate of volume loss with respect to time for 7 wt% starch films at constant relative humidity, 25% ± 5%. ■= 15 °C, ▲= 25 °C, and ♦ = 35 °C.**

As there are large differences in the behaviour of the starch films as compared to the caseinate films, an interesting next step would therefore be to incorporate small amounts of sodium caseinate into the starch film to see if the hydrophilicity and thus the rate of moisture absorption can be controlled. To investigate this systematically, the amount of starch used to make the films was constant at 7 wt%, with the amount of sodium caseinate added varying between 1 wt%, 2 wt%, 3.5 wt%, 7 wt% and 14 wt%. All the rehydration experiments were carried out at 30 °C and 25% ± 5% relative

humidity of the surrounding air. From Figure 5.8 it is clear that the amount of caseinate added to the starch system is important if the rehydration rate is to be controlled.

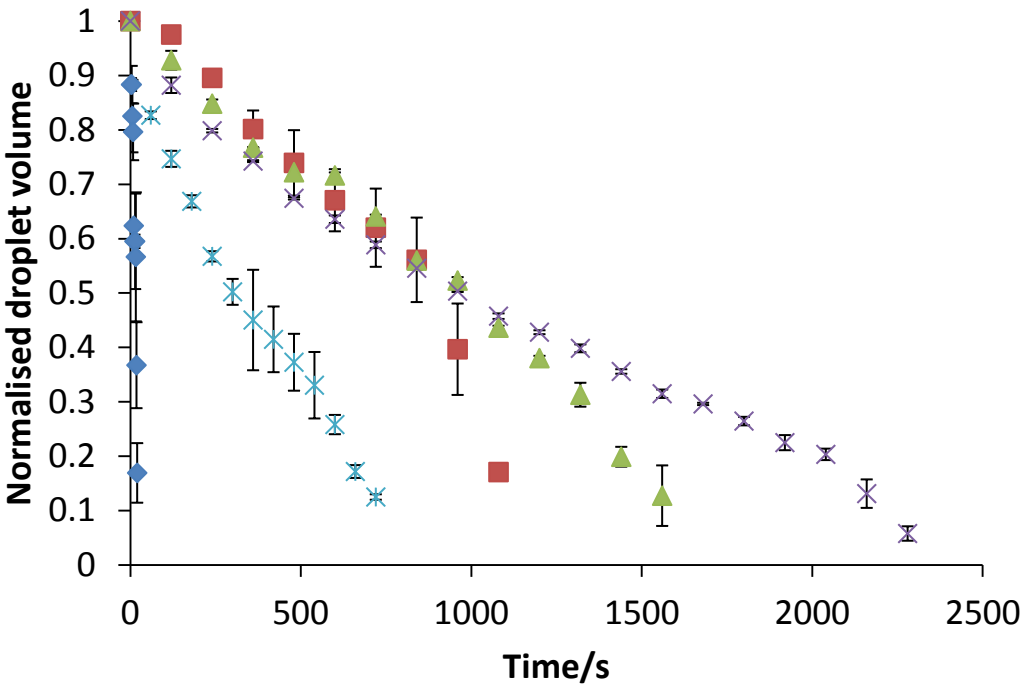


**Figure 5.8 - Normalised droplet volume as a function of contact area with respect to time at 30 °C and constant relative humidity, 25% ± 5%. ♦ = 7 wt% starch with 1 wt% caseinate, ✱ = 7 wt% starch with 2 wt% caseinate, ▲ = 7 wt% starch with 3.5 wt% caseinate, ■ = 7 wt% starch with 7 wt% caseinate, and × = 7 wt% starch with 14 wt% caseinate.**

Due to the large difference in rehydration seen between the starch film with 1 wt% casinate and that with 3.5 wt% caseinate, it seemed logical to investigate the case in which the starch film was mixed with 2 wt% caseinate, a mid-point between these two films. Figure 5.8 shows that this 2 wt% film does not have a rapid rehydration like 1 wt% caseinate, but it is still faster than 3.5 wt% caseinate, with the rehydration curve sitting nicely between the two.

As the concentration of caseinate is increased, more resistance to water is seen, gradually increasing towards, and infact surpassing the rate achieved for the pure 18 wt% sodium caseinate film. This trend is demonstrated further in Figure 5.9, where, if the curves from Figure 5.8 are approximated to be linear, a value $t_{0.5}$, that is, the time taken for half of the droplet volume to be lost, can be used as a comparison tool between the different film compositions.

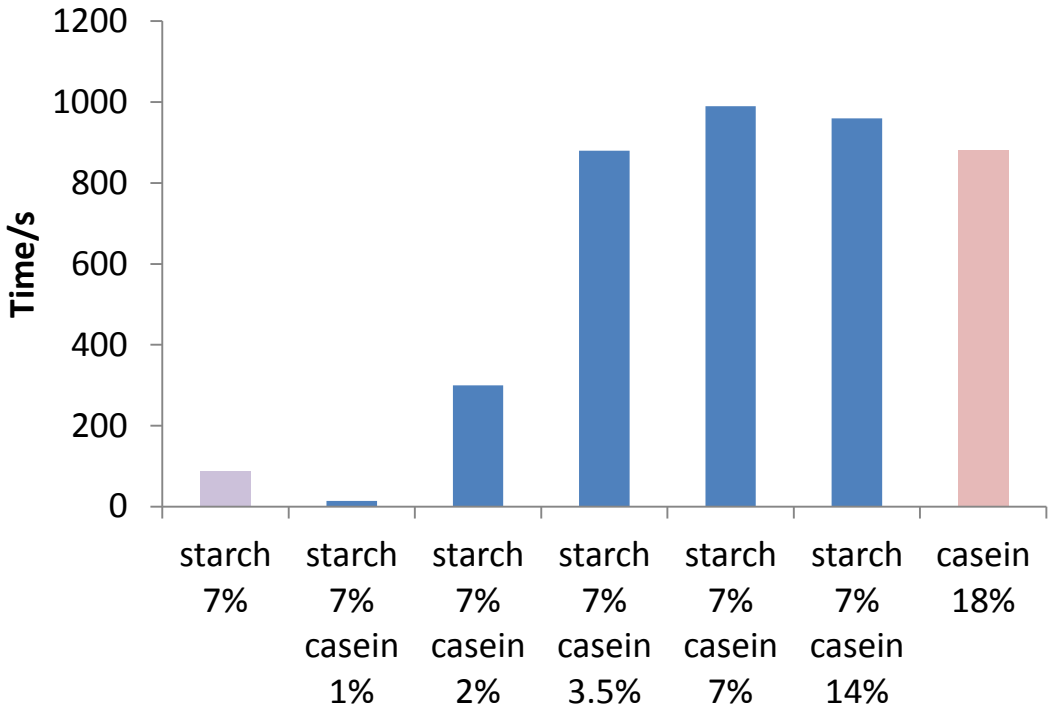


**Figure 5.9 - The $t_{0.5}$ measured at 30 °C and a constant relative humidity, 25% ± 5%, for rehydration of films of different composition.**

Figure 5.9 demonstrates well that the more sodium caseinate that is added to the 7 wt% starch system, the greater the film resistance to water penetration. For example when 1 wt% caseinate is added, the rehydration is very fast, not improving the resistance of the film to water, but in fact making it less resistant than the pure starch film. This could be due to discrete

regions of starch and casein forming within the film's structure, leading to weak sections of film in the drying process, and so allowing water to penetrate in these weak spots easily. This phenomenon only occurs at this mixture concentration, as by adding more sodium caseinate a significant increase in $t_{0.5}$ is seen. Once a concentration of 3.5 wt% caseinate is added, the resistance to water is equivalent to that of the pure sodium caseinate system. This is an important and valuable result, as it is more cost effective to have more starch and less sodium caseinate in the system, so by using this mixture, the same water resistance can be achieved at a lower production cost. When the amount of caseinate in the system is increased further to 7 wt% and 14 wt%, little improvement in water resistance is observed. In fact, at 14 wt% caseinate, the water resistance actually reduces a little. From these results, it is clear that the optimum system when considering both performance and cost would be the system containing 7 wt% starch and 3.5 wt% sodium caseinate.

### 5.3.2 Microstructural analysis of biopolymer systems

As a result of the interesting findings in the above section, an investigation into the microstructure of the various biopolymer films was conducted using both confocal scanning laser microscopy and scanning electron microscopy to investigate the film surfaces, principles and methods of which are discussed in Chapter 1.

#### 5.3.2.1 SEM investigation of film microstructure

The first technique used to investigate the different microstructures of the dried films was SEM. This technique was used to compare the structures of the pure 7 wt% starch and 18 wt% caseinate films. In Figure 5.10 the SEM

image of the starch film is shown. There are a large number of micro-cracks visible across the film surface, and these are likely to be the main reason why the rehydration of water into the starch based films is so fast. The cracks suggest a weak film structure and provide easy access points for the water droplets to penetrate the film and be absorbed.

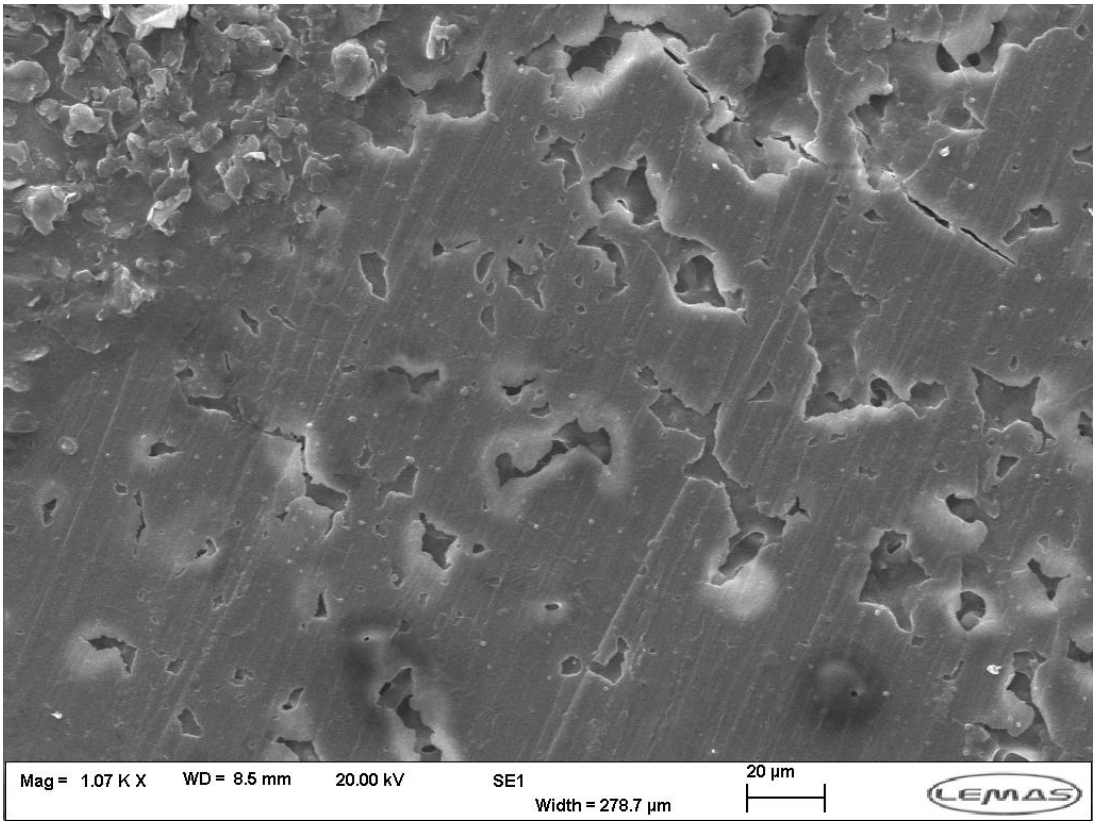


**Figure 5.10 - A SEM image of a starch film dried at 25 °C and 30% relative humidity.**

Figure 5.11 shows the sodium caseinate film surface structure. This film structure is much smoother and more homogeneous than that of the starch film, and no cracks are visible, suggesting the caseinate forms a strong, homogeneous polymer network which is more resistant to water penetration. The striations visible across the film are most likely due to the coating mechanism as the film is produced.

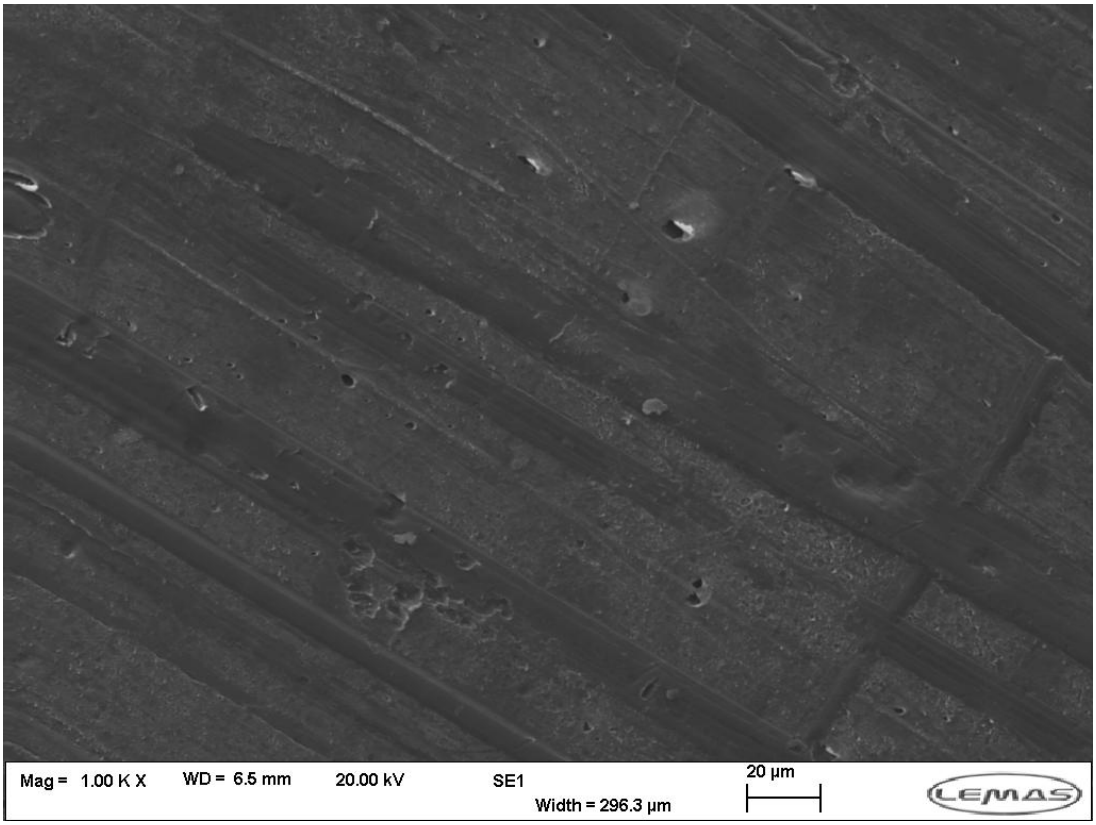


**Figure 5.11 - SEM image of caseinate film dried at 25 C and 30% relative humidity.**

From the two above images there is evidence that the structure of the starch and caseinate films are considerably different, and this could account for the differences seen in their water resistance.

### 5.3.2.2 CLSM investigation of film microstructure

Further to the SEM investigation of the film microstructure for the different biopolymer systems, it was felt that by using CLSM, a better insight into the structure would be gained as confocal microscopy allows both wet and dry samples to be analysed. The main drawback of this method is that a fluorescent dye must be added to the sample to stain either the starch or the casein constituents in order to distinguish between the two components of the film, and this dye has the potential possibility of changing how the biopolymer system behaves. For example, if the dye molecules induce

cross-linking, then the drying mechanism of the films may be altered, leading to an unrepresentative surface structure. However, by comparing the images from the CLSM with those in the previous section from SEM, this does not appear to be the case for these samples.

Figure 5.12 shows the 18 wt% sodium caseinate film surface structure, dyed with Rhodamine B. Again, like with the SEM image, the structure seems consistently homogeneous throughout the film. The darker spots are likely to be where the casein has formed agglomerates during drying, and so the dye here is more concentrated.

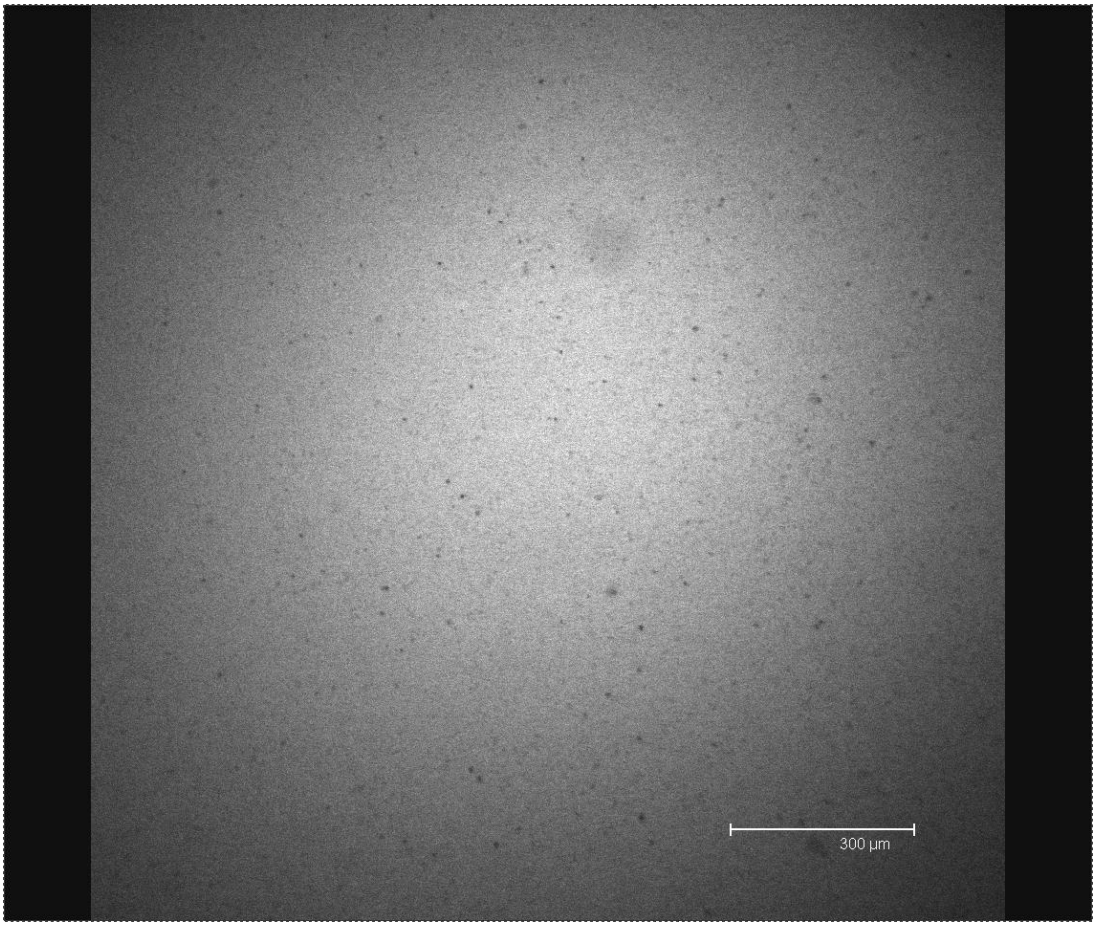


**Figure 5.12 - A CLSM image a of casein film dried at 25 °C and 30% relative humidity.**

Figure 5.13 shows the CLSM image for the pure starch system. This supports the image obtained from the SEM which showed many micro-

cracks, however here there is only one large crack to the bottom left corner of the image. The dark patches visible on the surface are likely to be starch granules, which have not gelatinised fully in the preparation process. These localised starch granules may also account for the starch films having a weaker structure than the casein films.

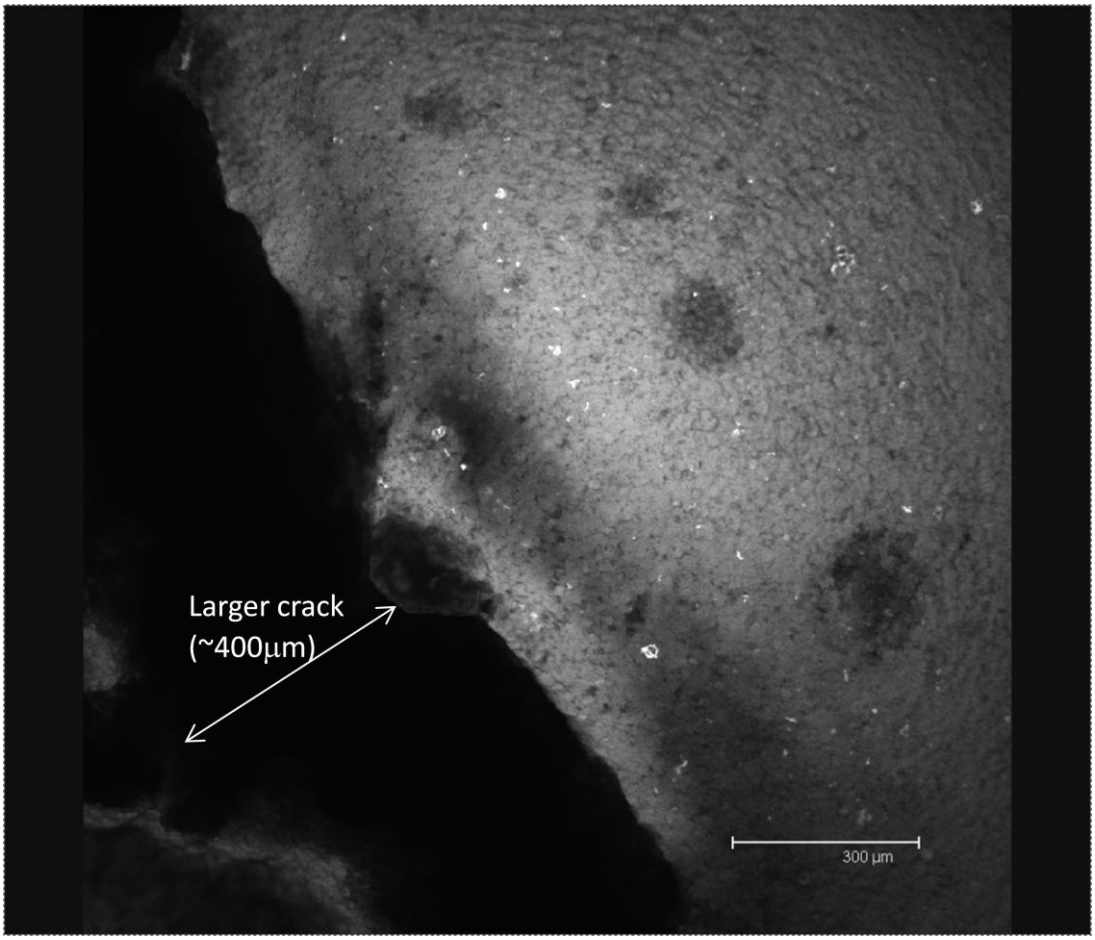


**Figure 5.13 - A CLSM image of a starch film dried at 25 °C and 30% relative humidity.**

While there are clear differences in the structures of the starch and the caseinate films, it is particularly interesting to note the effect of adding casein to the starch solution on structure. From the results displayed in 4.3.1 it is evident that when only a small amount of casein is added, the film becomes less resistant to water than starch alone, but as gradually more casein is

added, the water resistance improves, eventually becoming as resistant if not slightly more resistant than casein alone. By looking at the microstructures of these films of different composition, an explanation as to why this occurs becomes apparent. Figure 5.14 shows the CLSM images of the surface of films with a) 1% casein and 7% starch, b) 3.5% casein and 7% starch, c) 7% casein and 7% starch, and d) 14% casein and 7% starch. Casein is fluorescing green. Figure 5.14a shows large, isolated aggregates of casein within a mostly starch based film. These localised areas likely provide easy access routes for the water to penetrate, due to the different drying mechanisms of the different components leading to a stress build-up and therefore cracking, thus leading to the faster rehydration rate seen in the experimental data. Figure 5.14b also shows localised casein agglomerates, however they are smaller and more frequent, although still not homogenous throughout the starch film. In Figure 5.14c there are less obvious casein areas throughout the film, they are smaller and more regular across the entire film. This formation results in a stronger polymer network, where the two biopolymers have a synergistic relationship to provide a marginally better water resistance to that of pure casein. Finally in Figure 5.14d there are very few flocs of casein, it is mainly finely dispersed throughout the film, again behaving in a similar fashion to pure casein. The homogenous nature of the film structure again suggests the starch and casein work together to form a strong resistance to water ingress. This provides strong evidence that to achieve optimum film performance at the lowest cost, a starch casein mix is an entirely viable alternative to pure casein. The images seen here help explain the experimental data, providing definitive evidence of the different

structures formed when the two biopolymers are mixed in different proportions.

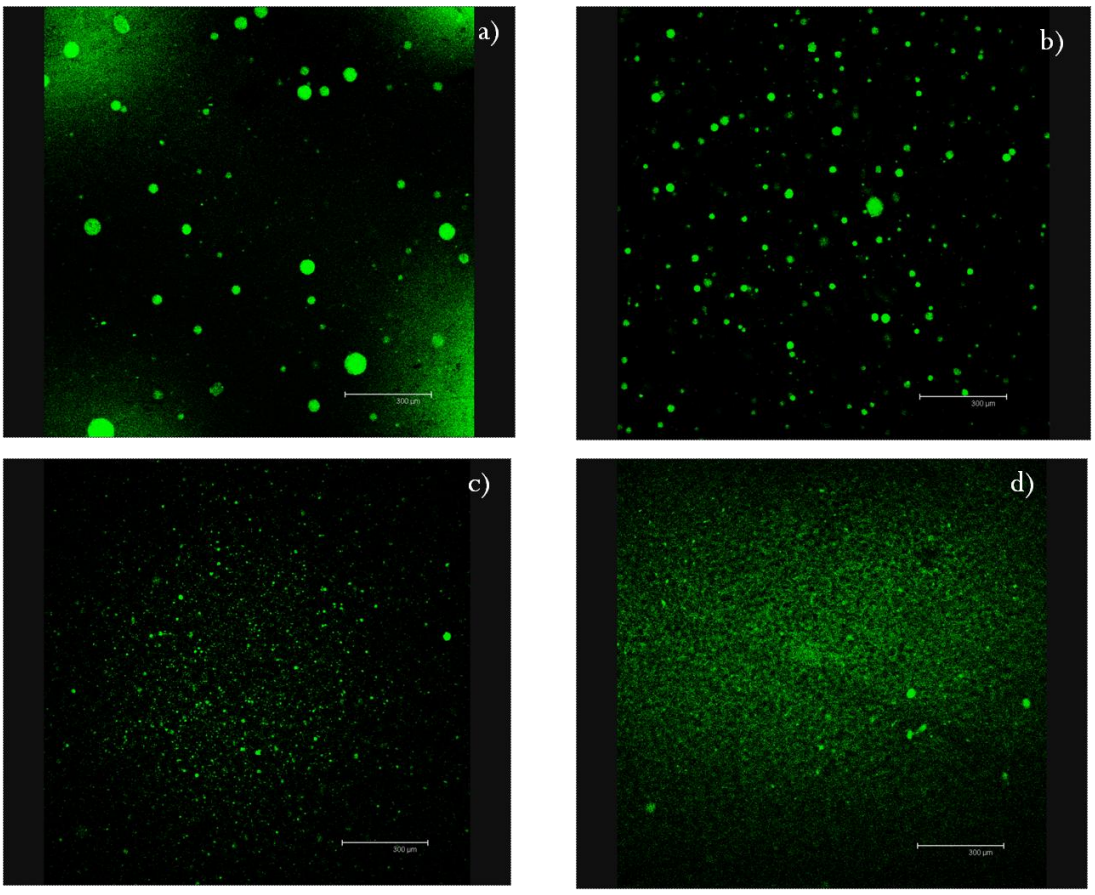


**Figure 5.14 - CLSM images of the surface of dried films with a) 1% casein and 7% starch, b) 3.5% casein and 7% starch, c) 7% casein and 7% starch, and d) 14% casein and 7% starch. The scale bar represents 300 μm length.**

### 5.3.3 Modelling rehydration

In order to be able to predict the behaviour of different types of films with regard to water absorption, it is useful to develop a model which simulates the disappearance of the water droplet. The model will need to take into account the volume loss due to both evaporation and diffusion into the film below it. However, in the simplest case, for example when a non-penetrable substrate is used, diffusion can be neglected from the model and thus an analytical expression can be derived to predict shrinkage of the droplet.

To obtain such a model first the volume and surface area of a partial sphere must be considered, (see Figure 5.15). The equation for the volume of a spherical cap is well known, but in order to apply it to the experimental results, it needs to be expressed in terms of *R* and *a*, the radius of the sphere itself, and the radius of contact, or the radius of the spherical cap, as shown below.

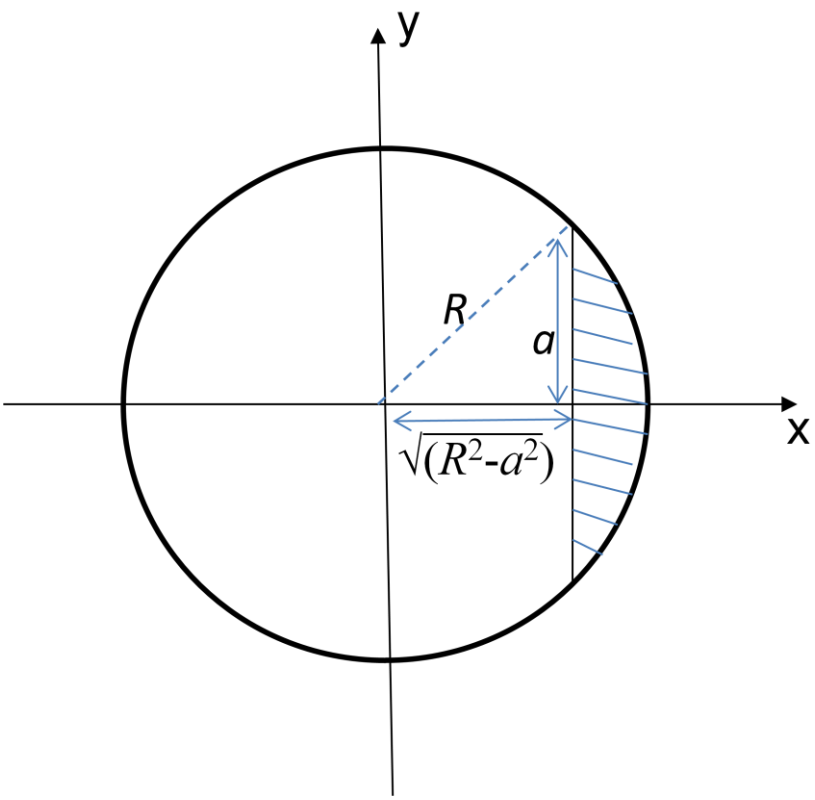


**Figure 5.15 - Finding the volume of a partial sphere in terms of *R* and *a*.**

The experimental data is expressed as volume of the droplet with respect to time and so by modelling the volume of a spherical cap with the initial conditions used in the experiment for *R* and *a*, the volume change due to evaporation and diffusion can be mapped to a model describing variation of *R* with time. Note that once again the droplet is assumed to be pinned so the

value of *a* is constant, as is indeed the case as seen in the experimental results.

The volume of the spherical cap shown above is given by equation 5.3.

$$V = \pi \int_{\sqrt{R^2+a^2}}^{R} y^2 dx = \int_{\sqrt{R^2+a^2}}^{R} (R^2 - x^{2)})dx$$

When integrated this gives:

$$V = \left[ R^2 x - \frac{x^3}{3} \right]_{\sqrt{R^2+a^2}}^{R},$$

which results in the following equation:

$$V = \pi \left[ \frac{2}{3} R^3 - R^2 \sqrt{R^2 - a^2} + \frac{\left(R^2 - a^2\right)\sqrt{R^2 - a^2}}{3} \right]$$

Simplified, this gives:

$$V(R,a) = \frac{2}{3}\pi R^3 \left( 1 - \frac{\sqrt{R^2 - a^2}}{R^3} \left( R^2 + \frac{a^2}{2} \right) \right) \qquad \textbf{5.3}$$

Similarly, the surface area of the cap can be expressed in terms of *R* and *a* as follows:

$$A = 2\pi \int_{0}^{\sin^{-1}\frac{a}{R}} R^2 d\theta \sin\theta,$$

By integratinging the above, we get:

$$A = 2\pi R^2 \left[ -\cos\theta \right]_0^{\sin^{-1}\frac{a}{R}}$$

which leads to the following expression for area in terms of *R* and *a*:

$$A = 2\pi R^2 \left(1 - \frac{\sqrt{R^2 - a^2}}{R}\right) \qquad \textbf{5.4}$$

If now this analogy is considered as a droplet on top of a film surface, as is seen in the experimental procedure, the droplet has a curvature of *R* and is in contact with the surface by a circular region of radius, *a*. This is shown in Figure 5.16.

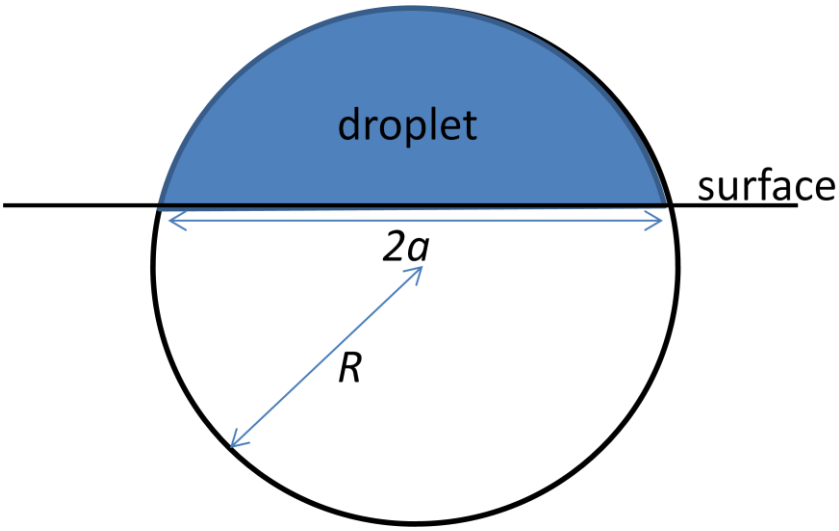


**Figure 5.16 - Droplet with a curvature of *R* and is in contact with the surface by a circular region of radius, *a*.**

An assumption is made that as the droplet dries out and evaporates, the contact area between the solid and the droplet, *a*, remains constant and is effectively "pinned" so the contact angle alters and is not in equilibrium, as in Figure 5.17. As the droplet dries, the radius of curvature, *R*, increases, so both volume and area of contact with the air decrease, as indicated in Figure 5.17.

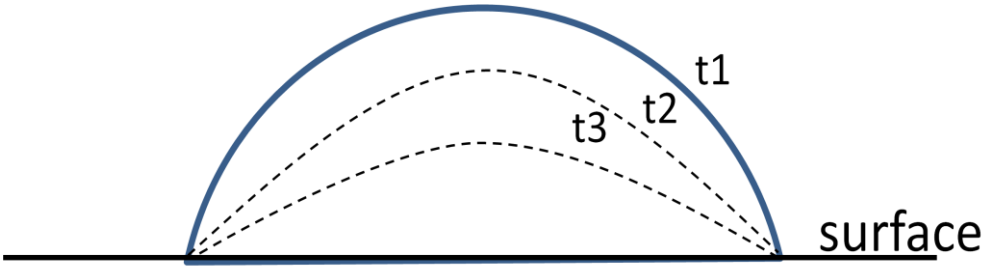


**Figure 5.17 - Schematic of a "pinned" droplet drying.**

The drying of the droplet is caused by two phenomena, a) the diffusion of liquid into the solid substrate, and b) evaporation of water into the surrounding air. As the contact area between the droplet and the solid phase does not change throughout the process, the diffusion problem can be solved for a dry substrate in contact with a wet circular patch of radius *a,* with a water concentration maintained as $c_w$=1 on the patch. The patch is always circular and wet.

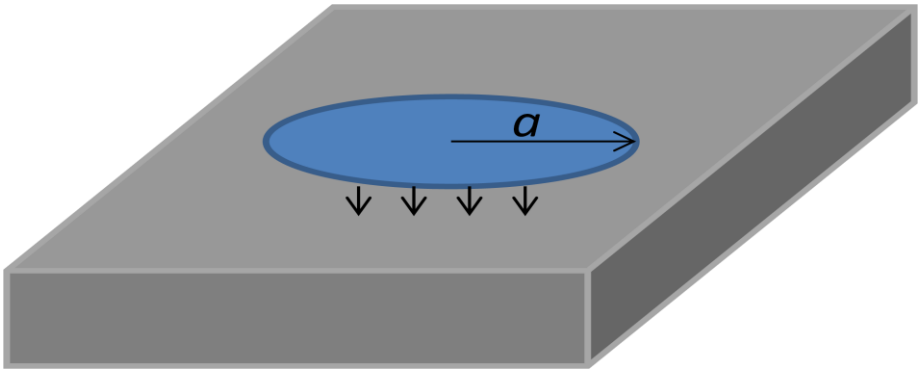


**Figure 5.18 - Illustration a circular patch on top of a substrate, modelled using COM-SOL.**

The flux $J_d$(t) can be obtained by numerically solving Fick's first law using a finite difference or finite element program such as COM-SOL (Datta and Rakesh, 2009), see Figure 5.18. $J_D$(t) is completely independent of both the shape and volume of the droplet, and only depends on the radius of the

circular patch, *a*, and time, *t*. It defines the amount of water per second penetrating the solid at any given time. In this way the problem concerned with diffusion of water into the film can be separated from that of evaporation and then be solved to obtain $J_D$(t).

The evaporation rate is given by an evaporation constant $K_{ev}$ multiplied by the surface area of the droplet-air interface:

$$Rate\ of\ evaporation = K_{ev}A(R,a).$$

The value of $K_{ev}$ is constant at a given temperature and relative humidity. It is useful to remember at this point that $K_{ev}$ is defined in terms of volume, as opposed to mass.

So the rate of change of the droplet volume is equal to the rate of volume of water lost to the solid and the rate of volume loss to the air:

$$\frac{dV}{dt} = -K_{ev}A(R,a) + (-J_D(t)) \qquad \textbf{5.5}$$

Using equations 5.3 and 5.4, the above equation can be expressed in terms of *R(t)*, noting that:

$$\frac{dV}{dt} = \frac{dR}{dt} \cdot \frac{dV}{dR}$$

Therefore:

$$\frac{dV}{dt} = \frac{2}{3}\pi\left(3R^2 - 2R\sqrt{R^2 - a^2} - \frac{R}{\sqrt{R^2 - a^2}}\left(R^2 + \frac{a}{2}\right)\right)\frac{dR}{dt} \qquad \textbf{5.6}$$

If this is substituted into equation 5.5, the following is obtained:

$$\left(3R^2 - 2R\sqrt{R^2 - a^2} - \frac{R}{\sqrt{R^2 - a^2}}\left(R^2 + \frac{a}{2}\right)\right)\frac{dR}{dt} = -3K_{ev}R^2\left(\frac{\sqrt{R^2 - a^2}}{R}\right) - \frac{3J_D(t)}{2\pi}$$

This can then be written as:

$$\frac{dR}{dt} = \frac{-K_{ev}\left(R^2 - R\sqrt{R^2 - a^2}\right) - \frac{J_D(t)}{2\pi}}{\left(R^2 - \frac{2}{3}R^2\sqrt{R^2 - a^2} - \frac{R\left(2R^2 + a^2\right)}{6\sqrt{R^2 - a^2}}\right)} \qquad \textbf{5.7}$$

This differential equation is best solved numerically, particularly as $J_D$(t)/$2\pi$ will be obtained by a numerical package, such as COM-SOL, and therefore is given in numerical form rather than as a closed form equation. However, in order to do this, $K_{ev}$ is needed. This can be determined by conducting an experiment where a droplet is placed on a substrate which is impenetrable to water. In this case, equation 5.7 reduces to:

$$\frac{dR}{dt} = \frac{-K_{ev}\left(R^2 - R\sqrt{R^2 - a^2}\right)}{\left(R^2 - \frac{2}{3}R^2\sqrt{R^2 - a^2} - \frac{R\left(2R^2 + a^2\right)}{6\sqrt{R^2 - a^2}}\right)} \qquad \textbf{5.8}$$

Since $J_D$(t) = 0 now. Equation 5.8 can be rearranged to give:

$$-K_{ev}t = \int_{R(0)}^{R(t)} \frac{R\sqrt{R^2 - a^2} - R^2 + \frac{a^2}{2}}{R\sqrt{R^2 - a^2} - R^2 + a^2}\,dR \qquad \textbf{5.9}$$

where, *R(0)* is the initial curvature of the droplet and *R(t)* is the radius of curvature at time, *t*.

Now, if a change of variable is made to equation 5.9 it can be expressed in a simpler form. Making the change of variable $R = a \cosh(\lambda)$ gives:

$dR = a(sinh\lambda)d\lambda$,

and,

$\sqrt{R^2 - a^2} = a \sinh \lambda$.

If $\cosh^{-1}R(t)/a$ is written as $\beta$ and $\cosh^{-1}R(0)/a$ is written as $\sigma$, the integral in equation 5.9 now becomes:

$$-K_{ev}t = a\int_{\sigma}^{\beta} \frac{(\cosh\lambda)(\sinh\lambda) - \sinh^2\lambda - 0.5}{(\cosh\lambda) - (\sinh\lambda)} d\lambda \qquad \textbf{5.10}$$

This can be factorised to:

$$\frac{-K_{ev}t}{a} = \int_{\sigma}^{\beta} \frac{(\cosh\lambda)(\sinh\lambda) - \sinh^2\lambda - 0.5}{(\cosh\lambda) - (\sinh\lambda)} d\lambda \qquad \textbf{5.11}$$

The hyperbolic functions sinh($\lambda$) and cosh($\lambda$) are defined as follows:

$$\sinh\lambda = \frac{e^{\lambda} - e^{-\lambda}}{2}$$

$$\cosh\lambda = \frac{e^{\lambda} + e^{-\lambda}}{2}$$

By rewriting equation 5.11 in terms of their exponentials, 5.12 is obtained:

$$\frac{-K_{ev}t}{a} = \int_{\sigma}^{\beta} \frac{0.5 - \frac{e^{-2\lambda}}{2} - 0.5}{e^{-\lambda}} d\lambda \qquad \textbf{5.12}$$

which, when multiplied by -1 and simplified, becomes:

$$\frac{2K_{ev}t}{a} = \int_{\sigma}^{\beta} e^{-\lambda} d\lambda \qquad \textbf{5.13}$$

Finally the integral is carried out to give:

$$\frac{2K_{ev}t}{a} = \left[e^{-\lambda}\right]_{\sigma}^{\beta} \qquad \textbf{5.14}$$

Considering cosh(x) can be written as $ln[(x^2-1)^{0.5} -x]$, evaluating the upper and lower limits in 5.14, equation 5.15 is obtained:

$$\frac{2K_{ev}t}{a} = \frac{1}{\frac{R(0)}{a} + \sqrt{\left(\frac{R(0)}{a}\right)^2 - 1}} - \frac{1}{\frac{R(t)}{a} + \sqrt{\left(\frac{R(t)}{a}\right)^2 - 1}} \qquad \textbf{5.15}$$

Equation 5.15 gives the desired variation of R(t) with t for a given initial radius of curvature R(0). It can easily be used in Excel to allow a model which can be compared to the raw data to be created. Upon solving this, a graph of the variation of the droplet volume with respect to time can be constructed using equations 5.9 and 5.3. By fitting this to experimental data, a value of $K_{ev}$ is obtained, based on the assumption that the evaporation constant is not dependant on the nature of the solid substrate with which the droplet is in contact.

#### 5.3.3.1 Fitting of experimental data to the model

As the model described above is for the case where an impenetrable substrate is used , the obvious experimental data for testing it are those from the droplet evaporation deposited on a metal substrate, with no polymer film on it. The result of this exercise can provide an evaporation correction factor for the rehydration plots in 5.3.1. The measured data for *R* as a function of time and for *a,* obtained from the observation of droplet data at 15 °C, 25°C, and 35°C, should yield a straight line according to equation 5.15, if the quantity $[(R(t)/a + ((R(t)^2/a^2)^{0.5} - 1)]^{-1}$ is plotted against time. It is assumed the evaporation is the rate limiting process. As the metal beam is impenetrable, this should indeed be the case. Figure 5.19 shows $[(R(t)/a + ((R(t)^2/a^2)^{0.5}$ -

1)]$^{-1}$ plotted against time, for the droplets at the three different temperatures. As expected, in each case a straight line is obtained.

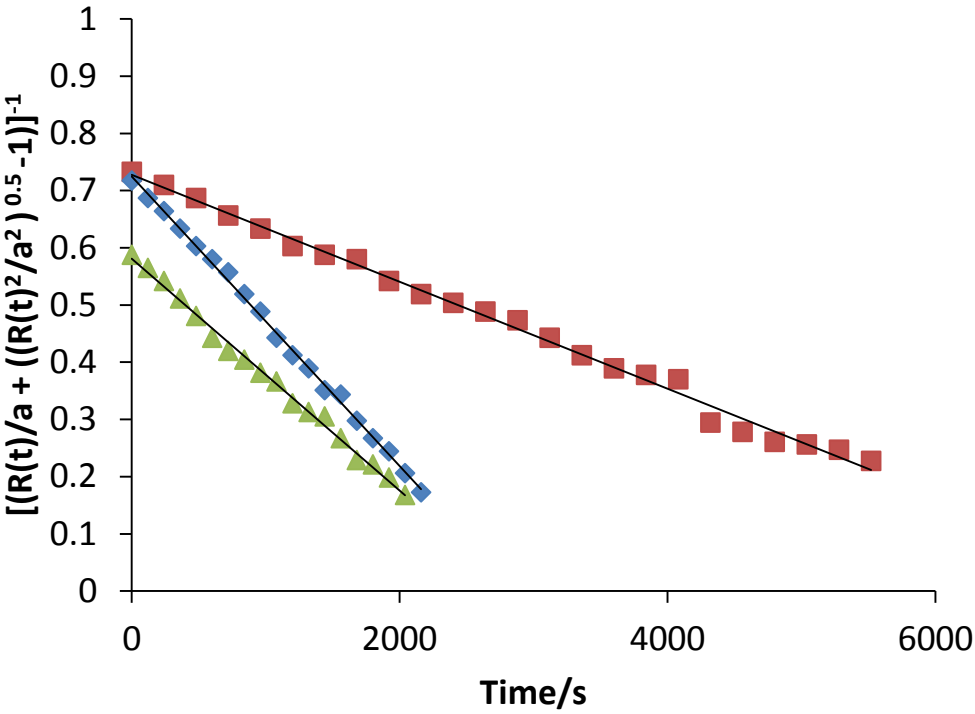


**Figure 5.19 - Using *R* and *a* values from droplets placed on a metal substrate to calculate the evaporation constant. ■= 15 °C, ▲=25 °C, and ♦ =35 °C.**

From the gradient of this line, $2K_{ev}/a$, $K_{ev}$ can be calculated. The y-intercept gives the value of $[(R(t)/a + ((R(t)^2/a^2)^{0.5} - 1)]^{-1}$. Figure 5.20 shows the $K_{ev}$ values extracted in this way for each temperature. This gives a linear relationship between $K_{ev}$ and temperature over the studied range, demonstrating the temperature dependence of the evaporation constant.

Following successful modelling of the droplets on a metal substrate, droplets on the starch mix and casein films were considered next. It is important to note here that the starch films cannot be modelled in this way, nor the starch-casein mix films which show a more starch-like behaviour, because

the droplets spread on these types of films, so the "pinning" effect necessary for this model to be valid does not occur, and the value of *a*, until now assumed constant also varies with time. The model has been applied to casein films at 15 °C, 25°C, and 35°C, and the films composed of 7 wt% starch and 3.5 wt% casein, and 7 wt% starch with 7 wt% casein.

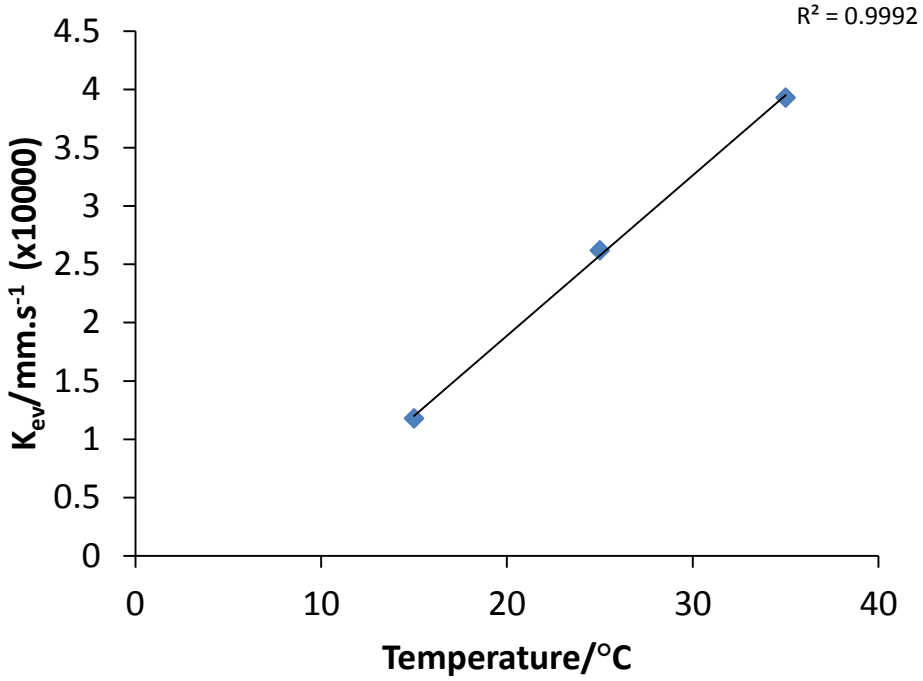


**Figure 5.20 - Evaporation constants plotted against temperature for a droplet evaporating from an impermeable substrate.**

Figure 5.21 shows the corresponding plots for the casein films at different temperatures. At 35 °C the trend is almost linear, suggesting that at this high temperature, diffusion is very slow and that the droplet essentially vanishes by evaporation. This could be that the film is in its glassy state, and so it takes a long time for water to begin to penetrate it, thus as a higher temperature drives evaporation faster, the droplet evaporation dominates.

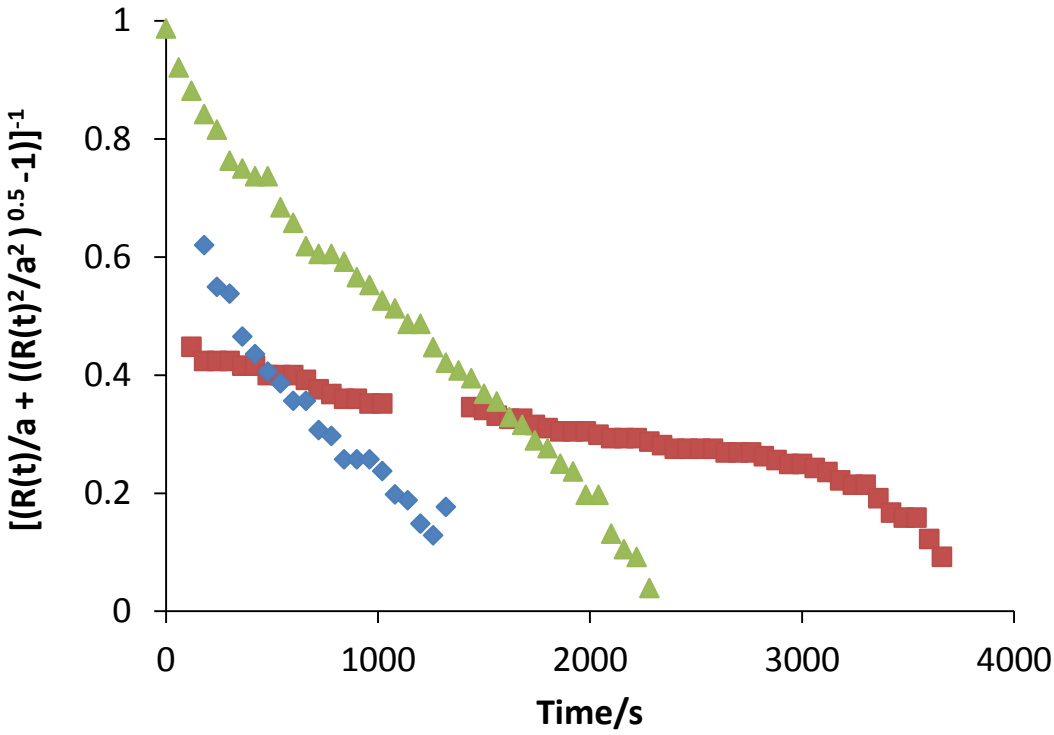


**Figure 5.21 - Using R and a values from droplets placed on casein films to calculate the evaporation constant. ■= 15 °C, ▲=25 °C, and ♦ =35 °C.**

The plot for 25 °C is also fairly linear, however not to the same extent as the 35 °C plot, suggesting that diffusion does start to have an effect at this temperature, most likely due to the slower evaporation rate, allowing time for the film to be penetrated, allowing the diffusion process to manifest itself. The curved nature of the plot at 15 °C supports this theory. As the temperature is decreased, evaporation becomes even slower and so towards the end of the droplet disappearance the plot is clearly no longer linear and is therefore not controlled solely by evaporation. Also, as the surface area of contact between the droplet and air decreases, so does the rate of evaporation. This means that the deviation towards the end of the process, due to diffusion, is most noticeable. This provides strong evidence

that the diffusion flux needs to be built into the model, so that a diffusion coefficient can be extracted. These results support the findings in Chapter 3 of the dehydration of these thin films, in that evaporation is the controlling factor, with diffusion playing a less significant role, slightly altering the results one may expect from the evaporation only case.

Figure 5.22 show the models for 7 wt% starch and 3.5 wt% casein, and 7 wt% starch with 7 wt% casein at 25 °C.

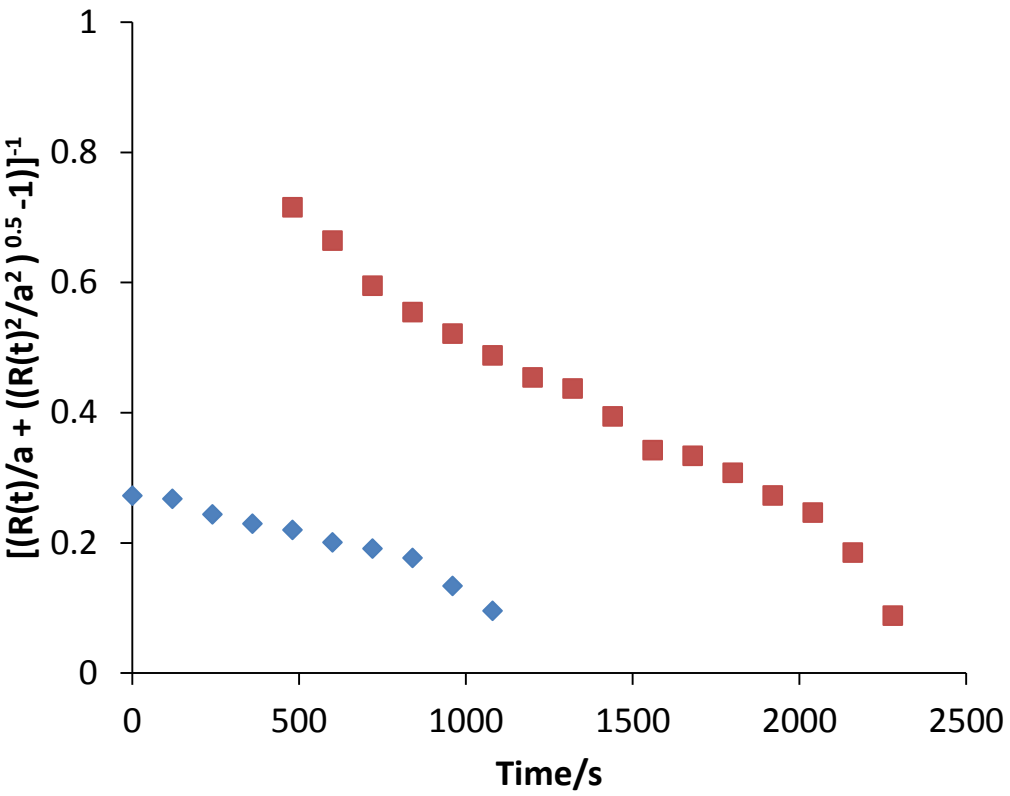


**Figure 5.22 - Using R and a values from droplets placed on a metal substrate to calculate the evaporation constant. ■= 7 wt% starch with 3.5 wt% casein and ♦ = 7 wt% starch with 7 wt% casein.**

Here, the plots are not linear throughout, but curved, emphasising that evaporation is not the only significant process for disappearance of water from the droplet. The different composition of the films is likely a key

contributor to determine which process will dominate, as starch does not give the same glassy film as casein, so diffusion, in this case, will be easier, thus its effect is seen throughout the experiment. In some cases, the droplet takes a few seconds to spread across the surface of the film before becoming "pinned" at a fixed contact area. This has been accounted for in the models, by starting the models from the point at which the droplet stops its lateral expansion.

Although the flux has not yet been obtained in the present work, some conclusions regarding the relationship between flux and time can be deduced by writing *J*, the flux, in terms of *C(0)*, *D* and *L*, the initial concentration, diffusion coefficient, and film thickness, to give the normalised flux, *J'*.

If Fick's second law is considered,

$$\frac{dc}{dt} = D\frac{d^2c}{dx^2} \qquad \textbf{5.16}$$

and written with *x* and *t* normalised by *R* and $R^2/D$ respectively, and *c* by *c*(0), then equation 5.16 can be rewritten in the normalised form.

$$\frac{dc'}{dt'} = \frac{d^2c'}{dx'^2} \qquad \textbf{5.17}$$

where

$$c' = c/c(0), \qquad x' = \frac{x}{R}, \qquad \text{and} \qquad t' = \frac{Dt}{R^2}.$$

For a fixed ratio of *R* to *L* (radius of wet patch to thickness of the film) *j'=f(t'),*or:

$$j' = DRf\left(\frac{Dt}{R^2}\right) \qquad \textbf{5.18}$$

Now initially it is expected that the ingress of water into the biopolymer film will be proportional to the surface area of the patch, i.e. ~ $R^2$. For this to be true, f(t') ~ $1/t^{0.5}$. Hence, initially;

$$j \sim \pi R^2\left(\frac{D}{t}\right)^{0.5} \qquad \textbf{5.19}$$

This conclusion is arrived at without actually solving 5.16, purely on the basis of the scaling form expected from *j*. For larger times, $t > R^2/D$, the lateral speed of water in the film away from the wet patch causes deviation from the equation (5.19), however equation 5.18 remains true, as long as R/L is the same. The form of *f(t')* however would need to be obtained by solving 5.16 numerically.

From this prediction, and the previous fitting of the evaporation model, it is quite clear that diffusion is not the controlling factor, and that a model needs to be developed to combine the two mechanisms of water loss from the droplet.

## 5.4 Conclusions

In this chapter a method to investigate the rehydration of a water droplet into thin biopolymer films consisting of casein and starch as well as those comprised of mixtures of the two, has been developed and validated. Rehydration curves, expressed as normalised droplet volume plotted against time show that temperature is a key factor in rehydration rate, for all film

compositions, but particularly for the starch-based films, where, above 15 °C, a very large increase in rate of droplet disappearance is observed. This difference in behaviour has been supported by SEM and CLSM images of the dried film surfaces, which indicate starch films to have a more imperfect structure as compared to casein.

Addition of casein to the starch films has been shown to decrease the rate of droplet disappearance, with equal ratio of casein to starch performing as well as the pure casein system. This could provide a more cost effective way of achieving the performance comparable to that of casein itself on an industrial scale. CLSM images of mixed films support the differences in rehydration behaviour between films, showing distinct casein regions in the poorer performing, fast rehydration films, as compared to a more homogenous mix of starch and casein in the films which have slower rehydration.

A model of a "pinned" droplet on a substrate has been developed, and validated using experimental data of droplet volume as a function of time, on an impermeable metal substrate at different temperatures. The linear relationship between $[(R(t)/a + ((R(t)^2/a^2)^{0.5} -1)]^{-1}$ and time seen in all cases indicated the evaporation is the main process responsible for the rehydration rate. A temperature dependence of the evaporation constant has also been demonstrated.

Finally, "pinned" droplets on casein films at different temperatures, and mixed films, have been modelled using this model. It was found that at higher temperatures, films give a linear behaviour indicating once again that evaporation is the limiting factor, but at lower temperatures, the plots

deviate towards the end, strongly indicating that diffusion is playing a role and therefore should be accounted for in the model. This will be considered in future work.

## 5.5 Further Work

With regard to the modelling part of this chapter, there is obvious further work that should be considered. The work above clearly shows that although evaporation is the dominant process in controlling the rate of droplet disappearance, in some cases the models deviate from the linear plot that indicates purely evaporation. Thus, diffusion must be incorporated into the model. Indeed, it is this deviation that is of interest so as to be able to obtain information regarding the ingress of water into the films. To do this, a numerical program such as COM-SOL needs to be used to calculate the diffusive flux as a function of time.

In addition, to complete the analysis, it would be useful to model the droplet disappearance for the case where the contact area is not fixed, such as is the case for the starch films. This could be achieved using a finite difference scheme with a moving boundary, similar to that used in Chapter 2 to model dehydration.

# Chapter 6 Conclusions

Throughout this thesis several aspects of moisture diffusion into and out of biopolymer films have been investigated. Dehydration of thin casein and starch based biopolymer films has been carried out systematically, under controlled conditions with varied temperature and relative humidity and fitted to mathematical simulations based on Fick's laws to reveal the dominant mechanisms behind dehydration of this type of film. Diffusion coefficients and evaporation constants for the differents films under different conditions have been extracted from the results to aid explanation of the different drying behaviours seen. Two novel methods to examine water ingress into biopolymers have been developed and validated. The first utilises ultrasonic waves to monitor the change in speed of sound across a cell containing biopolymer solution and a reservoir of water. As water diffuses into the biopolymer, the sound velocity decrease can be plotted as a function of position in the biopolymer solution or time, and standard curves of speed of sound vs. concentration are used to generate a concentration profile. Simulations of Fick's laws are used to model concentration profiles and a diffusion coefficient for water in the casein system, resulting in comparable values to those obtained in the dehydration experiments. The second method involves placing a water droplet onto a dried film as produced in the dehydration experiments and monitoring its disappearance by video camera under controlled conditions. Mathematical models of shrinkage of a droplet on a substrate with a fixed contact area have been derived and for the case

where the substrate is impenetrable has been modelled and compared with experimental data.

## 6.1 Key findings

### 6.1.1 Dehydration of thin biopolymer films

The most significant finding from this part of the work is that all the experimental drying data for different film compositions under different drying conditions, scales onto a single master curve when normalised by appropriate time scales. This suggests that the driving mechanism for dehydration is independent of the film composition and only the rates change when external conditions are modified. A novel model has been derived for such a drying process, in which not only the film shrinkage due to water loss is accounted for, but also the possibility of such a volume variation due to changes in the partial molar volumes of water and solid phases is considered.

Experimental results, when fitted to the mathematical simulations show that contrary to expectations, diffusion has relatively little role in the dehydration of these thin films. This is an important finding as many previous works use diffusion curves to predict the behaviour during drying, a prediction which would be inaccurate in this case.

Results obtained experimentally demonstrate that the films shrink during drying, and the mathematical calculations described in detail in Chapter 2 and applied in Chapter 3 demonstrate the importance of including shrinkage in the models, if they are to accurately represent the system in question.

Mathematical calculations applied to the experimental data show a poor fit when diffusion is the limiting factor, whether the diffusion is constant throughout the process, or it varies as a function of moisture content. Fitting the various models that have been developed show that evaporation is the dominant process in the dehydration of these thin biopolymer films, as a very good fit is obtained for the case where evaporation is the controlling process with infinitely fast diffusion. Of course, diffusion of water from the bulk has to occur for the films to dry, and the model for the case where evaporation is the limiting factor, with a fast but nevertheless finite diffusion provides the best fits to the experimental data.

The diffusion coefficient has been estimated from fits of the model to experimental results for a film thickness of 0.4 mm, at $5\times10^{-9}$ $m^2s^{-1}$, a reasonable value for a food based material. The evaporation constants have similarly been extracted, lying in the range $1.2\times10^{-7}$ $ms^{-1}$ at lower temperatures and high air humidities, to $3.6\times10^{-7}$ $ms^{-1}$ at higher temperatures and low air humidities.

Models were applied to drying data of adhesive samples used in industry. The results indicate that the model systems accurately describe the drying behaviour of such adhesive thin films too, with the theoretical predictions once again in excellent agreement with the experimental data provided for the dehydration of several starch and casein based commercial adhesive samples. Assuming a film thickness of 0.4 mm, as used in the model experiments, the evaporation constant is found to lie between $2.6\times10^{-7}$ $ms^{-1}$ and $3.7\times10^{-7}$ $ms^{-1}$, and the diffusion coefficient between $4.35\times10^{-9}$ $m^2s^{-1}$ and $5.95\times10^{-9}$ $m^2s^{-1}$, values which are in good agreement with the practical model starch and casein systems used in the rest of this work.

This work has demonstrated that relying on diffusion to predict the behaviour of thin films during drying is insufficient and evaporation is the key, and dominant process in driving dehydration.

### 6.1.2 Modelling dehydration of thin biopolymer films

The most significant finding in this chapter involves the incorporation of a moving boundary into the simulations. The effect of including film shrinkage in the diffusion and indeed evaporation equations causes significant deviation from the standard curve produced when for either diffusion or evaporation the film thickness is considered as constant throughout the dehydration process. Incorporating film shrinkage into the models, highlights the importance of the initial and final moisture contents of the film in question. For cases where evaporation is very dominant, exact analytical solutions to the drying problem are given involving film shrinkage. To our knowledge no such exact analytical results to this problem have been given before. For the cases involving both diffusion and evaporation, a new numerical method that changes the moving boundary conditions to fixed ones is devised, to allow a much simpler implementation of the problem, with higher accuracy. The method is based on a continuous redefining of the length scale, such that at any one time the film thickness in the redefined units is 1.

By incorporating both diffusion and evaporation into the simulation, the shape of the curve becomes more linear, demonstrating that the diffusion coefficient and evaporation rate are both potential limiting factors in the dehydration of thin biopolymer films.

### 6.1.3 Novel acoustic monitoring of water transport into biopolymer solutions

A novel method has been developed and validated for the investigation of water diffusion into biopolymer solutions using the Acoustiscan device built at the University of Leeds. The method has been validated using a sodium caseinate system, tested in replicate to give reproducible results.

The procedure has scope to test a variety of different compositions of biopolymer solution over a wide range of temperatures, and therefore is a useful tool in determining the diffusion properties of biopolymer systems.

A model based on Fick's second law of diffusion has been successfully fitted to the experimental data at various time intervals. The procedure has confirmed that two way diffusion occurs in the water-biopolymer system and the diffusion coefficients are found to be in the order of 2.0 $x10^{-10}$ $m^2.s^{-1}$ for water and 1.5 $x10^{-10}$ $m^2.s^{-1}$ for caseinate at t >8h and prior to that an order of magnitude faster at 1.0 $x10^{-9}$ $m^2.s^{-1}$.

### 6.1.4 Rehydration of thin biopolymer films

In this chapter the potential for a new method involving monitoring the shrinkage and disappearance of a water droplet on the surface of a biopolymer film was examined and validated at a series of temperatures on various films of different composition. As anticipated, temperature increases resulted in faster droplet disappearance. Starch- and casein- based films showed vastly different behaviours in the rate of droplet volume loss. When the two constituents were mixed, even for mixtures with casein content as low as 3 wt% with 7 wt% starch, much improved water resistance and slower ingress of water was found, as opposed to pure starch films.

Confocal and scanning electron microscopy demonstrated vast structural differences between the different film compositions, supporting the behaviours seen experimentally.

A particularly interesting finding is that on some of the thin films, in particular the casein- based, and casein containing films, the water droplet remains "pinned" on the surface of the film as it disappears. This led to a model derived to simulate evaporation of a "pinned" droplet on an impermeable substrate. The model was successfully validated using experimental data obtained from drying a water droplet on a metal beam, so that no ingress could occur, with results showing the desired linear trend between $[(R(t)/a + ((R(t)^2/a^2)^{0.5} -1)]^{-1}$ and time, indicating evaporation as the sole controlling factor. The evaporation constant was found to be a linear function of temperature over the temperatures investigated. This is likely due to a corresponding change in humidity as the temperature is increased, due to lack of accurate control, and any differences in droplet surface area.

When the model was applied to the biopolymer films, below 25 °C for the casein films, and for the mixed films at 25 °C, a linear trend between $[(R(t)/a + ((R(t)^2/a^2)^{0.5} -1)]^{-1}$ and time was not observed, supporting the hypothesis that diffusion is a significant factor.

## 6.2 Further research

There is a great deal of further work that would be interesting to carry out following the successful validation of the novel method which uses ultrasound to determine concentration profiles of water diffusion into biopolymer systems. The effect of temperature on diffusion is easily

examined using the Acoustiscan with support from temperature – speed of sound data already collected on the Resoscan for the sodium caseinate system. It would also be interesting and of great merit to this project to develop an understanding of how different composition biopolymer systems behave under the same conditions. The outcomes of these additional experiments will allow better understanding of the effect of temperature on diffusion of water into each sample, and the effects of adding crosslinkers and mixing systems on the diffusion of water can be examined.

By defining a diffusion coefficient for these different biopolymer systems, for example starch based, and synthetic acrylic based systems, an explanation as to why they behave so differently with respect to the issue of ice water resistance as outlined in chapter 1 could be uncovered. This knowledge could lead to an adhesive being designed which outperforms all currently available water based labelling adhesives.

it would be interesting to repeat the experiments with films of different thicknesses. Due to apparatus limitations, this could not be done using the current setup for large film thicknesses, but an experimental setup could be designed to cope with thicknesses upto 1-2 cm. By increasing the film thickness the importance of the role of diffusion in the drying process should become more prominent, and eventually diffusion will become the limiting mechanism for the drying of the film.

Over the last few years, casein- based adhesives have started to be phased out of use and replaced with synthetic alternatives. These synthetic adhesives are based on an acrylic polymer mixed with starch. Therefore it would be useful to repeat the dehydration experiments for a model acrylic

system to see if the synthetic polymer film can be modelled successfully to give the same mechanism of dehydration.

Further work to be considered with regard to the rehydration of thin films also includes applying the method to adhesive samples, to compare to the model starch- and casein- systems, and to provide industry relevant information about how the different compositions of adhesive behave under such a test.

With regard to the modelling part of the rehydration investigation, there is obvious further work that should be considered. Due to the fact that, in some cases the models deviate from the linear plot of $[(R(t)/a + ((R(t)^2/a^2)^{0.5} -1)]^{-1}$ as a function of time that indicates purely evaporation, diffusion must be incorporated into the model. In fact, it is the analysis of this deviation that will provide information regarding the diffusion of water into the films. To do this, a numerical program such as COM-SOL needs to be used to calculate the diffusive flux as a function of time, then this needs to be incorporated into the evaporation model, presented in Chapter 5, so that both processes are accounted for. It would be interesting to be able to compare the diffusion coefficients obtained from these models with those seen in the dehydration work, to see if they are related in any way.

Finally, it would be useful to model the droplet disappearance for the case where the contact area is not fixed, as seen for the purely starch- based films. This could be achieved using a finite difference scheme with a moving boundary, or by mapping of the problem to one with fixed boundary conditions as was done for dehydration in Chapter 2.

## 6.3 Limitations of this work

It is important at this stage to acknowledge that the work does have some limitations. One particular limitation that stands out is the lack of accurate control of relative humidity in both the rehydration work and the film shrinkage investigation. Another limitation, is the inability to raise and maintain the relative humidity above 50% during the dehydration experiments. Similarly, temperature cannot be maintained above 50 °C in the drying chamber at this time. These are limitations of the apparatus, and could be resolved by redesigning a chamber which can withstand these harsher conditions. A more accurate monitoring of the weight of a drying film could be achieved by using a data logger, which may help with the noisy rate of dehydration data. Finally, the method used to place the water phase on top of the biopolymer solution in the ultrasound experiments could be improved to prevent the biopolymer surface from being disturbed, and thus help avoid some of the anomalous speed of sound values seen in the bulk water phase. If more time was available, the experiment should also be conducted in different glass cells to remove the anomalies due to defects in the glass, for example micro-cracks, uneven surfaces etc., altering the sound velocity at particular heights.

## 6.4 Concluding statement

Throughout this thesis several important, original contributions to the field of diffusion of water in biopolymer films have been made. Two novel methods have been developed and validated, providing two different ways to monitor diffusion of moisture into wet biopolymer gels, and dried biopolymer films. By

monitoring the moisture loss of dying biopolymer thin films of different composition and under different external conditions, a single master curve has been discovered, that all the data scales onto by normalising time. And finally, films of such a small thickness have been shown to have dehydration mechanisms driven mostly by evaporation and not diffusion, suggesting the traditional diffusion modelling based on Fick's laws is insufficient to predict the drying behaviour of thin water-based biopolymer films, including industry standard adhesives used in bottle labelling. In particular, not only evaporation should be accounted for but also changes in the film thickness, which are often neglected in analysis of such data.

## References

AL-ASHEH, S., BANAT, F. & AL-LAGTAH, N. 2004. Separation of ethanol-water mixtures using molecular sieves and biobased adsorbents. *Chemical Engineering Research & Design,* 82**,** 855-864.

ALONSO, J. A., CABRIA, I. & LOPEZ, M. J. 2012. The storage of hydrogen in nanoporous carbons. *Journal of the Mexican Chemical Society,* 56**,** 261-269.

ANDERBERG, A. & WADSO, L. 2008. Method for simultaneous determination of sorption isotherms and diffusivity of cement-based materials. *Cement and Concrete Research,* 38**,** 89-94.

AOKI, T., YAMADA, N., TOMITA, I., KAKO, Y. & IMAMURA, T. 1987. Caseins are cross-linked through their ester phosphate groups by colloidal calcium phosphate. *Biochim Biophys Acta,* 911**,** 238-43.

ATKINS, P. & DE PAULA, J. 2006. *Atkins' Physical Chemistry*, Macmillan Higher Education.

BABALIS, S. J. & BELESSIOTIS, V. G. 2004. Influence of the drying conditions on the drying constants and moisture diffusivity during the thin-layer drying of figs. *Journal of Food Engineering,* 65**,** 449-458.

BAEZ-GONZALEZ, J. G., PEREZ-ALONSO, C., BERISTAIN, C. I., VERNON-CARTER, E. J. & VIZCARRA-MENDOZA, M. G. 2004. Effective moisture diffusivity in biopolymer drops by regular regime theory. *Food Hydrocolloids,* 18**,** 325-333.

BANASIAK, J. 2013. *Mathematical modelling in one dimension : an introduction via difference and differential equations,* Cambridge, Cambridge University Press.

BASMADJIAN, D. 2003. *Mathematical modeling of physical systems : an introduction,* Oxford, UK, Oxford University Press.

BLITZ J. 1963. *Fundamentals of Ultrasound,* London, Butterworth & co.

BOUCHARD, D., ZHANG, W. & CHANG, X. 2013. A rapid screening technique for estimating nanoparticle transport in porous media. *Water research,* 47**,** 4086-94.

BRADY, J. B. 1975. Reference frames and diffusion coefficients. *American Journal of Science,* 275**,** 954-983.

BRENNAN, W., BRIENS, L., BRIENS, C. & ZANIN, J. 2009. Using a new diffusivity model to accelerate the drying of biopolymer films. *Canadian Journal of Chemical Engineering,* 87**,** 761-765.

BUONOCORE, G. G., CONTE, A. & NOBILE, M. A. D. 2005. Use of a mathematical model to describe the barrier properties of edible films. *Journal of Food Science,* 70**,** E142-E147.

BUONOCORE, G. G., DEL NOBILE, M. A., DI MARTINO, C., GAMBACORTA, G., LA NOTTE, E. & NICOLAIS, L. 2003. Modeling the water transport properties of casein-based edible coating. *Journal of Food Engineering,* 60**,** 99-106.

CAMIRAND, W., KROCHTA, J. M., PAVLATH, A. E., WONG, D. & COLE, M. E. 1992. Properties of some edible carbohydrate polymer-coatings for potential use in osmotic dehydration. *Carbohydrate Polymers,* 17**,** 39-49.

CERNY, R., DRCHALOVA, J., HOSKOVA, S. & TOMAN, J. 1996. Methods for evaluation of water-proofness quality and diffusion properties of coating materials. *Construction and Building Materials,* 10**,** 547-552.

CHEMAT, F., ZILL E, H. & KHAN, M. K. 2011. Applications of ultrasound in food technology: Processing, preservation and extraction. *Ultrasonics Sonochemistry,* 18**,** 813-835.

CHEN, J. S., ETTELAIE, R., YANG, H. Y. & YAO, L. 2009. A novel technique for in situ measurements of stress development within a drying film. *Journal of Food Engineering,* 92**,** 383-388.

CHEN, L.-H., LI, X.-Y., ROOKE, J. C., ZHANG, Y.-H., YANG, X.-Y., TANG, Y., XIAO, F.-S. & SU, B.-L. 2012. Hierarchically structured zeolites: synthesis, mass transport properties and applications. *Journal of Materials Chemistry,* 22**,** 17381-17403.

CHICK, J. & USTUNOL, Z. 1998. Mechanical and barrier properties of lactic acid and rennet precipitated casein-based edible films. *Journal of Food Science,* 63**,** 1024-1027.

COSTELLA, A. M., TROCHMANN, J. L. & OLIVEIRA, W. S. 2010. Water sorption and diffusion coefficient through an experimental dental resin. *Journal of Materials Science: Materials in Medicine,* 21**,** 67-72.

CRANK, J. 1975. *The Mathematics of Diffusion,* Oxford, Oxford University Press.

CUSSLER, E. L. 1997. *Diffusion: mass transfer in fluid systems*, Cambridge university press.

CZAPUTA, K., BRENN, G. & MEILE, W. 2011. The drying of liquid films on cylindrical and spherical substrates. *International Journal of Heat and Mass Transfer,* 54**,** 1871-1885.

DA SILVA, W. P., ;, PRECKER JÜRGEN, W. & DE LIMA ANTONIO GILSON, B. 2009. Drying kinetics of lima bean (Phaseolus lunatus L.) Experimental determination and prediction by diffusion models. *International Journal of Food Engineering.*

DANIELEWSKI, M. & WIERZBA, B. 2009. Diffusion, drift and their interrelation through volume density. *Philosophical Magazine,* 89**,** 331-348.

DARKEN, L. S. 1948. Diffusion, mobility and their interrelation through free energy in binary metallic systems. *Transactions of the American Institute of Mining and Metallurgical Engineers,* 175**,** 184-201.

DATTA, A. K. 2007a. Porous media approaches to studying simultaneous heat and mass transfer in food processes. I: Problem formulations. *Journal of Food Engineering,* 80**,** 80-95.

DATTA, A. K. 2007b. Porous media approaches to studying simultaneous heat and mass transfer in food processes. II: Property data and representative results. *Journal of Food Engineering,* 80**,** 96-110.

DATTA, A. K. & RAKESH, V. 2009. *An Introduction to Modeling of Transport Processes: Applications to Biomedical Systems,* Cambridge, Cambridge University Press.

DAY, D. R., SHEPARD, D. D. & CRAVEN, K. J. 1992. A microdielectric analysis of moisture diffusion in thin epoxy/amine films of varying cure state and mix ratio. *Polymer Engineering and Science,* 32**,** 524-528.

DEL GROSSO, V. A. & MADER, C. W. 1972. Speed of sound in pure water. *J. Acoust. Soc. Am.,* 52**,** 1442-1446.

DELAHAYE, N., MARAIS, S., SAITER, J. M. & METAYER, M. 1998. Characterization of unsaturated polyester resin cured with styrene. *Journal of Applied Polymer Science,* 67**,** 695-703.

DHANPAL, P., YIU, C. K. Y., KING, N. M., TAY, F. R. & HIRAISHI, N. 2009. Effect of temperature on water sorption and solubility of dental adhesive resins. *Journal of Dentistry,* 37**,** 122-132.

DICKINSON, E., GOLDING, M. & POVEY, M. J. W. 1997. Creaming and flocculation of oil-in-water emulsions containing sodium caseinate. *Journal of Colloid and Interface Science,* 185**,** 515-529.

DRAGNEVSKI, K. I., ROUTH, A. F., MURRAY, M. W. & DONALD, A. M. 2010. Cracking of drying latex films: An ESEM experiment. *Langmuir,* 26**,** 7747-7751.

DRCHALOVA, J. & CERNY, R. 1998. Non-steady-state methods for determining the moisture diffusivity of porous materials. *International Communications in Heat and Mass Transfer,* 25**,** 109-116.

DRCHALOVA, J. & CERNY, R. 2003. A simple gravimetric method for determining the moisture diffusivity of building materials. *Construction and Building Materials,* 17**,** 223-228.

DURNING, C. J. & TABOR, M. 1986. Mutual diffusion in concentrated polymer solutions under a small driving force. *Macromolecules,* 19**,** 2220-2232.

EGERTON, R. F. 2005. *Physical principles of electron microscopy: an introduction to TEM, SEM and AFM*, Springer US.

ENOMAE, T., DOGOME, K. & ISOGAI, A. 2012. Evaluation of absorption of micro-droplets on paper for creation of paper-based microstructures. *Journal of Materials Science,* 47**,** 3554-3563.

EVINGUR, G. A. & PEKCAN, O. 2011a. Drying of polyacrylamide composite gels formed with various kappa- carrageenan content. *Journal of Fluorescence,* 21**,** 1531-1537.

EVINGUR, G. A. & PEKCAN, O. 2011b. Studies on drying and swelling of PAAm-NIPA composites in various compositions. *Polymer Composites,* 32**,** 928-936.

FIAT, A. M. & JOLLES, P. 1989. Caseins of various origins and biologically-active casein peptides and oligosaccharides - structural and physiological aspects. *Molecular and Cellular Biochemistry,* 87**,** 5-30.

FICK, A. 1995. On liquid diffusion. *Journal of Membrane Science,* 100**,** 33-38.

FISCHER, H., POLIKARPOV, I. & CRAIEVICH, A. F. 2004. Average protein density is a molecular-weight-dependent function. *Protein Science,* 13**,** 2825-2828.

FRISCH, H. L. & STERN, S. A. 1983. Diffusion of small molecules in polymers. *Crc Critical Reviews in Solid State and Materials Sciences,* 11**,** 123-187.

GENNADIOS, A. (ed.) 2002. *Protein-based films and coatings,* New York: CRC press.

GEORGIADIS, A., BRYANT, P. A., MURRAY, M., BEHARRELL, P. & KEDDIE, J. L. 2011. Resolving the film-formation dilemma with infrared radiation-assisted sintering. *Langmuir,* 27**,** 2176-2180.

GHOSH, A., ALI, M. A. & DIAS, G. J. 2009. Effect of cross-linking on microstructure and physical performance of casein protein. *Biomacromolecules,* 10**,** 1681-1688.

GRAHAM, T. 1833. LVIII. On the law of the diffusion of gases. *Philosophical Magazine Series 3,* 2**,** 351-358.

GRESKOVI, C. & STUBICAN, V. S. 1970. Change of molar volume and interdiffusion coefficients in system MGO-CR2-03. *Journal of the American Ceramic Society,* 53**,** 251-&.

GRIFFITH, J. D., MITCHELL, J., BAYLY, A. E. & JOHNS, M. L. 2009. In situ monitoring of the microstructure of detergent drops during drying using a rapid nuclear magnetic resonance diffusion measurement. *Journal of Materials Science,* 44**,** 4587-4592.

GUO, R. W., DU, X. Y., ZHANG, R., DENG, L. D., DONG, A. J. & ZHANG, J. H. 2011. Bioadhesive film formed from a novel organic-inorganic hybrid gel for transdermal drug delivery system. *European Journal of Pharmaceutics and Biopharmaceutics,* 79**,** 574-583.

HARTLEY, G. S. & CRANK, J. 1949. Some fundamental definitions and conceptsin diffusion processes. *Transactions of the Faraday Society,* 45**,** 801-818.

HENSHAW, P., PRENDI, L. & MANCINA, T. 2006. A model for the dehydration of waterborne basecoat. *Jct Research,* 3**,** 285-294.

HERNANDEZ, R. J. & GAVARA, R. 1994. Sorption and transport of water in nylon-6 films. *Journal of Polymer Science Part B-Polymer Physics,* 32**,** 2367-2374.

HOLT, C. & SAWYER, L. 1993. Caseins as rheomorphic proteins: interpretation of primary and secondary structures of the [small alpha]S1-, [small beta]- and [small kappa]-caseins. *Journal of the Chemical Society, Faraday Transactions,* 89**,** 2683-2692.

HORNE, D. S. 2002. Casein structure, self-assembly and gelation. *Current Opinion in Colloid & Interface Science,* 7**,** 456-461.

HOUGHTON, D. R., SMITH, R. N., EGGINS, H. O. W. & BRAVERY, A. F. 1988. Biodeterioration of paint -a state-of-the-art comment. *Biodeterioration 7.* Springer Netherlands.

HUANG, H. & HAGHIGHAT, F. 2002. Modelling of volatile organic compounds emission from dry building materials. *Building and Environment,* 37**,** 1127-1138.

JANJARASSKUL, T. & KROCHTA, J. M. 2010. Edible packaging materials. *In:* DOYLE, M. P. & KLAENHAMMER, T. R. (eds.) *Annual Review of Food Science and Technology, Vol 1.* Palo Alto: Annual Reviews.

KALTSA, O., MICHON, C., YANNIOTIS, S. & MANDALA, I. 2013. Ultrasonic energy input influence on the production of sub-micron o/w emulsions containing whey protein and common stabilizers. *Ultrasonics Sonochemistry,* 20**,** 881-891.

KAMPER, S. L. & FENNEMA, O. 1984. Water vapor permeability of edible bilayer films. *Journal of Food Science,* 49**,** 1478-1481.

KARBOWLAK, T., GOUGEON, R. D., RIGOLET, S., DELMOTTE, L., DEBEAUFORT, F. & VOILLEY, A. 2008. Diffusion of small molecules in edible films: Effect of water and interactions between diffusant and biopolymer. *Food Chemistry,* 106**,** 1340-1349.

KARGER, J. S., F. 2005. NMR studies of anomalous diffusion. *In:* HEITJANS, P. K., J.; (ed.) *Diffusion in Condensed Matter;.* Heidelberg, Germany,: Springer:.

KRISHNA, R. 2009. Describing the diffusion of guest molecules inside porous structures. *The Journal of Physical Chemistry C,* 113**,** 19756-19781.

KRZAK, M., TABOR, Z., NOWAK, P., WARSZYNSKI, P., KARATZAS, A., KARTSONAKIS, I. A. & KORDAS, G. C. 2012. Water diffusion in polymer coatings containing water-trapping particles. Part 2. Experimental verification of the mathematical model. *Progress in Organic Coatings,* 75**,** 207-214.

LI, Z. Y. & KOBAYASHI, N. 2005. Determination of moisture diffusivity by thermo-gravimetric analysis under non-isothermal condition. *Drying Technology,* 23**,** 1331-1342.

LUCEY, J. A. 2002. Formation and physical properties of milk protein gels. *Journal of Dairy Science,* 85**,** 281-294.

MAKI, D. P., ; THOMPSON, M.; 2006. *Introduction to mathematical modeling and computer simulation,* London, UK, Thomson Brooks/Cole.

MARCZAK, W. 1997. Water as a standard in the measurements of speed of sound in liquids. *J. Acoust. Soc. Am.,* 102**,** 2776-2779.

MAROULIS, Z. B., SARAVACOS, G. D., PANAGIOTOU, N. M. & KROKIDA, M. K. 2001. Moisture diffusivity data compilation for foodstuffs: effect of material moisture content and temperature. *International Journal of Food Properties,* 4**,** 225-237.

MARUCCI, M., RAGNARSSON, G., VON CORSWANT, C., WELINDER, A., JARKE, A., ISELAU, F. & AXELSSON, A. 2011. Polymer leaching from film coating: Effects on the coating transport properties. *International Journal of Pharmaceutics,* 411**,** 43-48.

MASON T. J., P. D. 2002. *Practical Sonochemistry,* Chichester, Horwood Publishing.

MAYACHIEW, P., DEVAHASTIN, S., MACKEY, B. M. & NIRANJAN, K. 2010. Effects of drying methods and conditions on antimicrobial activity of edible chitosan films enriched with galangal extract. *Food Research International,* 43**,** 125-132.

MEROUANI, S., HAMDAOUI, O., REZGUI, Y. & GUEMINI, M. 2013. Effects of ultrasound frequency and acoustic amplitude on the size of sonochemically active bubbles - Theoretical study. *Ultrasonics Sonochemistry,* 20**,** 815-819.

METAYER, M., LABBE, M., MARAIS, S., LANGEVIN, D., CHAPPEY, C., DREUX, F., BRAINVILLE, M. & BELLIARD, P. 1999. Diffusion of water through various polymer films: a new high performance method of characterization. *Polymer Testing,* 18**,** 533-549.

MUBASHAR, A., ASHCROFT, I. A., CRITCHLOW, G. W. & CROCOMBE, A. D. 2009a. Modelling cyclic moisture uptake in an epoxy adhesive. *Journal of Adhesion,* 85**,** 711-735.

MUBASHAR, A., ASHCROFT, I. A., CRITCHLOW, G. W. & CROCOMBE, A. D. 2009b. Moisture absorption-desorption effects in adhesive joints. *International Journal of Adhesion and Adhesives,* 29**,** 751-760.

NAHIMANA, H., ZHANG, M., MUJUMDAR, A. S. & DING, Z. S. 2011. Mass transfer modeling and shrinkage consideration during osmotic dehydration of fruits and vegetables. *Food Reviews International,* 27**,** 331-356.

NIZOVTSEV, M. I., STANKUS, S. V., STERLYAGOV, A., TEREKHOV, V. I. & KHAIRULIN, R. A. 2008. Determination of moisture diffusivity in porous materials using gamma-method. *International Journal of Heat and Mass Transfer,* 51**,** 4161-4167.

ONER, M., YETIZ, E., AY, E. & UYSAL, U. 2011. Ibuprofen release from porous hydroxyapatite tablets. *Ceramics International,* 37**,** 2117-2125.

PAUL, A., VAN DAL, M. J. H., KODENTSOV, A. A. & VAN LOO, F. J. J. 2004. The Kirkendall effect in multiphase diffusion. *Acta Materialia,* 52**,** 623-630.

PEL, L., BROCKEN, H. & KOPINGA, K. 1996. Determination of moisture diffusivity in porous media using moisture concentration profiles. *International Journal of Heat and Mass Transfer,* 39**,** 1273-1280.

PEPPAS, N. A. & BRANNONPEPPAS, L. 1994. Water diffusion and sorption in amorphous macromolecular systems and foods. *Journal of Food Engineering,* 22**,** 189-210.

PERRY, R. H. & GREEN, D. W. 1997. *Perry's Chemical Engineers' Handbook,* New York, McGraw-Hill.

PETERLIN, A. 1977. Diffusion with discontinous swelling. *Journal of research of the National Bureau of Standards-A Physics and Chemistry,* 81A**,** 243-250.

PINFIELD, V. J., POVEY, M. J. W. & DICKINSON, E. 1995. The application of modified forms of the Urick equation to the interpretation of ultrasound velocity in scattering systems. *Ultrasonics,* 33**,** 243-251.

PINFIELD, V. J., POVEY, M. J. W. & DICKINSON, E. 1996. Interpretation of ultrasound velocity creaming profiles. *Ultrasonics,* 34**,** 695-698.

POGANY, G. A. 1976. Anomalous diffusion of water in glassy polymers. *Polymer,* 17**,** 690-694.

POVEY, M. J. W. 1997. *Ultrasonic Techniques for Fluids Characterisation,* London, Academic Press.

POVEY, M. J. W. 1998. Ultrasonics of food. *Contemporary Physics,* 39**,** 467-478.

PRASAD, V., SEMWOGERERE, D. & WEEKS, E. R. 2007. Confocal microscopy of colloids. *Journal of Physics-Condensed Matter,* 19.

PRICE, P. E., WANG, S. & ROMDHANE, I. H. 1997. Extracting effective diffusion parameters from drying experiments. *Aiche Journal,* 43**,** 1925-1934.

QI, P. X., BROWN, E. M. & FARRELL JR, H. M. 2001. 'New views' on structure–function relationships in milk proteins. *Trends in Food Science & Technology,* 12**,** 339-346.

RAHIM, T., MOHAMAD, D., AKIL, H. M. & AB RAHMAN, I. 2012a. Water sorption characteristics of restorative dental composites immersed in acidic drinks. *Dental Materials,* 28**,** E63-E70.

RAHIM, T. N. A. T., MOHAMAD, D., AKIL, H. M. & AB RAHMAN, I. 2012b. Water sorption characteristics of restorative dental composites immersed in acidic drinks. *Dental Materials,* 28**,** E63-E70.

RAMIREZ, C., TRONCOSO, E., MUNOZ, J. & AGUILERA, J. M. 2011. Microstructure analysis on pre-treated apple slices and its effect on water release during air drying. *Journal of Food Engineering,* 106**,** 253-261.

REID, J. D. & BUCK, R. P. 1987. Dielectric properties of an epoxy-resin and its composite. 2. Solvent effects on dipole relaxation. *Journal of Applied Polymer Science,* 33**,** 2293-2303.

REJL, F. J., VALENZ, L. & LINEK, V. 2010. "Profile method" for the measurement of kLa and kVa in distillation columns. Validation of rate-based distillation models using concentration profiles measured

along the column. *Industrial & Engineering Chemistry Research,* 49**,** 4383-4398.

ROY, S., VENGADASSALAM, K., WANG, Y., PARK, S. & LIECHTI, K. M. 2006. Characterization and modeling of strain assisted diffusion in an epoxy adhesive layer. *International Journal of Solids and Structures,* 43**,** 27-52.

RUIZ-CABRERA, M. A., FOUCAT, L., BONNY, J. M., RENOU, J. P. & DAUDIN, J. D. 2005. Assessment of water diffusivity in gelatine gel from moisture profiles. I - Non-destructive measurement of ID moisture profiles during drying from 2D nuclear magnetic resonance images. *Journal of Food Engineering,* 68**,** 209-219.

RUIZ-LOPEZ, II, RUIZ-ESPINOSA, H., ARELLANES-LOZADA, P., BARCENAS-POZOS, M. E. & GARCIA-ALVARADO, M. A. 2012. Analytical model for variable moisture diffusivity estimation and drying simulation of shrinkable food products. *Journal of Food Engineering,* 108**,** 427-435.

SARAVACOS, G. D. & MAROULIS, Z. B. 2001. *Transport Properties of Foods,* New York, Marcel Dekker Inc.

SCHMIDT-HANSBERG, B., KLEIN, M. F. G., PETERS, K., BUSS, F., PFEIFER, J., WALHEIM, S., COLSMANN, A., LEMMER, U., SCHARFER, P. & SCHABEL, W. 2009. In situ monitoring the drying kinetics of knife coated polymer-fullerene films for organic solar cells. *Journal of Applied Physics,* 106.

SETH, D. & SARKAR, A. 2004. A lumped parameter model for effective moisture diffusivity in air drying of foods. *Food and Bioproducts Processing,* 82**,** 183-192.

SHERWOOD, T. K. 1931. Application of the theoretical diffusion equation to the drying of solids. *Trans AIChE,* 27**,** 190-202.

SHIH, H. H. & HAMED, G. R. 1997. Poly(ethylene-co-vinylacetate) based hot melt adhesives: I. Relating adhesive rheology to peel adhesion. *Journal of Adhesion,* 61**,** 231-245.

SIDERIDOU, I. D. & KARABELA, M. M. 2011. Sorption of water, ethanol or ethanol/water solutions by light-cured dental dimethacrylate resins. *Dental Materials,* 27**,** 1003-1010.

SMIGELSKAS, A. D. & KIRKENDALL, E. O. 1947. Zinc diffusion in alpha-brass. *Transactions of the American Institute of Mining and Metallurgical Engineers,* 171**,** 130-142.

STAUDT, P. B., TESSARO, I. C., MARCZAK, L. D. F., SOARES, R. D. & CARDOZO, N. S. M. 2013. A new method for predicting sorption isotherms at different temperatures: Extension to the GAB model. *Journal of Food Engineering,* 118**,** 247-255.

STRUMILLO, C., PAKOWSKI, Z. & ZYLLA, R. 1986. Computer design calculation for dryers with fluidized and vibrating fluidized-beds. *Journal of Applied Chemistry of the USSR,* 59**,** 1935-1942.

SUTERMEISTER, E. B., F.: 1939. *Casein and its industrial applications,* New York, Rreinhold.

SWAISGOOD, H. E. 1982. *Chemistry of milk proteins,* London, UK, Applied Science.

TABOR, Z., KRZAK, M., NOWAK, P. & WARSZYNSKI, P. 2012a. Water diffusion in polymer coatings containing water-trapping particles. Part 1. Finite difference-based simulations. *Progress in Organic Coatings,* 75**,** 200-206.

TABOR, Z., KRZAK, M., NOWAK, P. & WARSZYŃSKI, P. 2012b. Water diffusion in polymer coatings containing water-trapping particles. Part 1. Finite difference-based simulations. *Progress in Organic Coatings,* 75**,** 200-206.

TARI, O., KARA, S. & PEKCAN, O. 2011. Study of thermal phase transitions in iota carrageenan gels via fluorescence technique. *Journal of Applied Polymer Science,* 121**,** 2652-2661.

THURSBY, G. J., MACLEAN, A., HOGG, H. & CULSHAW, B. 2006. Ultrasound detection of damage in complex carbon fibre/metal structures. 61770P-61770P.

THUWAPANICHAYANAN, R., PRACHAYAWARAKORN, S., KUNWISAWA, J. & SOPONRONNARIT, S. 2011. Determination of effective moisture diffusivity and assessment of quality attributes of banana slices during drying. *Lwt-Food Science and Technology,* 44**,** 1502-1510.

TREYBAL, R. E. 1980. *Mass-transfer operations*, McGraw-Hill New York.

TSOCHATZIDIS, N. A., GUIRAUD, P., WILHELM, A. M. & DELMAS, H. 2001. Determination of velocity, size and concentration of ultrasonic cavitation bubbles by the phase-Doppler technique. *Chemical Engineering Science,* 56**,** 1831-1840.

URICK, R. J. 1947. A sound velocity method for determining the compressibility if finely divided substances. *Journal of Applied Physics,* 18**,** 983-987.

VAN LOO, F. J. J. 1990. Multiphase diffusion in binary and ternary solid-state systems. *Progress in Solid State Chemistry,* 20**,** 47-99.

WANG, B. X. & FANG, Z. H. 1988. Water-absorption and measurement of the mass diffusivity in porous-media. *International Journal of Heat and Mass Transfer,* 31**,** 251-257.

WANG, J. C. F. & RONNEBRO, E. C. E. An overview of hydrogen storage for transportation application. *In:* BIELER, T. R., CARSLEY, J. E., FRASER, H. L., SEARS, J. W. & SMURGERESKY, J. E., eds. Trends in materials and manufacturing technologies for transportation industries and powder metallurgy research and development in the transportation industry, 2005. 21-24.

WOOD, A. B. 1941. *A Textbook of Sound,* London, Bell and Sons.

YORK, R. L., BRATLIE, K. M., HILE, L. R. & JANG, L. K. 2011. Dead zones in porous catalysts: Concentration profiles and efficiency factors. *Catalysis Today,* 160**,** 204-212.

ZHANG, L. Z. & NIU, J. L. 2003. Effects of substrate parameters on the emissions of volatile organic compounds from wet coating materials. *Building and Environment,* 38**,** 939-946.

ZHAO, D., LI, M., ZHANG, D., BAIG, S. A. & XU, X. 2013. Reductive dechlorination of 2,4-dichlorophenol by Pd/Fe nanoparticles prepared in the presence of ultrasonic irradiation. *Ultrasonics Sonochemistry,* 20**,** 864-871.

ZOGZAS, N. P. & MAROULIS, Z. P. 1996. Effective moisture diffusivity estimation from drying data. A comparison between various methods of analysis. *Drying Technology,* 14**,** 1543-1573.

## List of Abbreviations

$A$ = area of droplet in contact with substrate ($m^2$)

$A_a$ = area of droplet in contact with air ($m^2$)

$a$ = contact radius of droplet with substrate (m)

$c_s$ = molar concentration of the solid phase ($mol.cm^3$)

$c_w$ = molar concentration of the water phase ($mol.cm^{-3}$)

$c_w^{eq}$ = equilibrium molar concentration of water ($mol.cm^{-3}$)

$D$, $D_w$ = diffusion coefficient of the water phase ($m^2.s^{-1}$)

$h$ = height of droplet (m)

$j_s$ = molar flux of the solid phase ($kg.m^{-2}.s^{-1}$)

$j_w$ = molar flux of the water phase ($kg.m^{-2}.s^{-1}$)

$K$ = evaporation constant ($m.s^{-1}$)

$\kappa$ = compressibility ($Pa^{-1}$)

$L$ = thickness of the film (m)

$L\infty$ = thickness of the film at equilibrium (m)

$R$ = radius of droplet curvature (m)

$t$ = time (s)

$V$ = normalised droplet volume ($m^3$)

$V_{in}$ = initial moisture concentration ($m^3$)

$V_f$ = final moisture concentration ($m^3$)

$V_s$ = molar volume of the solid phase ($m^3.mol^{-1}$)

$V_w$ = molar volume of the water phase ($m^3.mol^{-1}$)

$x$ = position in film (m)

$z$ = height in the film above the substrate (m)

$\alpha$ = mole fraction of water

$\Gamma$ = moisture ratio

$\rho$ = density ($g.cm^{-3}$)

$\tau$ = scaled time

$\phi$ = volume fraction of water

$\phi^{eq}$ = equilibrium volume fraction of water

# Appendix 1

**Table of properties of different composition thin films under different drying conditions**

| Film composition | Drying condition | $\phi\infty$ | $w\infty$ | $\tau$(diff) | $\tau$(evap) |
|---|---|---|---|---|---|
| Caseinate 18 wt% | 30°C, 30% RH | $7.1 \times 10^{-6}$ | $4.5 \times 10^{-5}$ | 4600 | $3.97 \times 10^{-4}$ |
| Caseinate 18 wt% | 40°C, 30% RH | $1.3 \times 10^{-5}$ | $3.9 \times 10^{-5}$ | 7500 | $6.20 \times 10^{-4}$ |
| Caseinate 18 wt% | 50°C, 30% RH | $1.1 \times 10^{-5}$ | $3.8 \times 10^{-5}$ | 5000 | $9.20 \times 10^{-4}$ |
| Caseinate 18 wt% | 30°C, 20% RH | $8.2 \times 10^{-6}$ | $4.1 \times 10^{-5}$ | 4400 | $4.55 \times 10^{-4}$ |
| Caseinate 18 wt% | 30°C, 40% RH | $6.6 \times 10^{-6}$ | $4.2 \times 10^{-5}$ | 14500 | $3.05 \times 10^{-4}$ |
| Starch 7 wt% | 30°C, 30% RH | $1.9 \times 10^{-6}$ | $1.3 \times 10^{-5}$ | 4000 | $4.8 \times 10^{-4}$ |
| Starch 7 wt% | 40°C, 30% RH | $2.4 \times 10^{-6}$ | $1.3 \times 10^{-5}$ | 7500 | $6.30 \times 10^{-4}$ |
| Starch 7 wt% | 50°C, 30% RH | $3.4 \times 10^{-6}$ | $1.2 \times 10^{-5}$ | 5500 | $8.70 \times 10^{-4}$ |

| | | | | | |
|---|---|---|---|---|---|
| **Starch 7 wt%** | **30°C, 20% RH** | **$3.3 \times 10^{-6}$** | **$1.5 \times 10^{-5}$** | **4000** | **$4.85 \times 10^{-4}$** |
| **Starch 7 wt%** | **30°C, 40% RH** | **$1.6 \times 10^{-5}$** | **$8.8 \times 10^{-6}$** | **11500** | **$4.05 \times 10^{-4}$** |
| **Mixed 9%:4.5%** | **30°C, 30% RH** | **$6.9 \times 10^{-6}$** | **$2.5 \times 10^{-5}$** | **3000** | **$7.05 \times 10^{-4}$** |
| **Mixed 9%:4.5%** | **40°C, 30% RH** | **$3.8 \times 10^{-6}$** | **$2.4 \times 10^{-5}$** | **7500** | **$6.45 \times 10^{-4}$** |
| **Mixed 9%:4.5%** | **50°C, 30% RH** | **$9.1 \times 10^{-6}$** | **$2.8 \times 10^{-5}$** | **7100** | **$6.80 \times 10^{-4}$** |
| **Mixed 9%:4.5%** | **30°C, 20% RH** | **$7.6 \times 10^{-6}$** | **$2.2 \times 10^{-5}$** | **2900** | **$7.05 \times 10^{-4}$** |
| **Mixed 9%:4.5%** | **30°C, 40% RH** | **$1.3 \times 10^{-5}$** | **$3.0 \times 10^{-5}$** | **12000** | **$3.68 \times 10^{-4}$** |

**Fortran code example used to simulate dehydration of water from a thin film**

```
c    Program to calculate the drying profile of a thin film,
consisting of solid and solvent
C     The rate of drying from top surface is assumed to be very
fast, hence keeping the outer
c      layer always at a concentration of vfe in equilibrium with
surronding air
c
c         R ETTELAIE  and  A Tasker                      16/02/2011
c
       DOUBLE PRECISION dt,dy,x(2),vf(0:1010,2),vfts(2),dx,alpha
       DOUBLE PRECISION vfe,vfini,Conv,fli,fli1,DifCur,timet,mu
```

```
      DOUBLE PRECISION fsolid,dfsolid
      INTEGER curr,prev
      INTEGER i,j,k,N,NSTEP,Nitr
c
      OPEN (1,file="xdata.txt")
      OPEN (2,file="result.txt")
c
c  initialise the values
c
c vf(i,curr) is the volume fraction of water at point (i-0.5)*dy
C  The true voulme fraction is vf(i,curr)/x(curr)
C   vfts(curr) is the volume fration at outer layer set to
c   vfe*x(curr) here.
c
      curr=1
      prev=2
      N=400
      Nitr=640000
      NSTEP=4000
      timet=0.0d0
      vfini=0.5d0
      alpha=0.1d0
      vfe=0.2d0
      x(curr)=1.0d0
      dy=1.0d0/dfloat(N)
      PRINT *,"******"
      PRINT *,"dy =",dy
      dt=dy*dy*0.1d0
      PRINT *,"dt =",dt
      PRINT *,"mu=",mu(0.1d0,0.5d0)
c
c
      Do i=0,N
        vf(i,curr)=vfini
      END DO
      vfts(curr)=vfe
c
c    Begin the iterations
c
      Do i=1,NSTEP
        dt=dy*dy*0.1d0*x(curr)*x(curr)
        Do j=1,Nitr
         dx= 2.0d0*
     &     mu( (vf(N,curr)+vfts(curr))/2.0d0,x(curr) )*
     &     ( vfts(curr)-vf(N,curr) )/ dy/(1.0d0 -
vfts(curr)/x(curr))
         curr=3-curr
         prev=3-prev
c
         x(curr)=x(prev)+(dx*dt)
         Do k=1,N-1
          DifCur=((vf(k-1,prev)-vf(k,prev)))*mu((vf(k-1,prev)+
     &       vf(k,prev))/2.0d0,x(prev))
          DifCur=DifCur+((vf(k+1,prev)-vf(k,prev)))*
     &       mu((vf(k+1,prev)+vf(k,prev))/2.0d0,x(prev))
```

```
          DifCur=DifCur*dt/dy/dy
          fli=dfloat(k)
          fli1=dfloat(k-1)
          Conv=fli*((vf(k+1,prev)+vf(k,prev))/2.0d0) -
     &       (fli1)*((vf(k,prev)+vf(k-1,prev))/2.0d0)
          Conv=Conv*dx*dt/x(prev)
          vf(k,curr)=vf(k,prev)+DifCur+Conv
         END DO
         DifCur=((vf(N-1,prev)-vf(N,prev)))*mu((vf(N-1,prev)+
     &           vf(N,prev))/2.0d0,x(prev))
         DifCur=DifCur*dt/dy/dy
         fli1=dfloat(N-1)
         Conv=-(fli1)*((vf(N,prev)+vf(N-1,prev))/2.0d0)
         Conv=Conv*dx*dt/x(prev)
         vf(N,curr)=vf(N,prev)+DifCur+Conv+(dx*dt/dy)
c
c      impose reflective boundary condition at film/solid interface
         vf(0,curr)=vf(1,curr)
         vfts(curr)=vfe*x(curr)
        END DO
        fsolid=0.0d0
        Do j=1,N
          fsolid=fsolid+vf(j,curr)
        END DO
c        fsolid=(fsolid)-((vf(N,curr)-vfts(curr))*dy/4.0d0)
        fsolid=x(curr)-fsolid*dy
        dfsolid=fsolid-(1.0d0-vfini)
        timet=timet+dfloat(Nitr)*dt
        PRINT *,"finished",i,"  dfsolid=",dfsolid," "
        PRINT *,"timet=",timet
        PRINT *,"vfts=",vfts(curr),x(curr),dx
        PRINT *,vf(1,curr),vf(N/4,curr),vf(N/2,curr),
     &    vf(3*N/4,curr),vf(N,curr)
c
        WRITE (1,110) timet,x(curr)
 110    FORMAT (f12.6," ",f8.6)
      END DO
      Do i=1,N
       WRITE (2,100) dfloat(i)*x(curr)/dfloat(N),vf(i,curr)/x(curr)
      END DO
 100  FORMAT (f9.6," ",f9.6)
      CLOSE (1)
      CLOSE (2)
      PRINT *,"**** END ****"
C
      STOP
      END

C       ~~~~~~~~~~~~~ ###################
~~~~~~~~~~~~~
```

```
        mu=D/x/x
c       PRINT *,x
c
      RETURN
      END
```

## MatLab code to simulate waterfall plot of speed of sound vs height vs time

```
% this will create the matrix that is used to create the surface
plot

%place this in a loop for all 28 files and use eval to change the
name
% use i as the looping integer

for i=1:27

 a=['Acoustiscan          trial(cell3_d13-01-12_t14-49_21).XLS_Scan'
int2str(i) '.xls'];

 importfile(a)

 % delete unwanted columns and rows

 data(:,2:7)=[];
 data(:,3:7)=[];


 data(1:6,:)=[];
 data(2:5,:)=[];
 data(3:6,:)=[];
 data(4:7,:)=[];
 data(5:8,:)=[];
 data(6:9,:)=[];
 data(7:10,:)=[];
 data(8:11,:)=[];
 data(79:82,:)=[];
 data(80:83,:)=[];
 data(81:84,:)=[];
 data(82:85,:)=[];
 data(83:86,:)=[];
 data(84:87,:)=[];
 data(85:88,:)=[];
 data(86:89,:)=[];
 data(87:90,:)=[];
 data(88:91,:)=[];
 data(89:92,:)=[];
 data(90:93,:)=[];
 data(91:94,:)=[];
 data(92:95,:)=[];
 data(93:191,:)=[];


 height = data;
 height(:,2)=[];
```

```
 height=height.';

 data(:,1)=[];
 data=data.';

 if (i < 2)
     z=data;
     else
     z=[z; data];
 end

end

time=[62.5;65;67.5;70;72.5;75;77.5;80;82.5;85;87.5;90;92.5;95;97.5;1
00;102.5;105;107.5;110;112.5;115;117.5;120;122.5;125;127.5];

c=ones(27,91)

surf(height,time,z,c)
colormap hsv
alpha(.4)
xlabel('Height (mm)')
ylabel('Time (H)')
zlabel('Speed of sound (m/s)')
az = -20;
el = 25;
view(az, el);
set(gcf,'Color',[1,1,1]);
```